44885

NAME OF AUTHOR/*NOM DE L'AUTEUR*_____DAUTET Danielle_____

TITLE OF THESIS/*TITRE DE LA THÈSE*_____Studies of intermediate energy fission_____

_____

_____

UNIVERSITY/*UNIVERSITÉ*_____Simon Fraser University_____

DEGREE FOR WHICH THESIS WAS PRESENTED/
  *GRADE POUR LEQUEL CETTE THÈSE FUT PRÉSENTÉE*_____Ph.D._____

YEAR THIS DEGREE CONFERRED/*ANNÉE D'OBTENTION DE CE GRADE*_____1980_____

NAME OF SUPERVISOR/*NOM DU DIRECTEUR DE THÈSE*_____Dr. B. D. PATE_____

DATED/*DATÉ*___May 6⁴ 1980___ SIGNED/*SIGNÉ*_____

PERMANENT ADDRESS/*RÉSIDENCE FIXE*_____
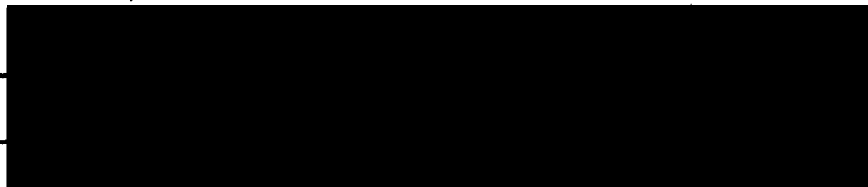
NOTICE

AVIS

The quality of this microfiche is heavily dependent upon the quality of the original thesis submitted for microfilming. Every effort has been made to ensure the highest quality of reproduction possible.

If pages are missing, contact the university which granted the degree.

Some pages may have indistinct print especially if the original pages were typed with a poor typewriter ribbon or if the university sent us a poor photocopy.

Previously copyrighted materials (journal articles, published tests, etc.) are not filmed.

Reproduction in full or in part of this film is governed by the Canadian Copyright Act, R.S.C. 1970, c. C-30. Please read the authorization forms which accompany this thesis.

La qualité de cette microfiche dépend grandement de la qualité de la thèse soumise au microfilmage. Nous avons tout fait pour assurer une qualité supérieure de reproduction.

S'il manque des pages, veuillez communiquer avec l'université qui a conféré le grade.

La qualité d'impression de certaines pages peut laisser à désirer, surtout si les pages originales ont été dactylographiées à l'aide d'un ruban usé ou si l'université nous a fait parvenir une photocopie de mauvaise qualité.

Les documents qui font déjà l'objet d'un droit d'auteur (articles de revue, examens publiés, etc.) ne sont pas microfilmés.

La reproduction, même partielle, de ce microfilm est soumise à la Loi canadienne sur le droit d'auteur, SRC 1970, c. C-30. Veuillez prendre connaissance des formules d'autorisation qui accompagnent cette thèse.

THIS DISSERTATION
HAS BEEN MICROFILMED
EXACTLY AS RECEIVED

LA THÈSE A ÉTÉ
MICROFILMÉE TELLE QUE
NOUS L'AVONS REÇUE

STUDIES OF INTERMEDIATE ENERGY FISSION

by

Danielle Marie Gabrielle Dautet nee Austrui

Maitrise es sciences, Universite de Paris, 1969

Doctorat de 3eme cycle, Universite de Paris, 1971

A THESIS SUBMITTED IN PARTIAL FULFILLMENT

OF THE REQUIREMENTS FOR THE DEGREE OF

DOCTOR OF PHILOSOPHY

in the Department

of

Chemistry

©Danielle Marie Gabrielle Dautet 1980

SIMON FRASER UNIVERSITY

April 1980

Title of Thesis/Project/Extended Essay

Studies of intermediate energy fission

Author:

(signature)

DAUTET   Danielle

(name)

May 6ᵗʰ 1980

(date)

APPROVAL

Name: Danielle Marie Gabrielle Dautet nee Austrui

Degree: Doctor of Philosophy

Title of Thesis: Studies of intermediate energy fission

Examining Committee:

     Chairman: C.H.W. Jones

          B.D. Pate
          Senior Supervisor

          R.G. Korteling

          A.C. Oehlschläger

          A.C. Arrott

          N. Sugarman
          External Examiner
          Professor, University of Chicago

              Date approved :   <u>April 24, 1980</u>

ABSTRACT

Fission induced by high energy particles was studied by means of two different techniques: mica track detector experiments (for fission of Au and U induced by 800 MeV protons and 400 MeV pions) and semi-conductor detector measurements (for fission of Au, Bi, Th and U induced by 480 MeV protons).

The total kinetic energy of the fission fragments was measured and found to be the same for a given fissioning system, within experimental errors, whether protons or pions were used as projectiles.

Angular correlation and angular distribution measurements led to average values of the fissioning system momentum parallel to the beam direction ($p_{//}$). From the results of a Monte Carlo calculation of the intra-nuclear cascade (performed with the computer code ISOBAR), an average excitation energy was deduced from the experimentally measured $p_{//}$. For thorium and uranium targets, it was found that the fission probability was

higher among nuclei possessing a low excitation energy (and a high angular momentum) at the end of the cascade step. This finding was confirmed, in the case of uranium, by a comparison of the widths of the fragment mass distributions obtained experimentally and calculated through the codes ISOBAR (for the cascade step) and EVA (for the evaporation step with competition between fission and particle emission).

The widths of fragment mass and total kinetic energy distributions were compared with the theoretical predictions of Nix and were found to be in reasonable agreement for gold and bismuth targets. The discrepancy observed in the case of thorium and uranium could be due to asymmetric fission events (from fission occuring at low excitation energy) for which the model is not valid.

All angular distributions in the center of mass system were found to be flat within experimental errors.

An attempt to determine the mass of the fissioning system was carried out but the quality of the measurements was not sufficient to obtain definitive value. While a mechanism involving simple "first-chance" fission was found improbable, it was not possible to distinguish between "last-chance" fission, or fission occuring at several stages of the de-excitation process.

DEDICACE

A la mémoire de ma mère: Dieu ne lui a pas permis de voir cette thèse, fruit de tant d'années de séparation et d'attente.

A mon père

A Henri et nos enfants qui ont du partager mon temps avec les exigeances de la recherche.

"Fission is a process of deadly fascination; had nature chosen her constants just a little differently, we should have been deprived of its potential for social good and spared its power for social evil."

D.H. Wilkinson

REMERCIEMENTS

TABLE OF CONTENTS

LIST OF TABLES

LIST OF FIGURES

INTRODUCTION

This thesis describes an attempt to obtain data bearing
on a long-standing problem in the area of nuclear fission,
namely when, in the evaporation de-excitation of an excited
heavy nucleus, fission does take place. The conventional
statistical model in its simplest form, with which much of
the radiochemical data on the yields of nuclei escaping
fission agrees, predicts that first chance fission (i.e.
fission early in the de-excitation process and hence at high
excitation energy) should be predominant for the heaviest
elements such as uranium and again for elements near silver.
For in between elements, such as gold and bismuth, fission
is expected to compete with evaporation over much of the
de-excitation sequence.

Data obtained for these same elements on the angular
correlation between emitted fission fragments and evaporated
particles, on the other hand, is understood in terms of
fission occuring primarily at the end of the de-excitation
process (last chance fission) and hence at low excitation
energy (Che.70), (Fra.75), (Wil.79).

As a result of previous work in this laboratory,

primarily by H.Blok and F.M.Kiely, experience had been
gained in the application of mica track detectors to fission
fragment spectroscopy, the mica had been calibrated, and
computer codes existed for data analysis. Thus, in the early
stages of this work, advantage was taken of this situation.
The contribution of the present author was in the extension
and improvement of the calibration data and analysis
programs, and then their application at the facilities
provided at the LAMPF accelerator (prior to TRIUMF being
operational) to experiments on fission induced by
intermediate energy protons and pions as LAMPF
experiment 104. The experimental contribution of the writer
was in the preparation for the experiment (target and mica
preparation,etc.) and in the scanning and analysis
afterwards. She was unable to travel to CRNL (for the
calibration irradiation) nor to LAMPF (for the fission
experiments); the irradiations were performed by the thesis
supervisor.

Later when TRIUMF produced protons beams of appropriate
quality, the program was extended to measurements with
semi-conductor detectors. This was accomplished as a small
part of TRIUMF experiment 6, in collaboration with H.Blok
and B.D.Pate who were working on that experiment. The

present author set up the experiment, and especially the electronics, in collaboration with the above mentioned, but took major responsability for running the experiment, and was solely responsible for target preparation and analysis of the subsequent data.

This experiment was not directed at obtaining fission-evaporation angular correlation data similar to that obtained at somewhat lower energies by others, and alluded to above. Instead, it concentrated on measurements on fission fragments themselves, and particularly on extraction of those fission parameters which might be expected to reveal the mass or excitation energy of the system undergoing fission.

In principle, the distribution in fissioning system mass should be accessible via simultaneous measurement of the energies and times of flight of both fragments from binary fission. In the end, the analysis of the present data showed its critical sensitivity to parameters which were beyond the scope of the present experiment to control, and the width of the distribution was obtained only with rather large uncertainty. These data and those obtained via a somewhat different analysis of data on two tracklengths plus their directions measured with mica sandwiches are, however,

still interesting to compare with theory in a general way.

The second possible avenue of examination was measurement of those parameters which might be affected by excitation energy at the moment of fission. These included the most probable values, and especially the widths, of the distributions in fragment kinetic energy and mass. In addition the center of mass momentum of the fissioning system was expected from previous work to be related to excitation energy, although the effect of post-fission de-excitation by particle evaporation was expected to affect the measurement of all these parameters.

Finally the angular distribution of the fission fragments with respect to the beam direction would lead to a value of the fission moment of inertia, which is expected to exhibit a sharp dependence on fissioning system mass in much of the subject mass region. Again, some difficulty was also expected in the extraction of this parameter, since the excitation energy also exerts an effect upon the fragment angular distribution through the nuclear temperature.

Much of the work in this thesis, therefore, was taken up in an exploration, during analysis of the experimental data, of the influence on parameter extraction of the complicating factors referred to above.

In the course of it, however, much fission fragment
spectroscopy was accomplished, some of it new and hence of
special interest. In particular, measurement of fission
fragment energies and fission center of mass momenta for the
pion-induced fission of gold was accomplished in comparison
with the corresponding data for proton-induced fission, and
these data were then available for comparison with theory.

In the organisation of what follows, the knowledge of
the field provided by the work of previous authors is first
reviewed. Then, the experimental procedures are outlined,
together with the techniques employed for analysis of the
data. Finally, the data are compared with the available
theories, and the data in the end accessible on fission-
evaporation competition are discussed.

I THEORETICAL CONSIDERATIONS

A) High energy fission

A characteristic difference between low (<50 MeV) and high (>100 MeV) energy nuclear reactions is illustrated in Fig.1 (taken from Mil.59) where the mass-yield curves for incident protons of 40- 480 and 3000 MeV upon bismuth have been plotted. It can be seen from this figure that the narrow mass distribution of the reaction products obtained at low bombarding energy becomes much wider as the energy increases. The products from high energy bombardment are spread over many mass numbers and, at the highest energies, all products with mass numbers less than that of the target are found with measurable cross-sections. Reactions induced by high energy particles are usually divided into four categories:

- spallation in which several nucleons or even groups of nucleons are emitted from the struck target nucleus.

Fig.1: Mass-yield curves for the irradiation of a bismuth target with 40, 480 and 3000 MeV protons.
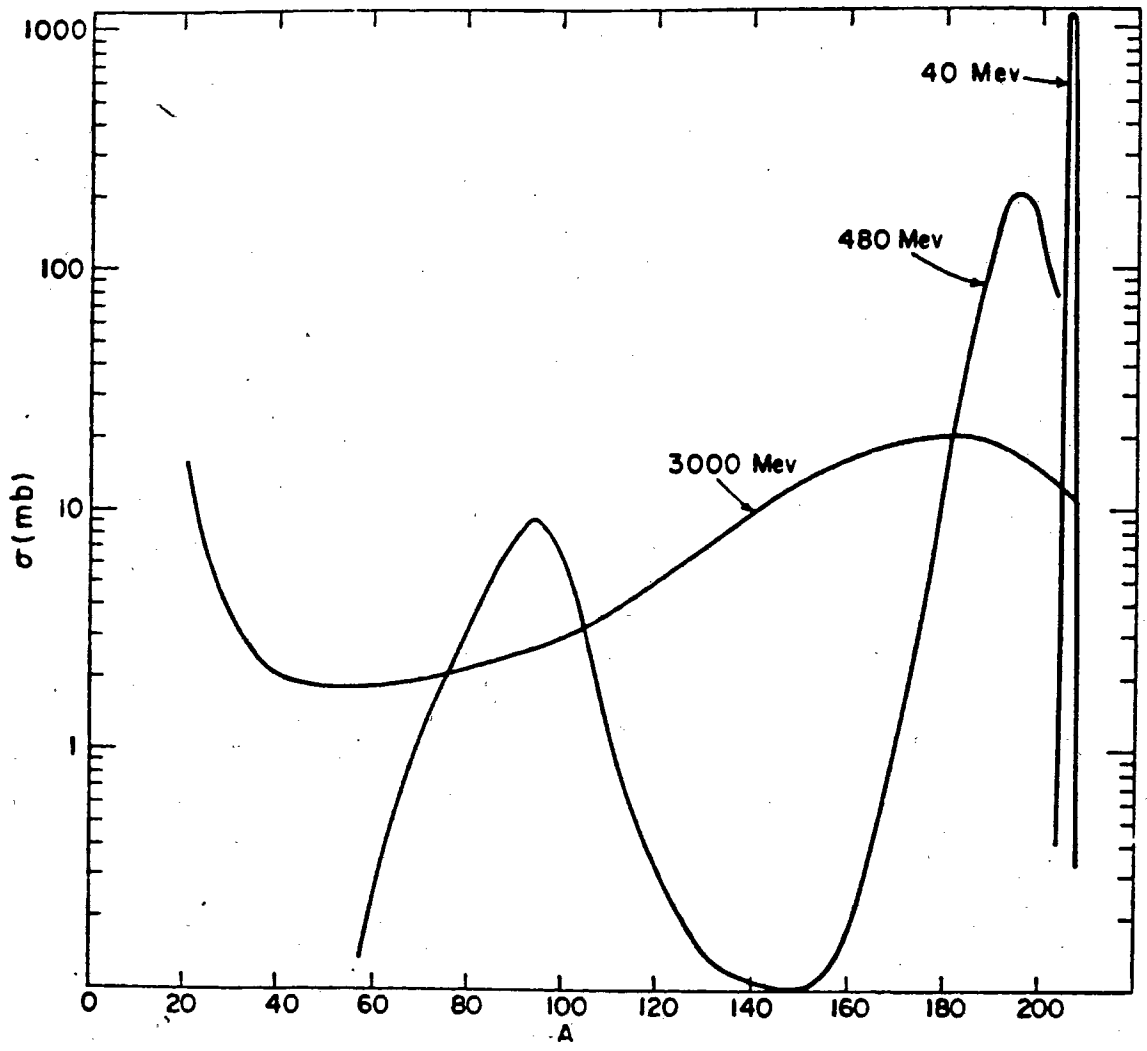
- fission (particularly characteristic of heavy nuclei) in which the struck nucleus splits into two or more fragments having roughly equal atomic masses.

- fragmentation in which relatively heavy fragments (^{8}Be, ^{12}C, ^{16}O and even ^{24}Na or ^{28}Mg) are generally ejected from the struck nucleus in a fast process and

- secondary reactions in which some particles or fragments released in the primary reaction have energies sufficient to cause further interactions with adjacent nuclei.

The shape of the mass-yield curve at 480 MeV bombarding energy has been explained (Mil.59) as follows: the products with mass number between 60 and 140 may be considered as fission products, in the light of the increased yield in this region for fissile targets which is absent for light targets, those with mass between 160 and 209amu as spallation products while those with a mass greater than that of the target as secondary products (neglecting the small contribution from π^- emission). It should be emphasized that the above categories are not mutually exclusive: for example, a fissile target nucleus struck by an incident particle may emit several particles in a spallation reaction and then may undergo fission. The wide

distribution in mass of the products indicates that Bohr's hypothesis (Boh.37) for low energy reactions, that the incident particle is initially absorbed by the target nucleus and the compound nucleus thus formed de-excites after equipartitioning of the energy, is no longer valid at high energies. Between 1947 and 1952 Serber (Ser.47), Goldberger (Gol.48), Chew and Goldberger (Che.52) proposed and developed a model to describe the wide distribution of radioactive products formed in the 200 MeV deuteron irradiation of ^{75}As (Cun.47).

1) The Serber and Weisskopf models

The Serber model describes the first step in a two step process. In this first stage, often called the "prompt cascade" or "nucleonic cascade" taking place in a very short period of time ($\sim 10^{-20}, 10^{-22}$ s), the incoming particle interacts with a single nucleon in the nucleus. The projectile and struck nucleon either escape from the nucleus or interact with other nucleons in a cascade. At the end of the cascade, the nucleus is left in an excited state and de-excites, in a second step, by the statistical emission of neutrons, protons, alpha-particles etc., or fission may

occur. This evaporation stage takes place on a longer time scale than the prompt cascade ($10^{-15}, 10^{-19}$ s), and is described by the formalism due to Weisskopf (Wei.37).

a) The nucleonic cascade

At kinetic energy of about 100 MeV, the wavelength associated with an incident proton becomes less than the average distance between nucleons, so that the incident particle will interact with one nucleon at a time. Another aspect is that the duration of the collision between the incident particle and the nucleon is short compared to the characteristic time interval for collisions between nucleons in the nucleus.

As the energy increases, there is an increasing probability that the bombarding particle will traverse the nucleus without any interactions, i.e, the nucleus becomes increasingly transparent to the bombarding particles. The nucleonic cascade may vary in complexity from such cases in which the projectile passes through the nucleus without making a single collision, to those in which very large cascades are generated. When collisions with one or several nucleons do occur, the struck nucleons may in turn strike other nucleons and contribute to the total excitation energy

of the nucleus, or escape from the nucleus. At incident energies above the pion production threshold, inelastic collisions must also be considered and will have an appreciable effect on the propagation of the cascade.

The generation of the cascade can be computed by the Monte Carlo method of Ulam and Von Neumann (Ula.47). The application of this method to the cascade calculation was outlined by Goldberger (Gol.48) and the first attempts were carried out in two spatial dimensions (Rud.56). However, since 1958, a treatment has been developed in three dimensions with the calculations performed by a computer (Met.58). Such a calculation follows step by step the development of the cascade by selecting via random numbers the kinematic conditions of the collisions: a random choice is made at every point in the calculation where a decision must be made and this choice is weighted according to the probability distribution for the event in question. The calculation is repeated for a sufficient number of projectile target pairs for the results to have statistical significance. All nucleons struck during the cascade are followed until they either leave the nucleus or, following further interactions, their energy becomes too low for them to escape. Over the years more sophisticated treatments of this model have been developed by Bertini (Ber.63,Ber.78),

Chen et al (Che.68,Che.71) and Harp (Har.74).

The computer code VEGAS developed by Chen et al (Che.71) has been modified lately by Harp (Har.74) to extend its calculations to higher energies. This version named ISOBAR was used in the present work to calculate the mass, energy and momentum distributions of the nuclei at the end of the cascade step for use in comparisons with the experimental data obtained.

b) The evaporation stage

All analyses of particle evaporation from excited residual nuclei remaining after the intranuclear cascade have used the statistical assumption and developments of the formalism first developed by Weisskopf (Wei.37). The probability per unit time that a particle of type i with binding energy B_i, mass M_i and spin s_i is emitted in the energy interval de_i at an energy e_i from a nucleus with excitation energy E is given by:

$$W(e_i)de_i = \frac{2s_i+1}{\pi^2 h^3} M_i \sigma_i(e_i) e_i \frac{\rho'(E-B_i-e_i)}{\rho(E)} de_i \qquad (I.1)$$

where $\sigma_i(e_i)$ is the cross-section for the inverse of the emission reaction, $\rho(E)$ is the density of energy levels of

the original nucleus at excitation energy E and $\rho'(E-B_i-e_i)$ is the density of energy levels of the nucleus remaining after the emission of particle i with kinematic energy e_i.

Crucial quantities in the above expression are the level densities $\rho(E)$ and $\rho'(E-B_i-e_i)$. In order to evaluate them, a nuclear model has to be assumed. If the Fermi gas model is chosen, the level density may be written as (Wei.37):

$$\rho(E) = C \exp[2(aE)^{1/2}] \tag{I.2}$$

where C and a are constants usually evaluated empirically.

The expression (I.1) has been used in many theoretical treatments of the evaporation stage following the intranuclear cascade (Lec.50), (Lec.52), (Yam.50), (Fuj.49), (Fuj.50), (Jac.56), (Rud.56) and (Dos.58). Recent important contributions are due to Hillman (private communication) who developed the computer code JULIAN.

Emission of a type i particle governed by equation (I.1) leads to a new nucleus whose behaviour is again governed by the same expression. Thus, the problem is one of an "evaporation cascade" which may be treated by the Monte Carlo method. Such a calculation has been performed by Dostrovsky et al (Dos.59) and extended by Porile and Tanaka (Por.64) to include the determination of the momentum of the

product nuclei resulting from long evaporation chains.

c) Competition between fission and particle emission during the evaporation stage

For high energy reactions, the possibility of fission must be included in the list of possible modes of de-excitation for each evaporation step.

Starting with a given value of the excitation energy, a random choice is made of the particle emitted in the first instance (proton, neutron or heavier particle). This choice depends on the probability ratios Γ_p/Γ, Γ_n/Γ, Γ_i/Γ or Γ_f/Γ where Γ is the total width and Γ_p, Γ_n, Γ_i and Γ_f are the widths for the emission of a proton, neutron, any particle i or fission respectively.

The fission width Γ_f was given by Bohr and Wheeler (Boh.39) for a model in which the nucleus was approximated by a uniformly charged liquid drop:

$$\Gamma_f = \frac{1}{2\,\pi\rho(E)} \int_0^{E-B_f} \rho(E-B_f-e)\,de$$

where $\rho(E)$ and $\rho(E-B_f-e)$ are the level densities of the excited nucleus before fission and of the nucleus at the saddle point respectively and B_f is the fission barrier.

For heavy nuclei where fission is important, the most important evaporation process is neutron emission, since charged particle emission is inhibited by increasingly large Coulomb barriers.

The expression for the neutron emission width was given by Weisskopf (Wei.37) as follows:

$$\Gamma_n = \frac{g\,m}{\pi^2 h^2} \times \frac{\sigma(E,e)}{\rho(E)} \int_0^{E-En} e\,\rho(E-E_n-e)\,de$$

where m is the neutron mass, $\sigma(E,e)$ is the cross section for the reverse process and g is the statistical weight for spin states. Using equation (I.2) for the two level densities $\rho(E-B_f-e)$ and $\rho(E-E_n-e)$ the following ratio is obtained:

$$\frac{\Gamma_f}{\Gamma_n} = \frac{h^2}{8mr_o^2 A^{2/3}} \times \frac{2Va_f(E-B_f)-1}{E-E_n} \times \frac{a_n}{a_f} \exp[2\sqrt{a_f(E-B_f)} - 2\sqrt{a_n(E-E_n)}] \quad (I.3)$$

where a_n and a_f are the respective level density parameters appropriate to the residual nucleus following neutron emission and the fissioning nucleus at the saddle point deformation. Expression (I.3) was used in a low energy calculation (FISMAP) of fission-evaporation competition by Blok (Blo.75).

The parameters a_n and a_f are expected to vary slowly and regularly with the mass of the nucleus; therefore, for a given excitation energy much larger than B_f or E_n, the main variation in the ratio Γ_f/Γ_n may be written as:

$$\frac{\Gamma_f}{\Gamma_n} = \text{Const. } \exp(B_f - E_n)\ f(a_f, a_n)$$

Thus, the probability that an excited nucleus, at a given excitation energy, will fission rather than emit a neutron , depends strongly upon the difference between the fission barrier B_f and the neutron binding energy E_n. If the neutron binding energy is much the smaller, the neutron emission will have a greater probability than fission and vice versa.

The simple formalism just described has been used to compute the fission-evaporation competition in high energy reactions by the Monte Carlo technique. The EVA code (Z.Fraenkel private communication) based on the earlier calculation by Dostrovsky et al (Dos.59) used, as an input, the characteristics of the excited nucleus after completion of the cascade as computed by the ISOBAR program. However this code could not be used in the case of gold or similar targets since the fission of elements lighter than thorium is not considered in the evaporation process.

d) First chance or last chance fission

The relative fissility of a nucleus may be measured through the parameter Z^2/A (related as will be seen below to the ratio of its Coulomb and surface energies), where Z and A are the nuclear charge and mass.

For nuclei at the end of the prompt cascade, competition may be significant between neutron evaporation and fission in a few or in all stages of evaporative de-excitation. Two extremes represented in Fig.2 could be postulated.

- Mechanism 1: last chance fission

If the various nuclei produced by the cascades have small fission widths due to an unfavourable Z^2/A value, the de-excitation, even at high energies, will occur almost exclusively by evaporation of neutrons. This loss of neutrons along the evaporation chain will increase the ratio Z^2/A (and the corresponding fissionability) and fission will occur towards the end of the chain when most of the excitation energy has been dissipated. Thus, this fission will be a fission at low energy preceded by a series of successive evaporations.

Fig.2: Schematic representation of "last-chance" fission (mechanism 1) and "first-chance" fission (mechanism 2).

MECHANISM 1

Target

Cascade

Neutron evaporation

Fissioning nucleus with high Z²/A and low excitation
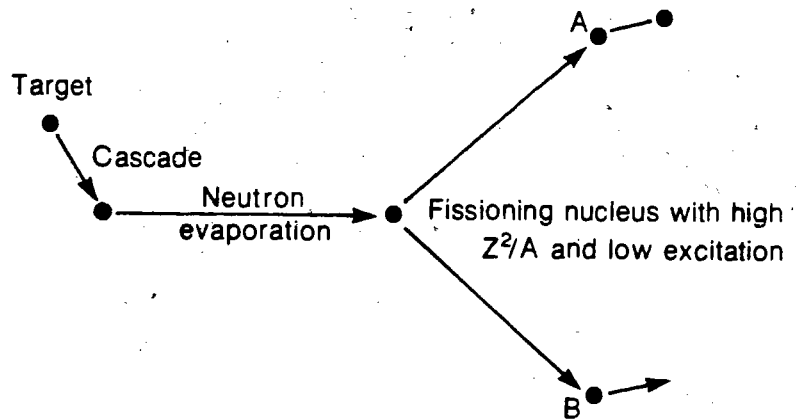
A and B : fission fragments - Evaporation of a few neutrons- Beta decay to stability

---

Target

Cascade

Fissioning nucleus with high excitation
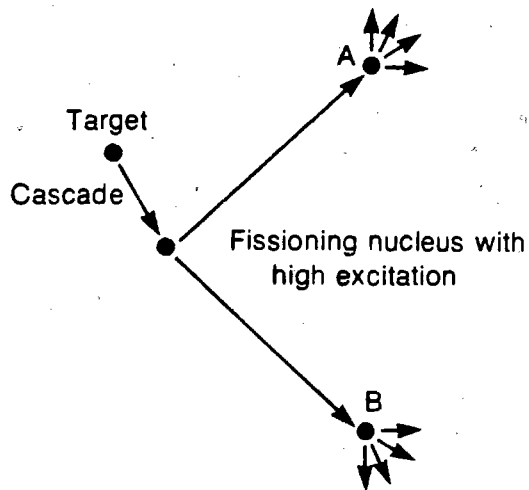
A and B : fission fragments - Multiple - neutron emission - Beta decay to stability

MECHANISM 2

- Mechanism 2: first chance fission

If the fission width increases significantly with the excitation energy, this will favour occurrence of fission in the early stages of de-excitation. In this case, a low Z^2/A ratio will be compensated by the high excitation energy which would increase the number of channels available for the fission of the deformed nucleus. This high energy fission would be different from fission at low energies in those respects affected by excitation energy. Since the kinetic energy of the fragments is, approximately independent of excitation energy (Lef.68), the excess energy appears in the form of excitation energy of the fragments which will then de-excite by evaporation of neutrons. First chance fission could also occur among nuclei possessing a low excitation energy after the cascade step.

Various experimental observations which seem to favour one mechanism or the other will be discussed later. It is possible that situations lying in between these two extremes do occur, producing a wide range of fissioning nucleus masses and, consequently, wide distributions in mass and energy of the fission products.

2) J.R Nix's theoretical predictions

The widths of distributions from the fission of
individual fissioning species as well as the most probable
values have been predicted theoretically by Nix (Nix.69) and
a brief outline of his work will be given here.

In order to study the properties of the division of an
idealized nucleus, a simplified version of the liquid-drop
model was used where the shape of the nuclear surface is
described by three smoothly joined portions of quadratic
surfaces of revolution (two spheroids connected by a
hyperboloidal neck). This shape is specified by means of a
parameterization which has six degrees of freedom: three
representing symmetrical deformations and the other three
describing asymmetrical deformations. This parameterization
has the great advantage of representing in a continuous way
the sequence of shapes from the original sphere through the
saddle and scission shapes, to the two fragments at
infinity.

The potential energy (which is the sum of the surface
energy and the Coulomb energy) of a deformed drop relative
to the spherical drop is given by:

$$V = E_s - E_{so} + E_c - E_{co}$$

where E_{CO} and E_{SO} are respectively the Coulomb and surface energies of the original spherical drop.

The surface energy of the spherical drop is:

$$E_{SO} = a_S A^{2/3} \{ 1-K[(N-Z)/A]^2 \} \quad \text{(Nix.69)}$$

with a_S =17.9439 MeV and K =1.7826.

The quantity E_{CO} is given by:

$$E_{CO} = a_C Z^2/A^{1/3} \quad \text{(Nix.69) with } a_C = 0.7053$$

The results of the calculations are given as a function of the dimensionless fissility parameter x defined as:

$$x = \frac{Z^2/A}{50.88 \{1-1.7826[(N-Z)/A]^2\}} \quad (I.4)$$

The potential energy V can also be expressed as:

$$V = [(B_S-1)E_{SO} + (B_C-1)E_{CO}] = [(B_S-1) + 2x(B_C-1)] E_{SO}$$

where x is the fissility parameter just defined.

The function B_S is the total surface energy of the drop in units of the surface energy of the spherical drop E_{SO} while, similarly, B_C is the Coulomb energy of the drop in units of E_{CO}. These two functions B_S and B_C depend only upon the six deformation coordinates which specify the shape of the drop.

Then, the kinetic energy of the system is calculated. This energy depends not only upon the shape of the drop but also upon the nature of the hydrodynamical flow of the fluid

inside the drop: a non-viscous irrotational flow was chosen. The transition-state method is used to calculate the probability that the nucleus is in a given state of motion when it passes through the vicinity of its saddle point. Having determined the probability distributions for the initial conditions near the saddle point, the next step is to perform the dynamical calculations which tell how the nucleus divides for a given set of initial conditions. This is done by solving Hamilton's equation of motion and this final step leads to the observable characteristics of the fission fragments at infinity, namely the most probable fission fragment energies and the widths of the distributions in total kinetic energy and fragment mass. These quantities can be compared with experimental results such as those obtained in the present work.

From comparison of this theory to existing experimental data, it was concluded (Nix.69) that this simplified version of the liquid drop model is not able to account for the properties of the division of heavy nuclei at low excitation energies. However, it reproduced approximately experimental fission fragment mass and energy distributions for the fission of heavy nuclei at high excitation energies and medium mass nuclei at all excitation energies.

The results of this theory offer the great advantage of being directly comparable to the experimental data since no adjustable parameters were used in the calculations.

B) Review of previous experimental results on high energy fission

Fission reactions have been studied extensively through radiochemical methods, track detectors or emulsions and semi-conductor detectors. Some general features follow from these experimental observations; however, there are still several unanswered questions and conflicting results particularly on the determination of when, in the evaporation chain, the fission occurs (first or last chance fission).

1) Mass distributions

All studies lead to the same conclusions that the well known double-peaked mass distribution, characteristic of low energy fission, changes over to a single peaked distribution characteristic of high energy fission (Ste.58). It was also found that this single peaked distribution became wider with increasing bombarding energy. Some evidence of the shift of

the mass distribution peak to lower mass numbers as the
energy of the incident proton increases was given by Jodra
and Sugarman (Jod.55), Sugarman et al (Sug.56) and Shamov et
al (Sha.56), but at high energy, the location of a single
peak, indicating the most probable fission fragment mass
becomes less certain. The earlier radiochemical
investigations were based on the assumption of prefission
emission of neutrons (or last chance fission) but the
results could be easily explained by a mechanism involving
fission in competition with evaporation at all stages of
de-excitation (Blo.80).

Various results have been reported in Table I where the
"fissioning nucleus" designates the most probable of a
distribution in fissioning nuclei.

2) Kinetic energy of the fission fragments

Several investigations on the kinetic energy of the
fission fragments lead to the same general description: the
kinetic energy distributions are symmetrically distributed
around a most probable value at which the two fragments have
the same energy. Single peaked energy distributions are in
accordance with the mass (and charge) distributions also
having a single peak.

TABLE I

Target	Projectile	Most probable A and Z	Assumed fission- -ing nucleus	Reference
^{nat}Ag	600 MeV p		A=104 estimated	(And.76)
Au	450 MeV p	$A_p = 87.5$ $Z_p = 38$	$^{175}_{76}Os$	(Kru.55)
Bi	450 MeV p	$A_p = 93$ $Z_p = 40$	$^{186}_{80}Hg$	(Kru.55)
	340 MeV p		$^{190}_{82}Pb$	Ref.6 in (Kru.55)
	450 MeV p		$^{186}_{80}Hg$	(Jod.55)
Pb	600 MeV p	$A_p = 93.2$ $Z_p = 40$	$^{}_{80}Hg$	(Hag.75)
Th	450 MeV p	$A_p = 103.5$ $Z_p = 43.5$	$^{207}_{87}Fr$	(Kru.55)
U	2.9 GeV p	$A_p - 110$		(Fri.65)

Among the important results of these studies is the finding that the kinetic energy of the incident particle does not contribute significantly to the kinetic energies of the products, but that these are determined essentially by Coulomb repulsion. This has been observed for heavy-ion induced fission (Vio.63) as well as high-energy light-particle induced fission (Dou.54). This feature will allow comparison of results from the present work with existing values of kinetic energy at very different bombarding energies than the one used in this study.

Some of the results found in the literature are reported in Table II where the kinetic energy E_K appears in column 4 and the distribution width (FWHM) is given when available.

3) Excitation energy of the fissioning nucleus

Several techniques yield information about the excitation energy of the fissioning nucleus. This energy has been estimated via its relationship to the energy transferred from projectile to target nucleus, from:

- the opening angle between the two fission tracks in nuclear emulsions (Ost.55): the difference between the observed angle and 180° is a measure of the momentum of the

TABLE II

Target	Method of measure	Projectile	E_K (MeV)	FWHM	Reference
nat Ag	Semi-cond. detectors	600 MeV p	62 ± 4	25 ± 3	(And.76)
Ta	Semi-cond. detectors	156 MeV p	119 ± 4	24 ± 0.8	(Ste.67)
Au	Semi-cond. detectors	25.5 MeV ^{3}He	138.6	17 ± 4	(Bri.63)
		120 MeV ^{4}He	136 ● 3	22 ± 6	(Pla.66)
Bi	Semi-cond. detectors recoil	25.5 MeV ^{3}He	145.4	18 ± 4	(Bri.63)
		120 MeV p	141 ± 3	24 ± 6	(Pla.66)
		450 MeV p	111		(Por.57)
U	recoil	450 MeV p	163 ± 8		(Sug.66)
	Semi-cond. detectors	156 MeV p	161 ± 2	31	(Ste.67)

nucleus before fission. The same information can be obtained from angular correlation measurements carried out with solid state detectors (Kow.62), (Kow.63), (Kow.64).

- recoil experiments (Por.57), (Sug.56), where the difference in the amount of recoiling radioactivity ejected in the forward direction over that ejected backwards, is a measure of the momentum of the struck nucleus.

Some experimental results are given in the following table where E^* is the mean excitation energy of the nuclei undergoing fission and $P_{//}$ is the mean value of the parallel component of the fissioning nucleus momentum.

Target	Projectile	E^* (MeV)	$P_{//}$(MeV/c)	Reference
Ta	450 MeV p	180		(Por.57)
Pb	600 MeV p	120-130		(Hag.75)
Bi	450 MeV p	155		(Por.57)
U	460 MeV p	165 ± 45		(Iva.57)
	660 MeV p	185 ± 60		(Iva.57)
	660 MeV p	240	340	(Obu.59)

4) First chance or last chance fission

The finding, from experimental observations, that several particles (mainly neutrons) are emitted during the evaporation stage of high energy fission is now well established. However, the controversy as to when these particles are emitted (before or after fission) is still not settled at the present time. In order to extract such data from results on the angular correlation between fission fragments and evaporated particles, it is assumed that the pre-fission neutrons are emitted isotropically in the center of mass of the fissioning nucleus while the post-fission neutrons are emitted isotropically in the center of mass system of the fully accelerated fragments. The knowledge of the number of pre- and post- fission neutrons is of great importance to the understanding of the fission process: the number of prefission neutrons is directly related to the competition between fission and neutron emission. Measurements of the number of prefission neutrons for several targets and bombarding energies will lead to the determination of the variation of ratio Γ_f/Γ_n of the fission width to the neutron emission width with energy and target mass. On the other hand, the number and kinetic

energy spectrum of the post-fission neutrons as a function of the fragment mass and the total kinetic energy of the two fragments will determine the total excitation energy and its partition between the two fragments.

Experimentally, the differentiation between pre- and post-fission neutrons requires the measurement of the energy and angular distribution of the neutrons with respect to the direction of the fission fragments and the measurement of the kinetic energy of the two fragments.

The first attempt of such measurements was carried out by Harding and Farley (Har.56a) in the case of ^{238}U bombarded with 147 MeV protons. In a previous measurement (Har.56b), it was found that an average 13.1 ± 1.6 neutrons were emitted per fission event. The measured forward/sideways anisotropy of these neutrons led to the conclusion that most of them were evaporated before fission (the ratio of the number of neutrons at 0° to the number of neutrons at 90° with respect to the fission fragments direction was $N(0^{\circ})/N(90^{\circ}) = 1.27 \pm 0.11$).

Similar studies were done with ^{209}Bi and ^{238}U targets irradiated with 155 MeV protons (Che.70) and ^{209}Bi, ^{232}Th, ^{233}U, ^{238}U and ^{239}Pu bombarded with 45 MeV alpha-particles (Fra.75). The results of these studies are summarized below:

Target	Projectile	Number of pre-fission neut.	Number of post-fission neut.	Reference
^{209}Bi	155 MeV p	6.9 ± 1.0	4.2 ± 0.5	(Che.70)
	45 MeV α	3.6 ± 0.2 *		(Fra.75)
^{226}Ra	12 MeV p	0.33±0.15	3.20±0.20	(Gay.77)
^{232}Th	45 MeV α	2.9 ● 0.9	4.4 ± 0.3	(Fra.75)
^{238}U	155 MeV p	5.8 ± 1.0	5.1 ± 0.5	(Che.70)
	45 MeV α	3.6 ± 1.6	4.6 ± 0.7	(Fra.75)

* total number of neutrons.

From the results listed in the table above, it is to be noted that while the number of post-fission neutrons remained approximately constant, the number of pre-fission neutrons increased with bombarding energy, suggestive of last chance fission.

Analysis by Fraenkel and others (Che.70) on the basis of the statistical model led to the conclusion that, while manipulation of model parameters could produce calculation results in agreement with these experimental data, the same parameter set could not simultaneously achieve agreement

with radiochemical data such as those due to Pate and
Poskanzer (Pat.61) or those in Table I.

Experiments conducted at 12 GeV projectile energy and
reported by Wilkins et al (Wil.79) also indicated a
preference for last chance fission.

5) Fission induced by pions

Most work on meson-induced fission has been done with
nuclear emulsions impregnated with heavy-element compounds.
Several studies of fission induced by slow π^- mesons are
reported in the literature but experimental data for high
energy pions are scarce.

Denisenko et al (Den.58) observed identical
distributions of ranges for uranium fission fragments
whether slow π^-, 300 MeV π^+ or 350 MeV protons were used
as projectiles. The ranges of the two fragments were found
to be equal, indicating a preference for symmetric fission.
An analysis of the light charged particles emitted in
uranium fission induced by 280 MeV π^+ (Iva.58) led to the
conclusion that the absorption of π^+ mesons occurs
predominantly in interactions involving a pair of nucleons
(n,p).

Most of the experimental results on pion-induced
fission were found to be in agreement with the following
mechanism:

the incident pion interacts with a pair of nucleons

$$\pi^- + n + p \longrightarrow n + n + 140 \text{ MeV}$$

$$\text{or} \quad \pi^- + p + p \longrightarrow n + p + 140 \text{ MeV}$$

and the rest energy of the pion is nearly all converted
into kinetic energy of the two nucleons, which may escape or
start a cascade.

When their energy is above 300 MeV, pions create more
or less the same effects as protons. The main difference is
due to their absorption inside the nucleus where their rest
mass is turned into excitation energy (i.e. a supplementary
deposit of 140 MeV is left inside the target nucleus). Apart
from this particular point, intra-nuclear cascades proceed
in the same manner as when they are initiated by protons.

C) Theory of track detectors

1) History

Various solid materials such as mica, glass and some
plastics are capable of registering tracks of highly charged
fragments. These tracks were first observed in 1959 by Silk

Most of the experimental results on pion-induced fission were found to be in agreement with the following mechanism:

the incident pion interacts with a pair of nucleons

$$\pi^- + n + p \longrightarrow n + n + 140 \text{ MeV}$$

$$\text{or} \quad \pi^- + p + p \longrightarrow n + p + 140 \text{ MeV}$$

and the rest energy of the pion is nearly all converted into kinetic energy of the two nucleons, which may escape or start a cascade.

When their energy is above 300 MeV, pions create more or less the same effects as protons. The main difference is due to their absorption inside the nucleus where their rest mass is turned into excitation energy (i.e. a supplementary deposit of 140 MeV is left inside the target nucleus). Apart from this particular point, intra-nuclear cascades proceed in the same manner as when they are initiated by protons.

C) Theory of track detectors

1) History

Various solid materials such as mica, glass and some plastics are capable of registering tracks of highly charged fragments. These tracks were first observed in 1959 by Silk

and Barnes (Sil.59) in mica with an electron microscope.
Price and Walker as well as other authors showed that the
diameter of these tracks may be enlarged by a preferential
chemical attack (or etching process) to a size where they
may be viewed with an optical microscope. The etching effect
has been demonstrated in solids of many different types:
ionic crystals (You.58),mica (Pri.62a,Pri.62b,Pri.62c),
glasses (Fle.63a) and plastics (Fle.63b).

An important advantage in the use of these detectors in
nuclear reaction studies is that there is a well defined
minimum rate of energy loss required before a fragment will
produce a track (as will be discussed later on). Thus,
these detectors offer unique advantages when heavy particles
must be studied under a variety of adverse conditions such
as intense background radiation, high temperature or low
event rate:

- a detector can withstand, without fogging or fading,
enormous doses of particles whose rates of energy loss are
less than the critical value of track formation.

- tracks can be formed and stored for long times.

- the preparation, development and observational
techniques are simple.

Use of these detectors has been expanding continuously

during the past decade in many fields of sciences
(Fle.65a,Fle.77).

2) Thresholds for detection

The concept of a critical rate of energy loss for track
formation was introduced by Fleischer et al .
(Fle.64a,Fle.65b). These authors calculated rates of energy
loss of various heavy ions as a function of the energy per
nucleon for three detectors, and their results for muscovite
mica are displayed in Fig.3, where the experimental points
are taken from (Fle.64a). The track registration efficiency
increases from 0 to 100% within the "transition region" and
the average tracklength increases from 0 to the full length
corresponding to the range. For each detector studied these
authors found such a "transition region" and defined a
critical energy loss rate $(dE/dx)_{crit}$ which appeared to be
independent of incident ion energy and atomic number.

The threshold or sensitivity of a detector will then be
defined as the minimum mass and/or energy of incident ions
which is detectable, that is which deposit the critical
value of energy loss rate so as to create enough damage to
leave an etchable track.

For example, for particles with energies less than

Fig.3: Track registration in muscovite mica. The curves give the calculated rates of energy loss of various heavy ions in mica as a function of the energy per nucleon.

L = LONG TRACKS
P = PARTIAL REGISTRATION
N = NO EFFECT
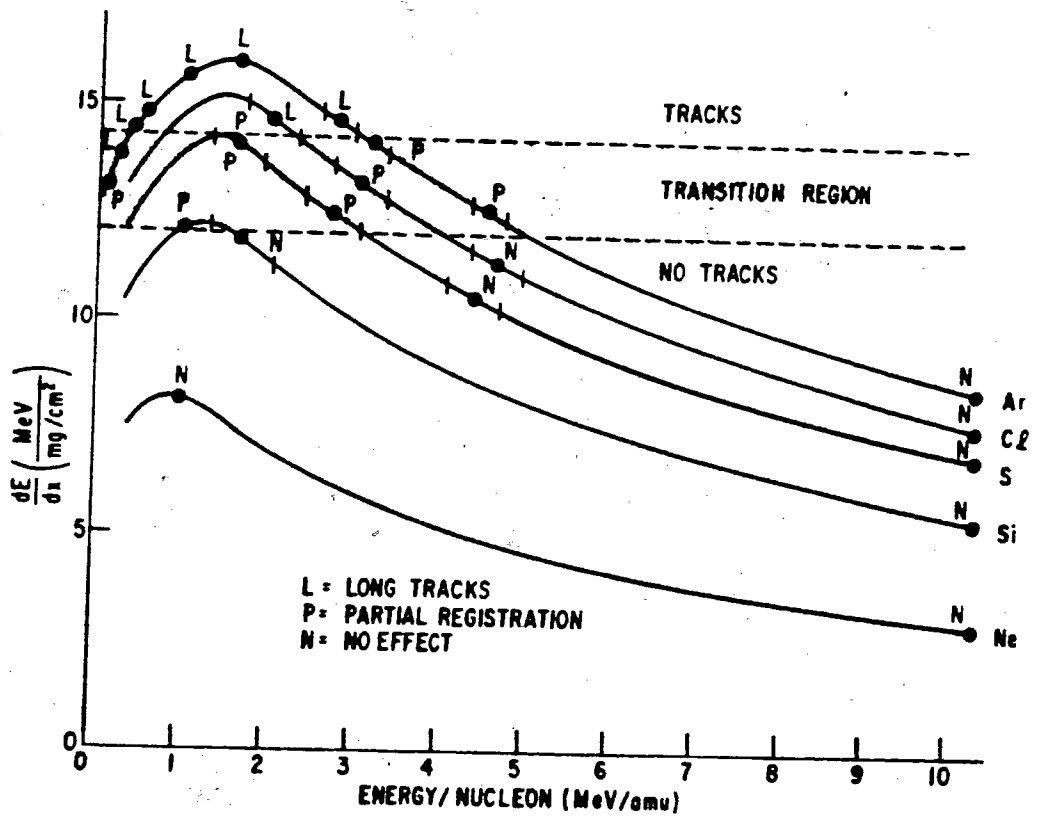
3 MeV/a.m.u, the mass must exceed 28 a.m.u in order to form tracks in the case of muscovite mica.

Natowitz et al (Nat.68) observed that ions of $Z<10$ do not leave, in mica detectors, tracks which could be etched out to their full length. These ions, however, damaged the mica sufficiently to give observable shallow "diamonds" after an etching time greater than one hour. A value of 10.1 MeV/mg.cm^{-2} for the critical energy deposition has been found by Blok et al (Blo.72) with a registration threshold lying between ion charge $Z=10$ and $Z=13$.

3) Track formation mechanisms

One of the most striking characteristics of track registering materials is the correlation of the track forming ability with their electrical conductivity. Insulators and some semiconducting glasses may register tracks while metals and the better semiconductors (such as silicon and germanium) do not. A model for the production of etchable particle tracks must account for this fact, as well as for the fact that different materials have different critical rates of energy loss for track formation. Several models for track formation have been proposed, with various

degrees of success, to account for experimental observations.

The first hypothesis as to how particle tracks might be formed was that direct atomic collisions produce interstitial atoms and vacant atomic sites ("displacement spikes" (Bri.54,Bri.56)). However, this direct displacement of atoms would be expected to occur equally in conductors and insulators and would become more prevalent near the end of the range of a charged particle where tracks often do not form.

The "thermal spike" model (Bon.61,Cha.63) led to several conclusions in contradiction with the experiment. The major criticism is that sensitivities of different materials do not relate in any regular manner with the known melting, softening or transformation temperatures of the detectors, as this model would suggest.

A model suggesting that track formation was governed by the total energy loss rate dE/dx had also to be rejected after its authors found contradictory experimental results (Fle.67a,Fle.67b).

The most successful model up to date is the one proposed by Fleischer et al (Fle.65c): the "ion explosion spike" model. The proposed multistep process is presented schematically in Fig.4. Following the primary ionization,

Fig.4: The ion explosion spike mechanism for track
formation in inorganic solids. The original ionization left
by the passage of a chaged particle (top) is unstable and
ejects ions into the solid, creating vacancies and
intersticials (middle). Later, the stressed region relaxes
elastically (bottom).

IONIZATION

ELECTROSTATIC
DISPLACEMENT

RELAXATION
AND
ELASTIC STRAIN
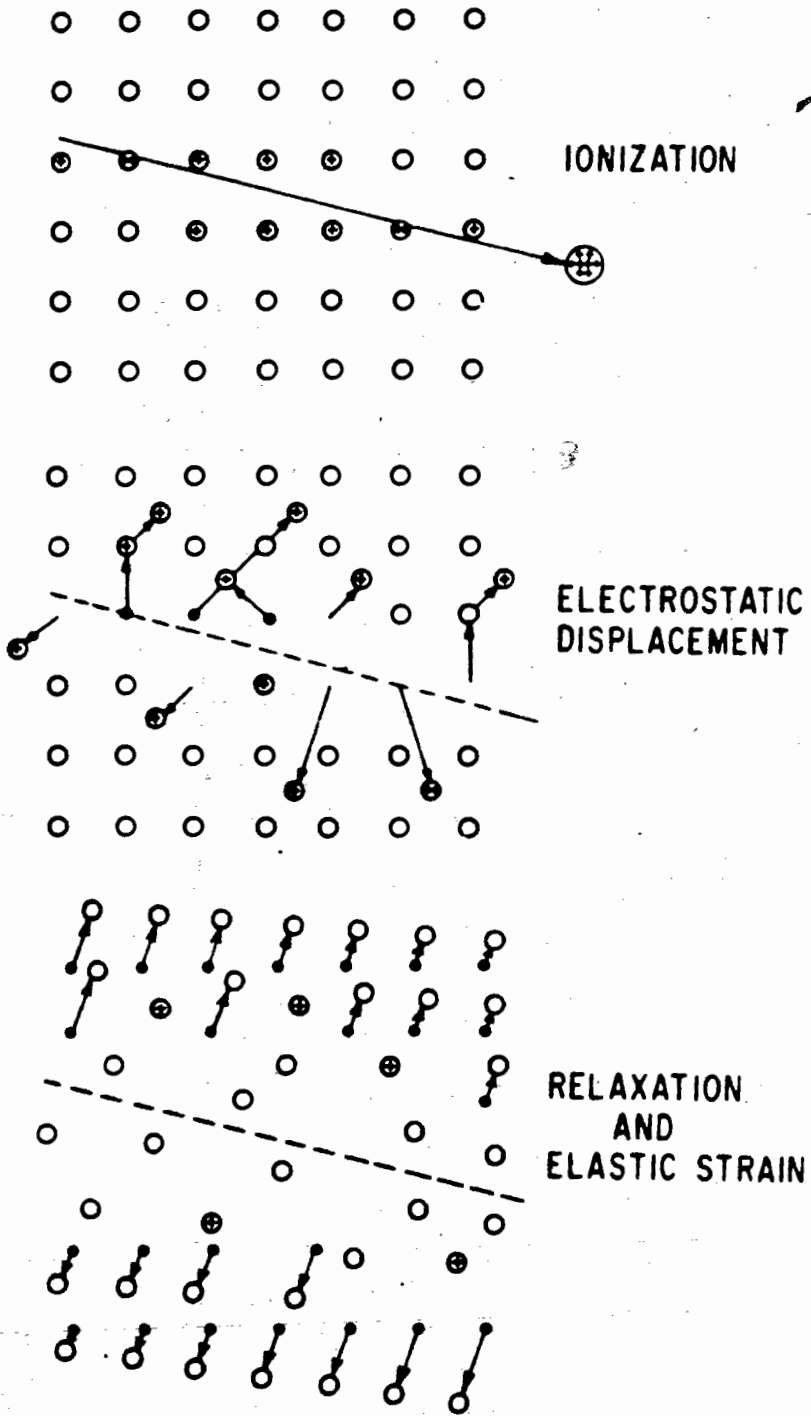
an array of interstitial ions and vacant lattice sites is produced by electrostatic repulsion after which elastic relaxation diminishes the local stresses by spreading the strain more widely. This model predicts correctly the conductivity dependence of track formation. It also predicts that a quantity somewhat different from dE/dx should determine the presence or absence of tracks: the number of ions formed per unit distance along the particle path or primary specific ionization. This quantity has been compared with dE/dx (Fle.67b) and shown (Pri.68) to be in better agreement with experiment. Katz and Kobetich (Kat.68) suggested that etchable damage is produced when a critical dosage of ionization energy is deposited at a critical distance from the ion's path by secondary electrons. This criterion predicts conditions for the formation of etchable tracks in three detectors (mica, Lexan polycarbonate and cellulose nitrate) in agreement with published data.

4) Track geometry and etching efficiency

The geometry of track etching is dictated in the simplest case by the simultaneous action of two etching

processes: chemical dissolution along the particle track at a linear rate V_T and general attack of the undamaged material at a lesser rate V_G (Pri.67,Pri.68a,Pri.68b). This process creates a cone which has the original track as its axis as shown in Fig.5 taken from (Pri.71) where it is assumed that V_G is isotropic and that V_T is constant over the length $V_T t$ etched during the time t. A layer of surface material of thickness $V_G t$ is removed at the same time that the etched track is developing so that both of the directly observable quantities, the track diameter D and the visible tracklength l, are the result of the competition between the effects of V_G and V_T. The smaller the excess of V_T over V_G, the smaller D and l will be (or the larger the cone angle $\theta = \arcsin V_G/V_T$). Geometrical relations giving the mesurable quantities in terms of etching parameters can be derived (Pri.71,Hen.71) both for a vertically incident particle (a) and a particle incident at a dip angle θ (b).

Various degrees of sophistication have been added to this very simple model after it was found experimentally that V_T was not constant along the tracks but rather increased with the ionization rate. The first detailed study for varying V_T was made by Fleischer et al (Fle.69). It was assumed that V_G was isotropic, which is true for glasses but

Fig.5: Track geometry with constant V_T and V_G:

    (a) for vertical incidence;

    (b) for incidence at dip angle θ .

(a)

ORIGINAL SURFACE

ETCHED SURFACE

2θ

PARTICLE TRACK

(b)

ORIGINAL SURFACE

2θ

ϕ
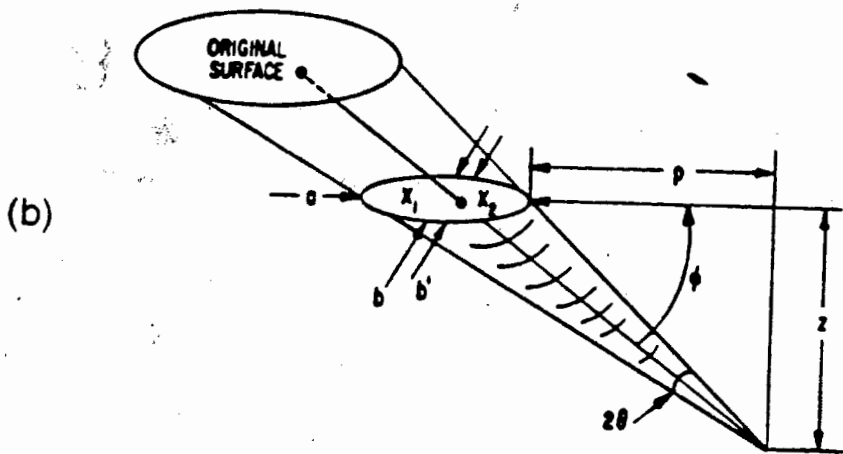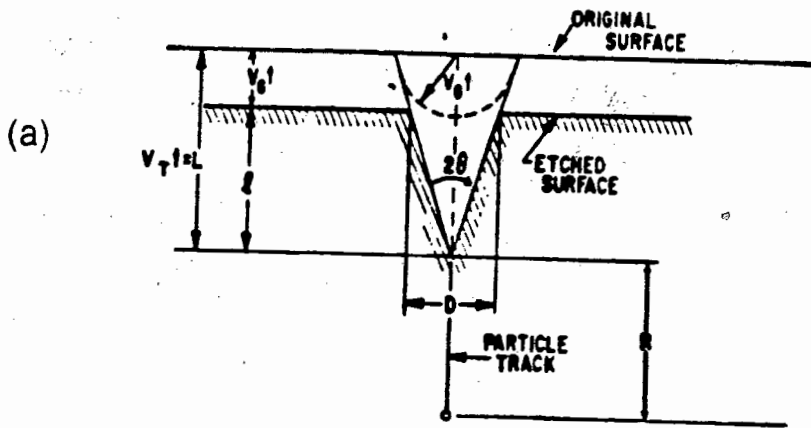
not for most crystals (where the rate of general attack as a function of crystal surface orientation can be elaborately complex). Somogyi et al (Som.73) developed a model (track-diameter kinetics) which is able to account for the most complex case of anisotropic solids with varying V_T. This model was improved later on (Som.77).

Tracks inclined at less than the cone angle θ to a surface are not revealed by etching as can be seen from Fig.6. As was showed in Fig.5, the angle θ depends on V_T and V_G. Fig.6 (a) shows that if the component normal to the etched surface of preferential etching along the track ($V_T \sin \theta$) is less than V_G, the material is removed so rapidly that the preferential etching fails to keep ahead: as a consequence, no track is revealed. Fig.6 (b) shows the case where $\phi = \theta$. Arcsin $V_G/V_T = \theta_C$ is the critical angle above which tracks will be registered.

This critical angle θ_C has been measured experimentally (Kha.72) and found to be 4° 30' $\pm$ 30' in the case of mica.

5) Comparison of tracklength data with theoretical stopping models

An energetic ion moving through a crystal interacts

Fig.6: Track registration geometry:

(a) for angle of incidence less than $\arcsin(V_G/V_T)$, the surface is removed at a greater rate than the normal component V_T and therefore no track is observed;

(b) $\arcsin(V_G/V_T)$ is the critical angle θ_C above which tracks are registered.
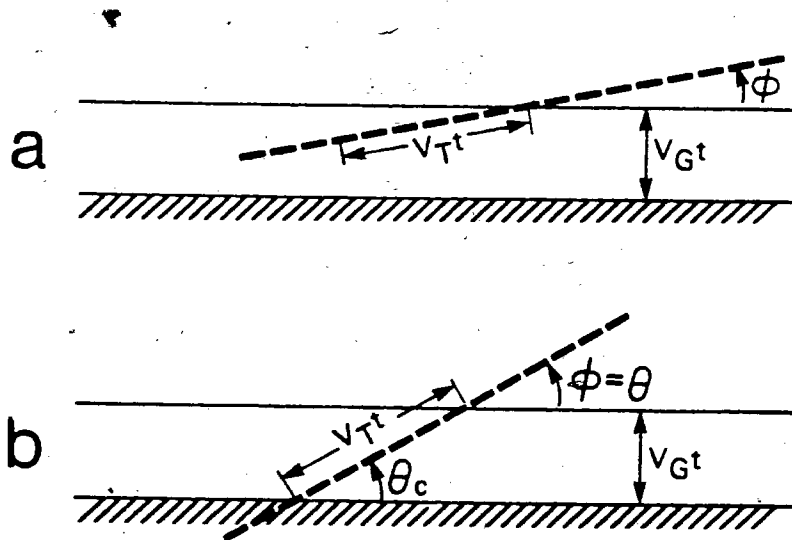
both with the positively charged nuclei and with the bound
or free electrons. For the nuclei, the ion is scattered by
its coulombic interaction with the positively charged nuclei
and kinetic energy is transferred to the atoms as a whole.
For electrons, one must consider both the excitation to
higher atomic energy levels and the ejection of electrons.
The ejected electrons, called delta rays, can produce
further excitation and ionization if they carry enough
energy. Nuclear stopping will be predominant at low ion
velocities, while electronic stopping will be predominant at
higher velocities. Generally, one considers that the two
effects are independent and separates the energy loss rate
into two components:

$$(-\frac{dE}{dx}) = (-\frac{dE}{dx})_{nucl} + (-\frac{dE}{dx})_{elec}$$

It has been suggested (Mor.70) that track formation is
not critically influenced by nuclear collisions since, if it
were, tracks would be expected to occur equally well in
conductors and insulators, and be more readily formed by low
velocity ions, both in direct contradiction to experimental
observations. These authors calculated that a fission
fragment with an energy of 60 MeV would displace only one
atom every 1 nm of the path length. This relatively large

spacing does not appear to fit in with the intense damage associated with a fission fragment track.

The energy loss due to electronic stopping is given by:

$$dE/dx = NS_e \qquad (I.5)$$

where N is the number of scattering centres per unit volume and S_e is the electronic stopping cross-section.

One of the properties of particle tracks is the fact that, in materials with the highest thresholds for registration, the distance to the point where a track-forming particle comes to rest exceeds the length over which preferential etching is observed. Therefore, the visible tracklength left by a particle will be smaller than its range in the particular stopping medium. The difference, called "range deficit" or "terminal tracklength deficiency", was recognized by Fleischer et al (Fle.64b) and Maurette (Mau.66) on the basis of studies with fission fragments, and was later put on a firmer basis by Price et al (Pri.68c). Although it is possible that a portion of the deficits observed was in fact caused by uncertainties in range-energy relations, Fleischer et al (Fle.75) formulated the conclusion (based upon several observations) that the deficit is real and of increasing magnitude for detectors of decreasing sensitivity.

The range R is related to the observed tracklength L by the relation:

$$R = L + \Delta L_t + \Delta L_s \qquad (I.6)$$

where ΔL_t is the terminal deficiency just discussed and ΔL_s is the apparent tracklength shortening due to the etching away of the undamaged mica surface.

From equations (I.5) and (I.6), the tracklength can be expressed as:

$$L = \frac{1}{N} \int \frac{dE}{S_e} - \Delta L_t - \Delta L_s \qquad (I.7)$$

Lindhard and Scharff (Lin.61) gave the electronic stopping cross-section as follows :

$$S_e(E) = \xi_e \, 8 \pi \, e^2 \, a_o \, \frac{Z_1 Z_2}{Z} \times \frac{v}{v_o} \qquad (I.8)$$

with $Z = (Z_1^{2/3} + Z_2^{2/3})^{3/2}$. The subscripts 1 and 2 refer to the penetrating ions and the stopping medium atoms respectively, e is the electronic charge, a_o the radius of the first Bohr orbit of hydrogen, v_o is the velocity of the electron in that orbit and v is the ionic velocity. The quantity ξ_e may vary with Z_1 approximately as $\xi_e \sim Z_1^{1/6}$.

In the literature, ξ_e is sometimes treated as an adjustable parameter (Dem.72) and Aras et al (Ara.65) found best agreement with fission fragment ranges in aluminum with

a value of $\xi_e = Z_1^{0.211}$. The same kind of study made by
Nakahara et al (Nak.69) led to a value of $Z_1^{0.212}$ for ξ_e. In
the case of heavy absorbers with Z values ranging from 74 to
92, Hontzeas et al (Hon.71) found that ξ_e had to be
dependent not only on the mass (or charge) of the fragment
but also on the mass (or charge) of the the atoms of the
stopping medium.

Expressions such as $\xi_e = Z_1^{0.7434} \exp[-0.7698\ (A_1 + A_2/A_2)]$

$$\text{or } \xi_e = Z_1^{0.8580} \exp[-0.8649\ (Z_1 + Z_2/Z_2)]$$

gave the best agreement when compared to experimental data.

The Z_2 value for a complex stopping medium is generally
taken as the weighted average for the various kinds of atoms
present. In the case of muscovite mica,
$KAl_2 (Si_3\ Al\ O_{10})(OH,F)_2$, there is an uncertainty in the
relative number of hydroxy and fluoride groups and an equal
number of these groups has been assumed. Average values are
then calculated as $\langle A \rangle = 20.0$ and $\langle Z \rangle = 9.9$ for the effective
mass and charge number of the mica stopping medium.
Integration of equation (I.7) with the expression of S_e
from equation (I.8) included yields:

$$L = \frac{2v_o Z A_1}{11.31 N \pi e^2 a_o Z_1 Z_2 \xi_e} \times \left[\frac{E}{A_1}\right]^{1/2} - \Delta L_t - \Delta L_s \qquad (I.9)$$

The tracklengths in mica should therefore be represented by:

$$L = b\ E^C - \Delta L \qquad (I.10)$$

where E is the energy of the penetrating ion in MeV/a.m.u and $\Delta L = \Delta L_t + \Delta L_s$. The exponent c is expected from equation (I.9) to have a value of 0.5 and, from the same equation:

$$b = \frac{2\ v_o}{11.31 N \pi e^2 a_o z_2} \times \frac{A_1}{z_1^{7/6}} (z_1^{2/3} + z_2^{2/3})^{3/2}$$

if L is expressed in cm while ξ_e is taken as $z_1^{1/6}$

$$\text{or}\quad b = 0.0552\ \frac{A_1}{z_1^{7/6}} (z_1^{2/3} + z_2^{2/3})^{3/2} \qquad (I.11)$$

When L is expressed in $mg.cm^{-2}$ then :

$$b = \frac{2 v_o d}{11.31 N \pi e^2 a_o z_2} \times \frac{A_1}{z_1^{7/6}} (z_1^{2/3} + z_2^{2/3})^{3/2}$$

where d is the density of the mica (taken to be $2.91 g.cm^{-3}$).

In the present work, ξ_e was chosen (as suggested by LSS theory) as $z_1^{1/6}$. Since the aim here was to obtain a calibration for the mica, another value of ξ_e would have given as good a result as the one chosen here. As will be seen later (section II-A-2-a), the experimental values of the parameter b and the values calculated by means of equation (I.11) were related through an empirical relationship. By setting $\xi_e = z_1^{0.212}$ instead of $z_1^{1/6}$, it was then found that the coefficients entered in this empirical relationship

would have to be different but the overall fitting of the experimental results was not affected by such a change.

As early as 1962, it has been observed (Tep.62) that the dependence of the range of several ions studied and their specific energy loss on their ionic nuclear charge Z was not monotonic.

Later, Ormrod et al (Orm.63,Orm.65) subjected the LSS theory of electronic stopping to a systematic experimental test in carbon and aluminum films at low energy E<<140 keV. Although the overall agreement with theory was reasonably good, they found a striking oscillatory behaviour of S_e as a function of the atomic number of the projectile. Fastrup et al (Fas.65,Fas.66,Hve.68) further extended the empirical information of the stopping process of heavy ions in carbon films. It was of particular interest to study the oscillation of S_e at higher projectile velocities where it is expected that effects such as electronic shell structure of the ions would be less important. Their data exhibit the same qualitative behaviour. The same type of observations were reported by other authors (Gil.64,Kap.66).

As will be seen later (section II-A-2-a), this oscillatory behaviour was also observed in the present calibration study. However, the objective of the calibration

experiments was not so much to check theoretical stopping models as to calibrate mica for determination of the tracklength of fission fragments. The comparison with theoretical stopping models of the variation of the tracklength as a function of energy can be used to this aim.

II EXPERIMENTS USING TRACK DETECTORS

A) Experiments with mica in a scattering array configuration

The scattering array configuration was used when angular distribution and tracklength information as a function of angle to the beam was needed for single tracks, but when coincidence information between tracks was not to be preserved.

1) Experimental techniques

a) Irradiation facilities and experimental set-up

- Calibration of the mica

Extraction of the distributions in fission fragment mass and energy from the distributions in tracklengths observed in mica requires a knowledge of the tracklengths in mica for a range of ions of known mass and energy. Such calibration data have been obtained previously

(Blo.72,Blo.74) for a series of ions from Al to Au, with
energies in the range 0 to 1 MeV per nucleon. However, data
for the heaviest ion studied (Au) were relatively few in
number and a gap in the data existed for ionic masses
between Au and Ag. Improved calibration data were needed in
the mass region above Ag since extrapolation of the
previously existing data to masses in the region of the
heavy mass peak from uranium fission was found to be
difficult and inaccurate. Such data were obtained in the
present work by tracklength measurements in mica of iodine
ions Rutherford-scattered off gold target nuclei.

The experimental arrangement used is shown
schematically in Fig.7. Irradiations of free-standing gold
targets of 180 μg.cm^{-2} thickness were made (by Dr. Brian
Pate in collaboration with Dr. David Ward of the Chalk River
Nuclear Laboratories) with a 132-MeV ^{127}I beam from the CRNL
tandem accelerator at Chalk River (Ontario). Beam currents
and irradiation times were those calculated beforehand to
produce track densities in the mica convenient for scanning.
Freshly cleaved sheets of mica were arranged around the
periphery of a 10-cm radius scattering chamber, inclined so
that the scattered projectile and target ions were incident
on the mica surface at a known 30-degree angle. This angle

Fig.7: Scattering chamber arrangement for the calibration
experiment at CRNL (the chamber used for irradiations at
Lampf was similar but a different size and angle of
incidence).

window   target   mica supports

30°

~5"
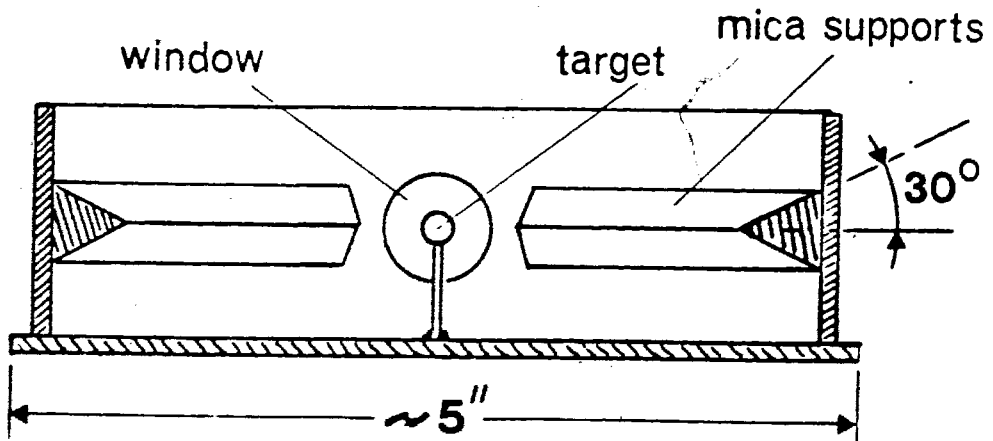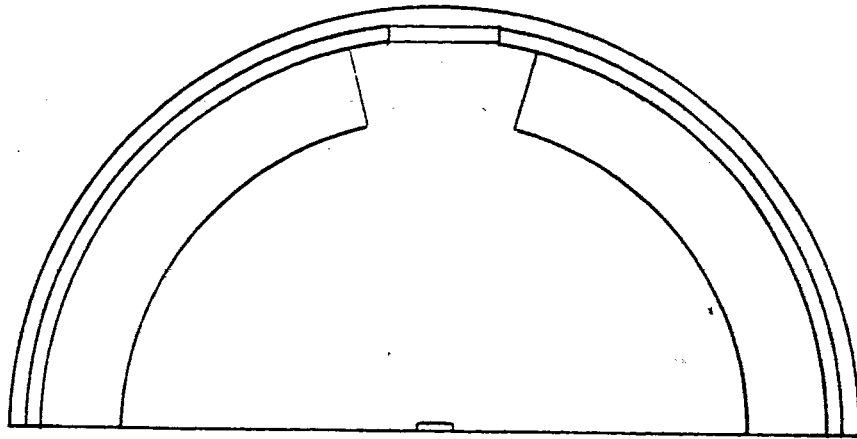
scattering chamber arrangement

ensured efficient track registration and also allowed
calculation of the actual tracklength from the measured
projection. Measurements could be made from 20 degrees to
160 degrees with respect to the beam direction.

Natural mica is known to contain trace quantities of
uranium (Gom.76,Gom.77) whose spontaneous fission produces
fossil tracks. The mica can be annealed by heating at high
temperature in order to remove these tracks. Total fading of
fission tracks in muscovite mica is reported in the
literature to occur after one hour heating at temperatures
ranging from $500^{\circ}C$ to $700^{\circ}C$ (Fle.75). Before irradiation,
the mica sheets were therefore heated at $500^{\circ}C$ for one and a
half hours. In case the natural tracks were not completely
removed by this heating procedure, the mica sheets were also
treated in 48% HF (ie HF solution in water which was 48% HF
by weight) at room temperature for two hours. This
pre-etching was expected to cause primordial tracks (or
their remnants) to be etched to large pits, which were
easily distinguishable from the tracks produced during
irradiation. However, no such primordial tracks were
observed during the scanning of the samples.

- Fission studies

The irradiations took place at Los Alamos (New Mexico)
with the Los Alamos Meson Physics Facility (LAMPF)
accelerator delivering a beam of 800 MeV protons. Targets of
gold, silver and uranium tetrafluoride were located in the
center of a 13cm radius chamber. Here again, the mica
detectors were arranged around the chamber at a known
45-degree angle and the experimental geometry was again as
shown in Fig.7. Prior to the irradiation, the micas were
annealed and also treated with HF and heated as described
earlier.

b) Target preparation

In both cases (mica calibration and fission study), the
gold and silver targets were free standing whereas the UF_4
was deposited on a free standing silver backing (of very
much lower fissility). The gold and silver used for target
preparation were of natural isotopic abundance and quite
pure: 6N gold shot (Alfa products*) and 5N silver needles
(Matheson, Coleman and Bell**). The UF_4 (with natural
uranium) was obtained from Research Organic/Inorganic
Chemical Corporation***.

The free standing target material was vacuum deposited
on a glass plate and then lifted very slowly from the glass

by surface tension with distilled water until the thin foil was floating entirely free on the surface of the water. The foil was then mounted and tightened on a 4.7cm by 5.5cm rectangular frame in the case of the fission study and on a 8mm diameter circular frame for the calibration experiment. Gold and UF_4 targets were mounted on aluminum frames and silver targets on reactor-grade graphite frames. Fission of the heavy element content of the aluminum was not intense enough to contribute significantly to the track density (via irradiation from the beam halo) in the case of the relatively fissile Au and UF_4 targets. For Ag, however, the interference was expected to be more serious and graphite frames relatively more free of heavy element impurities were used. The thickness of the targets was determined by weighing the glass plate before and after deposition of the target material; the area being known, the thickness in $\mu g.cm^{-2}$ was calculated assuming that the deposition of material was homogeneous. In order to improve the homogeneity of the targets, the glass plates were disposed symmetrically around the evaporating filament at a distance of the order of 30cm and the evaporation was conducted at a temperature very slightly greater than the metal boiling point which gave a slow and more uniform deposition. The

.evaporations were carried out at a pressure of $\sim 10^{-5}$ torr using a resistance heated tungsten filament.

A test of the target homogeneity was performed on a gold target. After evaporation, nine squares ($4cm^2$ each) were cut by scratching through the gold deposit on the glass plate, then the separated squares were lifted separately with distilled water as just described and weighed after drying. The weight values agreed to within 8% and the average thickness was in good agreement with the thickness calculated for the target as a whole. The target homogeneity can be taken as acceptable considering the fact that, in the 8% uncertainty the errors in the determination of the separately weighed areas were included.

The thicknesses of several UF_4 targets (ranging from $50\mu g.cm^{-2}$ to $300\mu g.cm^{-2}$) were checked by alpha counting and comparison with an uranium source of known mass. Following are some typical results :

Target thickness (in $\mu g.cm^{-2}$) determined	
by alpha counting	by weighing
47 ± 6	47 ± 2
172 ± 11	171 ± 3
302 ± 9	305 ± 4

As can be seen, the agreement between values determined
by alpha counting and by weighing was quite good, thus
establishing that the method for measuring the targets
thicknesses through their weight was valid and of sufficient
accuracy for the present purpose.

The target characteristics are shown in the following
table:

Experiment	Target element	Target thickness ($\mu g.cm^{-2}$)	Backing thickness ($\mu g.cm^{-2}$)	Frame size
fission	Au	514 ± 9		4.7x5.5 cm^2
	Ag	284 ± 5		4.7x5.5 cm^2
	UF$_4$	88 ± 4	Ag 177 ± 3	4.7x5.5 cm^2
calibration	Au	184 ± 3		4mm radius

c) Etching and scanning of the micas

After the irradiation, the micas were etched with 48%
HF at 20°C for a period of 20 minutes, conditions previously
found to be optimum (Blo.72), in order to form tracks
visible by optical microscopy. Since the angle at which the

scattered ions or the fission fragments entered the mica was fixed and known, only the projected length of the tracks needed to be measured via two-dimensional scanning. The scanning was achieved with a Zeiss microscope using a 63x air objective and 16x eyepieces giving a total magnification of 1000x. The scanned area was determined by means of two Mitutoyo mechanical gauges (having 0.01mm graduations) which measured displacements in two coordinates in the plane of the microscope stage. The projected track length was measured using an eyepiece graticule. This graticule as well as the dial gauges were calibrated by means of a Bausch and Lomb 0.01mm stage micrometer.

2) Data analysis and results

a) Calibration of the mica

The tracklengths from ions arriving at precisely known angles to the beam direction were measured and histograms were constructed. A fitting of these histograms using the "least squares" fit method was made by computer in order to extract the corresponding most probable tracklength value.

The fitted function was, as previously (Blo.74), a Gaussian with a tailing towards shorter tracklength:

For R< $R_{max}-T^2$ $P(R) = P_{max} \cdot \exp[T^2 \, (2R-2R_{max}+T^2)/2\rho^2]$

For R> $R_{max}-T^2$ $P(R) = P_{max} \cdot \exp[-(R-R_{max})^2/2\rho^2]$

where P_{max} is the maximum height of the distribution

R_{max} is the corresponding tracklength value

ρ is the width of the Gaussian (ρ=FWHM/2.355) and

T^2 is a tailing parameter.

Typical histograms and fitted curves are given in Fig.8 and 9. The number of tracks with length in a particular tracklength interval (in arbitrary units) is shown for iodine (Fig.8) and gold (Fig.9) at a 57 degree angle with respect to the beam direction. Fig.10 shows the same types of distribution at a 49° angle where tracklength values for I and Au were not different enough to give two distributions separately. However, the situation was handled easily with the fitting procedure and two most probable tracklength values extracted. Differentiation of Au from I ions in this and all other cases was easily accomplished via the predictions as to respective intensity as a function of angle calculated using Rutherford's scattering cross-section formula:

$$\frac{d\sigma}{d\Omega} = \left[\frac{Z_1 Z_2 e^2}{4E_i[A_2/(A_1+A_2)]} \times \frac{1}{\sin^2(\theta_{cm}/2)} \right]^2$$

where Z is the charge of the fragment and e the electronic charge.

Fig.8: Typical measured tracklength distribution for I ions fitted to the distribution function described in the text.
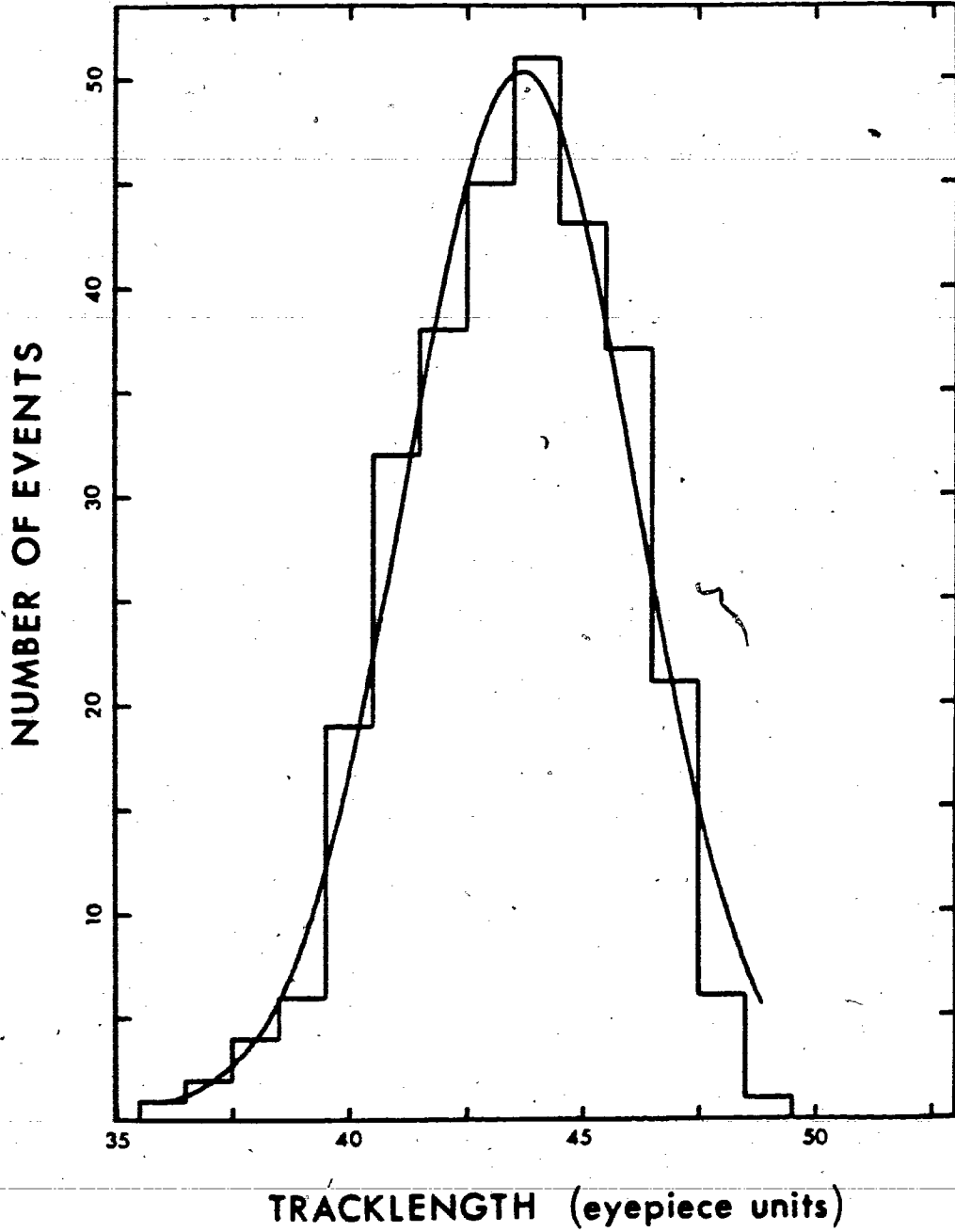
Fig. 9: Typical measured tracklength distribution for Au ions fitted to the distribution function described in the text.

NUMBER OF EVENTS

TRACKLENGTH (eyepiece units)
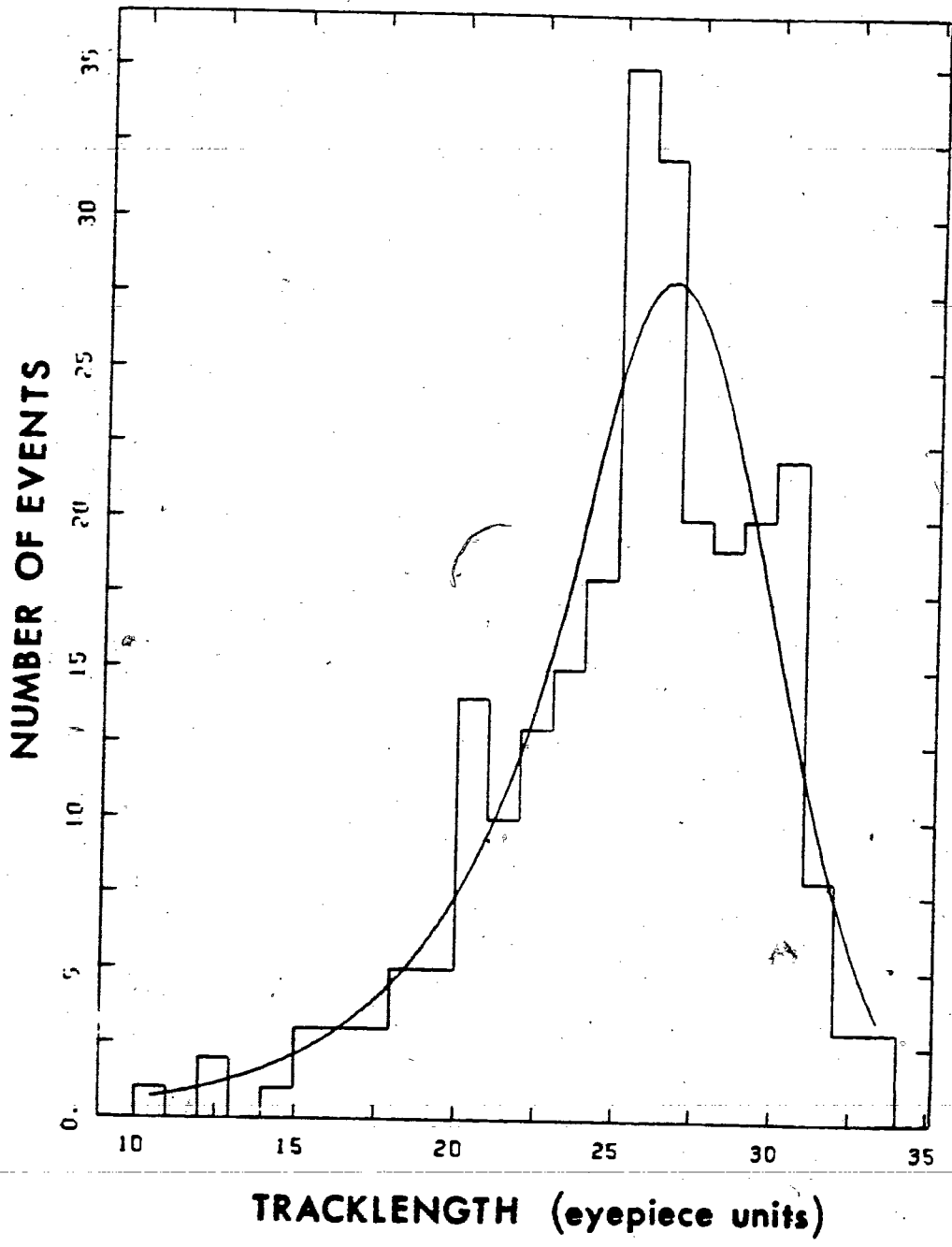
Fig.10: Measured tracklength distribution for both I and Au ions.

TRACKLENGTH (eyepiece units)
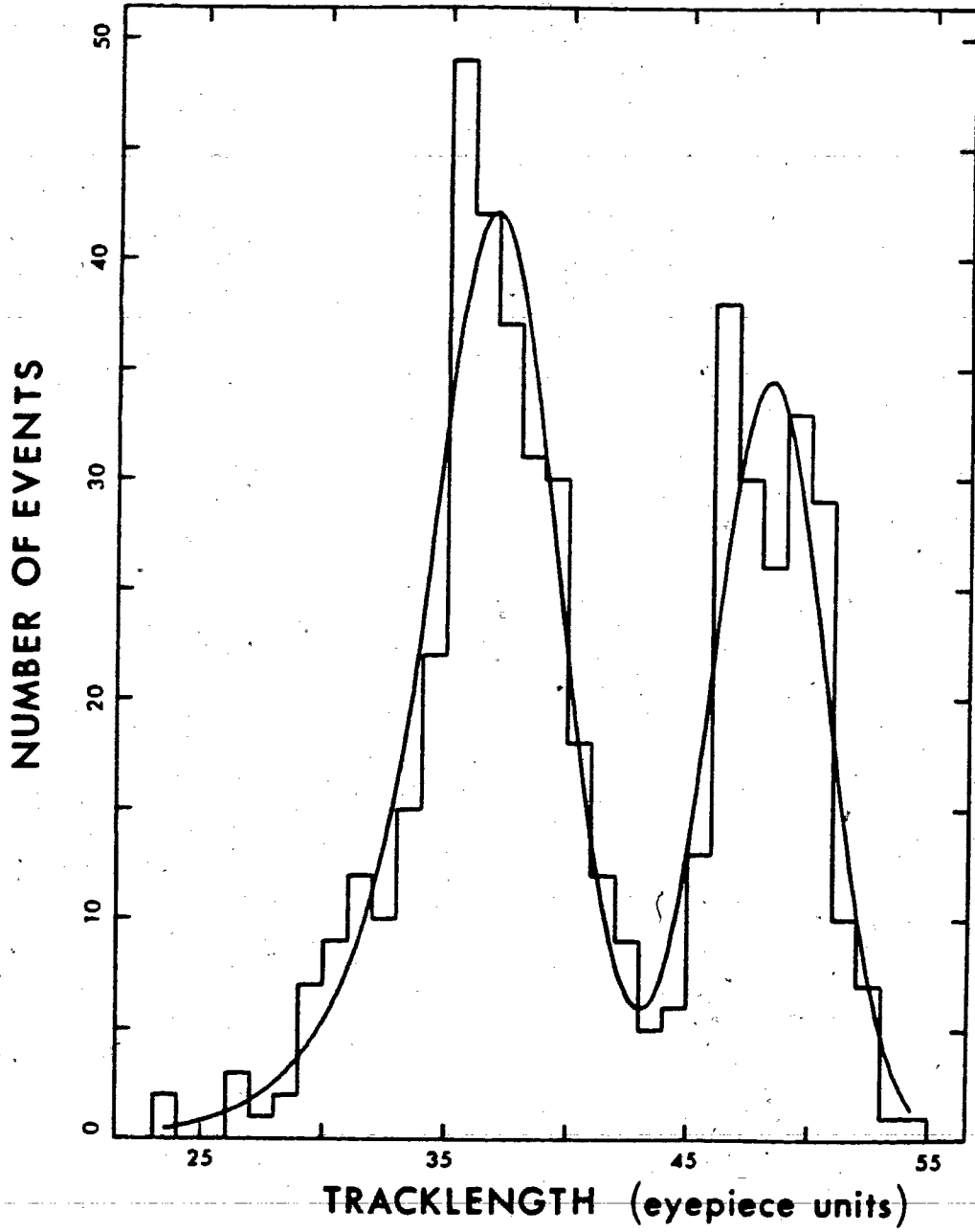
For gold, ρ was found to be (0.13 ± 0.02)mg.cm^{-2} and $T^2=(0.15\pm0.07)$mg.cm^{-2}. In the case of iodine : $\rho=(0.10\pm0.02)$mg.cm^{-2} and $T^2=(0.13\pm0.03)$mg.cm^{-2}. These results can be compared with the values reported by Blok et al (Blo.74) : for the same fitted function applied to all the ions studied, they determined $\rho=(0.08\pm0.01)$mg.cm^{-2} and $T^2=(0.077\pm0.020)$mg.cm^{-2}. Considering the fact that the experimental conditions were completely different (different target, projectiles, energy, scattering chamber) and that the scanning was done by a different person, one can consider the present results to be in reasonable agreement with those obtained previously. Therefore, the range distributions of all the ions studied was regarded in this work as represented by the same width and tailing parameters.

The tracklength values corresponding to the function maxima were taken as the most probable tracklength values after correction for the 30-degree angle of incidence on to the mica. The corresponding energies of the scattered ions were calculated via the conventional Rutherford scattering formula (Rut.11).

$$E_1 = \frac{[1+(A_1/A_2)^2 + 2A_1\cos\theta_{cm}/A_2]\ E_i\ A_2^2}{(A_1+A_2)^2}$$

$$E_2 = 2E_i(A_1/A_2)(1+\cos \theta_{cm})[A_2/(A_1+A_2)]^2$$

where the subscripts 1 and 2 refer to the scattered projectile and target nucleus respectively; A is the mass of the scattered fragments with an energy E in the center of mass, E_i is the kinetic energy of the incident projectile in the laboratory system and θ_{cm} is the center of mass scattering angle. The center of mass and laboratory angles θ_{cm} and θ_{lab} are related through the following equation:

$$\tan \theta_{lab} = \frac{\sin \theta_{cm}}{\cos \theta_{cm}+(A_1/A_2)}$$

which permits the conversion of the energy values to the laboratory system. These energies were not corrected for the energy loss by ions in the gold target since it was calculated to be 4% (and hence negligible) for the worst case of an incident iodine ion traversing the entire target thickness and then being scattered at backward angles.

The variation of the most probable tracklength as a function of energy for gold and iodine is plotted in Fig.11 together with the previous data for other ions (Blo.74). As one can see, the iodine data fall at the expected location and follow the general pattern of the other curves determined earlier. The present gold data are found to be in good agreement with the few values available previously.

Fig.11: Most probable tracklength as a function of incident energy for ions from Al to Au. Data for I and Au are from this work and the remaining data are from (Blo.74). Solid curves are calculated from equations (II.1), (II.2) and (II.3) in the text and dashed curves are best fit.

TRACKLENGTH (mg/cm²)

KINETIC ENERGY (MeV/a.m.u.)
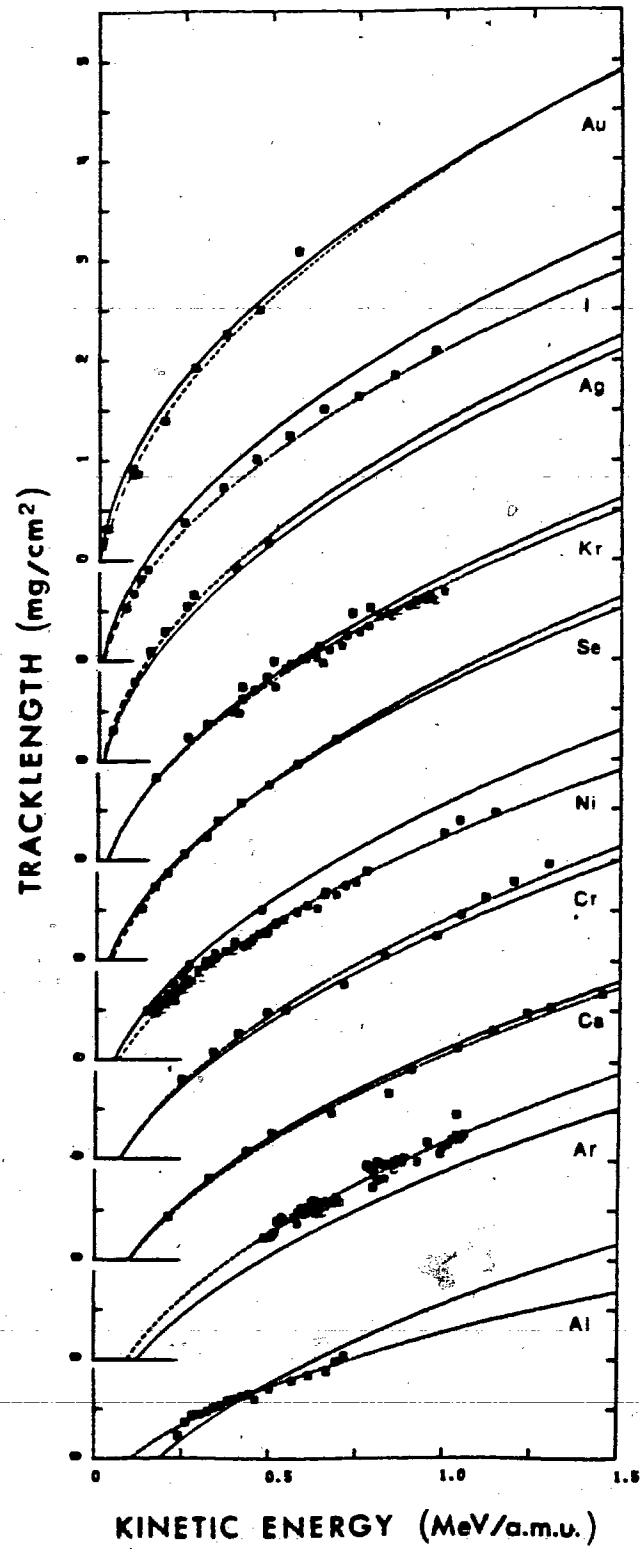
As described in section II-A, all the data shown in Fig.11 were expected to be represented by an equation of the form:

$$L = bE^c - \Delta L \qquad (II.1)$$

where L is the measured tracklength in $mg.cm^{-2}$, E is the incident ion energy in $MeV.amu^{-1}$, while b, c and ΔL are constants for a given ion.

Parameter b given by equation (I.11) (section I-C-5) will hereinafter be referred to as "b from theory" or "b_{th}", while the parameter c is expected (see equation (I.9)) to have a value of 0.5.

A first fitting of the new data for I and Au (and the previous data for other ions) with equation (II.1) was done by the least squares technique treating b, c and ΔL as free parameters. It was found that a value of $c=0.5$ (corresponding to the theory) fitted the data about as well as other values. Therefore, since c is expected to be independent of ionic composition and in order to reduce the number of degrees of freedom by one, it was fixed at the 0.5 value for all ions and the tracklength data were refitted with ΔL and b as variables. The best fit values of b and ΔL, then obtained are reported in Table III and compared with b_{th}. As can be seen from this table, the b and ΔL values for Al

TABLE III

Ion	b_{fit}	ΔL_{fit}	b_{th}	$b+b_{th}$	chi squared
Al	1.88 ± 0.08	0.61 ± 0.06	2.41	4.29	0.023
Al_1	2.45 ± 0.03	1.00 (fixed)	2.41	4.86	0.095
Ar	3.15 ± 0.09	0.97 ± 0.08	2.94	6.09	0.239
Ca	3.00 ± 0.07	0.94 ± 0.07	2.78	5.78	0.079
Cr	3.29 ± 0.11	0.88 ± 0.10	3.27	6.56	0.067
Ni	2.98 ± 0.05	0.76 ± 0.03	3.42	6.40	0.337
Se	3.58 ± 0.04	0.76 ± 0.03	4.18	7.76	0.003
Kr	3.31 ± 0.11	0.57 ± 0.09	4.33	7.64	0.455
Ag	3.80 ± 0.16	0.41 ± 0.08	4.94	8.74	0.026
I	3.53 ± 0.04	0.44 ± 0.03	5.52	9.05	0.012
Au	4.37 ± 0.15	0.44 ± 0.07	7.34	11.71	0.109

ions did not follow the trends exhibited by the rest of the data. However, if ΔL was fixed at 1.00 mg.cm^{-2} for Al (more in accord with the values for other light ions), the best fit value obtained for b was 2.45 $\pm$ 0.03 with an acceptable chi-squared value of 0.095. The curves corresponding to the best fit parameter values are shown as broken lines on Fig.11.

For the application of these data to the analysis of fission fragment tracks, a single formula giving tracklength over the range of ionic masses and energies covered by the fission fragments would be most desirable. An earlier analysis of these calibration data by the author (Dau.78) led to a general formula based on the ratio b/b_{th} as a function of the ionic nuclear charge Z fitted to a monotonic function of the form:

$$b/b_{th} = a + b \exp(-cZ) .$$

However, it was later found that a formula arbitrarily giving $b+b_{th}$ as a function of the ion mass A led to much more coherent results especially in the case of ions heavier than Se (i.e in the region where the fission fragments are expected to be located). The best fit values of b added to the corresponding values of b_{th} are shown plotted against ionic mass in Fig.12 ; the best fit values of ΔL as a

Fig.12: Best fit values of the parameter b added to the
corresponding theoretical values (b_{th}) as a function of the
ionic mass. The curve is a fitted function from equation
(II.2) in the text. The error bars correspond to the
uncertainty of the fitting process.
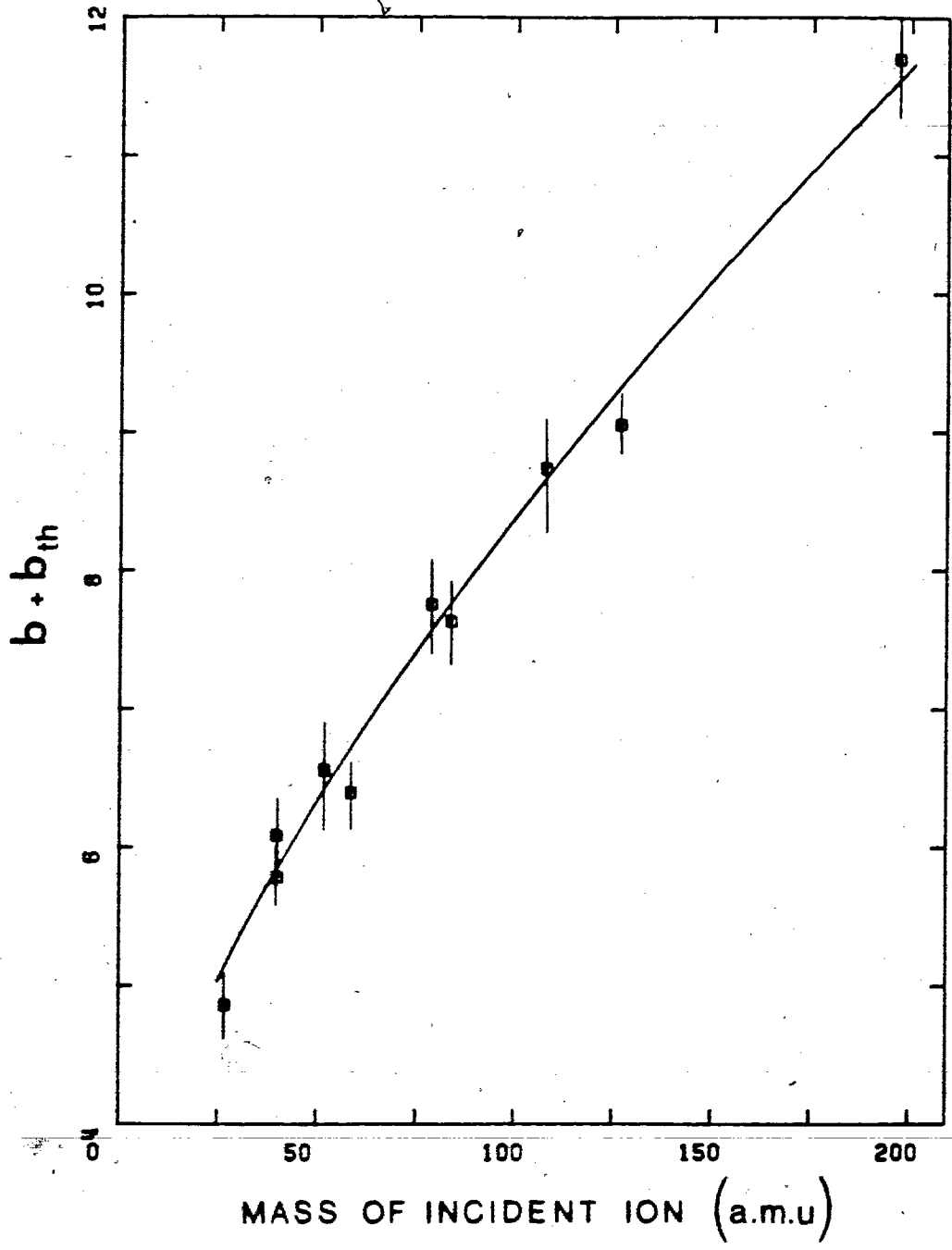
function of the ionic nuclear charge are reported in Fig.13. In both Figures 12 and 13, the error bars correspond to the uncertainty of the fitting process.

The application of these data to analysis of range distributions observed for fission fragments necessitates an interpolation to parameter values intermediate to those for which experimental data now exist. The apparent departure from monotonic variation of these parameters with ionic nuclear charge and mass shown in Fig.12 and 13 make such an interpolation difficult. (Such oscillations were reported earlier (Blo.74,Dau.78)). In order to obtain a convenient interpolation procedure, the data in Fig.12 were fitted to a monotonic function of the form:

$$b + b_{th} = c + d A^{2/3} \qquad (II.2)$$

whereas the data in Fig.13 were fitted to a function of the type:

$$\Delta L = e + f \exp(-gZ) \qquad (II.3)$$

The fitted function are plotted as the curves on those figures. The best fit parameters were found as follows:

for equation (II.2): $c = 2.84 \pm 0.22$

$d = 0.257 \pm 0.011$

in relation (II.3): $e = 0.17 \pm 0.20$

$f = 1.65 \pm 0.21$

$g = 0.04 \pm 0.02$

Fig.13: Best fit values of ΔL as a function of the ionic

nuclear charge. The curve represents a fitted function from

equation (II.3) in the text. The error bars correspond to

the uncertainty of the fitting process.
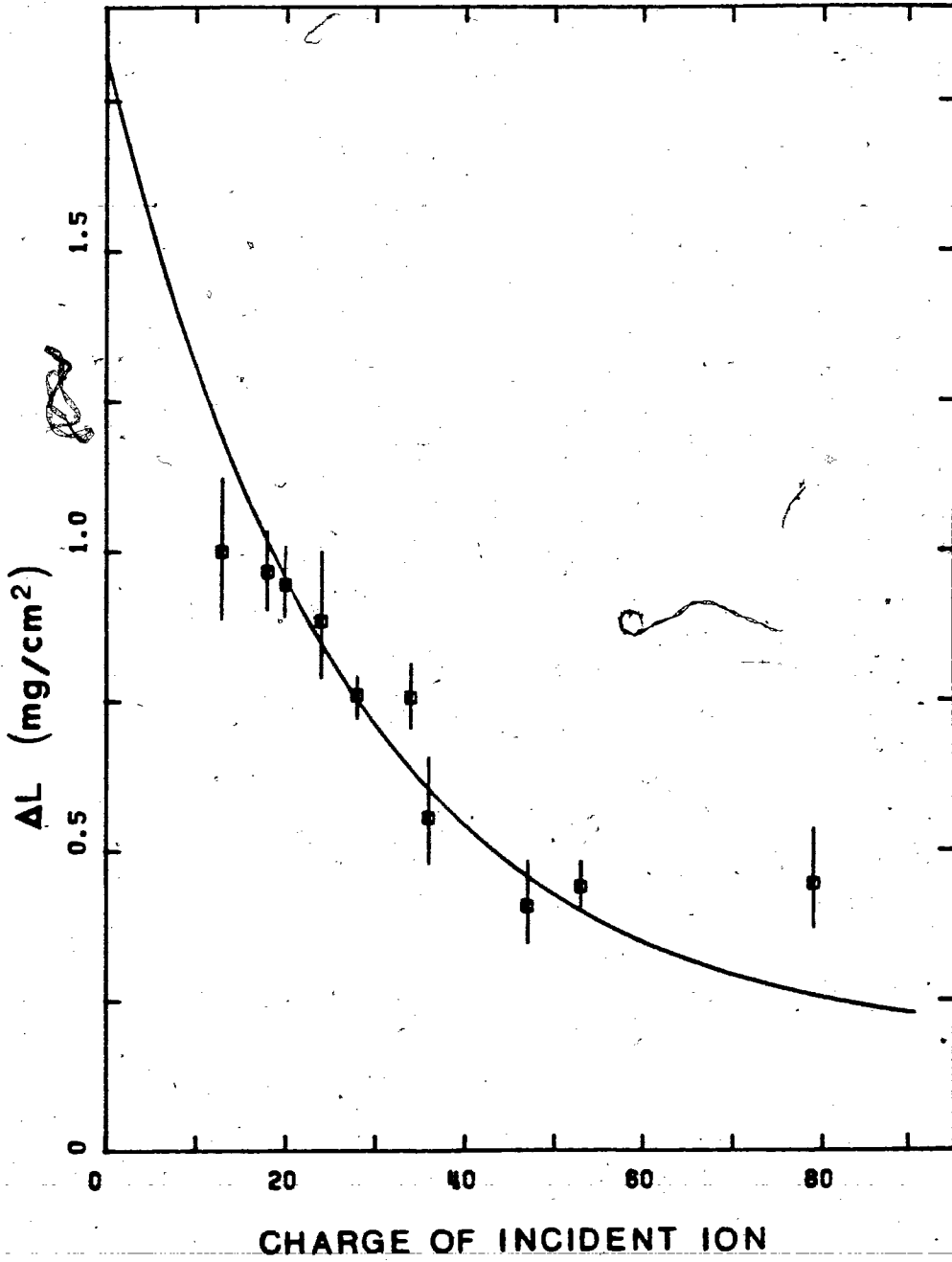
Values for b and ΔL taken from the curves in Fig.12 and 13
and inserted into equation (II.1), led to tracklength-energy
relationships which are shown plotted in Fig.11 as solid
curves. The discrepancy between the calculated and the
best-fit relationships is the largest for Al which is close
to the ionic charge treshold (found at Ne) for track
registration in mica but is otherwise less than 15% .
This is considered to constitute an acceptable error for the
present purpose. This set of relationships constitutes the
mica calibration which was used for the fission studies
using the mica as a detector.

b) Fission studies

Tracklength distributions were measured by scanning of
micas exposed at several angles between 20° and 160° with
respect to the beam direction; these distributions were then
fitted to Gaussian functions in order to obtain the most
probable value of the respective projected tracklength. The
angle of incidence of the fission fragments to the mica
being known, this projected tracklength value was converted
into a real tracklength value (expressed in mg/cm^2). The
curve giving the most probable tracklength as a function of
the laboratory angle was then analyzed using the program

RADICS (for RAnge DIstribution CalculationS) written by H.Blok and modified for the present work in order to include the new mica calibration relationships just described.

A brief outline of the program will be given here and a detailed description can be found in (Blo.75).

The mass of the fissioning system A_t being entered as a parameter, for each combination of fragment masses A_1 and A_2 (such that $A_1 + A_2 = A_t$), a kinetic energy of each fragment is calculated. In order to do so, it was assumed that the scission configuration was that of two tangent charged spheres. The total kinetic energy is then given by:

$$E = C \frac{Z_1 Z_2}{A_1^{1/3} + A_2^{1/3}} \qquad (II.4)$$

where the subscripts 1 and 2 refer to the fission fragments. The constant C is obtained by normalization of the calculated average total kinetic energy release to the energy E_t (calculated by the program from the data due to Nix (Nix.69) or entered as a parameter) for the case of symmetric fission such that:

$$C = E_t \frac{2 A_s^{1/3}}{Z_s^2} \qquad (II.5)$$

where E_t is the total kinetic energy release for the case of symmetric fission (i.e tangent spheres of equal Z_s and A_s).

Combining (II.4) and (II.5), one obtains:

$$E(A_1, A_2) = E_t \frac{2 A_s^{1/3}}{Z_s^2} \times \frac{Z_1 Z_2}{A_1^{1/3} + A_2^{1/3}}$$

In order to transform these energies from the center of mass system into the laboratory system, it was necessary to know the momentum of the fissioning system.

Porile and Sugarman (Por.57), (Por.60) and Alexander et al (Ale.63) found that the momentum component transferred to the target nucleus and parallel to the beam axis $(P_{//})$ increased with the excitation energy E^* of the residual cascade nucleus. The following relation has been widely used for many targets:

$$E^*/E_{cn} \sim 0.75 \, P_{//}/P_{cn}$$

where P_{cn} and E_{cn} are respectively the momentum and excitation energy of a hypothetical compound nucleus formed by the fusion of proton and target nucleus. The coefficient of proportionality has been taken as above by some authors (Cre.68), (Lag.76), (And.79) while, in other studies (Che.68), (Hog.69), different values were used. In the present work, the correlation coefficient between $P_{//}$ and E^* was obtained from the results of the intranuclear cascade calculations using the computer code ISOBAR. Fig.14 shows such a correlation in the case of a gold target with an

Fig.14: Average value of the momentum parallel to the
beam axis ($p_{//}$) corresponding to a given excitation energy
E^* as calculated by the ISOBAR code for a gold target
irradiated with 800 MeV protons.

p in MeV/c = p in (MeV.amu)$^{1/2}$ x 30.52

Au+800 MeV protons

EXCITATION ENERGY E* (MeV)

AVERAGE VALUE OF p// (MeV/c)
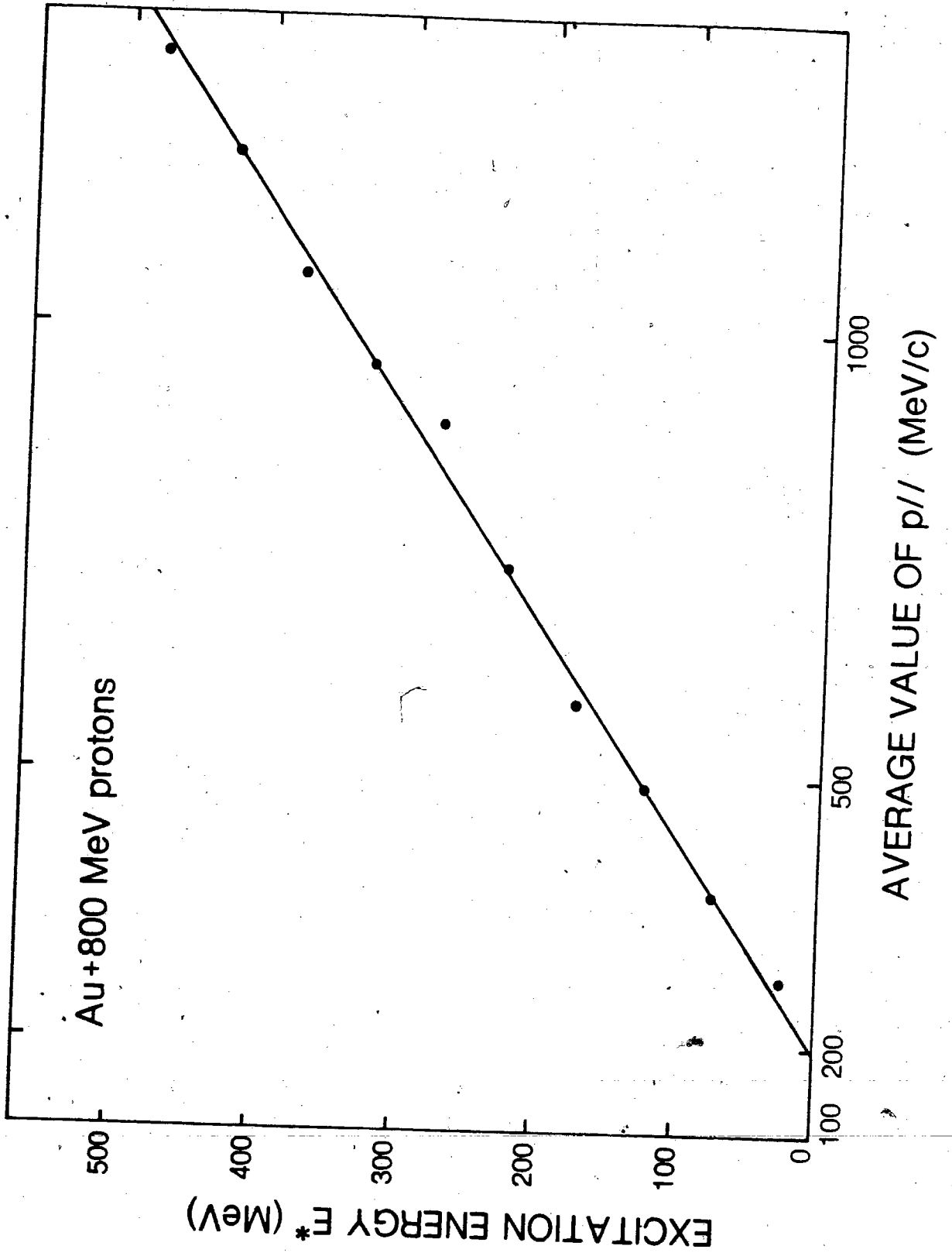
incident proton energy of 800 MeV where:

$$E^*/E_{cn} = 0.89 \; P_{///}/P_{cn} - 0.1$$

A similar expression was obtained for an uranium target

bombarded with 800 MeV protons:

$$E^*/E_{cn} = 0.91 \; P_{///}/P_{cn} - 0.1$$

The error in the fittig procedure being ± 0.02 and ± 0.03

for gold and uranium respectively, a single value of 0.90

for the correlation coefficient was used for both targets.

The analysis by the program RADICS was carried out by

entering the excitation energy E^* as an adjustable

parameter.

A broadening of a presumed Gaussian fragment kinetic

energy distribution was entered into the calculation

(Nix.69), as well as the effects of the experimental angular

resolution and the target thickness. This latter will also

shift the measured mean energy value.

For each mass, a range distribution was then calculated

using the range-mass-energy relationship previously

established from the mica calibration and the above energy

distribution. The distribution for each mass was then

weighed by a factor corresponding to the yield for that mass

obtained by assuming either a single Gaussian mass yield

distribution or two Gaussians, or a triple Gaussian.

Finally the weighted range curves for each fragment mass were added together for all the masses in order to give a total fission fragment range distribution in the laboratory system. This calculation was performed for each laboratory angle where a tracklength distribution was measured, so that a direct comparison could be made with the experimental results. This comparison was carried out by adjusting parameters entered in the program until an agreement with the measured range distributions was achieved.

For the study of fission at low bombarding energy where formation of a compound nucleus was expected, the fitting of the RADICS program results to the experimental data was achieved (Blo.75) by adjusting the total kinetic energy released and the excitation energy which were therefore the quantities determined by the analysis. In the present high energy fission study, the mass of the fissioning system was not known and was therefore taken as an adjustable parameter. The total kinetic energy in the center of mass system obtained from the experiments conducted with semi-conductor detectors (see section III-B-3) was entered as a known value and fixed (assuming that there is essentially zero variation of the fission energy between the bombarding energies of the two studies of 480 MeV and

800 MeV). The calculated range was then fitted to the experimental data with the mass A_t and the excitation energy E^* of the fissioning nucleus used as adjustable parameters. A change in the value of the mass A_t will shift the calculated curve of ranges as a function of the laboratory angle to higher or smaller range values. On the other hand, a change in the excitation energy will act upon the slope of the curve.

The experimental curves as well as the calculated ones are shown in Fig.15 and 16 in the case of gold and uranium respectively. The best agreement between calculation and experiment was achieved for the following values of mass and excitation energy of the fissioning nucleus:

Target	A_t (amu)	E^* (MeV)
Au	190 ± 5	150
UF_4	234 ± 2	95

Fig.15: Most probable tracklength (in mg/cm^2) measured in mica as a function of the laboratory angle for a gold target irradiated with 800 MeV protons. The upper and lower curves are the fitting with the program RADICS for values of the fissioning mass A_t of 195 amu and 185 amu respectively. The triangles represent the best fit for A_t=190 amu. The dip in the curves observed at a 90° angle is due to the fission fragments energy loss in the target.

Au 800 MeV protons

experimental data
△ RADICS $A_T = 190$ amu
① ---- $A_T = 195$ amu
② ---- $A_T = 185$ amu

LABORATORY ANGLE (degrees)
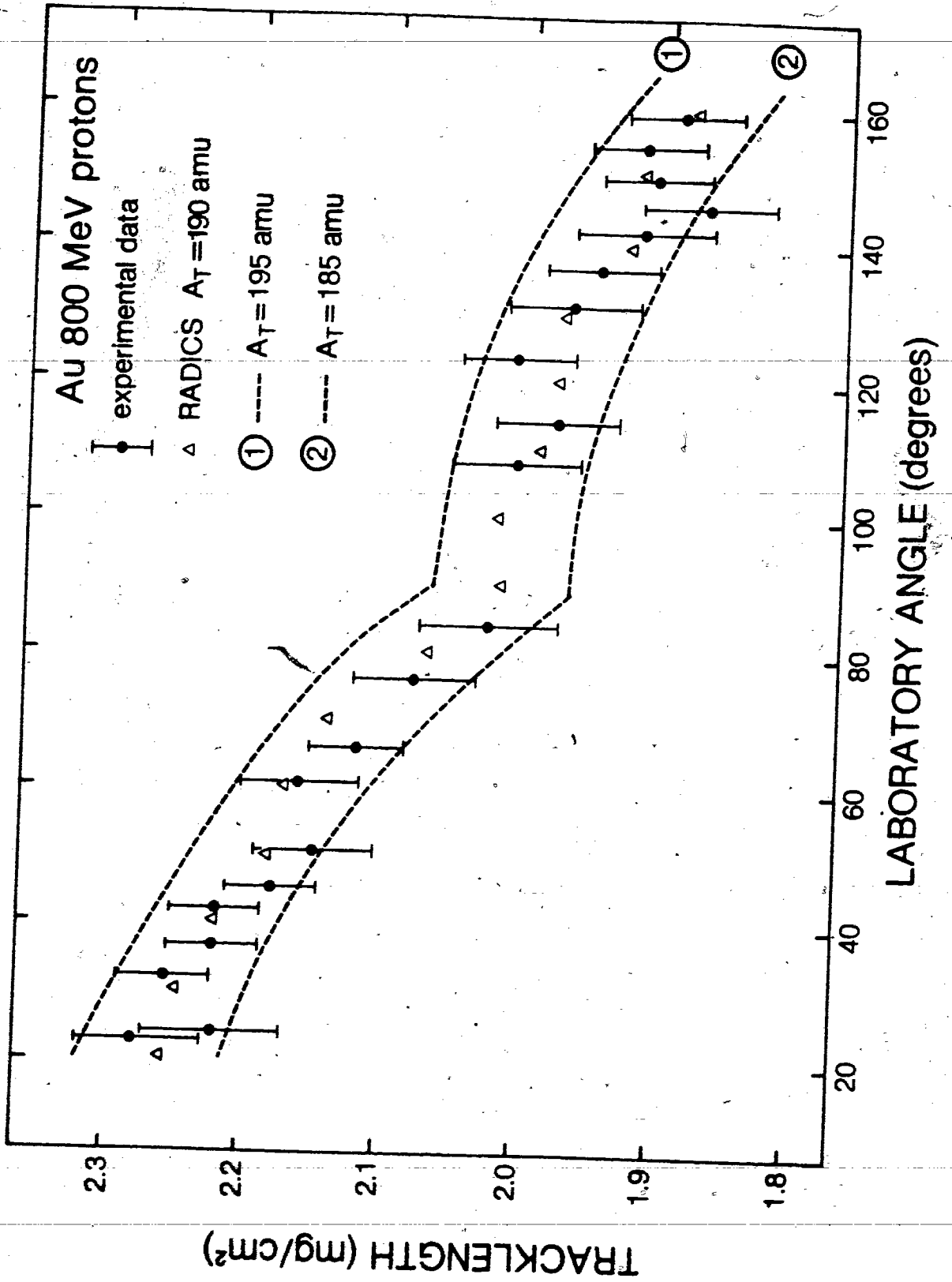
TRACKLENGTH (mg/cm²)

Fig.16: Most probable tracklength (in mg/cm^2) measured in mica as a function of the laboratory angle for an uranium target irradiated with 800 MeV protons. The upper and lower curves are the fitting with the program RADICS for values of the fissioning mass A_t of 236 amu and 232 amu respectively. The triangles represent the best fit for A_t=234 amu.
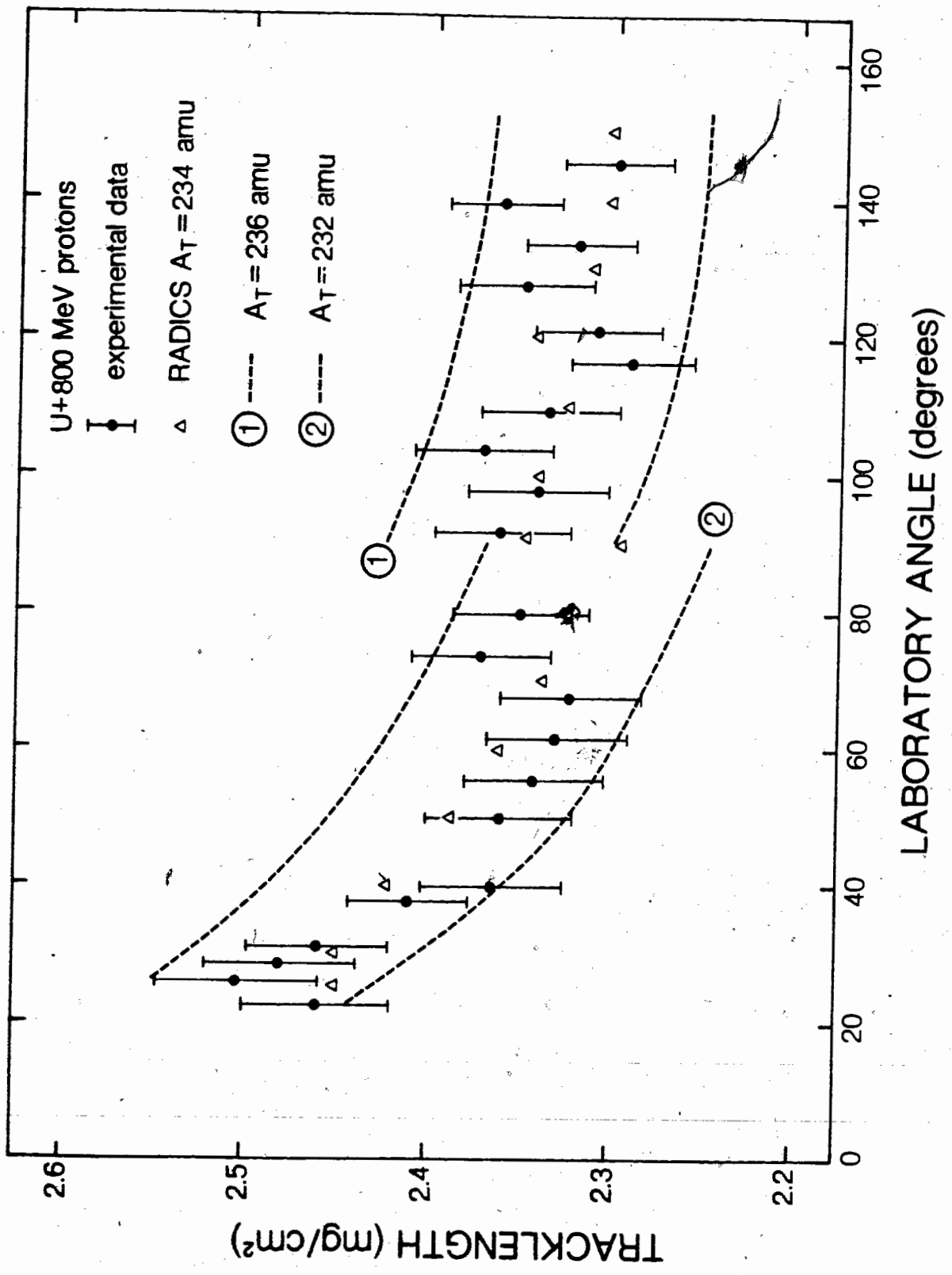
B) Experiments with mica in a sandwich configuration

The sandwich method has already been investigated and used in a few cases for measurements. It was proposed by Cieslak et al (Cie.66) who described the preparation of mica sandwiches and studied the average efficiency of track registration for several angles of incidence to the mica surface ranging from 6° to 90°. The average efficiency of observation of fission fragment coincidences was estimated to be (96 ± 5)%. However the aim of this study was to establish a method that could be used in experiments to obtain cross-section data for high-energy fission. Mica sandwiches were used (Hud.69) to measure the fission cross-sections of U, Bi, Au, and Ag targets bombarded with 0.6 to 29 GeV protons. The sandwich method has been used more rarely in order to extract the mass and energy distributions of the fission fragments. Ait-Salem et al (Ait.68) investigated the low energy neutron induced fission of ^{238}U by means of acetylcelluloid detectors in a sandwich configuration. They obtained mass and kinetic energy distributions of fission fragments in a manner comparable to

that used in the present work except for the fact that they used theoretical mass-energy relationships. Remy et al (Rem.70) carried out the same type of study on ternary fission using polycarbonate (makrofol) sandwiches. Like previous authors, they obtained energy and fragment mass distributions by using theoretical mass-energy relationships. In contrast, the studies presented here, as well as the work of Kiely et al (Kie.73), used the empirical relationships between projectile mass (charge) and range obtained from independent calibration experiments.

The sandwich method was utilized when track coincidence information (identifying binary fission) was more important than precise data on the variation of fragment intensity with respect to the beam direction. The sandwich configuration is shown schematically in Fig.17.

1) Experimental techniques

a) Irradiation facilities and experimental set-up

Irradiations of gold, silver and UF_4 targets in a mica sandwich configuration were made at LAMPF (Los Alamos) with 800 MeV protons and 400 MeV π^+ mesons. The mica sandwiches

Fig.17: Schematic view of a mica sandwich configuration.

beam

mica

mica
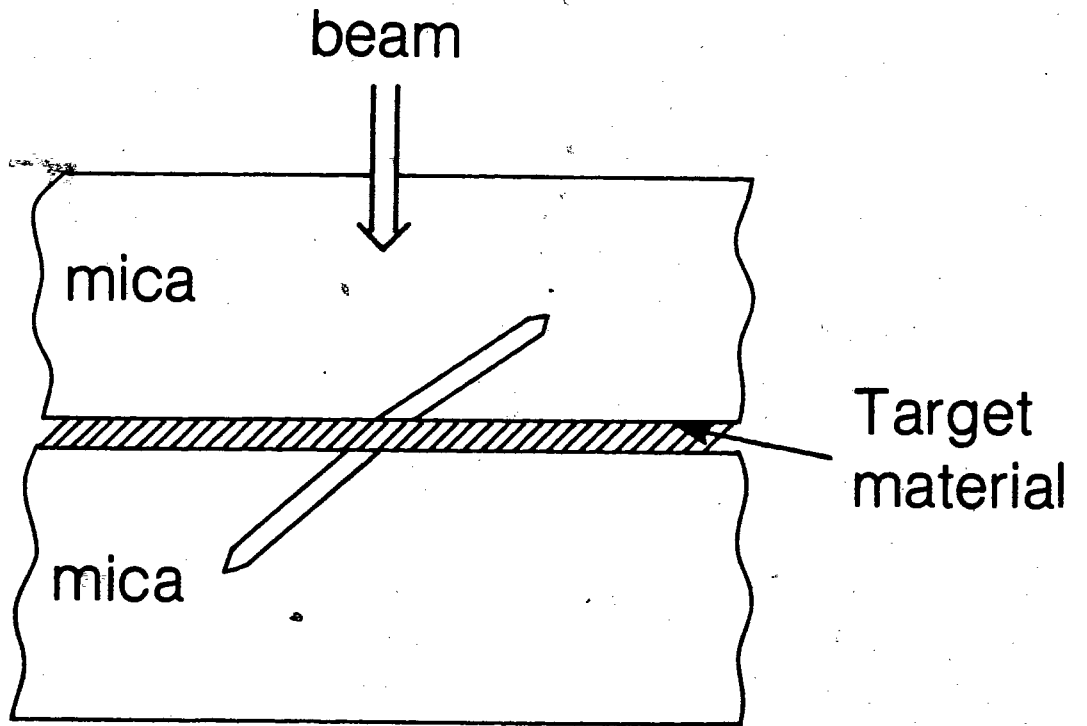
Target
material

were mounted in aluminum holders and irradiated directly in the beam with the mica plane perpendicular to the beam direction.

b) Target preparation

Squares of mica (2.5x2.5cm^2 in size) were cleaved and the appropriate target material was vacuum deposited on one of the freshly cleaved surfaces. Tne two sheets of mica were then clamped together at one edge (to insure retention of their respective positions) by two pieces of lucite glued with cyclohexanone, placed in an aluminum holder and screwed together in order to obtain a close contact of the clean mica surfaces. The amount of material deposited was, as previously, determined by weighing. The thicknesses of the targets used had values ranging between 100μg.cm^{-2} and 200μg.cm^{-2}.

c) Etching and scanning of the micas

After irradiation, the sandwiches were wedged open with a teflon thread in order to expose the interior surfaces to the etchant. The target material was then dissolved off with aqua regia and the micas were etched with HF under the same conditions as previously described. After washing and drying, the two parts of the sandwiches were then restored

to tight contact and mounted on a glass microscope slide. The scanning was done with a 100x oil immersion objective and an overall magnification of 1600x.

The target being located in between the two mica detectors, when a fission event occurred producing fragments directed towards the mica surfaces, each mica detector registered one of the fission fragments and the scanning of the sandwiches gave a coincidence measurement between fragments from the same fission event. Since the fission fragments entered the mica detectors at various angles, a measure of these angles was necessary in order to obtain the real track lengths. Therefore, a third Mitutoyo gauge (having 1μm graduations) was fitted to the microscope stage in order to allow measurements along the focussing axis and hence three-dimensional scanning. The depth of a track (that is the projected track length along the viewing axis), was obtained as the difference between readings of this third gauge when focussed on each end of the track. The projected track length on the mica surface was measured as before by means of the eyepiece graticule; then the real track length as well as the incident track angle were obtained by a simple geometrical calculation.

Some difficulties occurred in the measurement of the

depth of the track due to the utilisation of the oil immersion objective. The drop of oil surrounding the objective was found to produce a capillary attraction for the cover glass, which was lifted out of contact with the mica sample as soon as the microscope stage was lowered. As a result, the depth measurements were erroneous and gave a value far too large. This effect was eliminated by fitting several brass rings around the objective, heavy enough to overcome the capillary attraction.

The three-dimensional scanning measurements have been tested by using a sample from the calibration experiment where the tracks entered the mica with a known 45° angle. Two different sets of measurements have been carried out on the same sample: one set where the cover glass was placed directly onto the mica to be measured and one set where another small sheet of mica (without tracks) was inserted between the cover glass and the calibration mica in order to simulate measurements on the lower half of the mica sandwich.

The two sets of measurements in three dimensions led to tracklength and angle of incidence values with and without the inserted mica. The results are summarized in the following table:

air objective, two dimensional scanning assuming 45° incidence		oil objective, three dimensions scanning			
no mica inserted	with mica inserted	without mica inserted		with mica inserted	
length (μ)	length (μ)	length (μ)	angle (o)	length (μ)	angle (o)
9.14±0.22	9.22±0.22	9.50±0.37	46.5±2.1	9.47±0.37	45.9±2.1

This table shows that the three dimensional scanning led to acceptable results. However, the errors quoted here for the angle values are optimistic since only the uncertainty in the reading of the gauges has been taken into account. It is also assumed that, at the time the readings were made, the microscope was focussed reasonably precisely at the extremity of the track. This was probably true in this particular case as tracks incident on the mica at a 45° angle are relatively easy to scan. However, during the scanning of a sandwich, it was often much more difficult to determine when the ends of tracks were in focus,

particularly those which entered the mica at an angle greater than 70° (since they were viewed almost end-on). In the case of sandwich measurements, an uncertainty of ±6° is therefore estimated to be more realistic.

Several conditions had to be fulfilled by two tracks in order to be recognized as members of the same pair i.e. coming from the same fissioning nucleus. They had to be in opposite hemispheres with respect to the stage plane and have the same point of origin. Their projections had to be roughly colinear (within ~15°) and both in the field of view. This last condition could lead to the rejection of events entering the mica with a small angle of incidence since the separation of the mica surfaces during irradiation was not zero.

The two experimental arrangements previously described (scattering array and sandwich) give complementary information on the fission process. Two dimensional scanning of micas from the scattering array will lead primarily to the angular distributions of the fission fragments. This information could also be obtained from the three dimensional measurements but, due to the difficulty in measuring very shallow and very deep tracks, the angular distributions will have large uncertainties at angles below

20° and over 70° compared to the mica surface. The scanning of sandwiches being a coincidence measurement, the center of mass momentum could be deduced from the divergence between the tracks of the same pair: this quantity cannot be extracted from the scattering array measurements.

2) Data analysis

a) Treatment of the data

During the scanning of a mica sandwich, for each track of an observed pair, the projected length and the depth were measured. The absolute errors on these measurements were one eyepiece unit (or 0.16μ) and 0.20μ respectively. However, these errors (being statistically distributed) did not affect the position of the maxima in the measured tracklength distributions (and consequently in the calculated mass and energy distributions of the fission fragments) but did contribute to their widths. The depth measurements were corrected for the difference in refractive index between the oil used for the immersion objective and the mica. The refractive index of the oil was measured, at room temperature, with a Bausch and Lomb refractometer (model Abbe 3L) and found to be 1.5134 $\pm$ 0.0002.

The refractive index values for mica, given in the literature, range from 1.551(Han.70) to 1.6117 (Jen.57,Ros.65). An average value of 1.584 was chosen for the calculations.

Snell's law describes the refraction at a boundary between two substances having indices of refraction n and n' :

$$n \sin \phi = n' \sin\phi' \qquad (II.6)$$

where ϕ and ϕ' are respectively the angle of incidence and the angle of refraction as shown in Fig.18.

During the microscope measurements, the angle of incidence ϕ will always be small and, as a consequence (see eq.II.6), the angle of refraction will also be small. Under these circumstances, a good approximation is obtained by setting the sines equal to the angles themselves:

$$n \phi = n' \phi'$$

Since, in the particular case of mica and oil, n is greater than n', a ray of light coming from point A in the mica will be directed farther from the normal after refraction and will seem to be coming from point B (see Fig.18). If d' is the measured depth of a track, the true depth d will then be greater than d':

$$d = d'n/n'.$$

Fig.18: Light path and measurements of the depth with an oil immersion objective.

oil objective

oil
refractive index n'

d'

d

mica
refractive index n

B

A

light
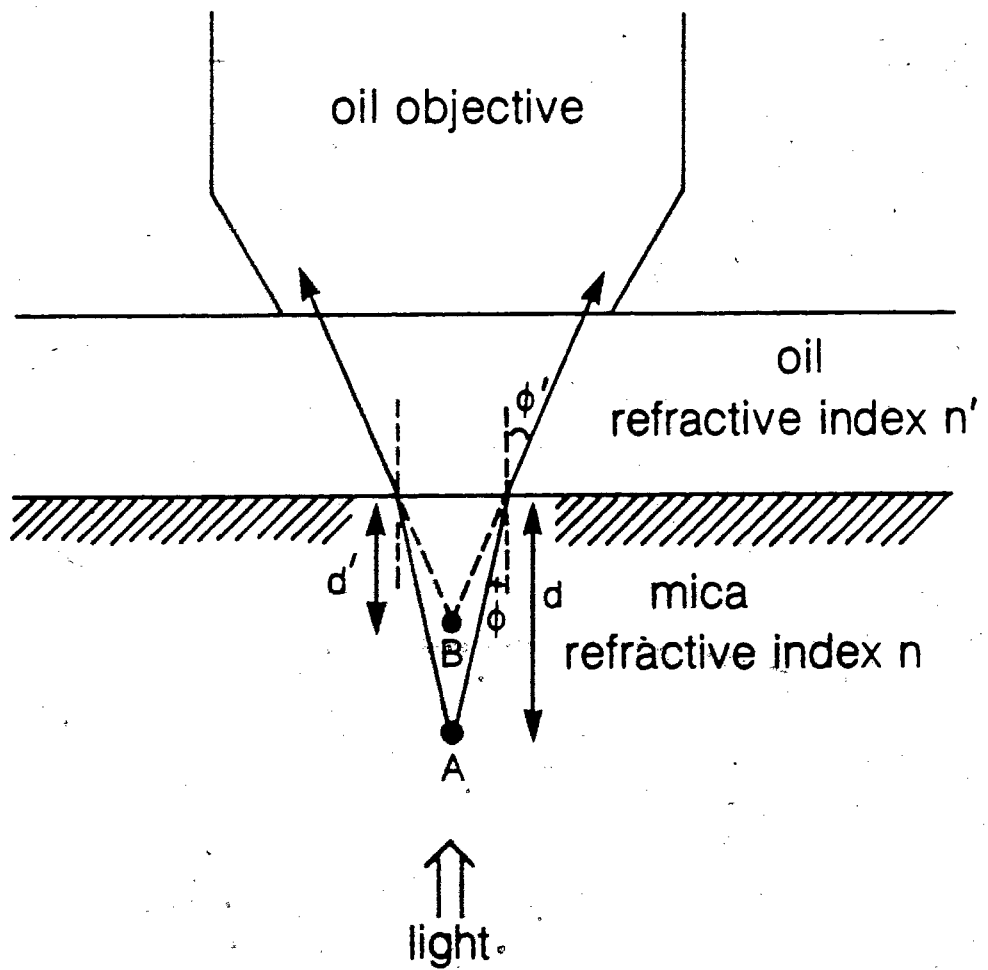
The air layers present between the cover glass and the
mica or inside the sandwich were kept constant by means of
the weight mentioned earlier (section II-B-1-c). No
correction for the refractive effects of these air layers
was then necessary, since a ray of light entering an air
layer or the cover glass with an angle of incidence a will
emerge with the same angle after being refracted twice.

The tracklength data were treated with a computer
program called SANDY (written by M.Kiely) modified for the
present work by insertion of the new set of mica calibration
data.The calculation of the center of mass momentum and
corrections for it have also been added.

The calibration data were entered as a set of
parameters relating, for a given tracklength, the energy of
a fission fragment to its mass. These calibration parameters
were obtained as follows: for each tracklength value from 2 μ
to 15 μ taken in 0.2 μ increments, masses ranging between 27
and 170 a.m.u were assigned. For each of these assigned
masses, the energy was calculated through equations (II.1),
(LI.2) and (II.3). Such a calculation implied that the
relationship between the charge Z and the mass A of the
fission fragments was known. The "unchanged charge
distribution" or UCD postulate (Goe.49,Fri.63), assuming

that both fragments bear the same neutron to proton ratio as
the fissioning nucleus, has been used. In the fission
studies, this ratio had to be assumed and the impact of this
assumption will be discussed further.

The calculated energy values were then fitted (still for
a given tracklength) to a fourth degree polynomial in the
mass:

$$E = \sum_{i=1}^{5} a_i \, A^{i-1}$$

The set of coefficients a_i constitutes the calibration
data used by the program SANDY.

From the measurements of the projected length and the
depth of the tracks, this program calculated the real
tracklength as well as the incident track angle which led to
tracklength distributions and angular distributions in each
hemisphere. Then, the analysis was carried out in two
different steps:

- Initially, it was assumed that there was no center
of mass motion and therefore the two fragments were emitted
with an angle of 180° between them. Conservation of the
momentum can be written as:

$$p_1 + p_2 = 0 \qquad (II.7)$$

where p_1 and p_2 are the momenta of the two fragments, which can be expressed as a function of the mass of the fragment and its energy in MeV/a.m.u : $p = A \sqrt{2E}$. Therefore equation (II.7) becomes:

$$A_1 \sqrt{2E_1} + A_2 \sqrt{2E_2} = 0 \quad \text{or} \quad A_1^2 E_1 = A_2^2 E_2$$

In order to carry out the calculations, the mass of the fissioning system A_t had to be given as an input to the program. Here again, some difficulties will arise in high energy fission when A_t is distributed. The bearing of this choice of the total mass on the results will be seen later on. Given a value of A_t, then $A_1 + A_2 = A_t$.

The system was thus solved through the following set of equations:

$$A_1^2 E_1 = A_2^2 E_2 \qquad (II.8)$$

$$E_1 = \sum_{i=1}^{5} a_i A^{i-1} \qquad (II.9)$$

$$E_2 = \sum_{j=1}^{5} \bar{a}_j A^{j-1} \qquad (II.10)$$

$$A_1 + A_2 = A_t \qquad (II.11)$$

Expanding equations (II.9) and (II.10) and replacing in equation (II.8), as a function of only one fragment mass (A_1

or A_2), a six order polynomial is produced. Among the six roots obtained, four (two complex and two negative roots) were immediately rejected. The two remaining solutions were real and positive and the one whose value was less than the fissioning nucleus mass A_t was kept. In the very few cases where two possible values of the fragment mass were found, the pairs of tracks leading to those results were taken out of consideration. From the mass of one fragment, the mass of the second fragment and the energies E_1 and E_2 were then calculated using equations (II.11),(II.9) and (II.10).

- In a second step, the effects of center of mass motion were taken into account. The center of mass momentum (P_{cm}) was taken as unknown but directed along the beam axis. The laboratory angles θ_1 and θ_2 at which the two tracks were observed were assumed to be measured accurately, and, for each pair of tracks, a center of mass momentum was calculated such that the fragments in this center of mass were emitted with a 180° angle between them.

A set of equations similar to the one presented previously permitted the calculation of the mass and energy of the fragments, their center of mass momenta as well as the energies and emission angles (θ'_1, θ'_2) in the center of mass system. Any measurement uncertainty in the angles will be

reflected in the width of the calculated center of mass momentum distribution.

This calculation was made by considering each pair of tracks in their particular center of mass system: they had new emission angles θ'_1 and θ'_2 calculated previously. The measured tracklength l, which was the projection of the real tracklength L, was not changed in the process, but a new tracklength L', corresponding to the new angles, was calculated. The relation $L = l/\cos\theta$ became $L' = l/\cos\theta'$ in the center of mass system.

Changing the real tracklength meant changing the combination of mass and energy of the fragments ; therefore, the previous calculation was repeated with the corrected data L'_1, L'_2, θ'_1 and θ'_2 in order to find the corrected energies.

b) Tests performed using known fission reactions

The three dimensional scanning technique together with the previously described calibration of mica as a heavy particle spectrometer have been tested with the well characterised fission of ^{238}U induced by 14 MeV neutrons and ^{235}U induced by thermal neutrons.

A UF_4 sandwich was irradiated with 14 MeV neutrons

produced by the TNC model 9900 neutron generator located at Simon Fraser University and subjected to etching and microscopic examination as described above. After processing of the data, the following results were obtained in the case of 14 MeV neutron-induced fission of ^{238}U.

The tracklength distributions in the forward and backward hemispheres (relative to the direction of the incident neutron) are presented in Fig.19. It is seen in this figure that the tracklength in the forward hemisphere is slightly larger than in the backward hemisphere, indicating the presence of a small center of mass momentum contribution. These two distributions combined give the total tracklength distribution (shown in Fig.20) whose full width at half maximum (FWHM) is 5.3μ.

The track angular distribution is displayed in Fig.21. This distribution was expected to be nearly isotropic. However, the shape observed in Fig.21 could be explained as the result of several experimental problems:

- As seen in section (I-C-4) the critical angle for track registration in mica detectors has been determined to be ~5°. Therefore, most fission fragments emitted at 85-95° with respect to the normal to the mica surface will not leave recognizable tracks, while tracks at nearby angles will be difficult to recognize.

Fig.19: Fragment tracklength distributions in the forward and backward hemispheres from mica sandwich measurements for the system UF_4+14 MeV neutrons.

UF$_4$+ 14 MeV neutrons
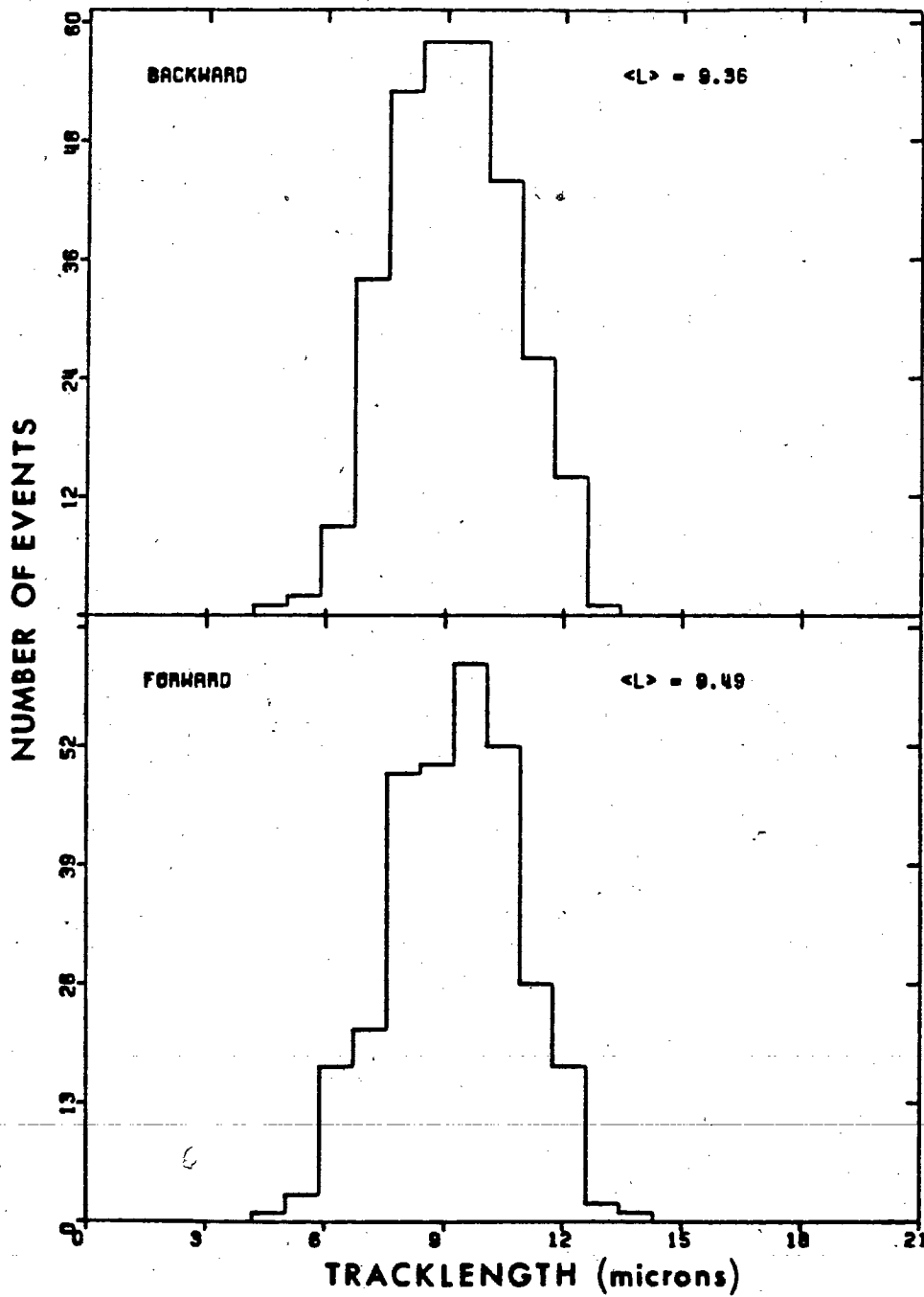
Fig.20: Distribution of the fragment tracklength sum
(forward and backward hemispheres added) for the system
UF_4+14 MeV neutrons.

$\langle L \rangle = 9.42$

$UF_4 + 14$ MeV neutrons

NUMBER OF EVENTS

TRACKLENGTH (microns)
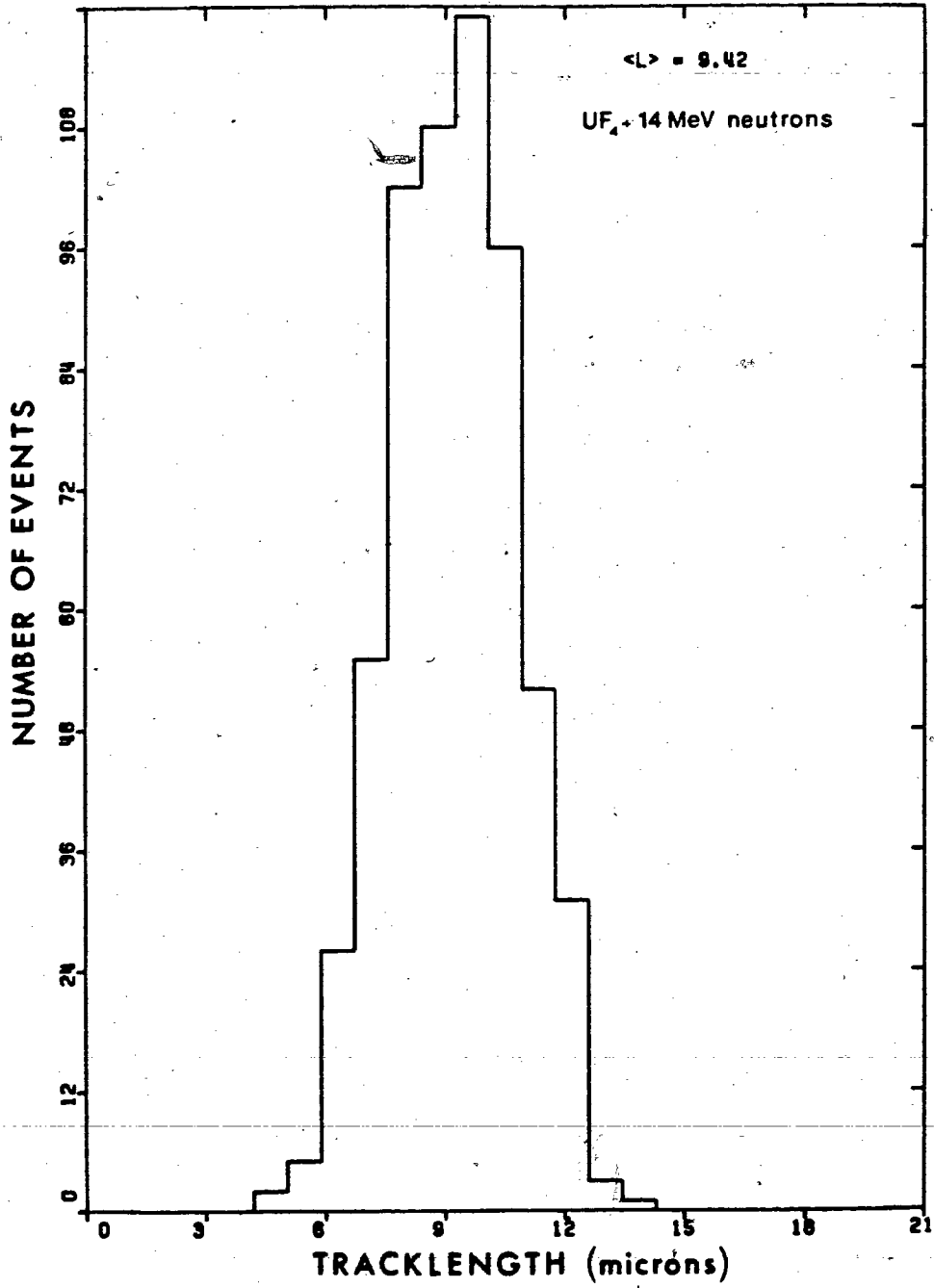
Fig.21: Angular distribution of the fission fragments
obtained with a mica sandwich for the system UF_4+14 MeV
neutrons: number of events per unit solid angle as a
a function of the angle in the laboratory system.

UF$_4$+ 14 MeV neutrons
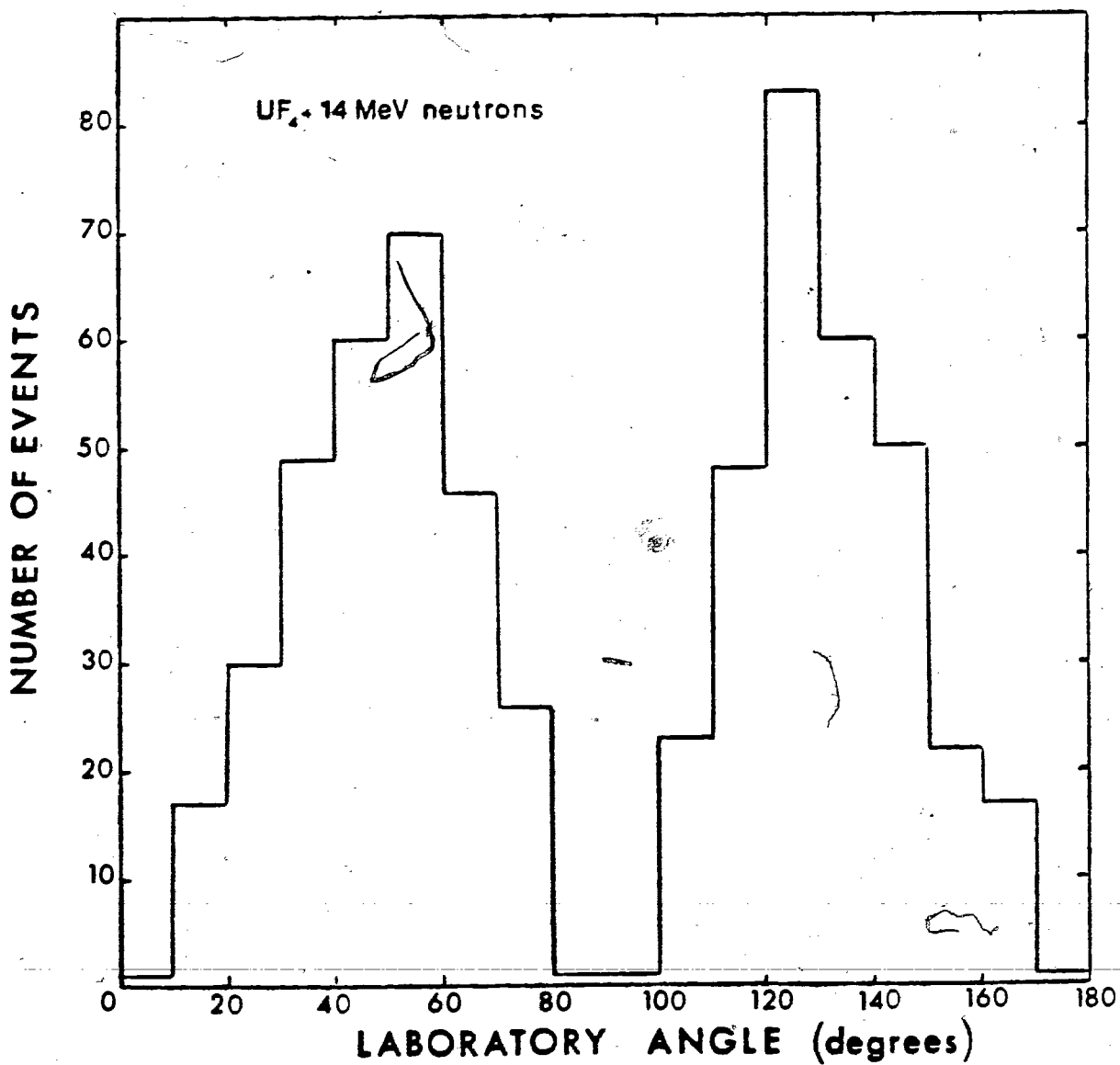
- The irreducible spacing between the mica sheets during irradiation caused tracks of the same pair to be separated in the field of view by a distance, which became larger for angles approaching $0°$ to the mica surface. As a result, the probability also became larger of a track pair being rejected as arising from a single fission event. These two effects could explain the gap observed in the angular distributions around $90°$ to the beam.

The problems encountered at angles $<20°$ to the beam axis were due to the difficulty (described earlier) of accurate measurements of tracks entering the mica nearly normal to the surface. Because of all the difficulties just mentioned, the angular distributions obtained with the sandwich method are not useful. However, the distribution in direction of one track of a pair with respect to the direction of the other could still be measured. Such a distribution is shown in Fig.22 where a pronounced peak corresponding to nearly colinearity indicates a small center of mass effect.

Fig.23 gives the center of mass momentum distribution with an average value of 2.6 $(MeV.amu)^{1/2}$ and a FWHM=35 $(MeV.amu)^{1/2}$.

The average values of the fragment kinetic energies obtained after correction for the center of mass motion were

Fig.22: Distribution of angular divergence between the fragment track directions for the system UF_4+14 MeV neutrons.

NUMBER OF EVENTS

DIVERGENCE (degrees)

<DIV> = 0.4
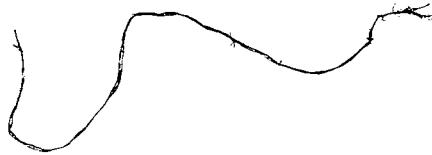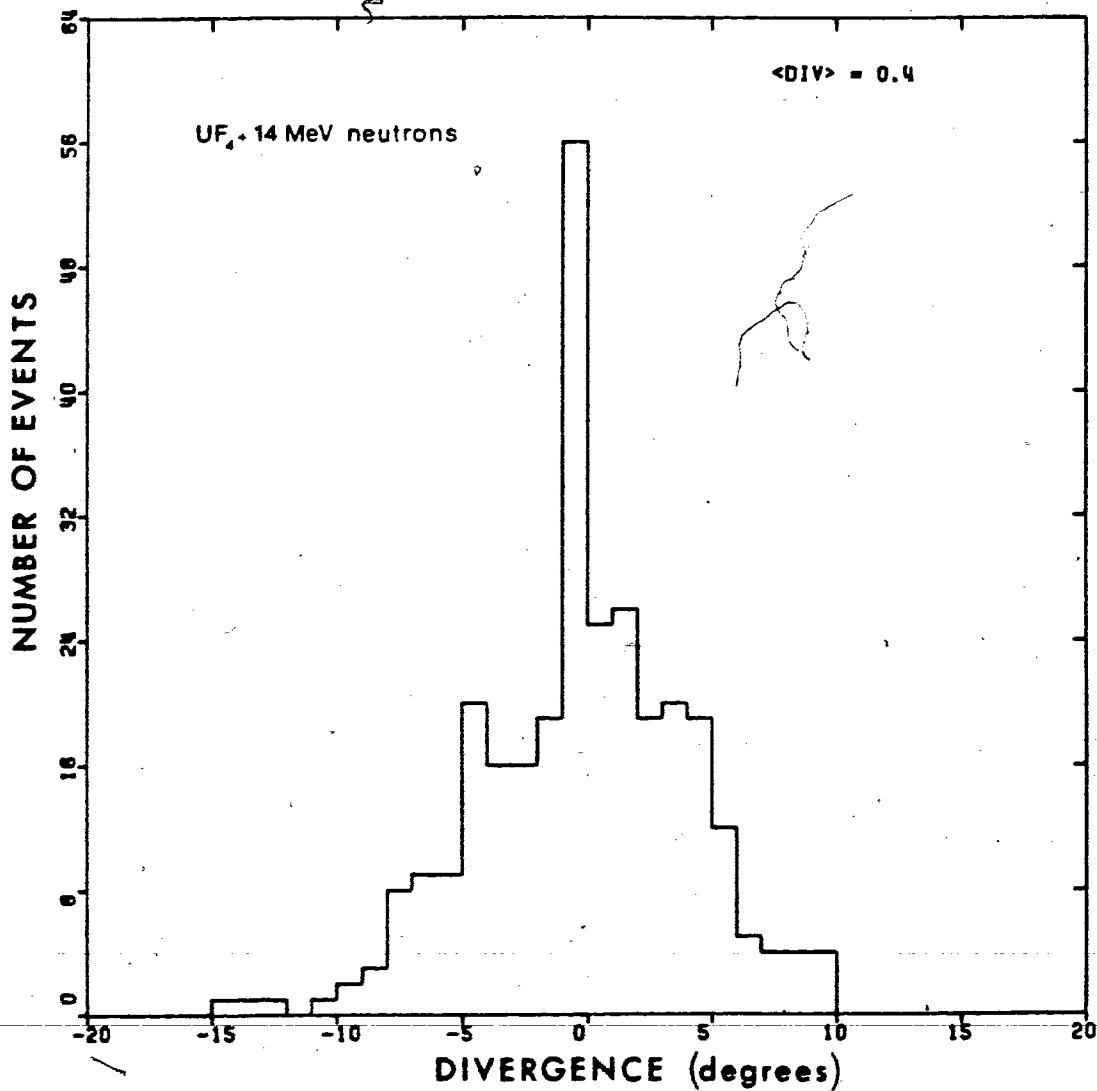
UF$_4$ + 14 MeV neutrons

Fig.23: Distribution of the deduced center of mass momentum (p_{cm}) of the fissioning nuclei from system UF_4+14 MeV neutrons.

Histogram of NUMBER OF EVENTS versus CENTER OF MASS MOMENTUM $(MeV.amu)^{1/2}$. Labelled UF_4, 14 MeV neutrons, $<P> = 2.6$.
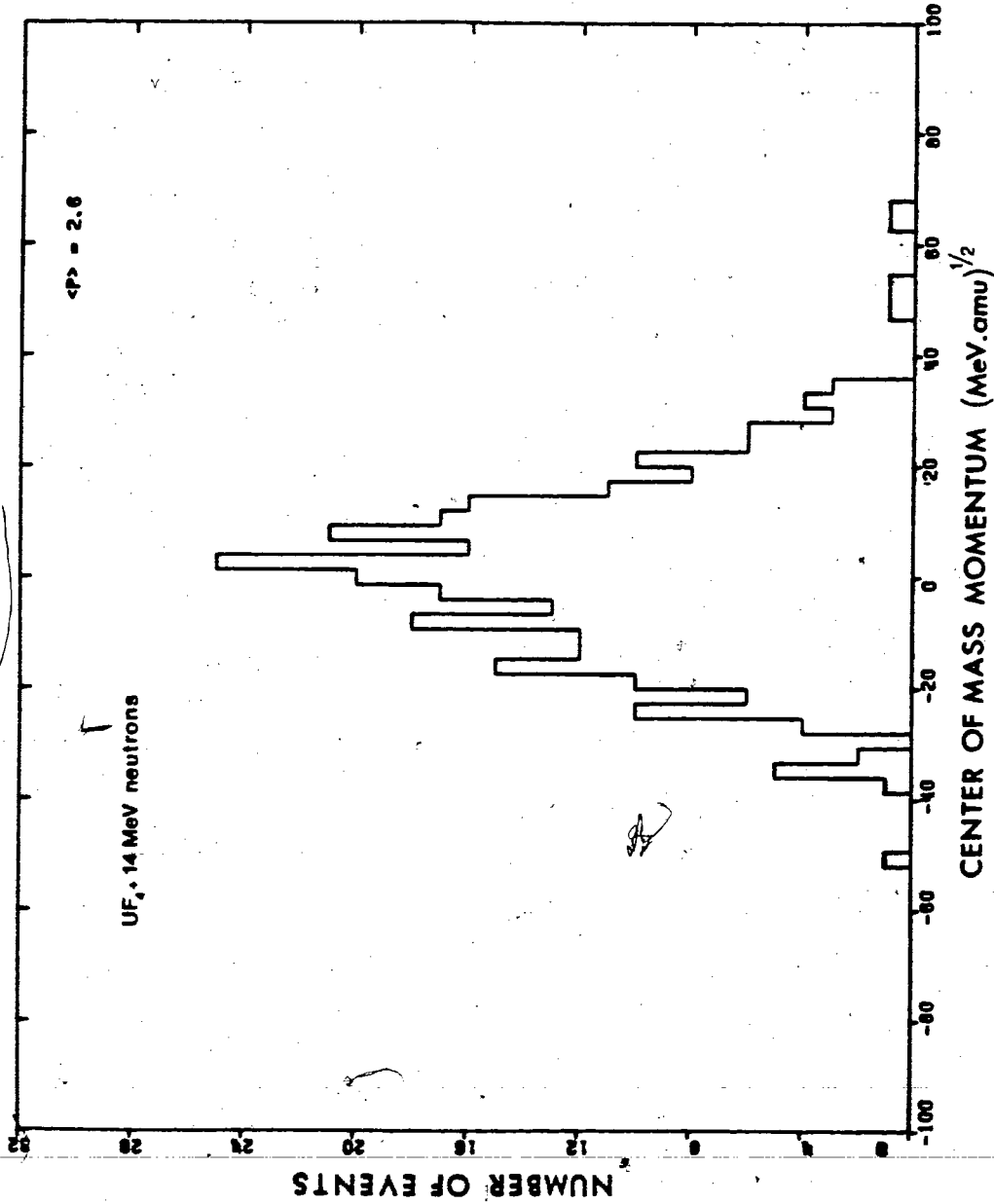
106 MeV for the light fragment and 72 MeV for the heavy one. This leads to an average value of 178 MeV for the total energy released. The total kinetic energy distribution displayed in Fig.24 shows a FWHM of 65 MeV.

The mass distribution is given in Fig.25. A fitting of this distribution as the sum of two Gaussian functions led to most probable values of 100.2 a.m.u and 138.0 a.m.u for the two peaks. This fitted function is shown as the curve on the figure while the experimental data are given by the histogram.

A second test of the sandwich technique was performed in a similar way but using, this time, the thermal neutron induced fission of ^{235}U. The sandwich was prepared as previously said and irradiations made at Simon Fraser University using the same neutron generator. The neutrons were slowed down to a thermal energy by interposing, before the sandwich, a thick block of paraffin.

The results are shown in Fig.26 to 28. Here, the average values of the fragments kinetic energy were found to be 103 MeV and 68 MeV for the light and heavy fragments respectively as shown in Fig.26. The total kinetic energy distribution from Fig.27 shows an average value of 171 MeV and a FWHM = 75 MeV.

Fig.24: Deduced total fission fragment kinetic energy
distribution for the system UF_4+14 MeV neutrons.
The solid curve is the result of a fit to a Gaussian function.

UF$_4$ + 14 MeV neutrons

NUMBER OF EVENTS

TOTAL ENERGY (MeV)

Fig.25: Deduced fission fragment mass distribution for the system UF_4+14 MeV neutrons. The solid curve is the result of a fit to the sum of two Gaussian functions.

UF$_4$ + 14 MeV neutrons

NUMBER OF EVENTS
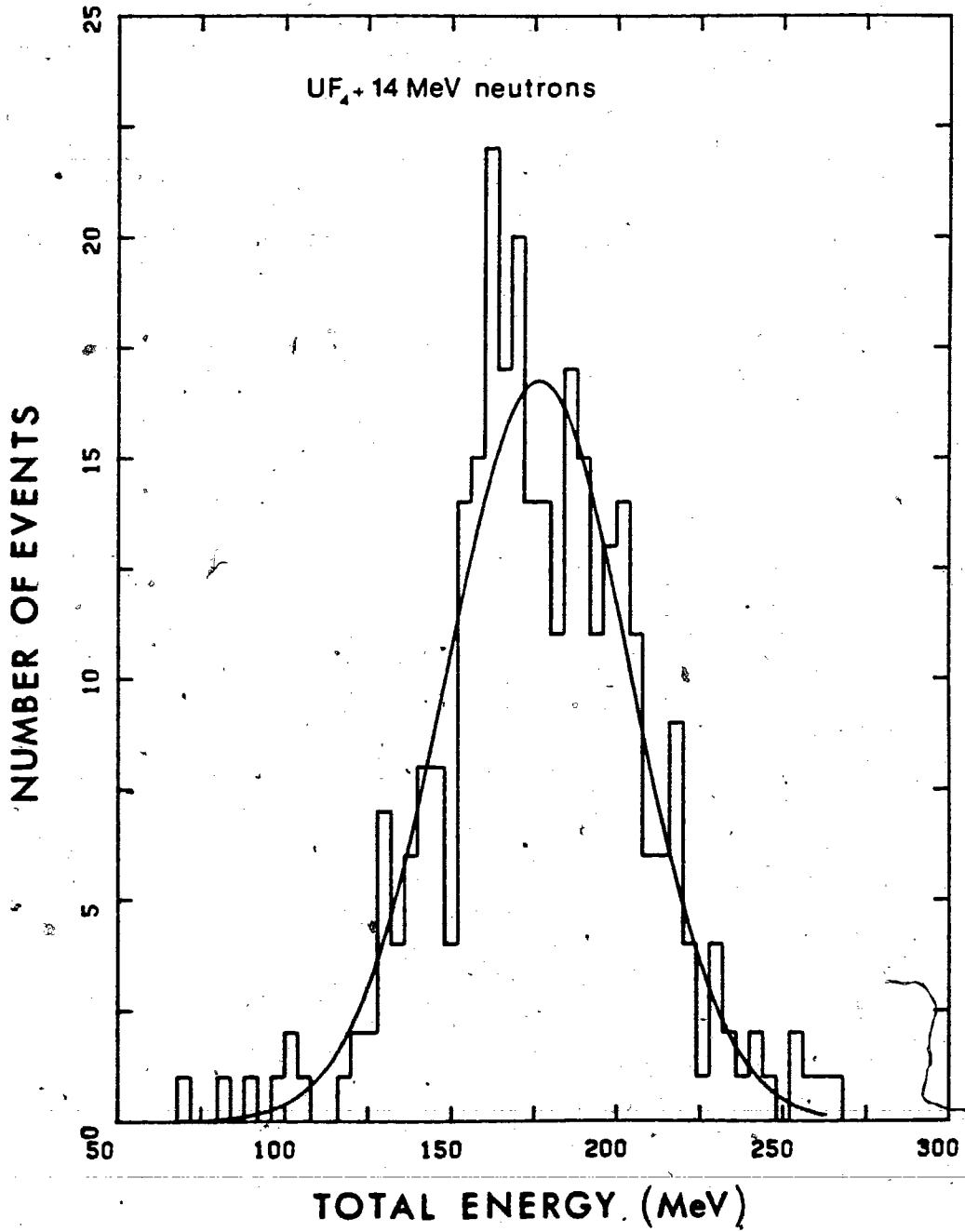
FRAGMENT MASS (a.m.u.)
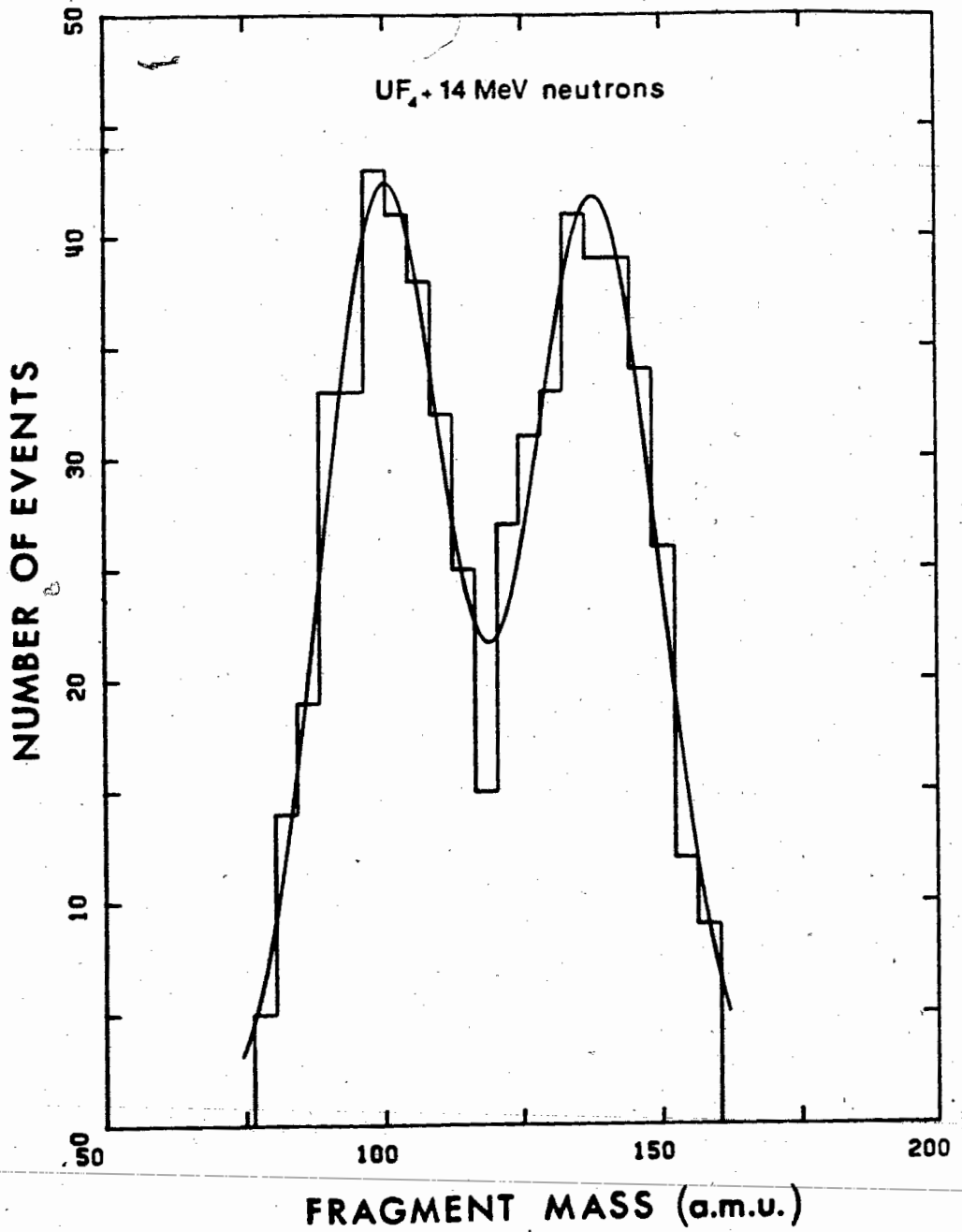
Fig.26: Deduced kinetic energy distributions for the
light and heavy fission fragments for the system UF_4+thermal
neutrons.

UF$_4$+ thermal neutrons

LIGHT   <E> = 103

HEAVY   <E> = 68

NUMBER OF EVENTS

FRAGMENT ENERGY (MeV)
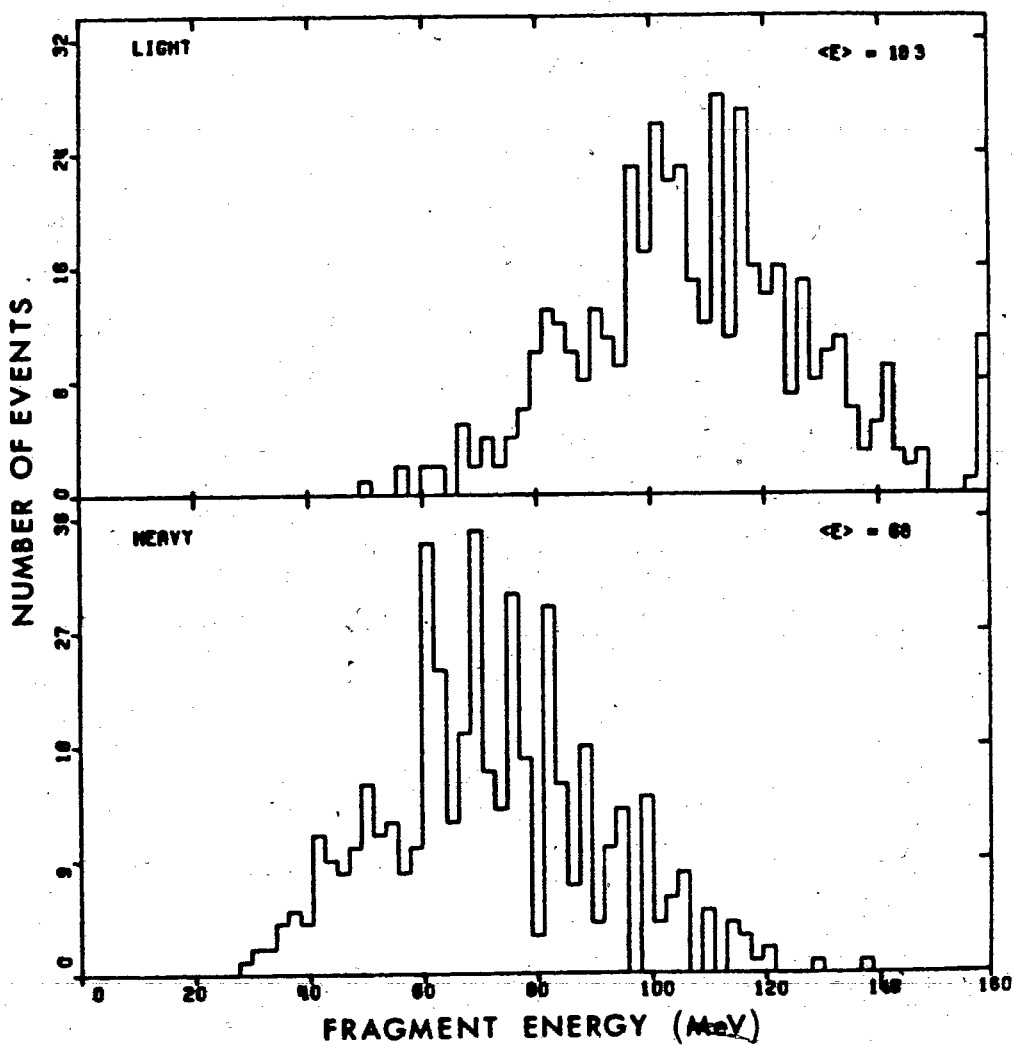
Fig.27: Deduced total fission fragment kinetic energy
distribution for the system UF_4+thermal neutrons.
The solid curve is the result of a fit to a Gaussian function.

UF$_4$+ thermal neutrons
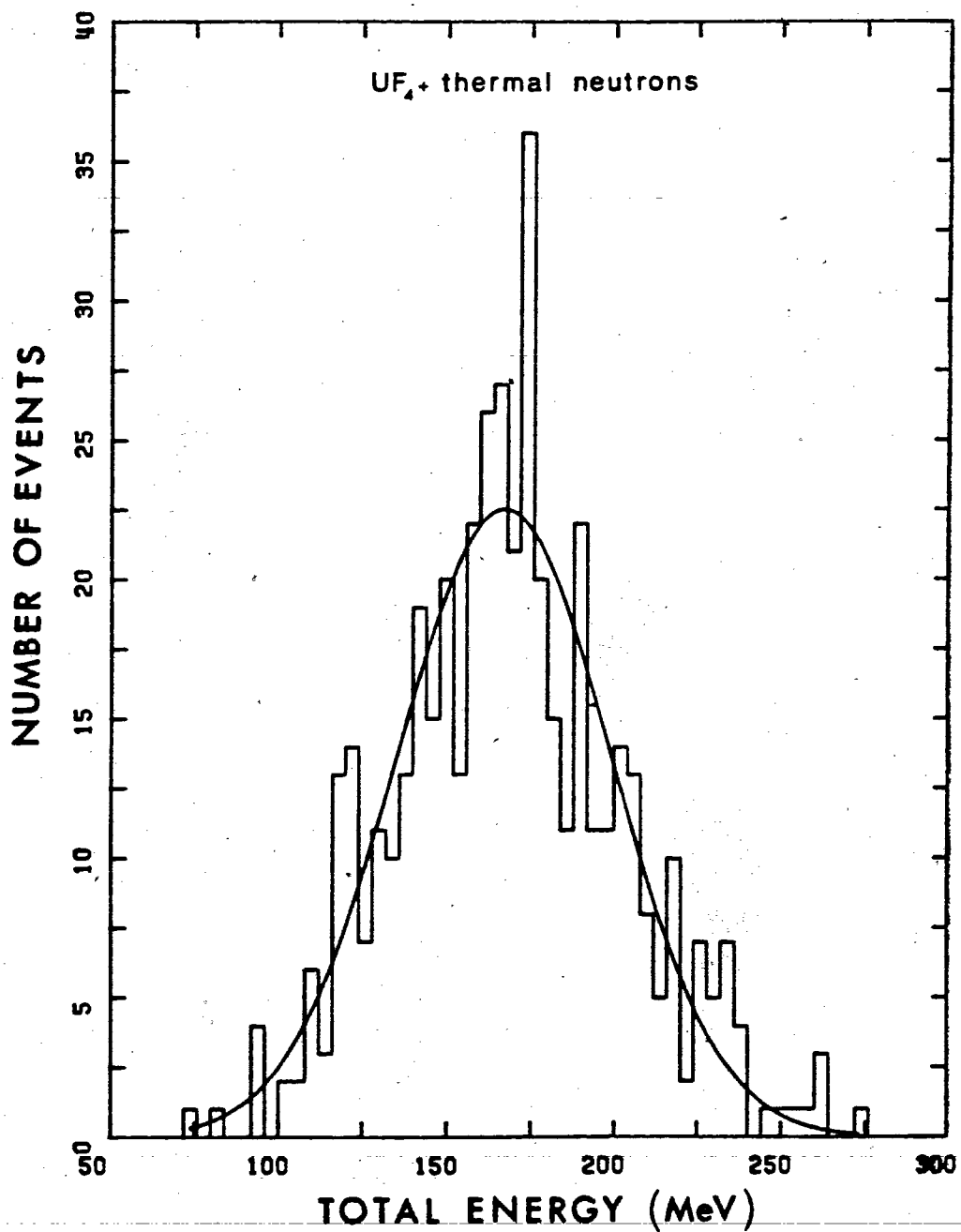
The mass distribution is given in Fig.28 where the curve represents the fitting of the data with the sum of two Gaussian curves. The most probable values of the two fragments masses were found to be 93.2 and 141.4 a.m.u.

The estimation of the uncertainties in these two cases was simplified by the fact that the mass of the fissioning system was known as was the neutron to proton ratio. Hence, the error on the energy was a result of the uncertainty in the measurements and in the mica calibration. The measurements of tracklength and depth are statistically distributed around an average value and the uncertainty in these measurements will not act strongly upon the position of the most probable value of the energy distribution, but will contribute to its width.

From the calibration curves Fig.11, it can be seen that the discrepancy between the general formula obtained in order to allow interpolations and the experimental data, will introduce an uncertainty in the energy. This uncertainty will vary depending upon the mass and energy of the fission fragments and can be estimated from Fig.11. In the case of uranium fission, the closest calibration curves corresponding to the fragments mass will be the iodine curve for the heavy fragment and the silver curve for the light

Fig.28: Deduced fission fragment mass distribution for the system UF_4+thermal neutrons. The solid curve is the result of a fit to the sum of two Gaussian functions.

UF$_4$ + thermal neutrons

NUMBER OF EVENTS

FRAGMENT MASS (a.m.u.)
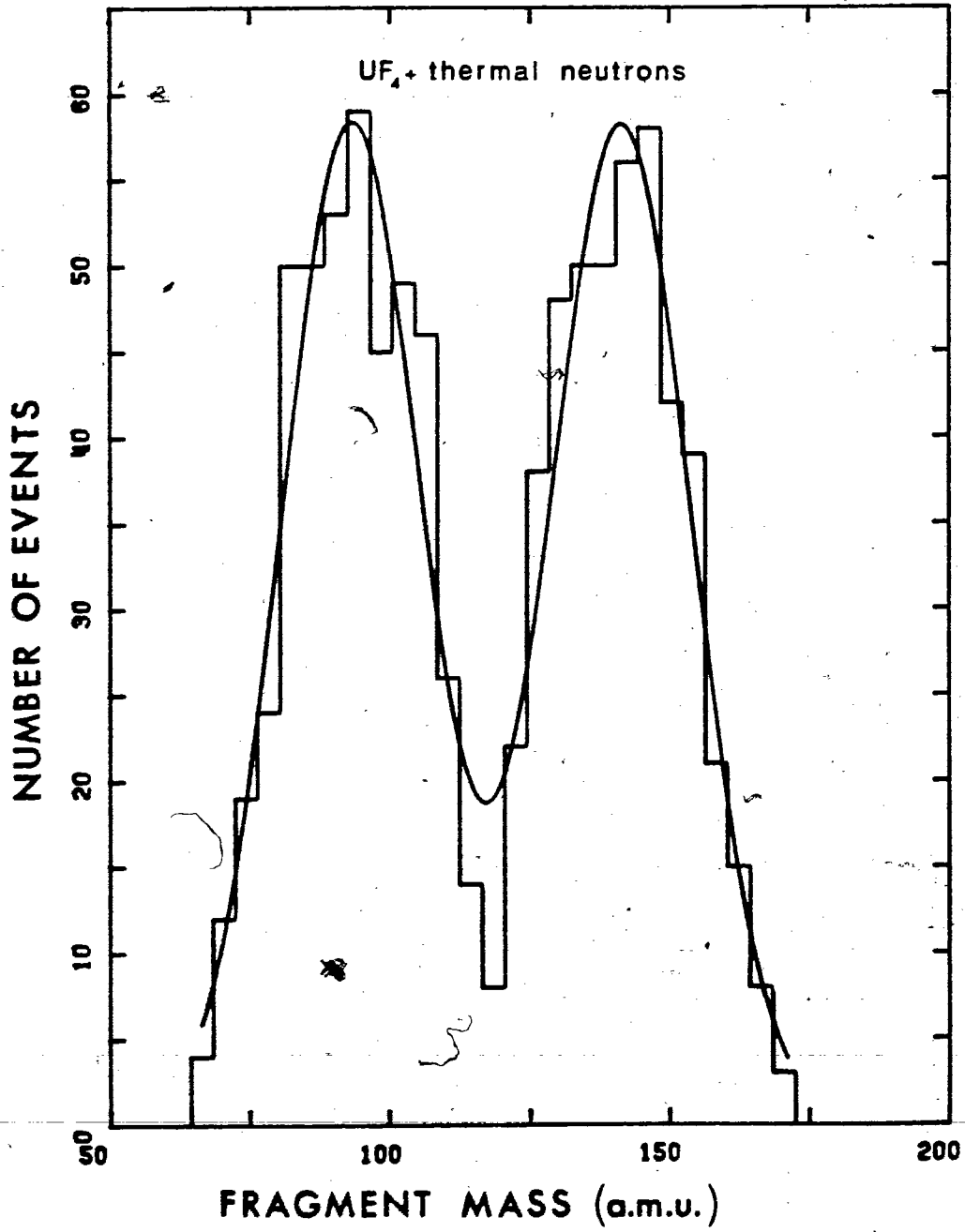
one. For the corresponding energies of around 70 MeV and
100 MeV, it can be estimated that the error is of the order
of 2 MeV and 8 MeV respectively. The error on the total
fission energy will then be around 10 MeV.

Since fragment energy and mass are inter-related for a
given tracklength, an estimation of the errors through
standard calculation cannot be easily performed. However,
the sensitivity of the results to some of the parameters can
be tested by means of the computer program. The influence of
the calibration was investigated by artificially changing
the general formula. It was found that the mass
distributions and the maxima of the peaks were quite
insensitive to such a change, the resulting shift being
smaller than the uncertainty in the fitting procedure.
Therefore, the error attributed to the mass of the fission
fragments will be that of the fitting process.

The calculated center of mass momentum will carry the
uncertainty in the energy and the mass. The estimated error
was 0.1 $(MeV.amu)^{1/2}$ in the case of 14 MeV neutron-induced
fission.

c) Comparison with literature

The interest in the knowledge of the average total kinetic energy of the fragments from uranium fission dates as far back as the discovery of the fission phenomenon itself in 1939. Henderson (Hen.40) made a calorimetric measurement of the energy released in a 13g sample of metallic natural uranium bombarded with moderated neutrons. He obtained a value of 177 MeV±1% per fissioning nucleus. This measurement was repeated in 1955 by Leachman and Schafer (Lea.55) and led to a value of 167.1±1.6 MeV. A previous measurement of the fragment velocities with a time of flight method carried out by Leachman (Lea.52) gave a result of 168±2 MeV. An independent calorimetric determination was made later by Gunn et al (Gun.57) who found a value of 166±2 MeV.

The study of mass yields, fine structure of the mass distributions, energy of each fragment, number of neutrons emitted etc.. led to a huge amount of publications on uranium fission induced by thermal neutrons. Only a few results will be presented here in order to compare with those of the present work. They are summarized in Table IV where the most probable values of the mass of the fragments

TABLE IV

$\langle A_H(amu)\rangle$	$\langle A_L(amu)\rangle$	$\langle E_H(MeV)\rangle$	$\langle E_L(MeV)\rangle$	$\langle E_{tot}(MeV)\rangle$	Reference
		67	98	165 ∓ 2	(Ste.57)
139.92±0.10	96.08±0.10	68.4 ±0.7	98.8 ± 1.0	168.3 ±1.7	(Mil.62).
139.43 σ = 5.36	96.57 σ = 5.36	70.34	101.56	171.9 ±1.4 σ = 10.9	(Sch.66)
		69.27±0.17 σ=8.32±0.01	100.02±0.26 σ=4.62±0.01	168.88±0.40 σ=11.01±0.02	(Asg.70)
138.7 σ= 5.60	97.3 σ= 5.6	70.8 σ= 7.5	100.6 σ= 5.2	171.4 ±0.2 σ= 10.7	(Asg.77).
138.8 σ= 5.7	97.2 σ= 5.7	70.6 σ= 7.6	100.4 σ= 5.1	171.0 ±0.4 σ= 10.7	(Asg.78)
139.5 ± 0.1 σ= 5.6 138.6	96.5 ± 0.1 σ= 5.6 94.9	70.4 ±0.2	101.4± 0.2	171.8 ±0.5 σ= 10.3	(Uni.74)
141.4 ± 0.8 σ = 12.7	93.2 ± 0.8 σ = 12.5	68 ± 8	103 ± 2	171 ± 10 σ= 32	Present work

(A_H=mass of the heavy fragment,A_L=mass of the light fragment), their energy (E_H,E_L) and the total kinetic energy (E_{tot}) are reported with the corresponding standard deviations when available.

As can be seen from this table, the results of the present study for the most probable values are in good agreement with the published data. However, the standard deviations obtained here are larger due to a poor resolution of the sandwich measurements compared to silicon surface barrier detectors.

The 14 MeV neutron-induced uranium fission has been less extensively studied and most of the work was done on ^{235}U isotope. Stevenson et al (Ste.60), by calorimetric measurement obtained an average total fragment kinetic energy of 174±4 MeV and 175±2 MeV for respectively ^{235}U and ^{238}U fission induced by 14 MeV neutrons. Comparison between literature and the present work is given in Table V.

A direct comparison can be made with the work of Ait-Salem et al (Ait.68) who measured ^{238}U fission induced by 15.3 MeV neutrons by means of acetylcelluloid track detectors in a sandwich configuration. The mass distribution obtained by these authors together with a fitting to the sum of two Gaussian curves is given in Fig.29. The fitting

TABLE V

$\langle A_H(amu)\rangle$	$\langle A_L(amu)\rangle$	$\langle E_H(MeV)\rangle$	$\langle E_L(MeV)\rangle$	$\langle E_{tot}(MeV)\rangle$	Reference
				175 ± 2	(Ste.60)
138.7				168.6± 3 σ = 12.2	(Gon.67)
137.4 136.0* σ= 8.9	100.0* σ = 8.9			168.5	(Ait.68)
		69 ± 1	96 ± 1	165 ± 1.4 166.4	(Are.72)
138.0±0.7 σ = 11.7	100.2±0.7 σ = 11.3	72 ± 8	106 ± 2	178 ± 10 σ = 27.8	Present work

♣ : results of the fitting of Ait-Salem et al. data with the sum of two gaussian functions.

Fig.29: Fission fragment mass distribution obtained from sandwich measurements made by Ait-Salem et al for the system ^{238}U+15.3 MeV neutrons. The solid curve is the result of a fit to the sum of two Gaussian functions.

UF$_4$ + 14 MeV neutrons
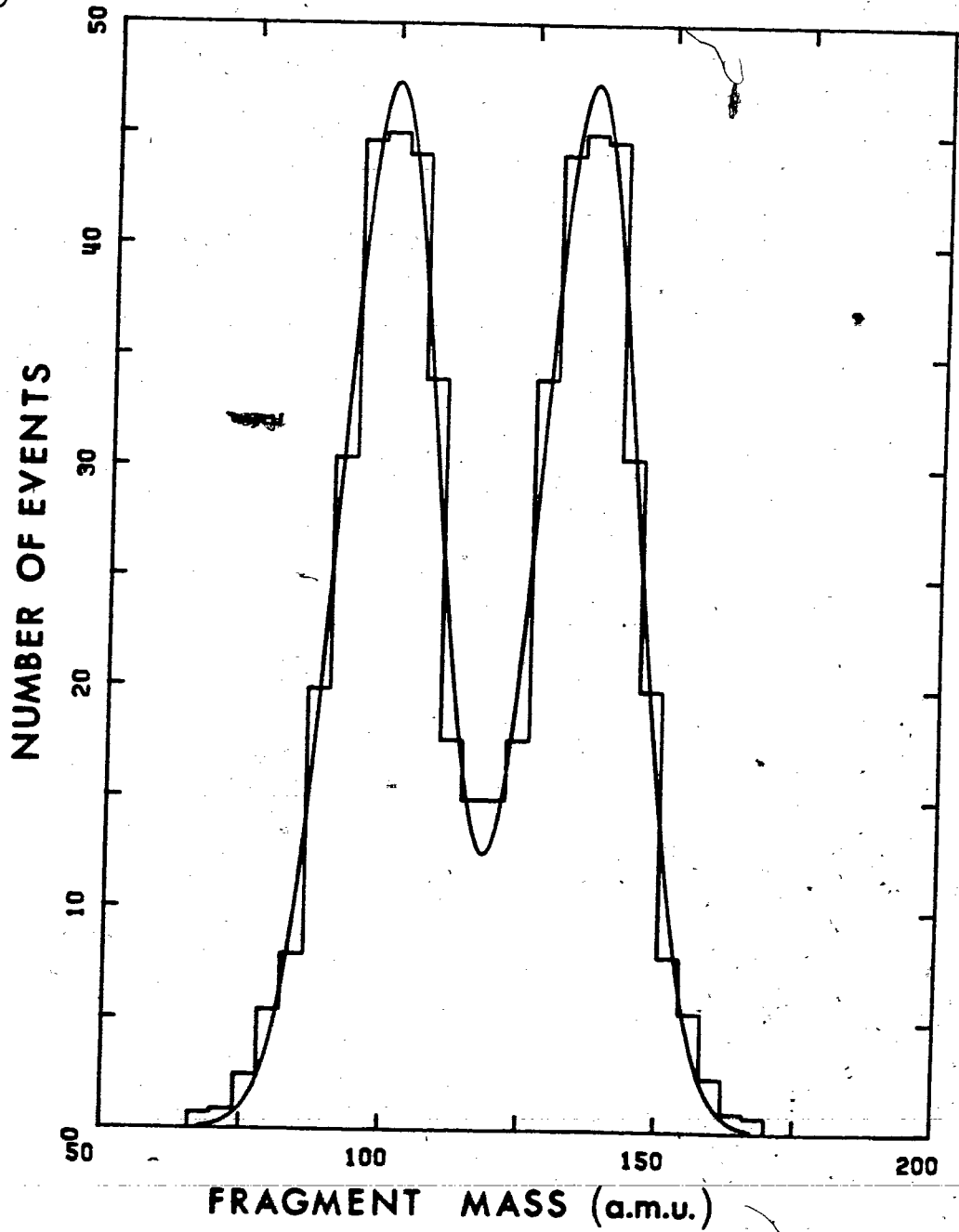
process gave 100.0±0.3 a.m.u and 136.0±0.3 a.m.u for the most probable values of the light and heavy fragment masses respectively and a standard deviation of 8.9 a.m.u for each peak.

The mass distributions obtained by these authors and in the present work are directly compared in Fig.30 where one can see that the agreement between the two is good. The distribution from the present study is here again slightly broader (FWHM=27 a.m.u against 21 a.m.u) which could be a result of poorer resolution with mica than with acetylcelluloid or/and of poorer statistics. Results of radiochemical measurements carried out by Cuninghame (Cun.57) and Broom (Bro.62) are also reported on the same figure.

3) Results

After the presentation of the experimental results, the influence of the parameters involved will be discussed and the results summarized on a tabular form.

a) Uranium fission

The results of uranium fission induced by 400 MeV π^+ mesons are shown in Fig.31 to 36.

Fig.30: Deduced fission fragment mass distribution for the system UF_4+14 MeV neutrons. The two histograms show the results of Ait-Salem et al (1) and the present study (2). The data represented by points are from radiochemical studies of Cuninghame (■) and Broom (●).
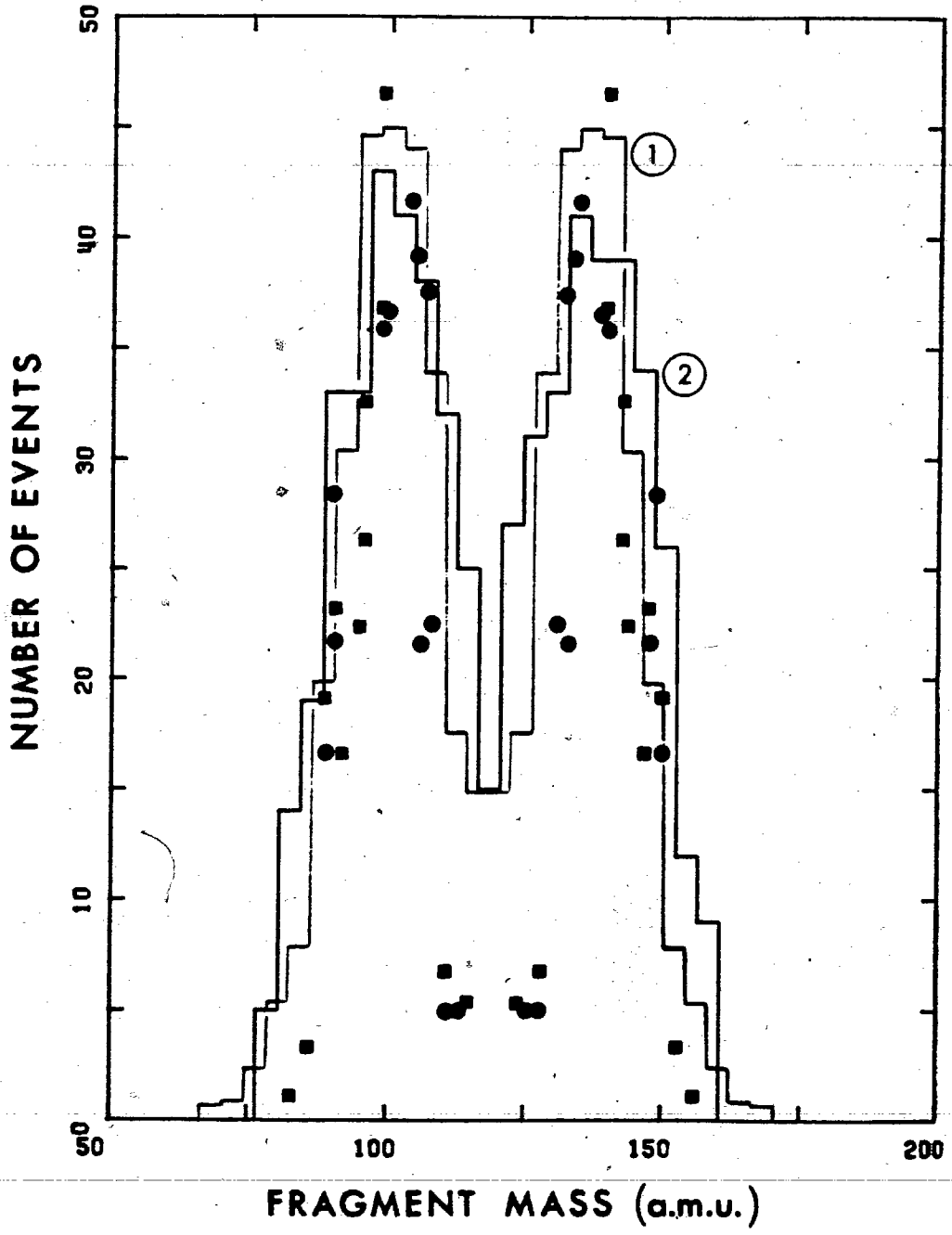
Fig.31 shows the tracklength distributions in both hemispheres. The difference in the average length between the forward and the backward hemisphere is much greater than in the case of 14 MeV neutrons induced fission, indicating a larger center of mass motion. The total tracklength distribution of Fig.32 has a FWHM of 3.5μ. The divergence in degrees between the direction of one track of a pair and the direction of the other is given in Fig.33. Here again, a larger value is obtained compared with that from 14 MeV-neutron fission, showing a larger center of mass momentum. From the distribution of this momentum on Fig.34, an average value of 15.3 (MeV.amu)$^{1/2}$ is obtained. The total kinetic energy distribution is given in Fig.35. The mass distribution of Fig.36 indicates a symetric fission process.

b) Gold fission

The tracklength distributions for the gold fission induced by 800 MeV protons are given in Fig.37 and 38 while the center of mass momentum distribution is shown in Fig.39. Fig.40 displays the total kinetic energy distribution with an average value of 123 MeV. The mass distribution of Fig.41 indicates a preferential splitting of the fissioning nuclei into two fragments of equal mass (symetric fission).

Fig.31: Fragment tracklength distributions in the forward
and backward hemispheres from mica sandwich measurements for
the system UF_4+400 MeV pions.

UF$_4$ + pions
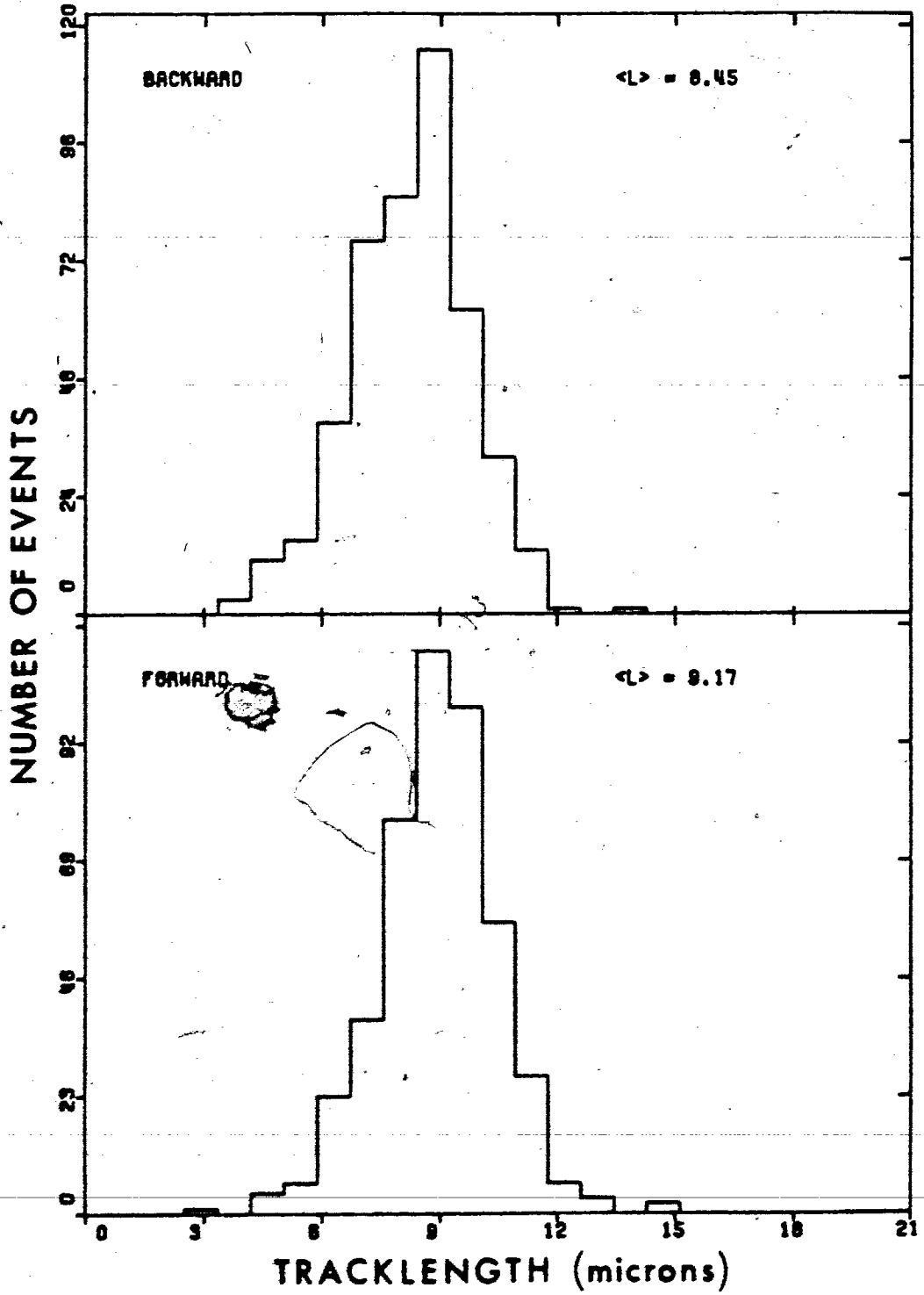
BACKWARD   <L> = 8.45

FORWARD   <L> = 8.17

NUMBER OF EVENTS

TRACKLENGTH (microns)

Fig.32: Distribution of the fragment tracklength sum
(forward and backward hemispheres added) for the system
UF_4+400 MeV pions.

NUMBER OF EVENTS

TRACKLENGTH (microns)

$<L> = 8.81$

UF_4 + pions

Fig.33: Distribution of angular divergence between the
fragment track directions for the system UF_4+400 MeV pions.

A histogram titled with annotations "<DIV> = 5.0" and "UF₄ + pions." The horizontal axis is labeled "DIVERGENCE (degrees)" ranging from -20 to 20. The vertical axis is labeled "NUMBER OF EVENTS" with values 0, 7, 14, 21, 28, 35, 42, 49, 56.
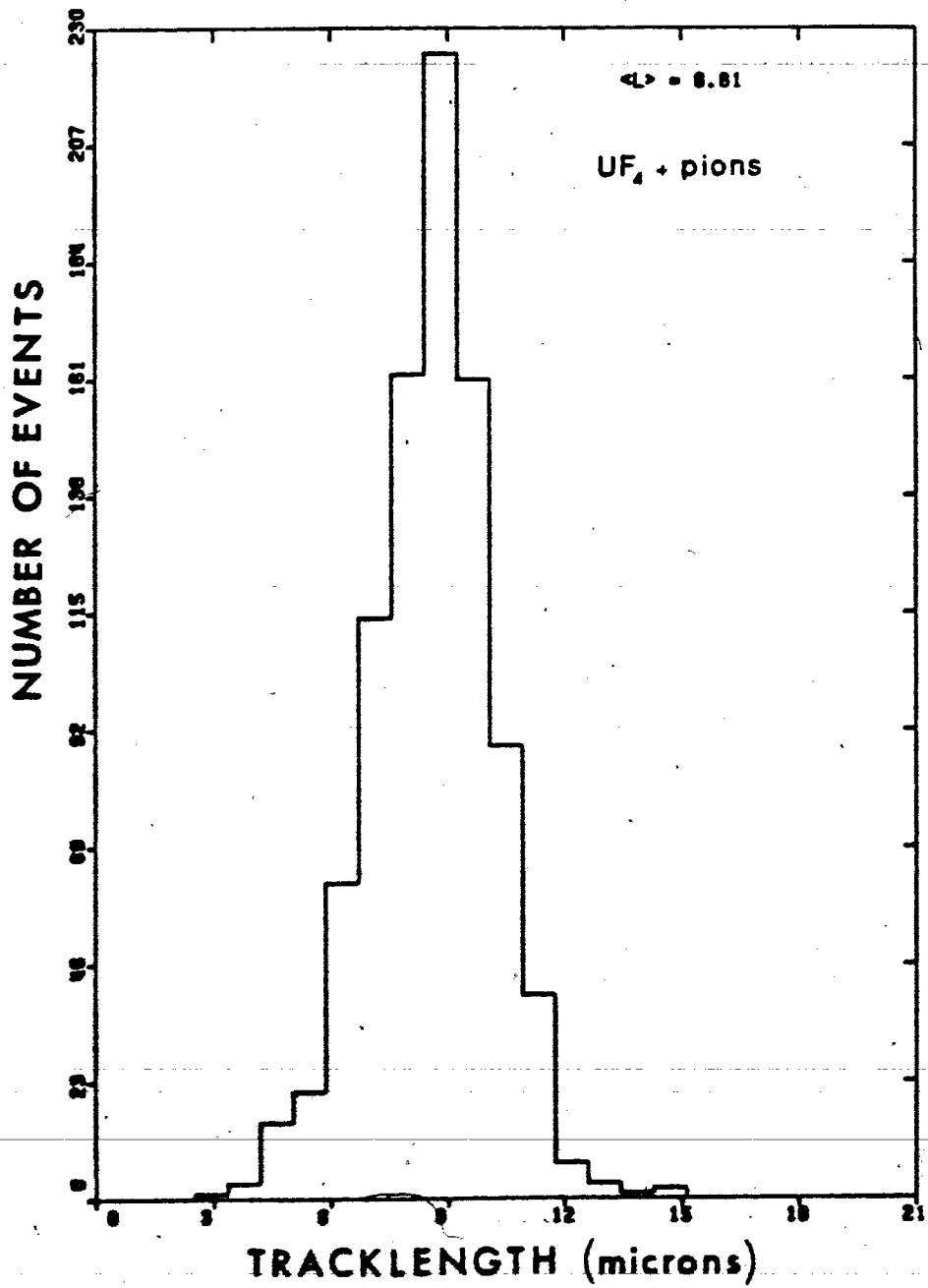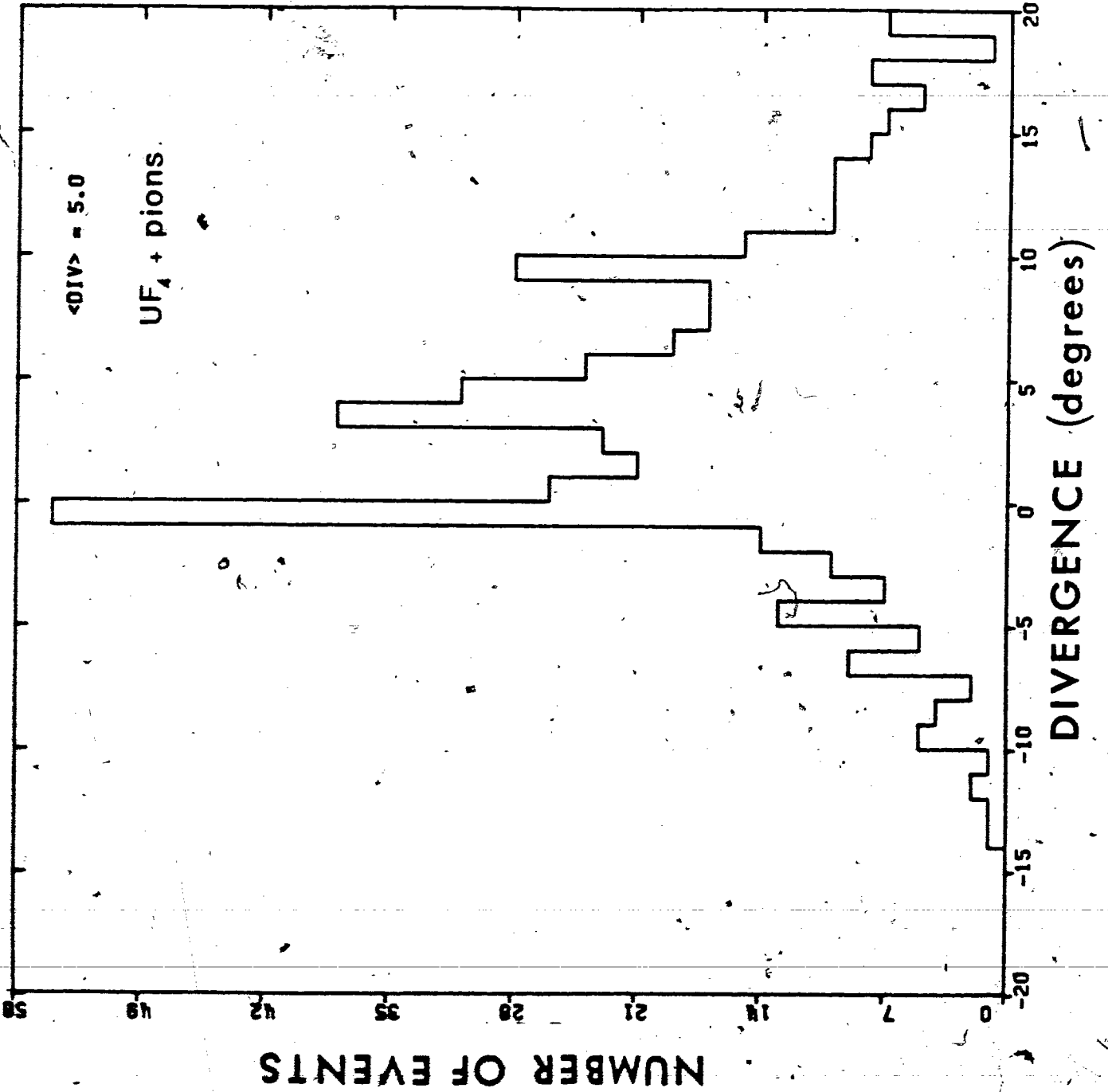
Fig.34: Distribution of the deduced center of mass momentum (p_{cm}) of the fissioning nuclei from system UF_4+400 MeV pions.

$\langle P \rangle = 15.3$

$UF_4 + pions$

CENTER OF MASS MOMENTUM $(MeV.amu)^{1/2}$

NUMBER OF EVENTS
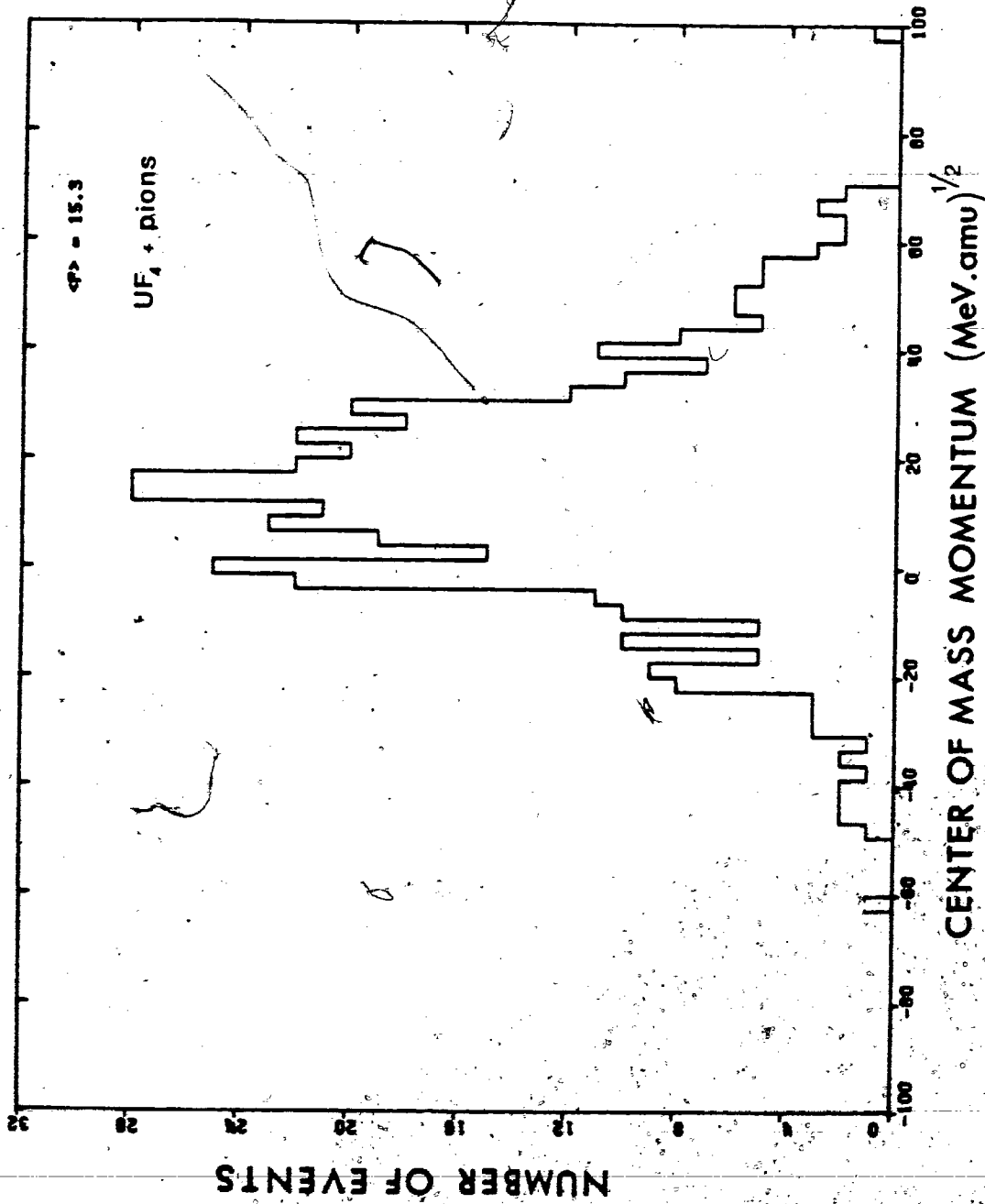
Fig.35: Deduced total fission fragment kinetic energy
distribution for the system UF_4+400 MeV pions.
The solid curve is the result of a fit to a Gaussian function.

UF$_4$ + pions
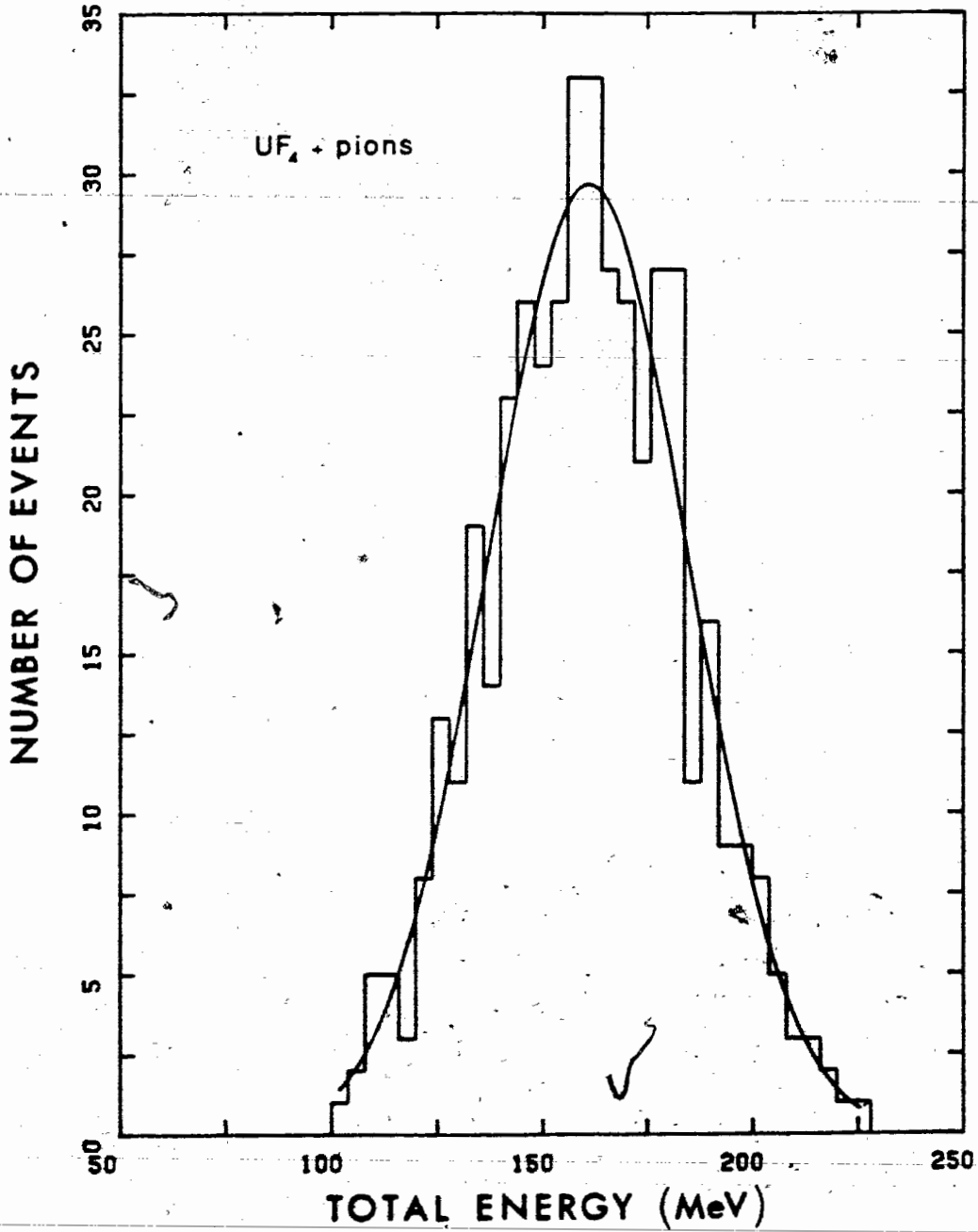
Fig.36: Deduced fission fragment mass distribution for
the system UF_4+400 MeV pions.
The solid curve is the result of a fit to a Gaussian function.

UF$_4$ + pions
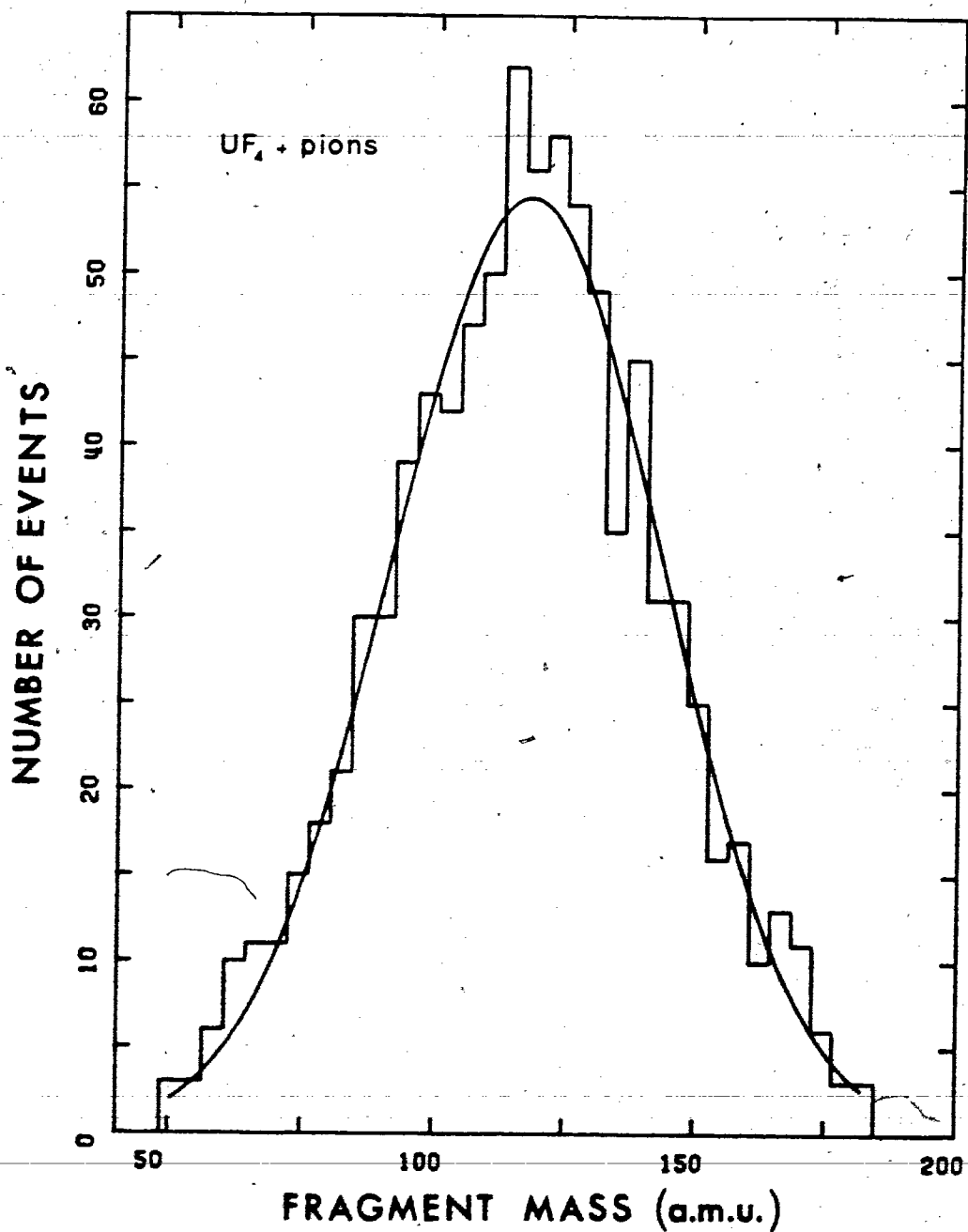
Fig.37: Fragment tracklength distributions in the forward
and backward hemispheres from mica sandwich measurements for
the system Au+860 MeV protons.

BACKWARD   <L> = 6.92
            Au + protons

FORWARD   <L> = 7.90

NUMBER OF EVENTS

TRACKLENGTH (microns)
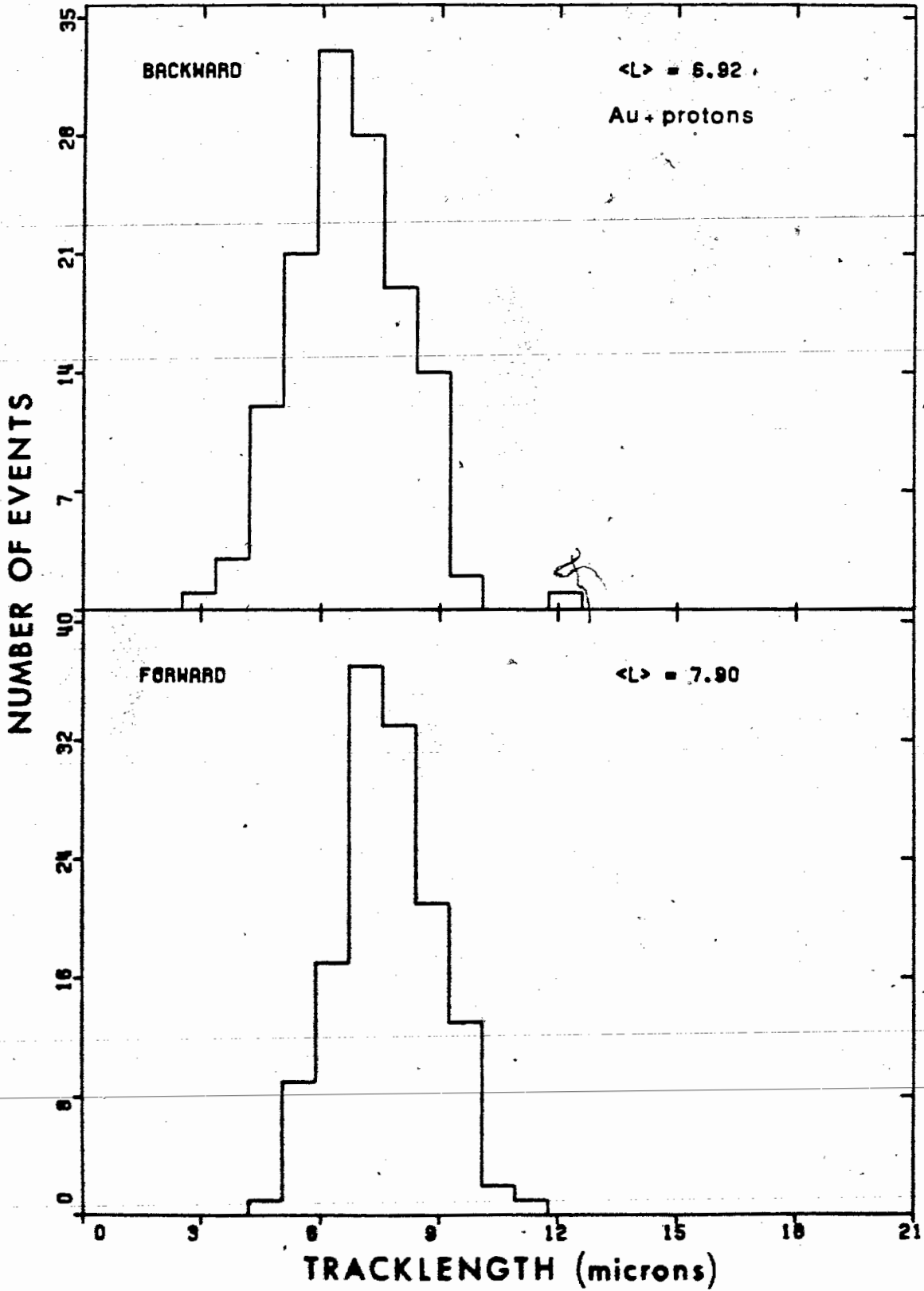
Fig.38: Distribution of the fragment tracklength sum
(forward and backward hemispheres added) for the system
Au+800 MeV protons.
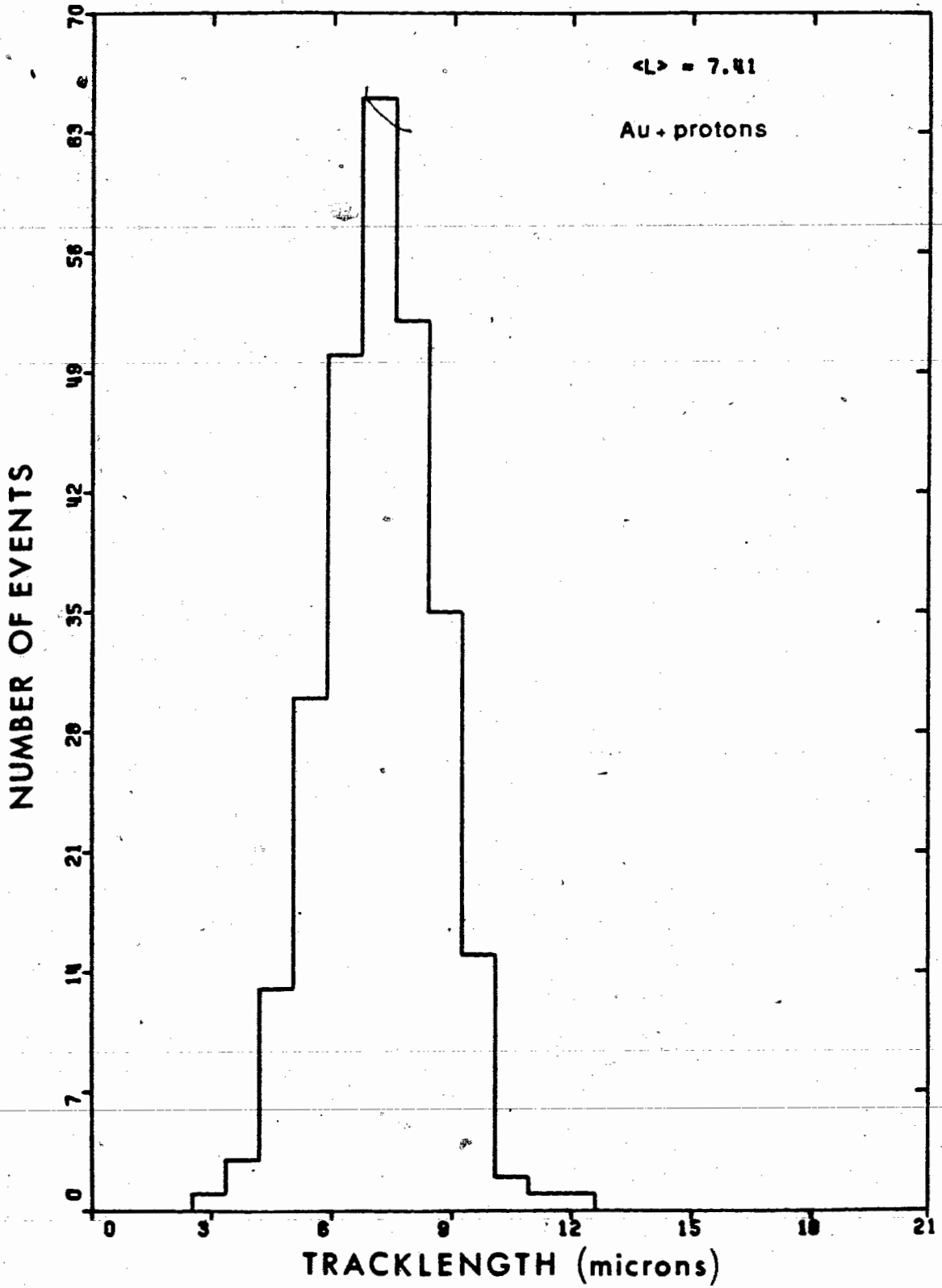
Fig.39: Distribution of the deduced center of mass
momentum (p_{cm}) of the fissioning nuclei from system
Au+800 MeV protons.
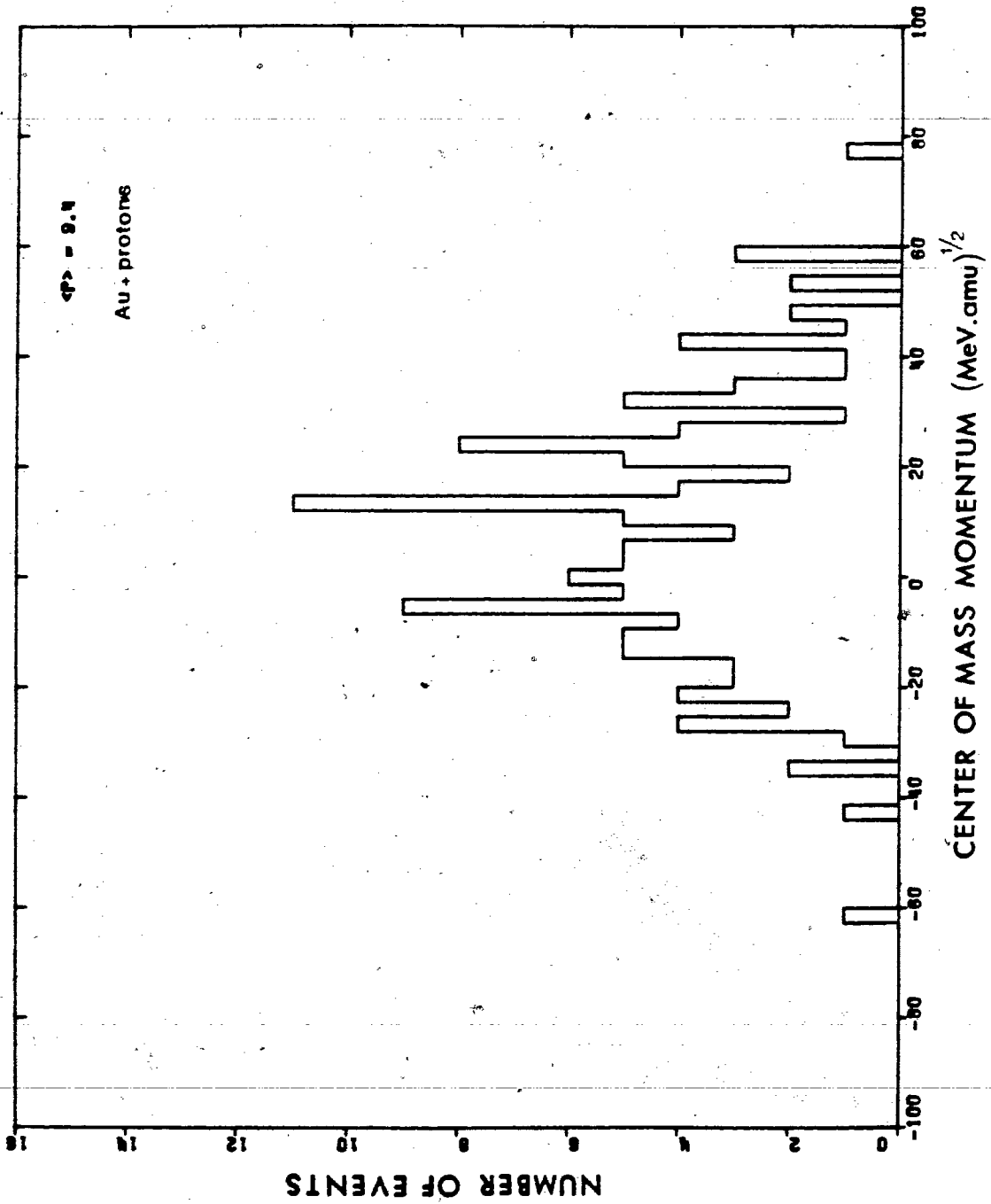
131 - a

Fig.40: Deduced total fission fragment kinetic energy
distribution for the system Au+800 MeV protons.
The solid curve is the result of a fit to a Gaussian function.

Au + protons

NUMBER OF EVENTS

TOTAL ENERGY (MeV)
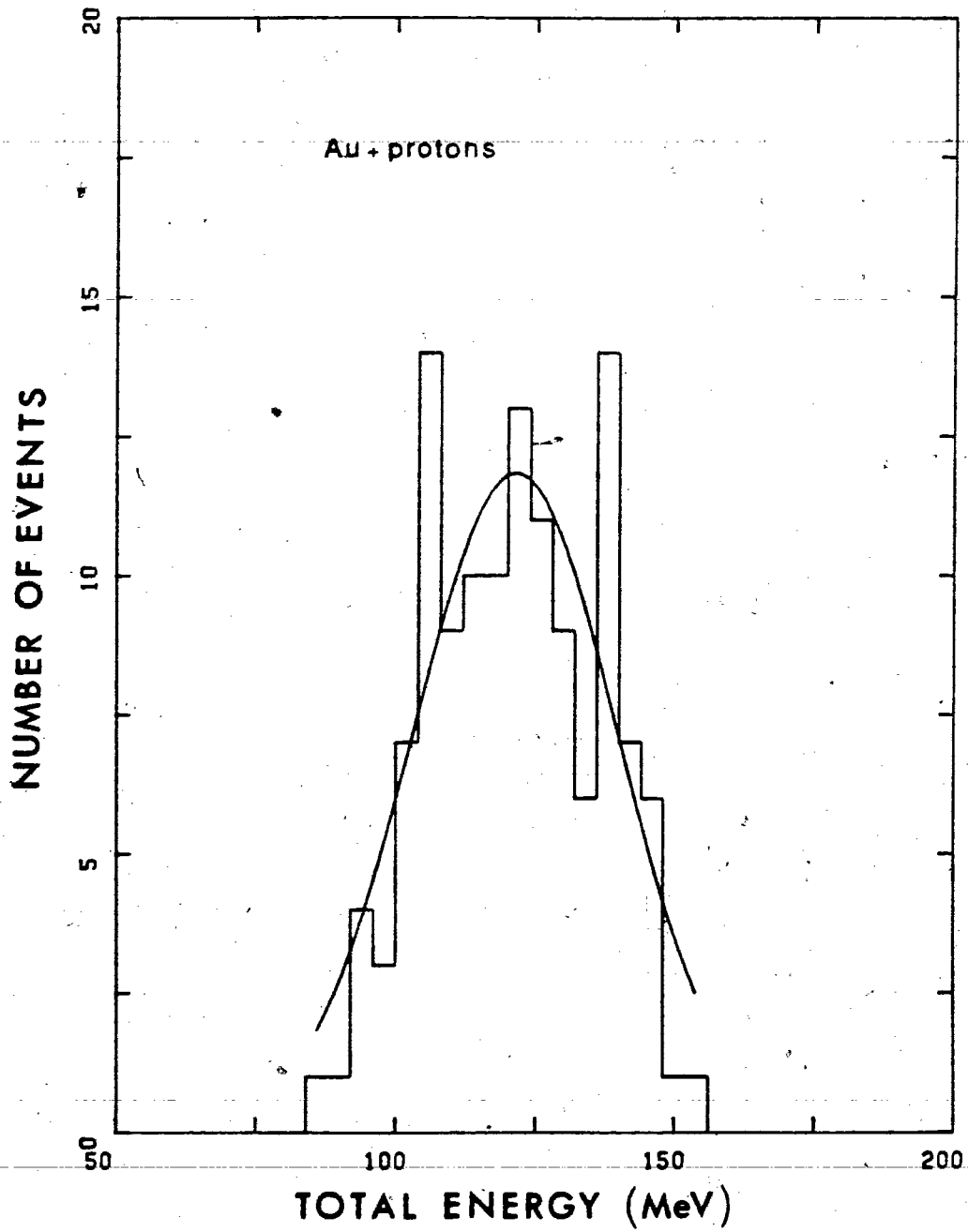
Fig.41: Deduced fission fragment mass distribution for
the system Au+800 MeV protons.
The solid curve is the result of a fit to a Gaussian function.
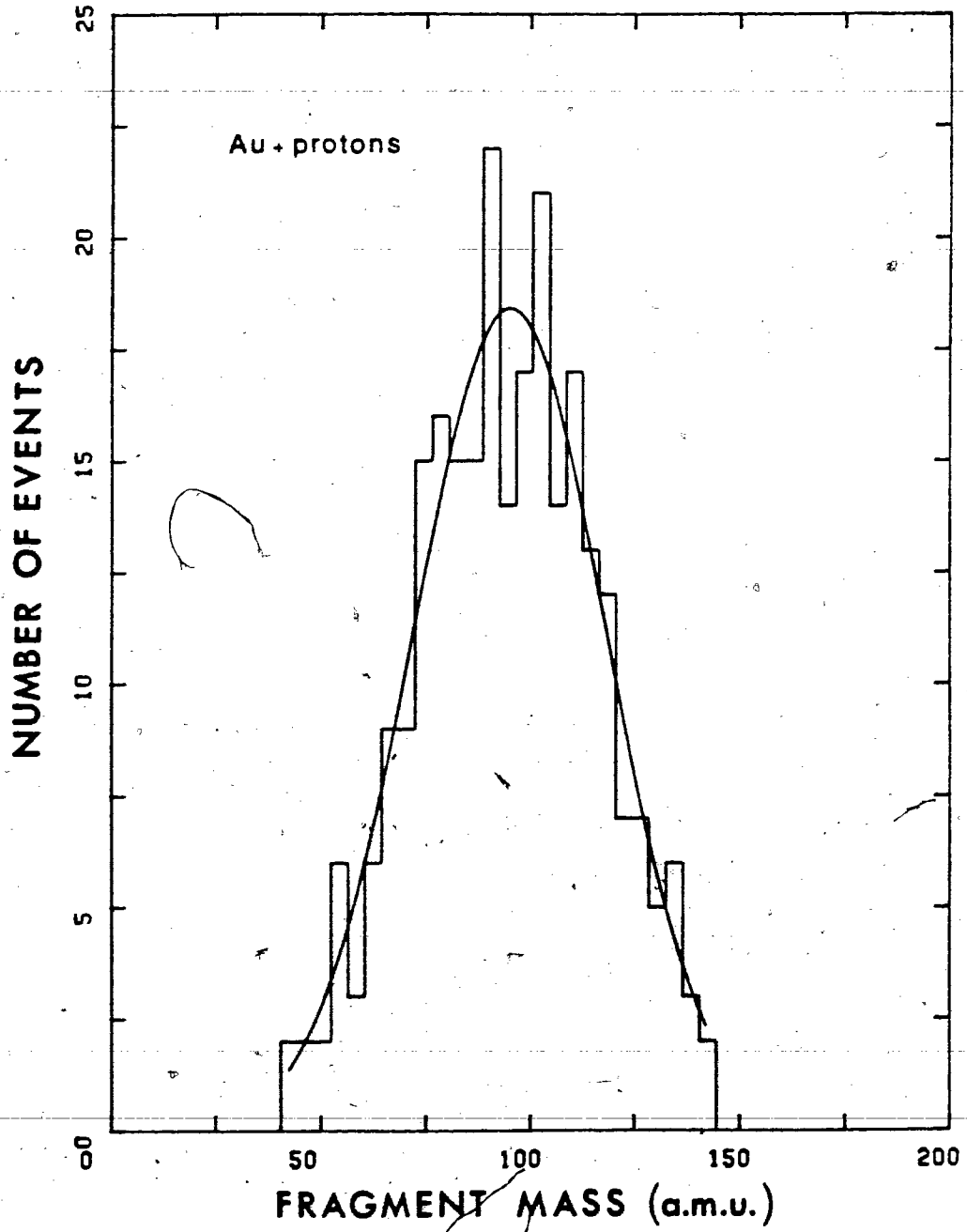
The same distributions in the case of gold fission induced by 400 MeV π^+ are given in Fig.42 to 46. They are respectively, the tracklength distributions in both hemispheres (Fig.42), the total tracklength (Fig.43), the center of mass momentum (Fig.44), the total kinetic energy (Fig.45) and the mass distribution (Fig.46).

c) Silver fission

In both cases of silver sandwiches irradiated with 800 MeV protons and 400 MeV π^+ mesons, fission tracks have been observed. However, these tracks were so short that they were very difficult to measure. The tracks having no recognizable direction, the coincidence between one track in one hemisphere and a track in the other hemisphere, was impossible to establish. These measurements of silver fission could only be made with a very low track density: if only one track at a time is present in the field of view, then, if another track is seen in the other mica, there is no certainty, but a good probability that they both belong to the same pair. However, the depth of these tracks would be very difficult to measure and subject to a large uncertainty.

Fig.42: Fragment tracklength distributions in the forward

and backward hemispheres from mica sandwich measurements for

the system Au+400 MeV pions.

BACKWARD   \<L\> = 7.26

Au + pions

FORWARD   \<L\> = 7.57

NUMBER OF EVENTS

TRACKLENGTH (microns)
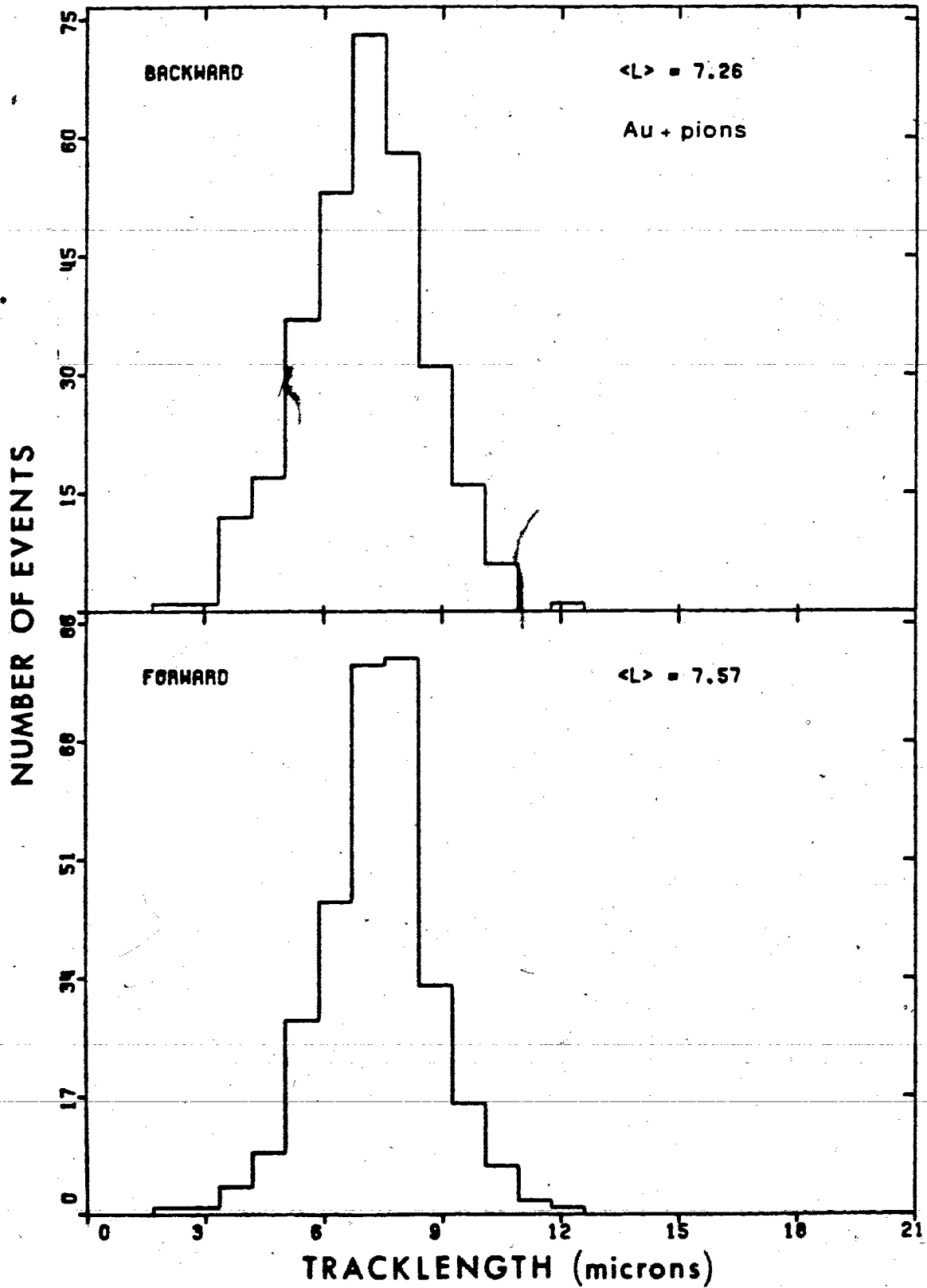
Fig.43: Distribution of the fragment tracklength sum
(forward and backward hemispheres added) for the system
Au+400 MeV pions.
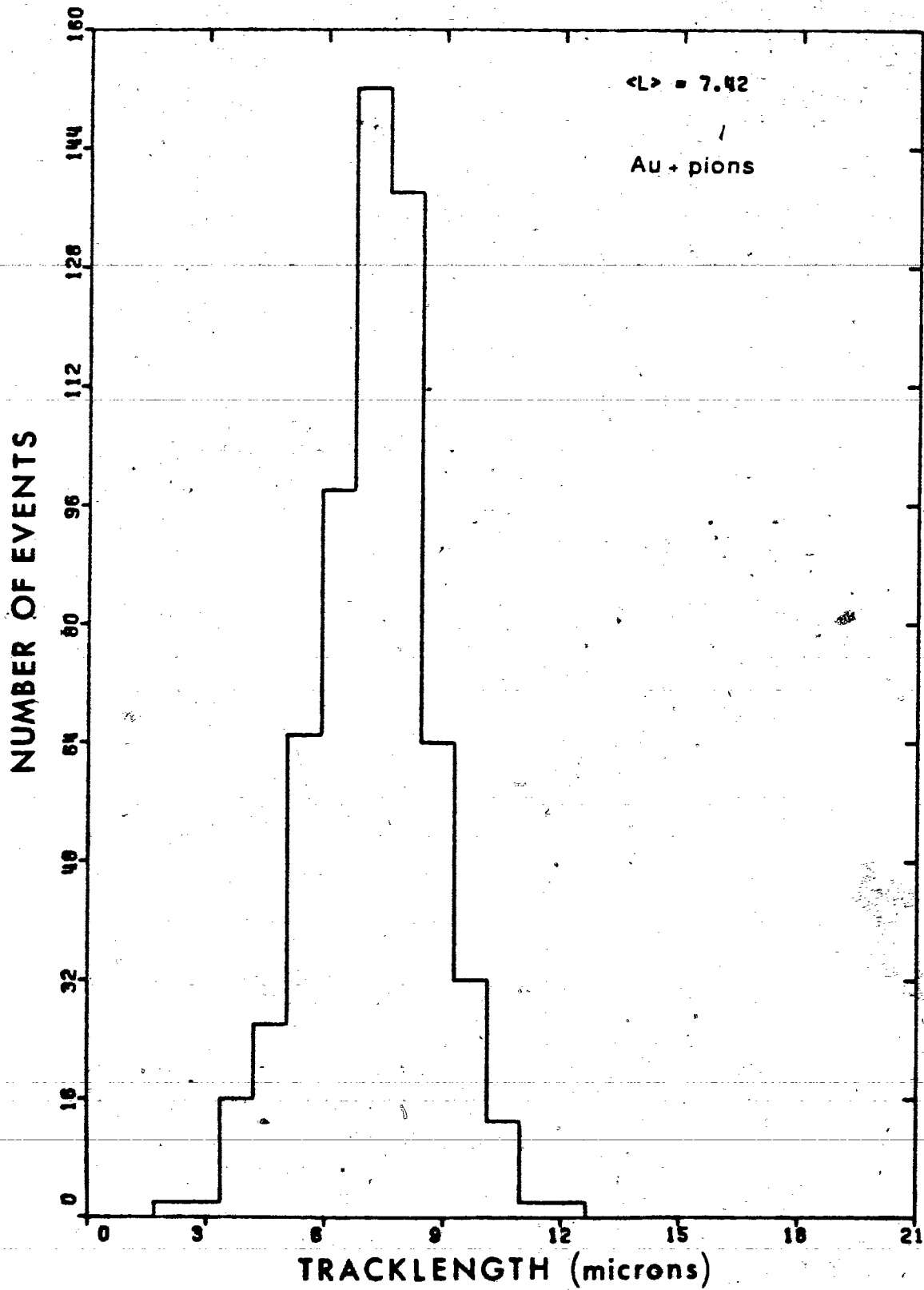
Fig.44: Distribution of the deduced center of mass momentum (p_{cm}) of the fissioning nuclei from system Au+400 MeV pions.
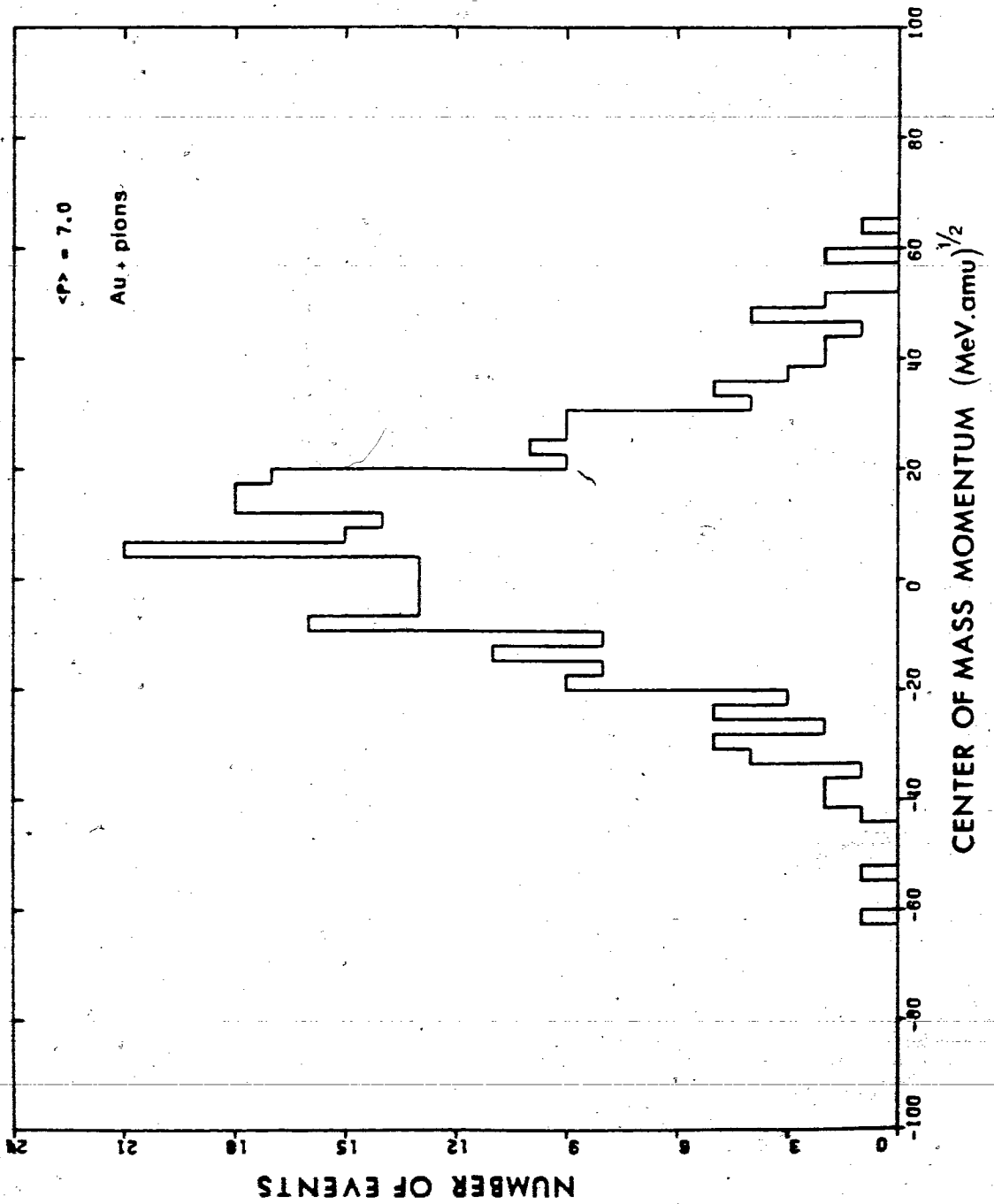
Histogram of NUMBER OF EVENTS versus CENTER OF MASS MOMENTUM $(MeV.amu)^{1/2}$. Labels: $<P> = 7.0$, Au + pions.

Fig.45: Deduced total fission fragment kinetic energy
distribution for the system Au+400 MeV pions.
The solid curve is the result of a fit to a Gaussian function.

Au + pions

NUMBER OF EVENTS

TOTAL ENERGY (MeV)
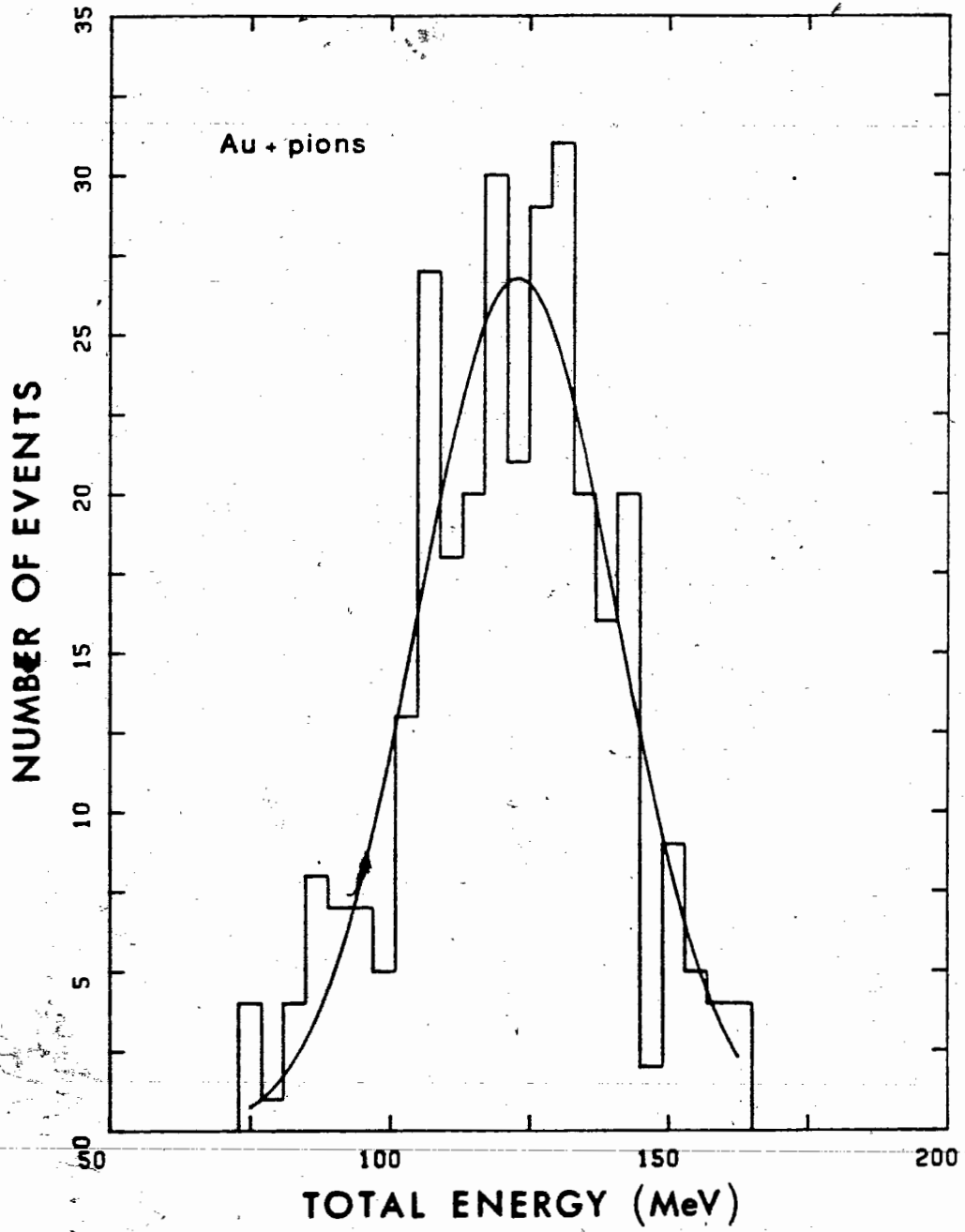
Fig.46: Deduced fission fragment mass distribution for
the system Au+400 MeV pions.
The solid curve is the result of a fit to a Gaussian function.

Au + pions
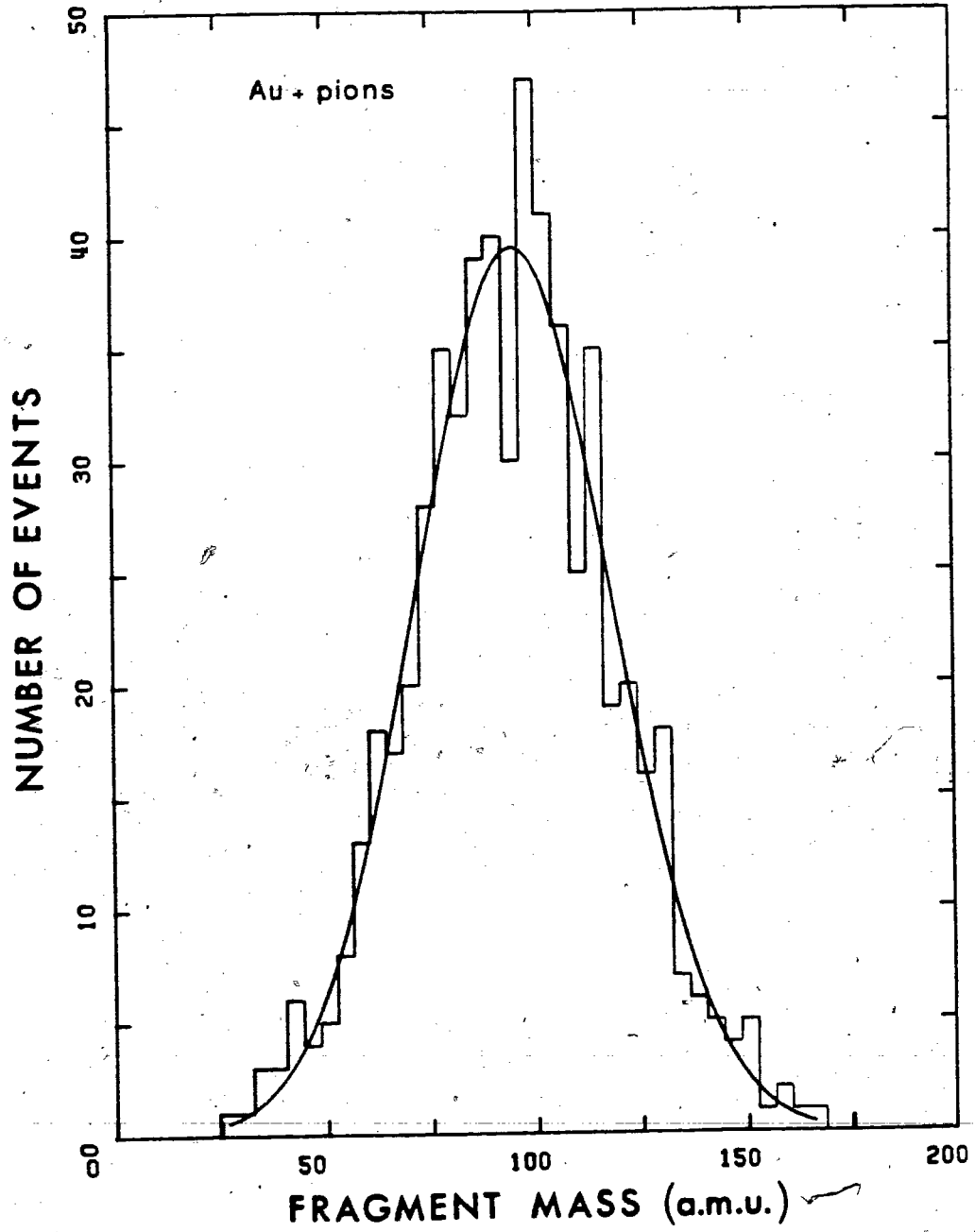
d) Influence of the different parameters on the derived data from the above neasurements

The value of the total kinetic energy will be influenced, as previously said, by the calibration formula but also by the choice of the fissioning mass and, as a consequence, by the corresponding neutron to proton ratio. The symetric fission of uranium will lead to fragment masses around 117 a.m.u which will lie between the silver and the iodine calibration curves. For an average 81 MeV energy, the discrepancy in the calibrations will give an uncertainty between 2 and 8 MeV for the silver and iodine curves respectively. An average value of 5 MeV can be taken and, as a consequence, the error on the total energy would be of the order of 10 MeV. This uncertainty of 5 MeV for each fragment is somewhat pessimistic if one considers that in the case of the silver calibration curve, the general formula gives an energy which is higher than the experimental one whereas it is the opposite situation in the case of the iodine calibration curve.

If the same procedure is followed for the case of gold, the fission fragments will be located between the krypton and the silver calibration curves. This will imply an

uncertainty of the order of 1 MeV for each fragment hence an error of 2 MeV on the total kinetic energy.

The uncertainties resulting from the choice of the fissioning nucleus mass and the neutron to proton ratio cannot be dissociated since one cannot change one without changing the other. Sensitivity of energy, mass and center of mass momentum was tested through the computer program by changing the mass or the charge of the fissioning system.

An error of 5 a.m.u in the value of the fissioning system mass (with the same charge Z and thus different Z/A ratios) led to an uncertainty of 5 MeV and 6 MeV in the fission energy of gold and uranium respectively. A change of one unit in the value of Z for a fixed mass gave a shift of 1.7 MeV in the total kinetic energy for gold while the energy in the case of uranium changed by 2.7 MeV. Therefore, an uncertainty of 5 a.m.u on the fissioning mass and one unit on its charge will lead to errors of 6.7 MeV and 8.7 MeV on the fission energy of gold and uranium respectively.

The mass distributions proved to be sensitive only to the given fissioning mass but not its charge. In all cases, the maximum of the mass distribution was located at half the value of the given total mass. Therefore, an uncertainty of

5 a.m.u in this mass will imply an error of 2.5 a.m.u on the average value of the fission fragment mass.

The value of the center of mass momentum is not very sensitive to the total mass or charge of the fissioning system. A change of 5 a.m.u in the mass and one unit in the charge will affect the value of p_{cm} by 0.2 (MeV.amu)$^{1/2}$ in the case of gold fission and 0.5 (MeV.amu)$^{1/2}$ for uranium.

The experimental results, with associated uncertainties and the corresponding standard deviations of the distributions are summarized in Table VI.

TABLE VI

Target	Projectile	Chosen fissio - ning system	Average mass of fission fragments in a.m.u	Average total energy in MeV	Average center of mass momentum (MeV.amu)$^{1/2}$
UF$_4$	400 MeV π$^+$	234 X 91	117.0 ± 2.5 σ = 26.1	162 ± 15 σ = 24	15.3 ± 0.5 σ = 14.7
Au	800 MeV p	190 X 77	95.0 ± 2.5 σ = 23.1	123 ± 9 σ = 18.3	9.4 ± 0.2 σ = 14.0
Au	400 MeV π$^+$	190 X 77	95.0 ± 2.5 σ = 23.4	123 ± 9 σ = 17.9	7.0 ± 0.2 σ = 13.8

III EXPERIMENTS CONDUCTED WITH SEMI-CONDUCTOR DETECTORS

A) Experimental techniques

1) Experimental set-up

These experiments were carried out at TRIUMF at the University of British Columbia using a proton beam delivered by the TRIUMF cyclotron. This cyclotron accelerates H$^-$ ions and several proton beams can be extracted by interception of the H$^-$ internal beam with appropriately located stripping foils. The proton beam energies can be chosen from 180 MeV to 525 MeV but irradiations in the present work were performed at a 480 MeV bombarding energy, the highest energy available for which beam delivery was most reliable.

Targets and detectors were located inside a scattering chamber which is located in the Beam Line 4A at the facility. This chamber (about 1.5 m in diameter) contained four arms for mounting detectors which could be moved and positioned to 0.1 degree accuracy. A multiple target ladder

(holding up to four targets at a time) was located in the center of the chamber and could be raised or lowered to position the desired target into the beam. All arms and target ladder were remotely controlled from an area where electronic equipment and the data acquisition system were located. The electronic equipment is shown in block diagram form in Fig.47, Fig.48, Fig.49.

The fission fragments were registered in two silicon surface barrier detectors (ORTEC model BF-040-400-60) whose active area was 400 mm^2. The sensitive depth was given by the manufacturer as 60 μ minimum and the gold electrode located in front of the detector had a thickness of 40 μg.cm^{-2}.

These detectors and the associated amplifier systems were calibrated in energy before and after each experiment using fragments of known energy from the spontaneous fission of ^{252}Cf.

2) Target preparation

Gold, bismuth and uranium tetrafluoride targets were prepared by vacuum deposition onto a VYNS backing. As in section (II-A-1-b) the target thickness was obtained by weighing. VYNS resin is a polyvinylchloride-acetate

Fig.47: Block diagram of electronic apparatus employed in measurements of angular distributions. The events were recorded on tape by a PDP 15 computer.
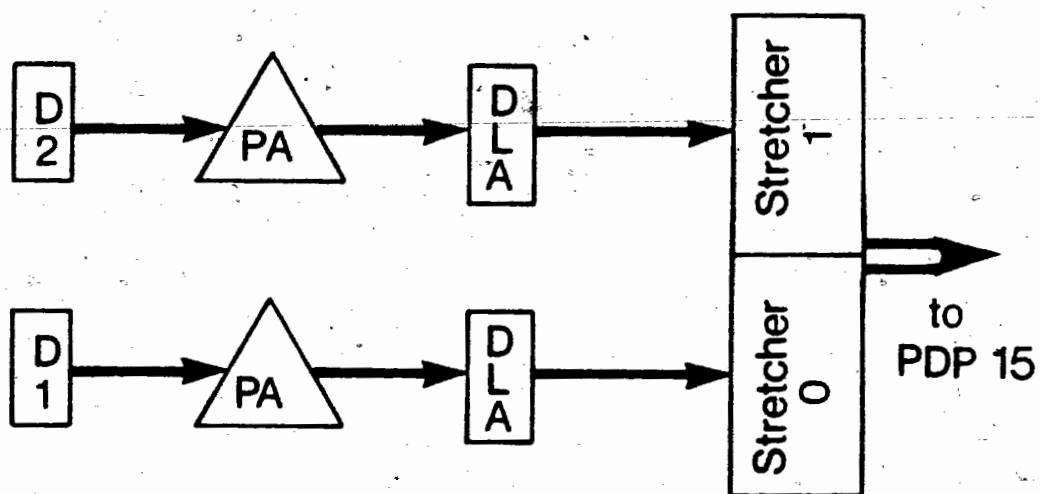
D1, D2 : detectors
PA : preamplifier (ORTEC 125)
DLA : delay line amplifier (ORTEC 460)

Fig.48: Block diagram of electronic apparatus employed in measurements of angular correlations.
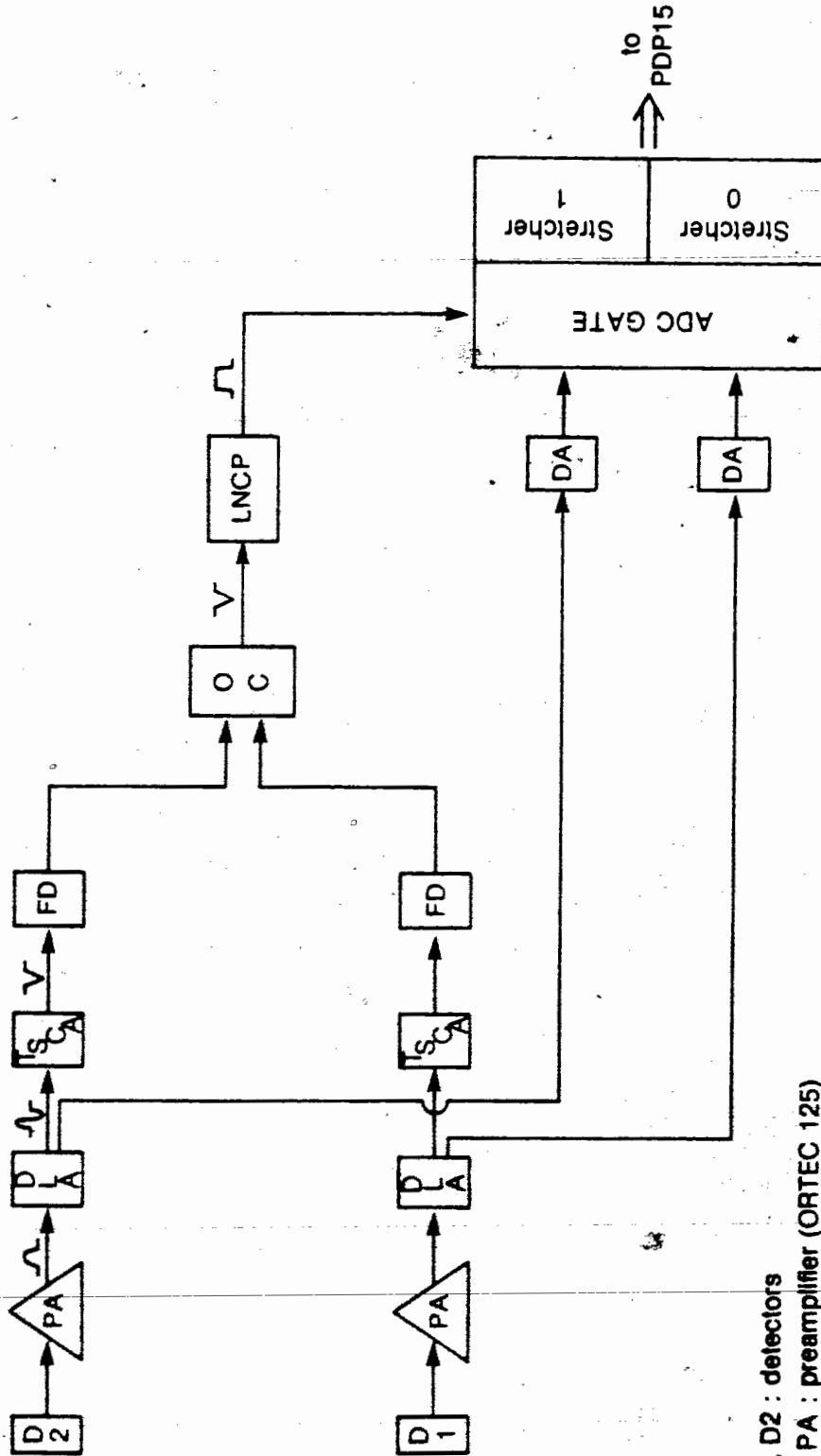
D1, D2 : detectors

PA : preamplifier (ORTEC 125)

DLA : delay line amplifier (ORTEC 460)

TSCA : timing single channel analyser (ORTEC 455)

FD : fast discriminator (Le Croy 621 BLZ)

OC : overlap coincidence (Le Croy 364 ALP)

DA : delay amplifier (ORTEC 427)

LCNP : logic converter negative to positive (TRIUMF C202)

Fig.49: Block diagram of electronic apparatus employed in measurements of energy plus time of flight between fission fragments.

to PDP15
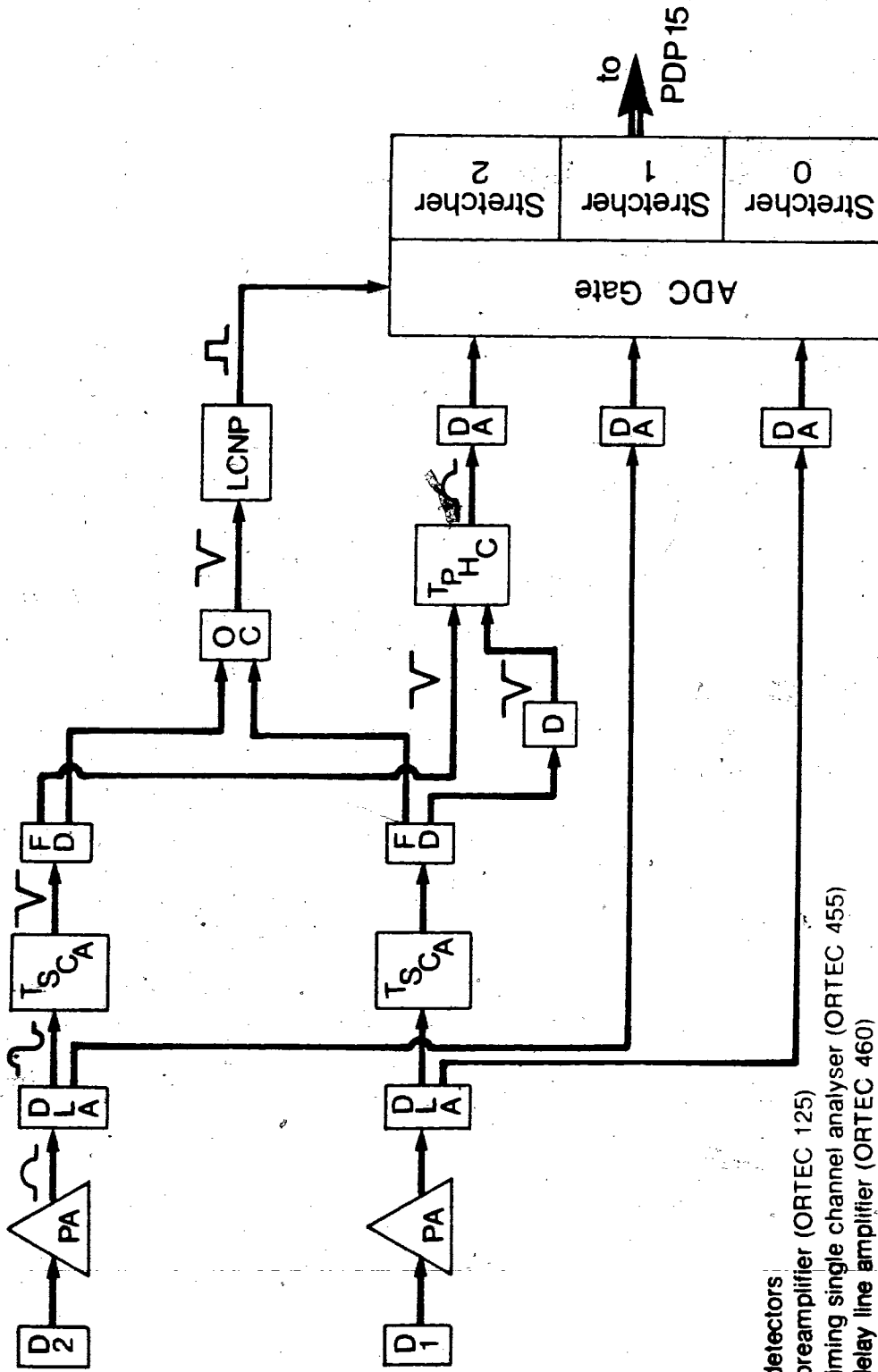
D1. D2 : detectors
PA : preamplifier (ORTEC 125)
TSCA : timing single channel analyser (ORTEC 455)
DLA : delay line amplifier (ORTEC 460)
FD : fast discriminator (LeCroy 621 BLZ)
OC : overlap coincidence (LeCroy 364 ALP)
LCNP : logic converter negative to positive (TRIUMF C202)
D : delay box (TRIUMF B007)
TPHC : time to pulse height converter (ORTEC 467)
DA : delay amplifier (ORTEC 427)
ADC : analog to digital converter

copolymer which has been found to produce good quality films with excellent chemical resistance and tensile strength (Pat.55). The VYNS as a white powder is first dissolved in cyclohexanone. Then, a small amount of the solution is allowed to expand on the surface of a water-filled container at room temperature. The thickness of the film can be controlled by the speed of expansion. It is finally lifted from the water and placed onto the appropriate aluminum frames. The film thickness in the range 10-50 μg.cm^{-2} can be determined visually with good precision ($\pm$ 5μg.cm^{-2}) by the colour changes from reflected light (Pat.55). The homogeneity can also be checked by visual examination.

No thorium compounds tried were found to give satisfactory results under vacuum deposition. The thorium targets were therefore prepared differently : a water solution of thorium nitrate (Th(NO$_3$)$_4$ 4H$_2$O from Fisher Scientific Company) of known concentration was prepared. An area of the VYNS film was then delimited precisely by wetting with a water solution of insulin as a wetting agent. A known amount of thorium nitrate solution was then deposited on this area and evaporated by infra-red heating, with a constant rotational movement in order to improve the homogeneity. The thickness of these targets was calculated

from the area of the dry spot (generally around 4 to 5 cm^2) and the weight of thorium deposited, and was subject to a greater uncertainty than the targets prepared by vacuum deposition, as was the target homogeneity. Attempts to measure the target homogeneity by alpha-particle backscattering were thwarted by the fragility of the targets, especially after their exposure to vacuum.

The targets used in the experiments with semi-conductor detectors had the following characteristics:

Target element	Target thickness ($\mu g.cm^{-2}$)	VYNS backing thickness ($\mu g.cm^{-2}$)	Frame size
Au	256 ± 4	35 ± 3	8.2x6.3 cm^2
Bi	210 ± 3	35 ± 3	8.2x6.3 cm^2
UF$_4$	40 ± 2	35 ± 3	8.2x6.3 cm^2
Th	51 ± 6	35 ± 3	8.2x6.3 cm^2

3) Types of measurements

For all measurements, two fission detectors were

employed: they were set at different positions with respect to the beam and registered single or coincident events, depending upon the type of measurement to be carried out. The various schemes of electronic apparatus are shown in Fig.47, Fig.48, Fig.49.

a) Angular distributions

One of the fission detectors ,used as a monitor, was left at a 90° angle with respect to the beam while the other was moved from 20° to 160°. For a known number of fission fragments registered by the monitor counter, fragment energy spectra were registered from the movable detector (without coincidence requirements) for a series of angles with respect to the beam direction. The target was oriented at a 45° angle with respect to the beam and two measurements were taken with the movable detector at 90° : once with the detector looking directly at the target material and once through the backing. Thus, from the energy difference between these two target positions, the fission fragments' energy loss in the backing material was determined for this particular angle and corrected for at all other angles of measurement. The magnitude of this correction at a 90° angle was of the order of 5 MeV.

While both detectors were registering single events, it could be shown that these single events were in fact due to fission fragments. The spectra obtained from both detectors were gaussian distributions whose maxima gave a most probable value of the energy in the range of 60 to 80 MeV. This energy is far too large to be deposited in the known detector thickness by possible lighter fragments produced from the reaction systems studied. From range-energy curves for charged particles in silicon, it can be deduced that the maximum energy deposited in a 60 µ thickness of silicon (i.e the detector's sensitive depth) is 2.3 MeV for protons and 9.2 MeV for alpha particles. Thus, the events corresponding to background from this source could be easily discriminated. Heavier fragments than alphas (and other than fission fragments) are produced with probabilities much too small to account for the intensities observed and their energy spectra are of a quite different form. Secondly, when a coincidence condition was imposed requiring simultaneous registration of two such energetic particles, the angular correlation for such events was found to be strong and centered near 180° while the energy spectrum was identical to that registered for single events. Thus, the

latter spectrum is clearly that of binary fission fragments
from the subject targets.

b) Angular correlations

As described in the previous section, one detector was
left at a 90° angle while now the other detector was located
at angles ranging from 60° to 100° with respect to the beam
and coincident events were registered between them via the
apparatus in Fig.48. A secondary emission beam monitor was
used for normalization purposes. For a known number of
counts registered by the fixed fragment detector, the number
of fragment-fragment coincidences registered between the two
fission detectors was measured as a function of the
detector-detector angle. The distribution in coincidence
rate as a function of the angle could be approximated with a
gaussian function whose maximum gives directly access to the
centre of mass momentum of the fissioning system.

Special attention was taken to center the proton beam
in order that the fission fragments were effectively emitted
from the center of the chamber. This insured that the
measured angles at which the detectors were positioned were
identical to the angles at which the fragments were emitted.

c) Time of flight measurements

For these experiments, one detector was set at a $40°$ angle with respect to the beam and located at a 50cm distance from the target, the second detector being at a $135°$ angle and a distance of 11cm, and the detector-detector angle being close to that at which the maximum coincidence rate was observed. Coincident events between the detectors were registered, and for each event the two energies and the time difference between the detector pulses (i.e between the times of arrival of the two fission fragments) was recorded via the electronic apparatus of Fig.49. For the time measurement, the detector farther away from the target was used as a "start" signal whereas the detector close to the target was the "stop" signal in the time to amplitude converter. The target was, as previously, oriented at a $45°$ angle with respect to the beam direction.

The time calibration of the output of the model ORTEC 467 time to amplitude converters was achieved by applying signals at the inputs of the TAC with varying time differences, typically of the order of 50 nanoseconds and fitting the resulting data to a straight line whose slope gave the relationship between channel number and time. The

time origin (i.e the time on the TAC output scale when the
fission event took place) was the most difficult to
evaluate. It was estimated by calculating the time of flight
of fragments with the most probable mass and energy, with
the necessary assumption that the fissioning system mass was
known. During the analysis of the experimental data, it
developed that this zero time was of critical importance as
far as a measure of the total fissioning mass was concerned:
its influence will be discussed in section (III-B-3-b).

For this particular experiment, the fission detectors
were protected from a high counting rate of electrons (with
an energy below ~15 keV) from the target by free standing
silver foils; their thickness was determined by calibrating
the detectors using a ^{252}Cf source with and without the
foils, thus obtaining the energy loss of the californium
fission fragments in the silver. This calculation was made
using the tables of stopping power as a function of energy
by Northcliffe (Nor.70) for fragment masses A=141 and
107 a.m.u (Ner.60) and atomic numbers Z=55 and 43
respectively (Wat.69).

B) Data analysis and results

1) Angular distributions

The energy spectra collected from the movable detector at various angles between $20°$ to $160°$ with respect to the beam direction and from the detector fixed at $90°$ were fitted to Gaussian functions and then integrated. As mentioned previously (section III-A-3-b) no coincidence was required between the events registered by both detectors. The number of events registered by the movable detector, normalized to the same number of counts in the detector used as a monitor, led to angular distribution curves.

The analysis of these curves can be made by using a statistical theory developed by Halpern and Strutinski (Hal.58) and Griffin (Gri.59). The angular distribution of the fragments depends upon the angular momentum I introduced by the projectile and on the fraction of it converted into orbital momentum between the fragments. This fraction can be characterized by the parameter K where K is the projection of I on the separation axis between fission fragments.

The K distribution for a given nuclear temperature was
predicted to be a Gaussian (Hal.58), (Hui.69):

$$F(K) \sim \exp(-K^2/2K_o^2)$$

where the variance of the distribution (designated as K_o^2)
is expressed in terms of the temperature of the nucleus at
the saddle point t and the effective moment of inertia $\mathcal{J}_{eff}$
through the relation:

$$K_o^2 = t\mathcal{J}_{eff}/h^2$$

Huigenza et al (Hui.69) derived an overall angular
distribution which was used in the KNOTTY computer code
(Blo.77) in order to fit the experimental results and
extract a K_o value. Unfortunately, it was not possible to
fit the results of the present study with the KNOTTY code
due to the lack of anisotropy, in the center of mass system,
shown by all angular distributions measured. A similar
observation was made on the angular distributions measured
with the mica detectors in a scattering array configuration
(i.e two dimensional scanning).

The number of tracks counted in a given solid angle as
a function of the angle with respect to the beam in the
center of mass system is shown in Fig.50(a) for a gold target
irradiated by 800 MeV protons. Fig.50(b) displays the results
obtained with the semi-conductor detector measurements for

Fig.50: Fragment angular distributions in the center of
mass system:

        a) measured with mica detectors for a gold target
irradiated with 800 MeV protons

        b) measured with semi-conductor detectors for an
uranium target irradiated with 480 MeV protons.
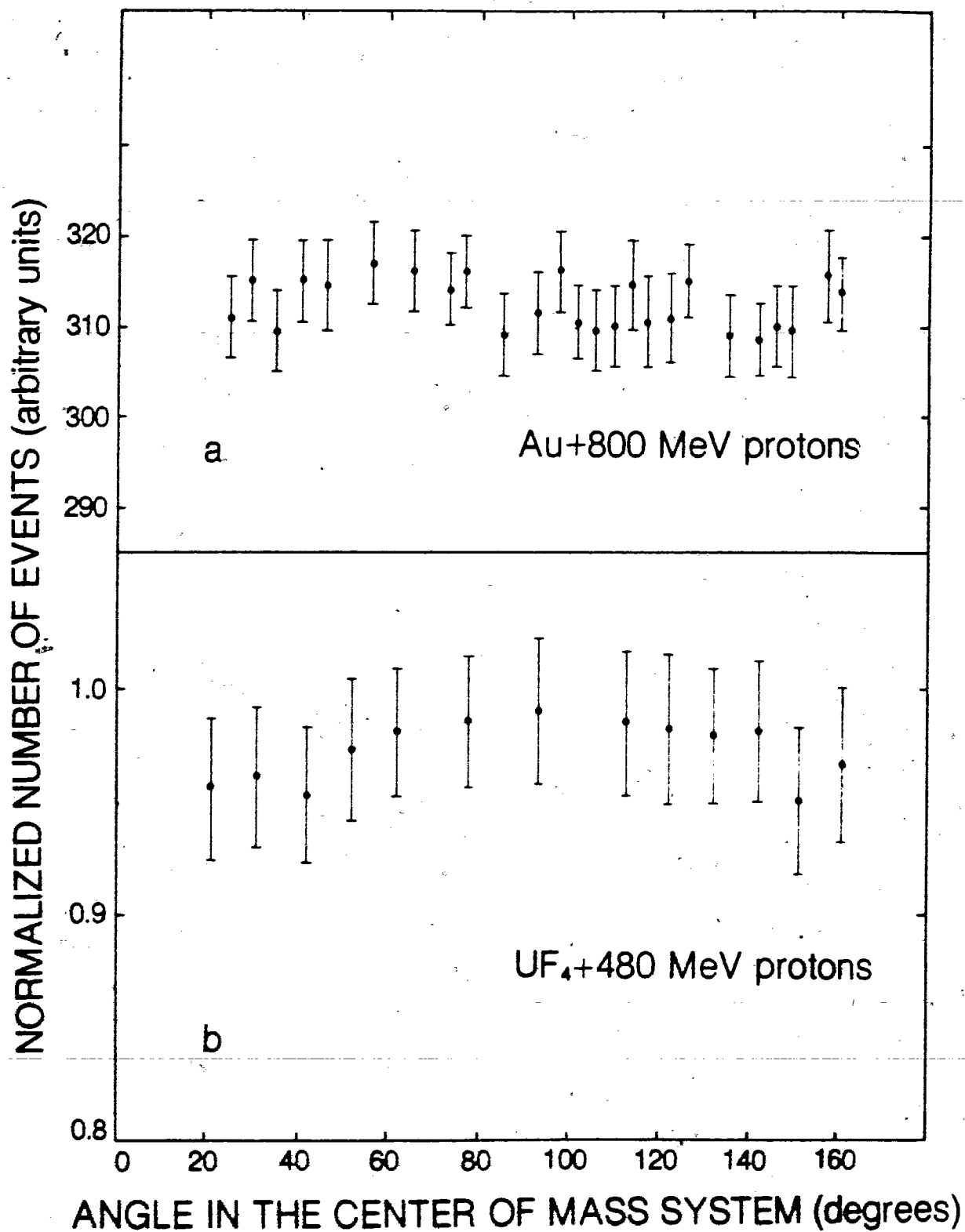
the system UF_4+480 MeV protons. As can be seen, the distributions are practically flat within the experimental errors. Since this type of result will lead to very large values of K_o, the computer code was unable to provide a fit of the experimental data.

While some authors measured angular distributions showing no anisotropy within experimental error, (Obu.61), (Obu.62), several investigators reported a surprising effect: in high proton energy bombardments, the anisotropy seemed to favour 90° instead of 0° and 180° (Loz.55), (Loz.56), (Mea.58), (Val.60).

An explanation for this reversal was suggested by Halpern (Hal.59): the fast incident particle, during its passage through the heavy nucleus, hits one or two nucleons and projects them with rather low energies into a direction at right angles to its path. These nucleons travel through the nucleus playing the role of a beam of particles which is directed at right angles to the original beam. They therefore give "inverted" anisotropies.

The results of this work shown in Fig.50(b) could be seen as displaying very faintly such an anisotropy at 90°.

2) Angular correlations

For each angle θ_2 where the movable detector was positioned, a value of the coincidence rate (normalized to the same number of counts in the monitor) was obtained. The angle θ_2 at which maximum coincidence rate was measured depends on the target nucleus: it was found to be 82° for gold, 84° for bismuth, 87° for thorium and 88° for uranium. A typical distribution from angular correlations measurements is given in Fig.51 for a Th target. For each experimental point of such a distribution, the projection of the fissioning system momentum along the beam axis $(p_{//})$ can be calculated since the energy in both detectors was also measured.

It can be shown that :

$$p_{//}^2 = \frac{A_t \, E_{tot} \, \cos^2\theta_2}{1+\sin^2\theta_2} \qquad (III.1)$$

where A_t is the mass of the fissioning nucleus and E_{tot} is the total energy of both fragments.

Equation (III.1) was derived assuming that the fission mass division was symmetrical which is a reasonable average assumption for high energy induced fission.

Fig.51: Measured fragment-fragment angular correlation for the system Th+480 MeV protons.
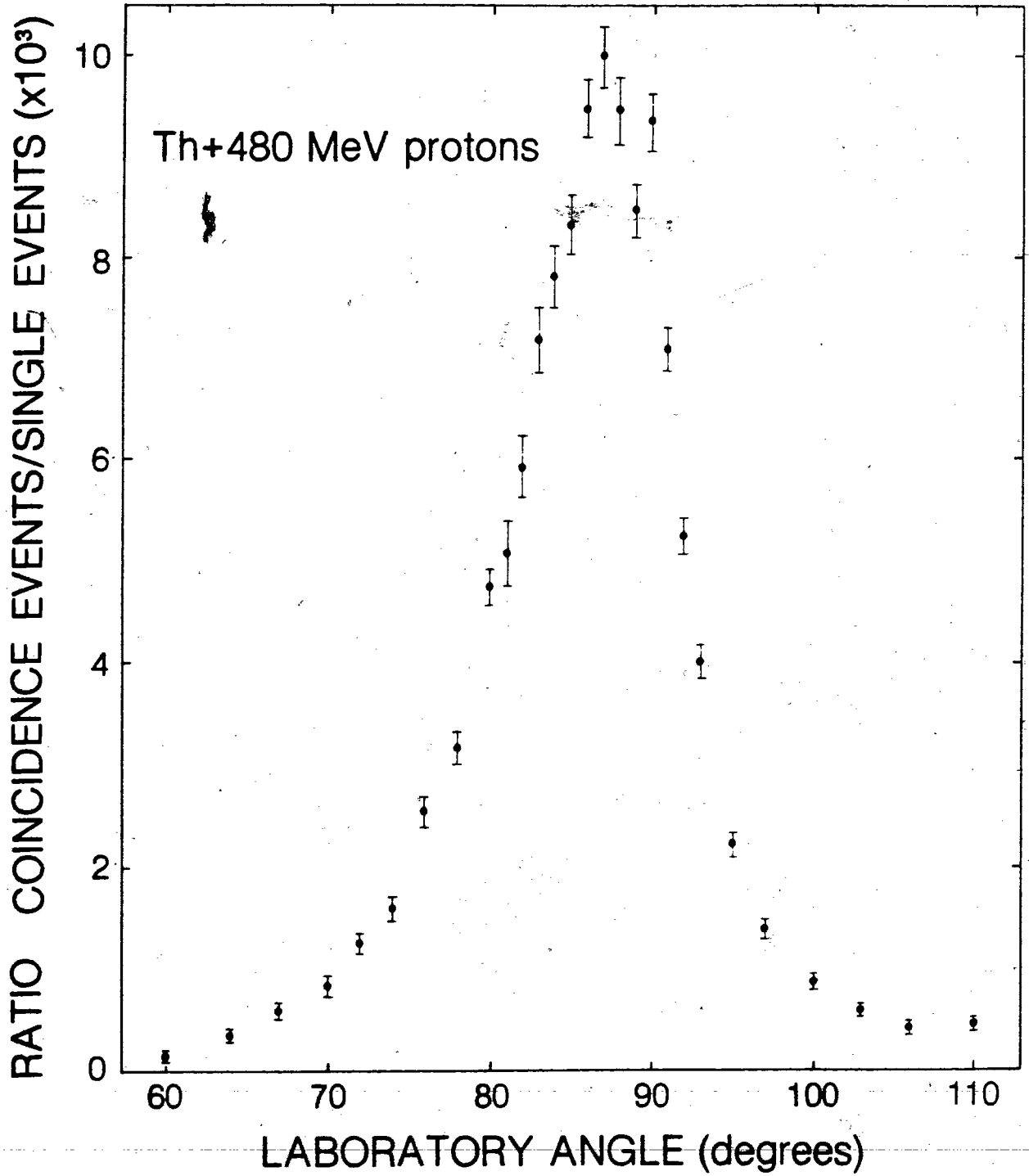
Fig.52: Center of mass momentum distribution ($p_{//}$) derived from fragment-fragment angular correlation for the fissioning system Au+480 MeV protons. Histogram shows results of calculations by the ISOBAR code.

p in MeV/c = p in (MeV.amu)$^{1/2}$ x 30.52
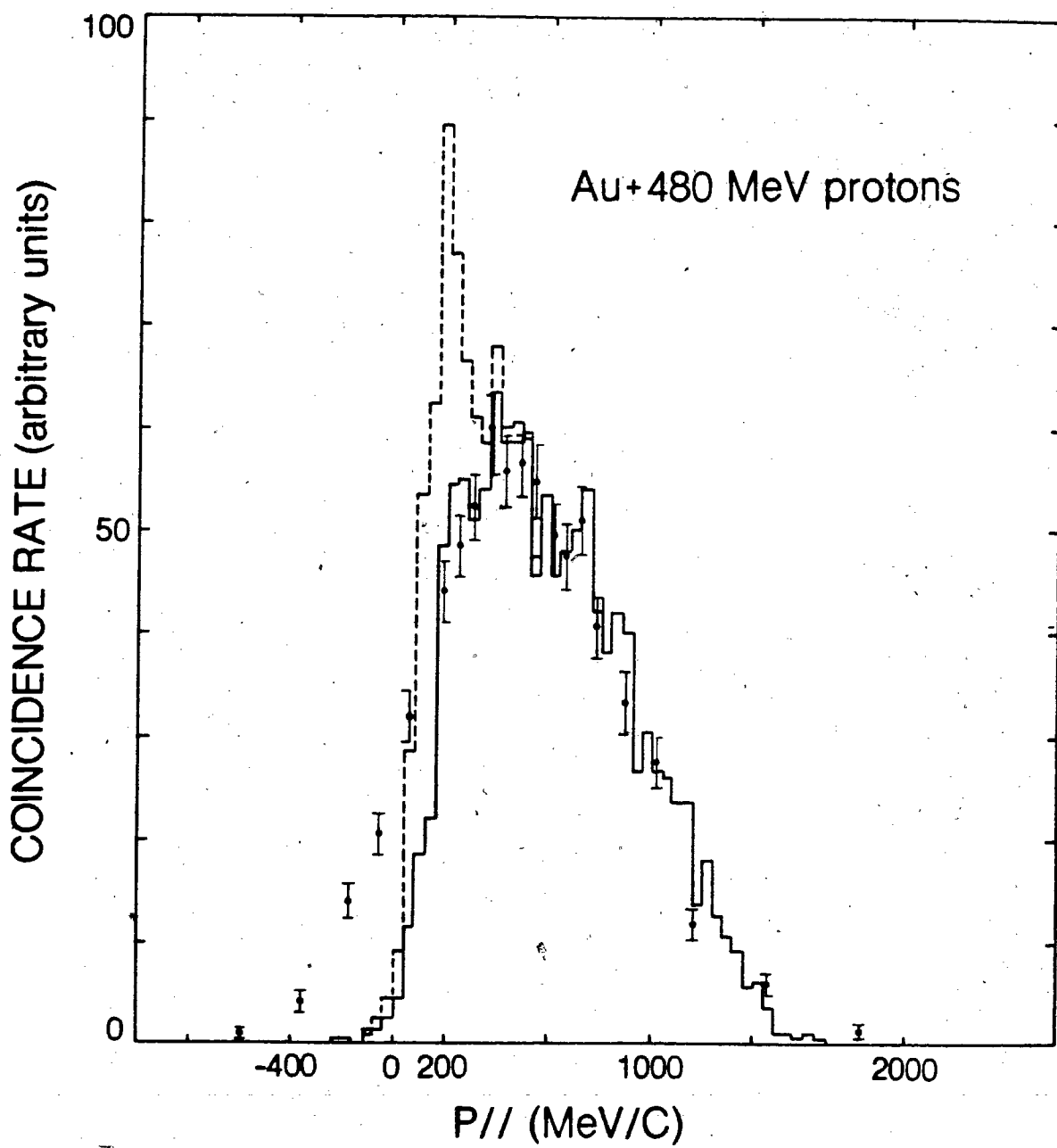
Au+480 MeV protons

Fig.53: Center of mass momentum distribution $(p_{//})$ derived from fragment-fragment angular correlation for the fissioning system Bi+480 MeV protons. Histogram shows results of calculations by the ISOBAR code.
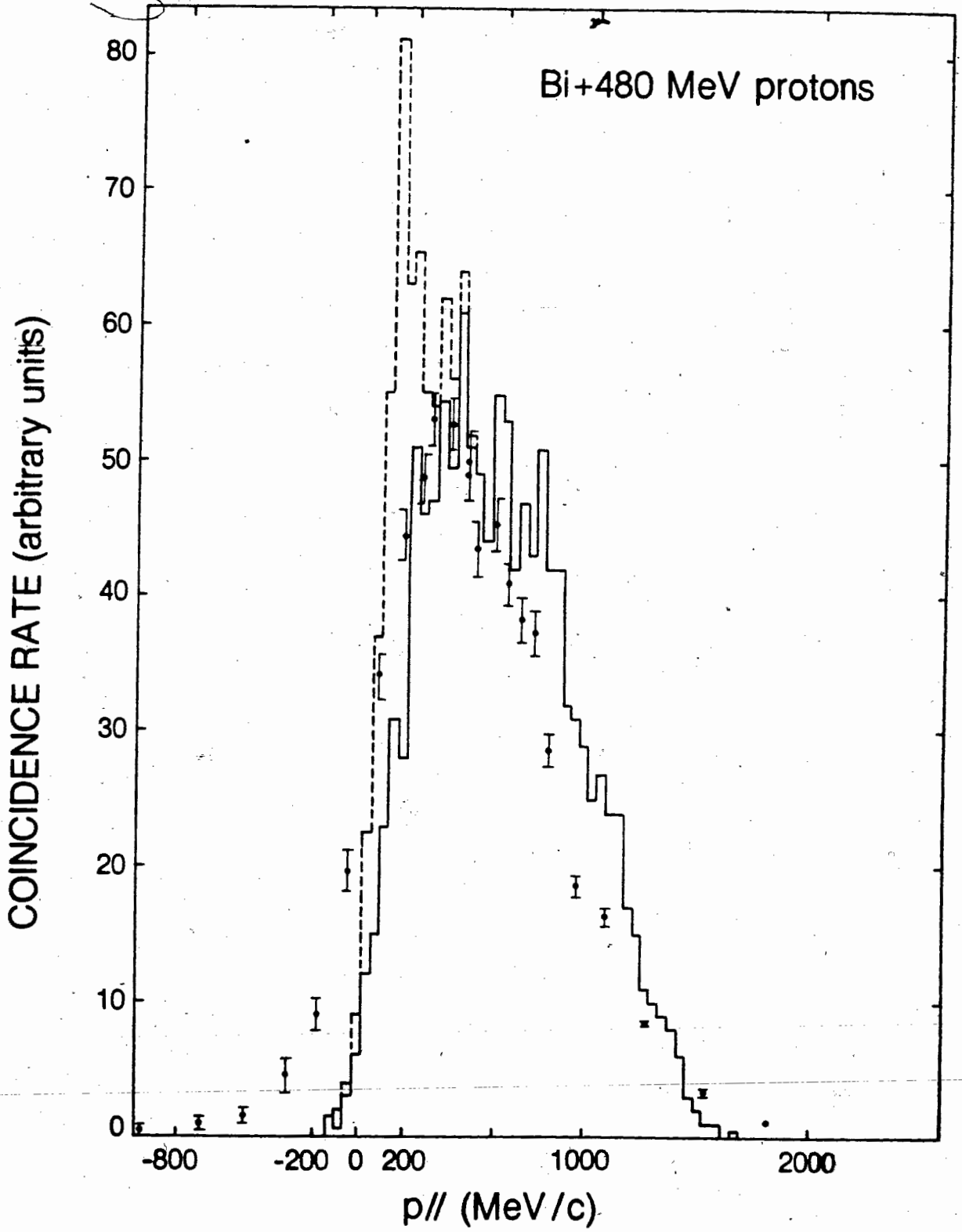
Fig.54: Center of mass momentum distribution ($p_{//}$) derived from fragment-fragment angular correlation for the fissioning system Th+480 MeV protons. Histogram shows results of calculations by the ISOBAR code.
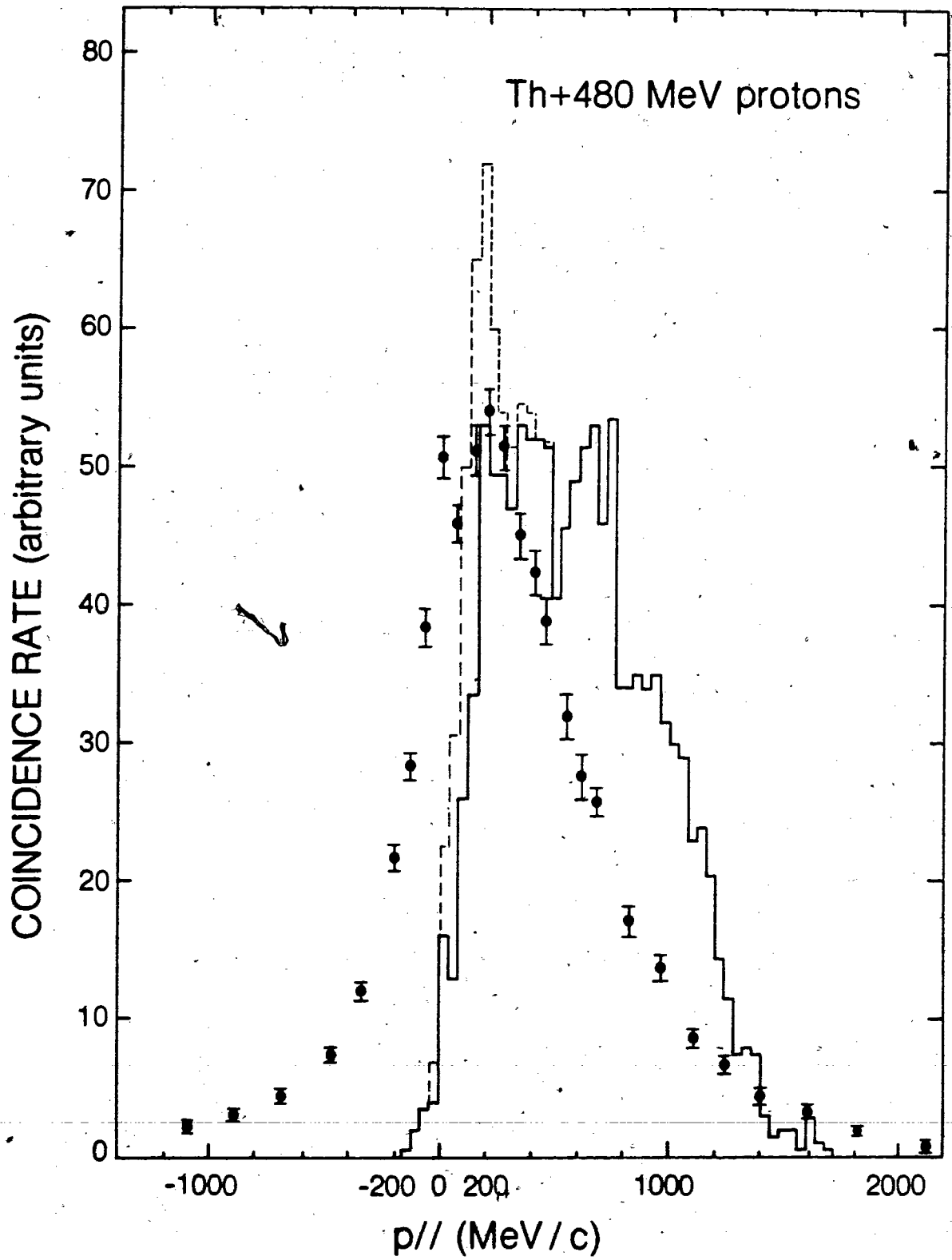
Fig.55: Center of mass momentum distribution ($p_{//}$) derived from fragment-fragment angular correlation for the fissioning system UF_4+480 MeV protons. Histogram shows results of calculations by the ISOBAR code.

UF$_4$ + 480 MeV protons
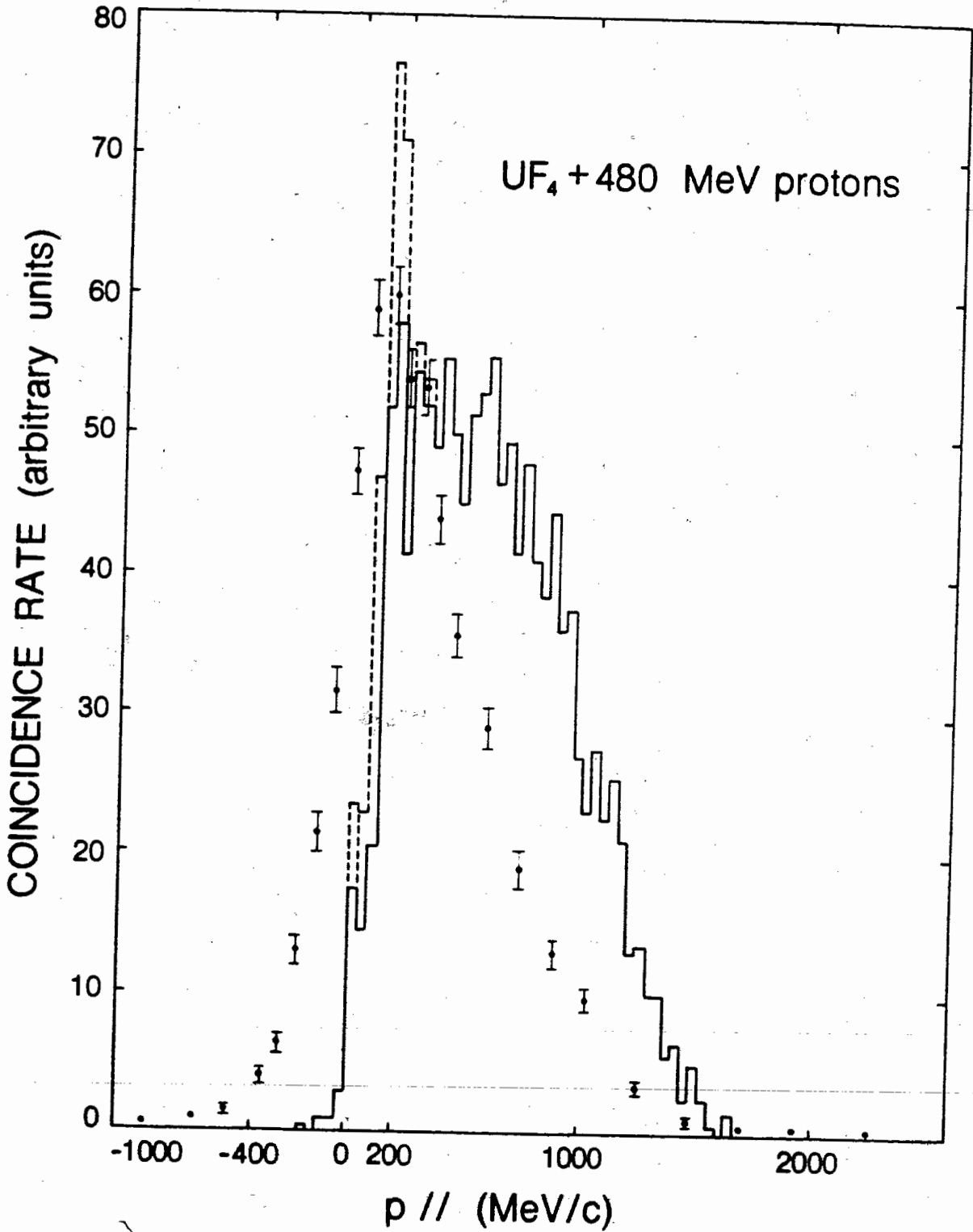
Therefore, from each angular correlation distribution a distribution in $p_{//}$ was calculated. Such distributions are shown in Fig.52-53-54-55 where experimental data have been compared to the results of a cascade calculation made through the computer code ISOBAR. The calculated distribution in momentum along the beam axis is shown as the broken line histogram on these figures.

One can notice that the sharp peak corresponding to low values of the momentum is considerably decreased when these events resulting in an excitation energy below the fission barrier are rejected (solid line histogram). This phenomenon can be observed on all target elements, however, it is most pronounced with the light target elements (Au and Bi) due to a higher value of the fission barrier ($\sim$20 MeV compared with about 5 MeV for Th and U).

It can be seen on these figures that the experimental curves are shifted (with respect to the results of the ISOBAR calculation) towards lower momentum values, the magnitude of this shift increasing with the mass of the target.

3) Time of flight experiments

a) Treatment of the data

The data from these experiments could be analyzed in three different ways, that is through three different options of the computer program MANIAC (written by H.Blok and modified for the present study to include the third option and several types of corrections for center of mass motion and energy loss).

These options are (briefly):

- Option 1 :

The measured energy and the difference in time Δt between the signals coming from the fragments in coincidence were used to determine the fission fragment masses A_1 and A_2 through the relation :

$$\Delta t = \frac{d_2}{v_2} - \frac{d_1}{v_1} = \frac{d_2 (A_2)^{1/2}}{(2E_2)^{1/2}} - \frac{d_1 (A_1)^{1/2}}{(2E_1)^{1/2}} \qquad (III.2)$$

For this option, the mass A_t of the fissioning system had to be given as an input to the program which searched all combinations of A_1 and A_2 (such that $A_1 + A_2 = A_t$) until the difference in time Δt was identical to the experimental value.

- Option 2 : This used conservation of momentum in order to calculate the fission fragments masses as well as the center of mass momentum, provided again that the mass of the fissioning system was known. Here again, the assumption of the center of mass momentum having the same direction as the beam was made in order to carry out the calculations. The momentum conservation is written as :

$$p_1 + p_2 = p'_1 + p'_2 + p_{cm} \qquad (III.3)$$

where p_1 and p_2 are the laboratory momenta of the fission fragments, p'_1 and p'_2 are the momenta in the center of mass system and p_{cm} is the center of mass momentum.

Relation (III.3) becomes:

$$p_1 + p_2 = p_{cm} \qquad (III.4) \qquad \text{since the fragments}$$

are emitted at a 180° angle in the center of mass, so that $p'_1 + p'_2 = 0$.

By projection of the momenta on the beam axis and on an axis perpendicular to the beam, equation (III.4) is equivalent to the two following equations:

$$p_1 \cos\theta_1 + p_2 \cos\theta_2 = p_{cm} \qquad (III.5)$$

$$p_1 \sin\theta_1 + p_2 \sin\theta_2 = 0 \qquad (III.6)$$

where θ_1 and θ_2 are the angles between the beam direction and p_1 and p_2 respectively. The angle corresponding to p_{cm} is assumed to be zero (see assumption made earlier).

The mass A_t of the fissioning system is assumed which leads to another relation:

$$A_1 + A_2 = A_t \qquad (III.7)$$

where A_1 and A_2 are the fission fragments masses.

By expressing p_1 and p_2 as a function of the fission fragments masses and energies and solving the system of equations (III.5), (III.6) and (III.7), the masses A_1 and A_2 can be calculated:

$$A_1 = \frac{A_t \, E_2 \, \sin^2\theta_2}{E_1 \, \sin^2\theta_1 + E_2 \, \sin^2\theta_2} \qquad (III.8)$$

then $A_2 = A_t - A_1$

After A_1 and A_2 are known, the quantity p_{cm} is calculated through equation (III.5).

In a last step, the energy values in the laboratory system were converted to the center of mass system, via :

$$E' = E - \frac{\sqrt{2EA} \, p_{cm} \cos\theta}{A_t} + \frac{A p_{cm}^2}{2A_t^2} \qquad (III.9)$$

where E' and E are the energies in the center of mass and in the laboratory systems respectively. After correction for energy loss in the foils, the target and the backing, the energies of both fragments in the center of mass system were calculated together with the total fission energy.

- Option 3 : This combined both the previous options and was of greater interest since it allowed a determination of the mass of the fissioning system. However, the value of the fissioning system mass obtained proved to be highly sensitive to some of the different parameters involved as will be explained further.

In this case, the fission fragment masses A_1 and A_2 were calculated by solving the system of equations (III.2) (from option 1) and (III.6) (from option 2). Then $A_t = A_1 + A_2$

- Procedure for analysis

The data were first collected from the tape and could be displayed as distributions of the number of events per channel number for both detectors and for the time difference Δt. After a calibration step where all calibrations for energy and time were entered, the same distributions were given as a function of the energy (in MeV) and time (in nanoseconds). An example of such results is given in Fig.56-57-58 where the energy in the detector close to the target (Fig.56), the energy in the second detector (Fig.57) and the time of flight (Fig.58) are shown for a Bi target. Options 1,2 or 3 of the MANIAC program could then be applied directly to these data.

Typically, the experimental data from a given target were analyzed through the following sequence:

Fig.56: Energy distribution from the system Bi+480 MeV protons measured by the semi-conductor detector 11cm from the target and at a 135° angle with respect to the beam direction.

FRAGMENT ENERGY (MeV)
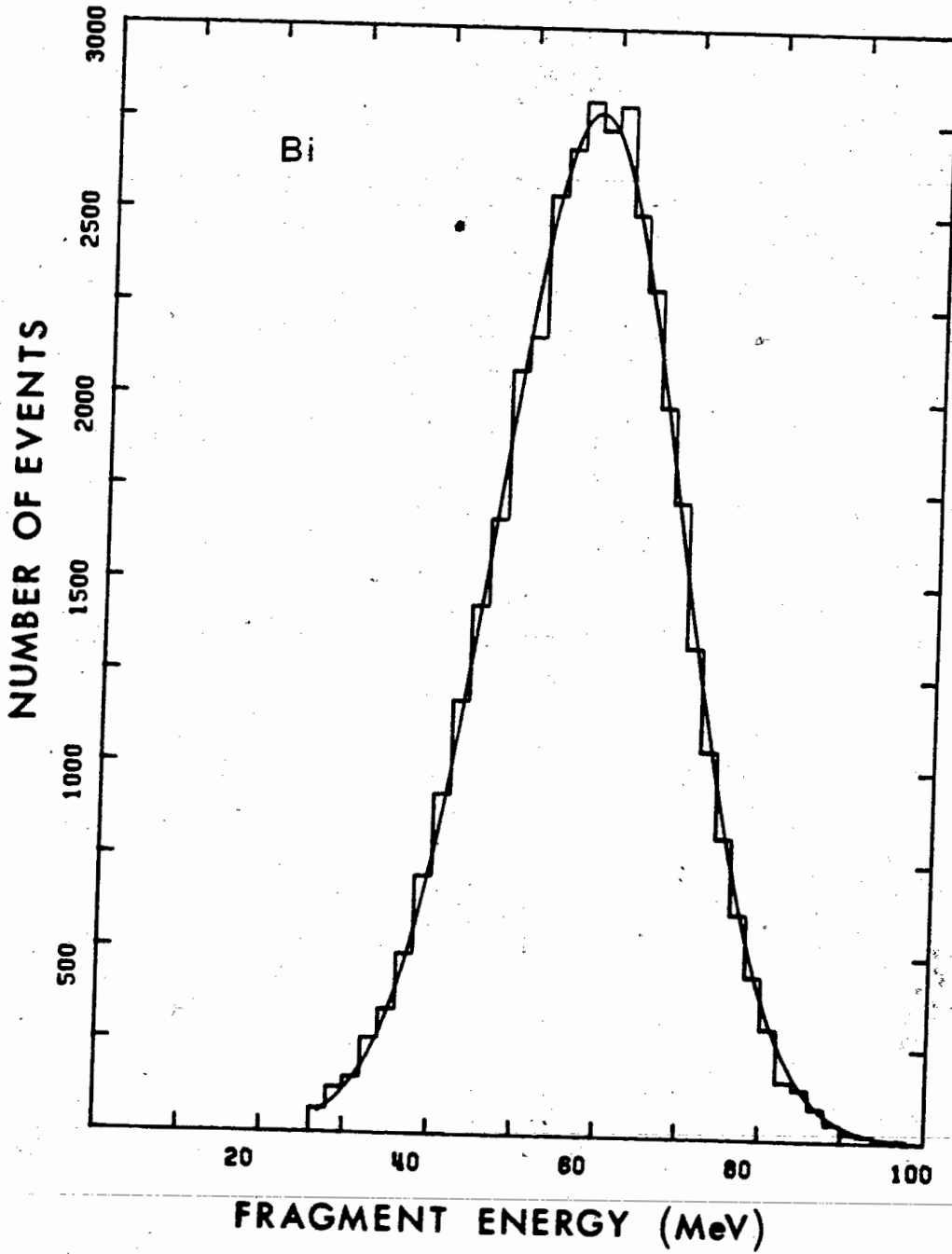
Fig.57: Energy distribution from the system Bi+480 MeV protons measured by the semi-conductor detector 50cm from the target and at a 40° angle with respect to the beam direction.
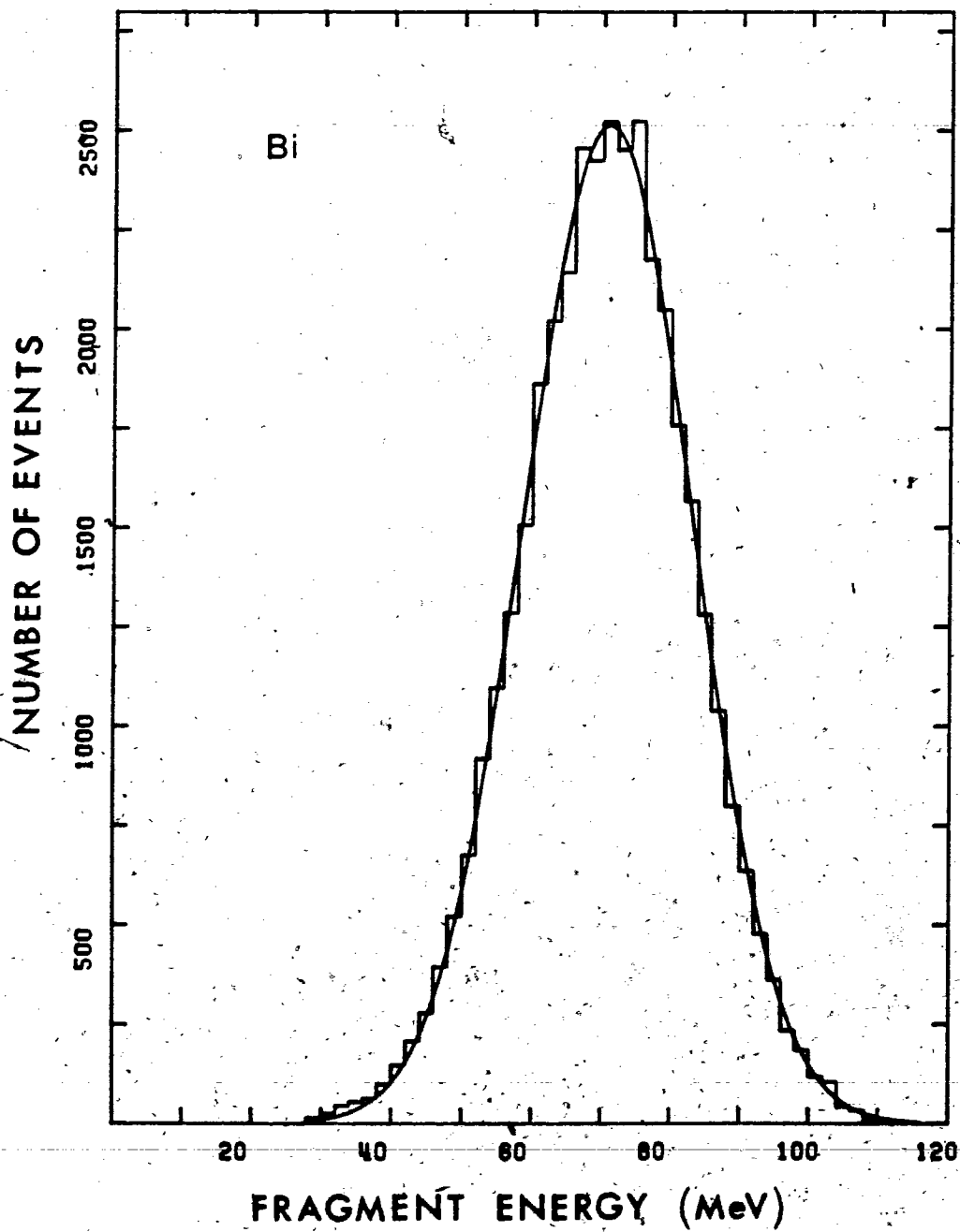
Fig.58: Difference in time of flight between the fission fragments from the system Bi+480 MeV protons.

NUMBER OF EVENTS

Bi

TIME OF FLIGHT (nanosec)
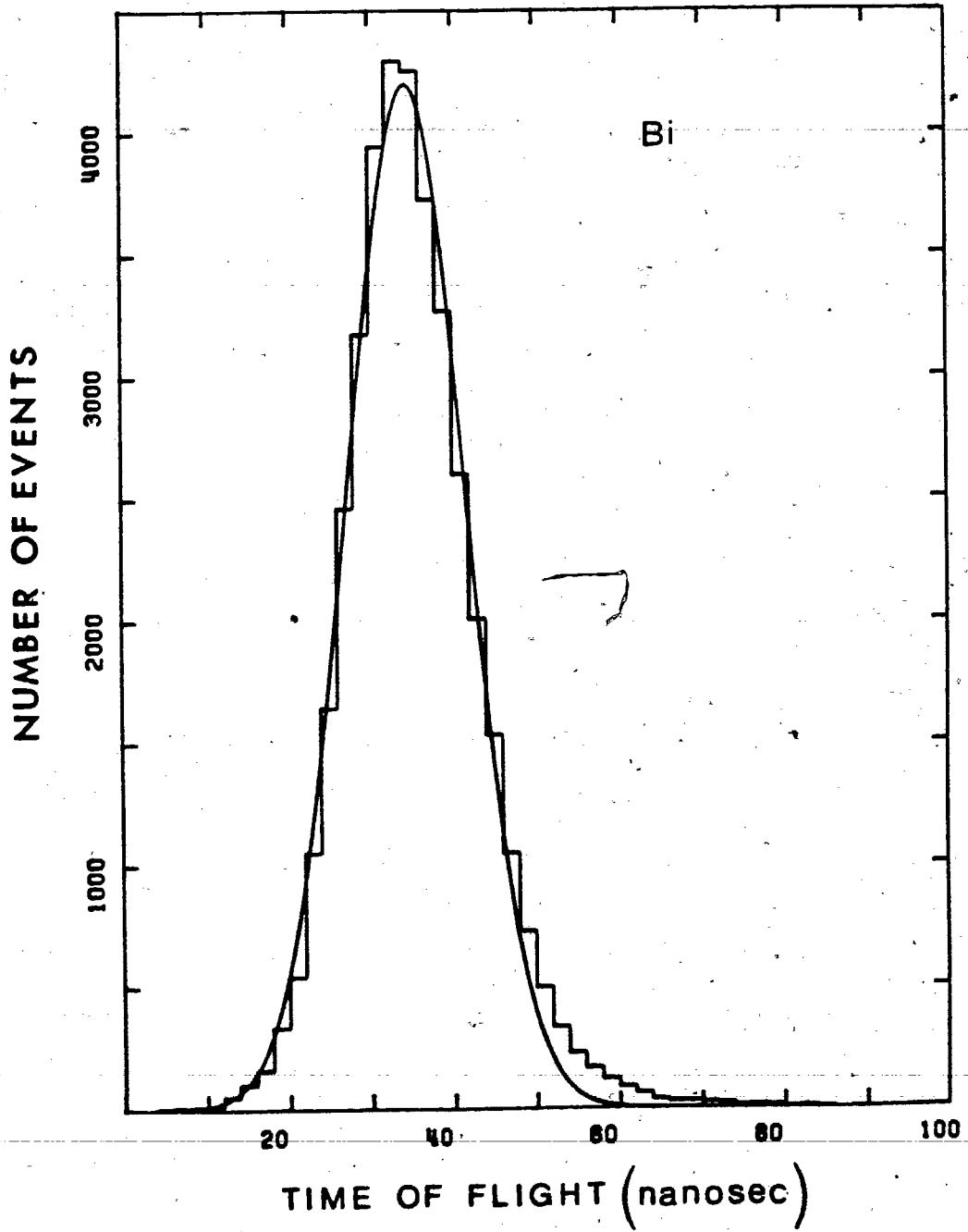
Fig.59: Calculated mass distribution for the system
Bi+480 MeV protons measured in the detector 11cm from the
target and at a 135° angle with respect to the beam
direction.

FRAGMENT MASS (a.m.u.)
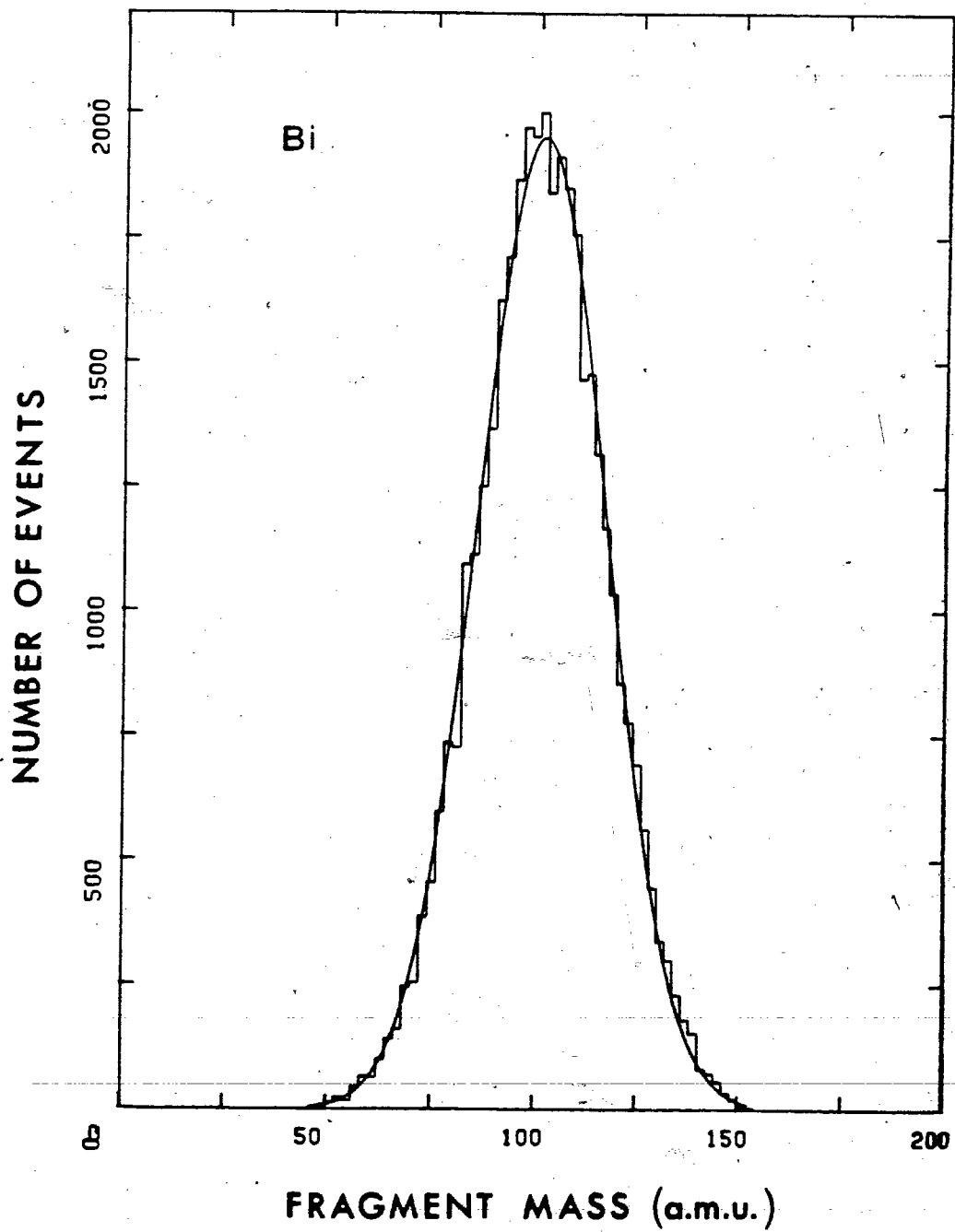
Fig.60: Calculated mass distribution for the system
Bi+480 MeV protons measured in the detector 50cm from the
target and at a 40° angle with respect to the beam
direction.

Bi

NUMBER OF EVENTS

FRAGMENT MASS (a.m.u.)
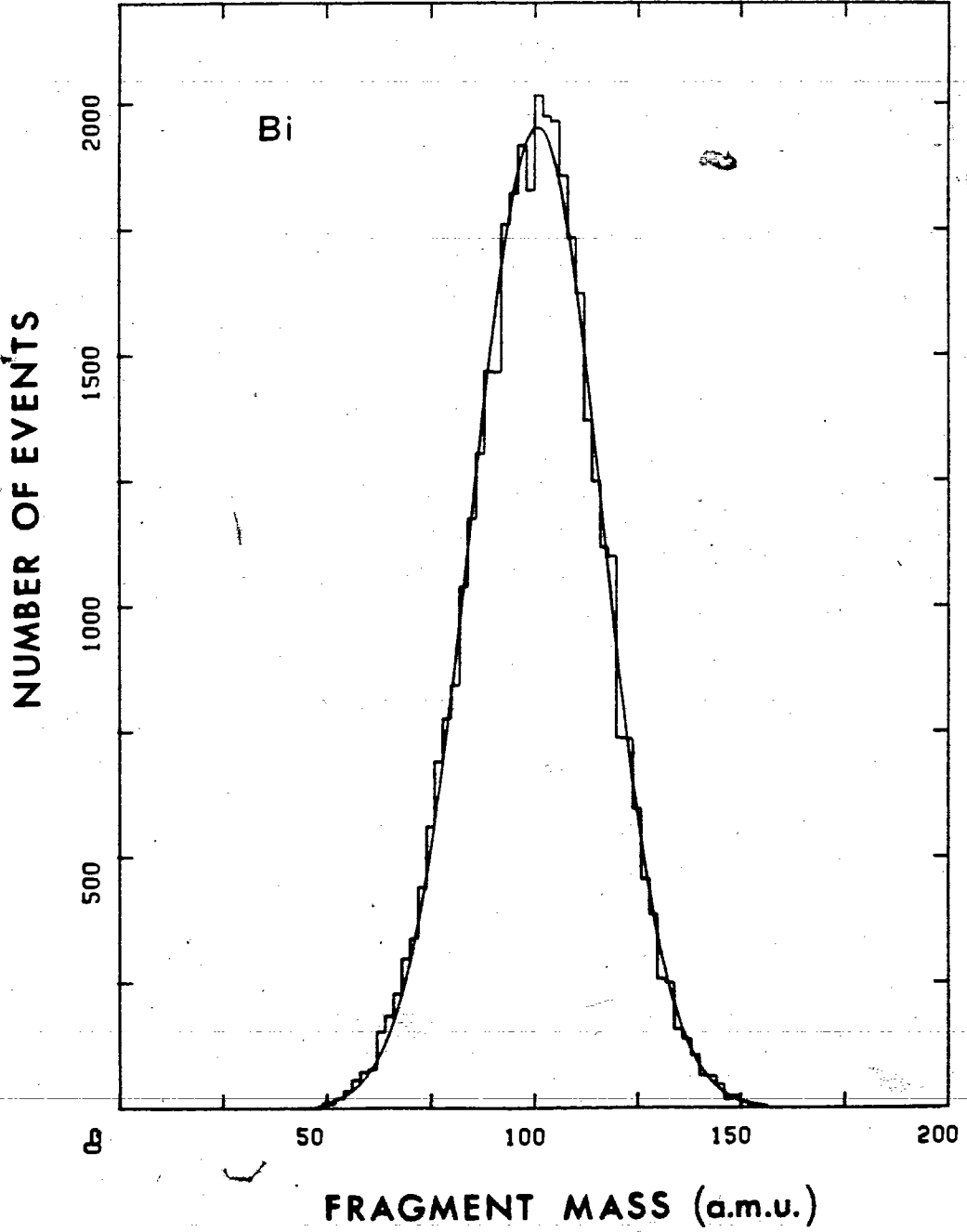
Fig.61: Fission fragment energy distribution in the
center of mass of the fissioning system Bi+480 MeV protons
measured in detector 11cm from the target.

Bi

NUMBER OF EVENTS

FRAGMENT ENERGY (MeV)
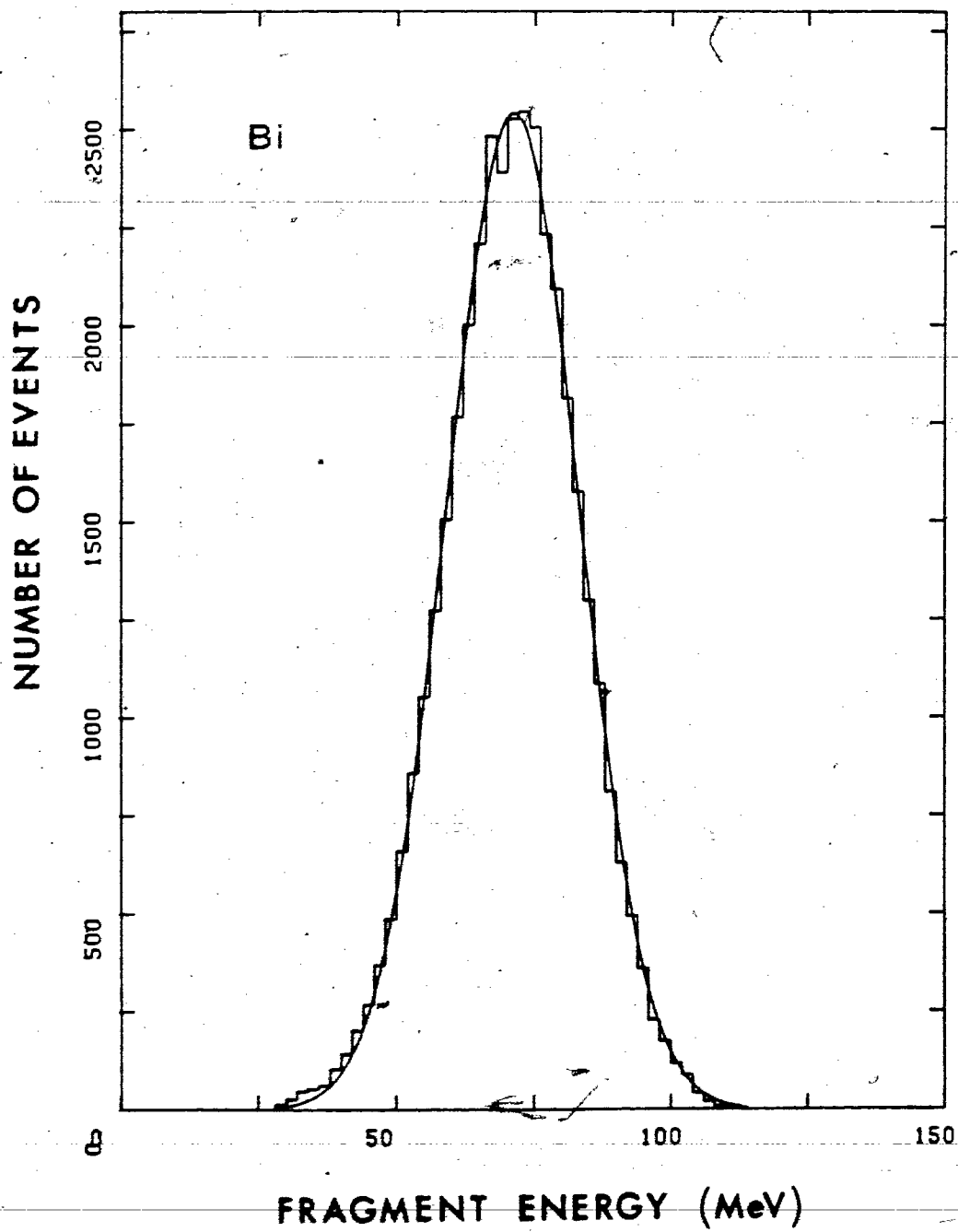
Fig.62: Fission fragment energy distribution in the center of mass of the fissioning system Bi+480 MeV protons measured in detector 50cm from the target.

Bi

NUMBER OF EVENTS

FRAGMENT ENERGY (MeV)
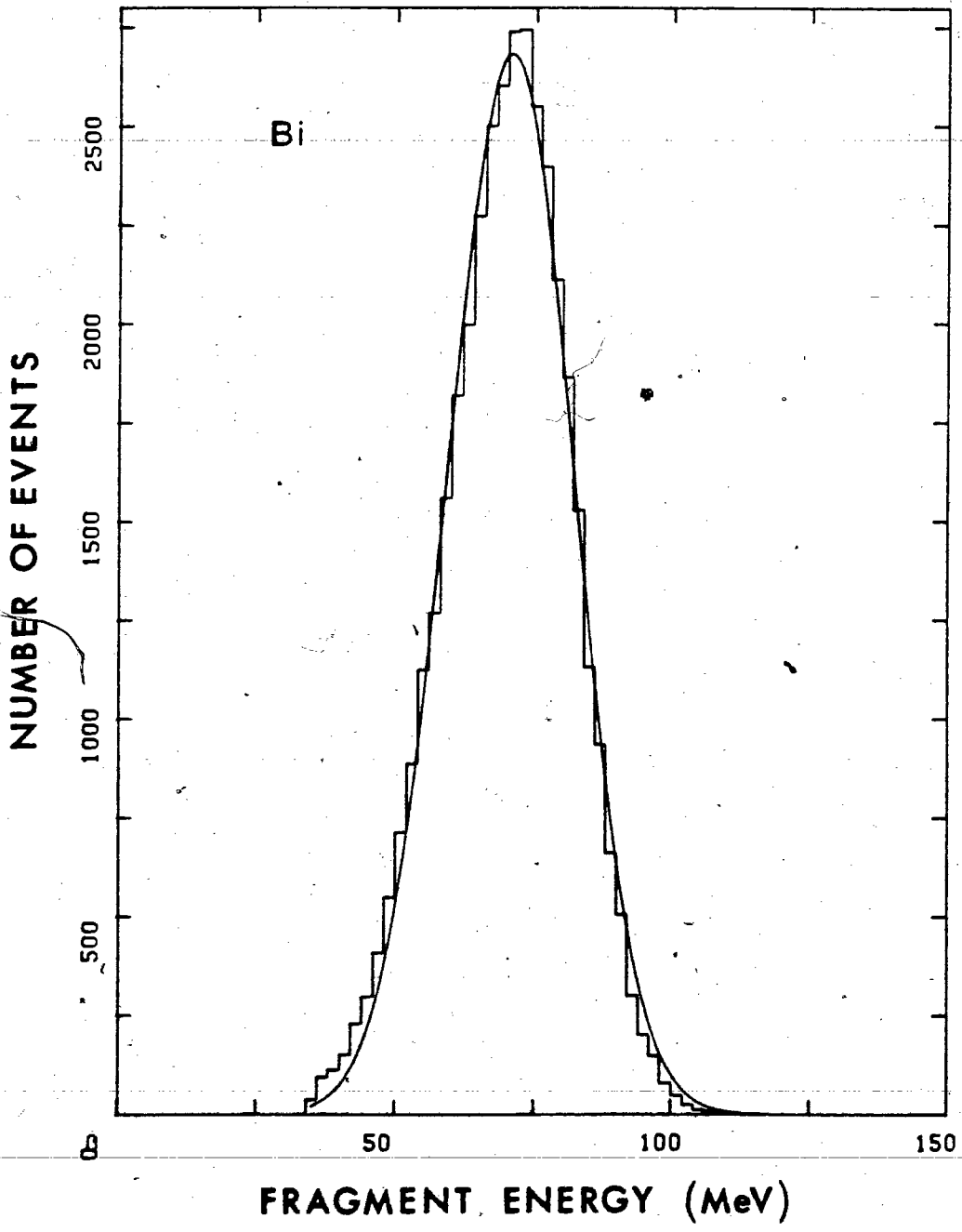
Fig.63: Measured total kinetic energy in the center of
mass system for Bi+480 MeV protons.

Bi

NUMBER OF EVENTS

3000
2500
2000
1500
1000
500

0 25   125   175

TOTAL ENERGY (MeV)
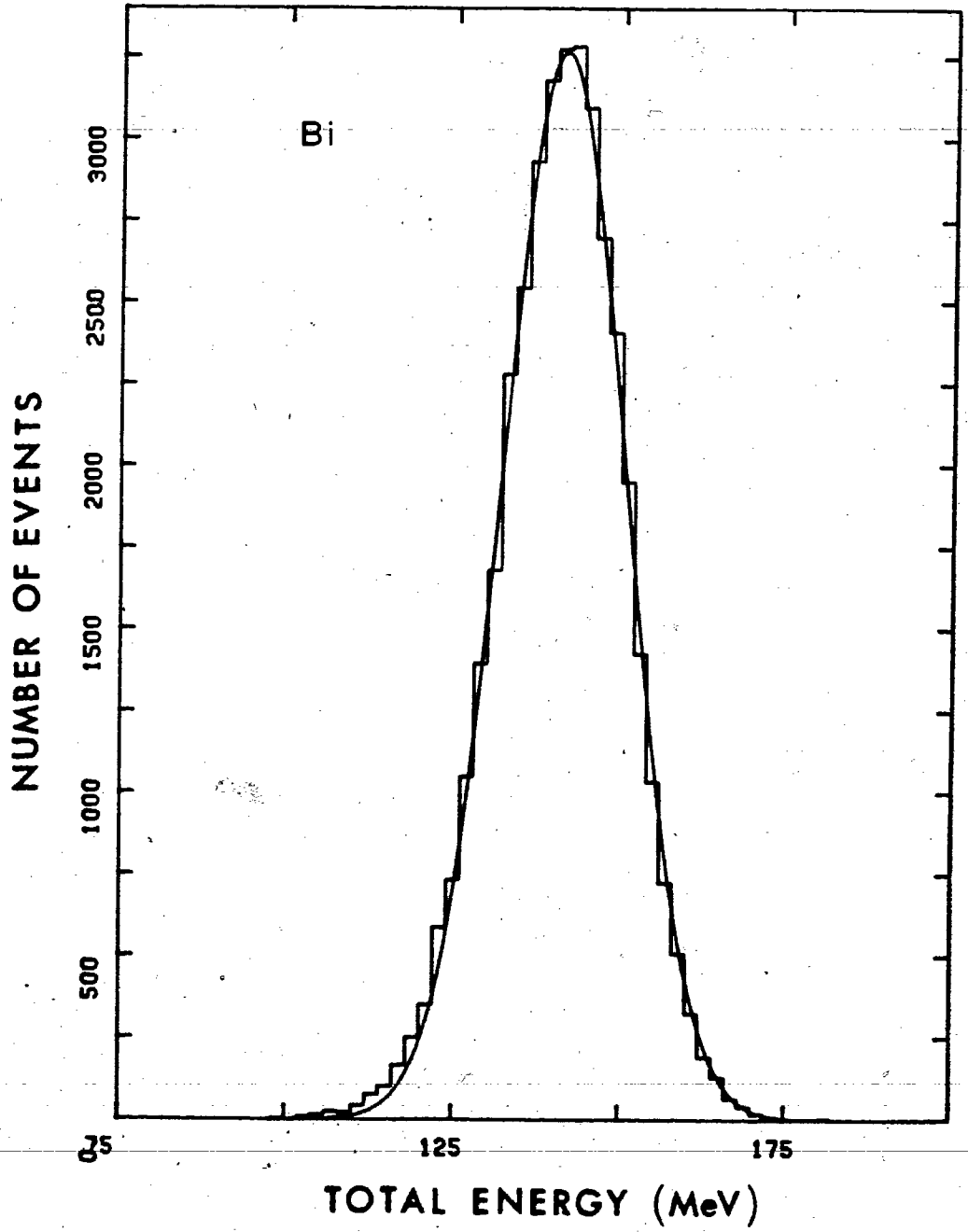
Fig.64: Deduced center of mass momentum distribution of the fissioning system from Bi+480 MeV protons.

p in MeV/c = p in $(MeV.amu)^{1/2}$ x 30.52

Bi

NUMBER OF EVENTS

CENTER OF MASS MOMENTUM $(MeV.amu)^{1/2}$
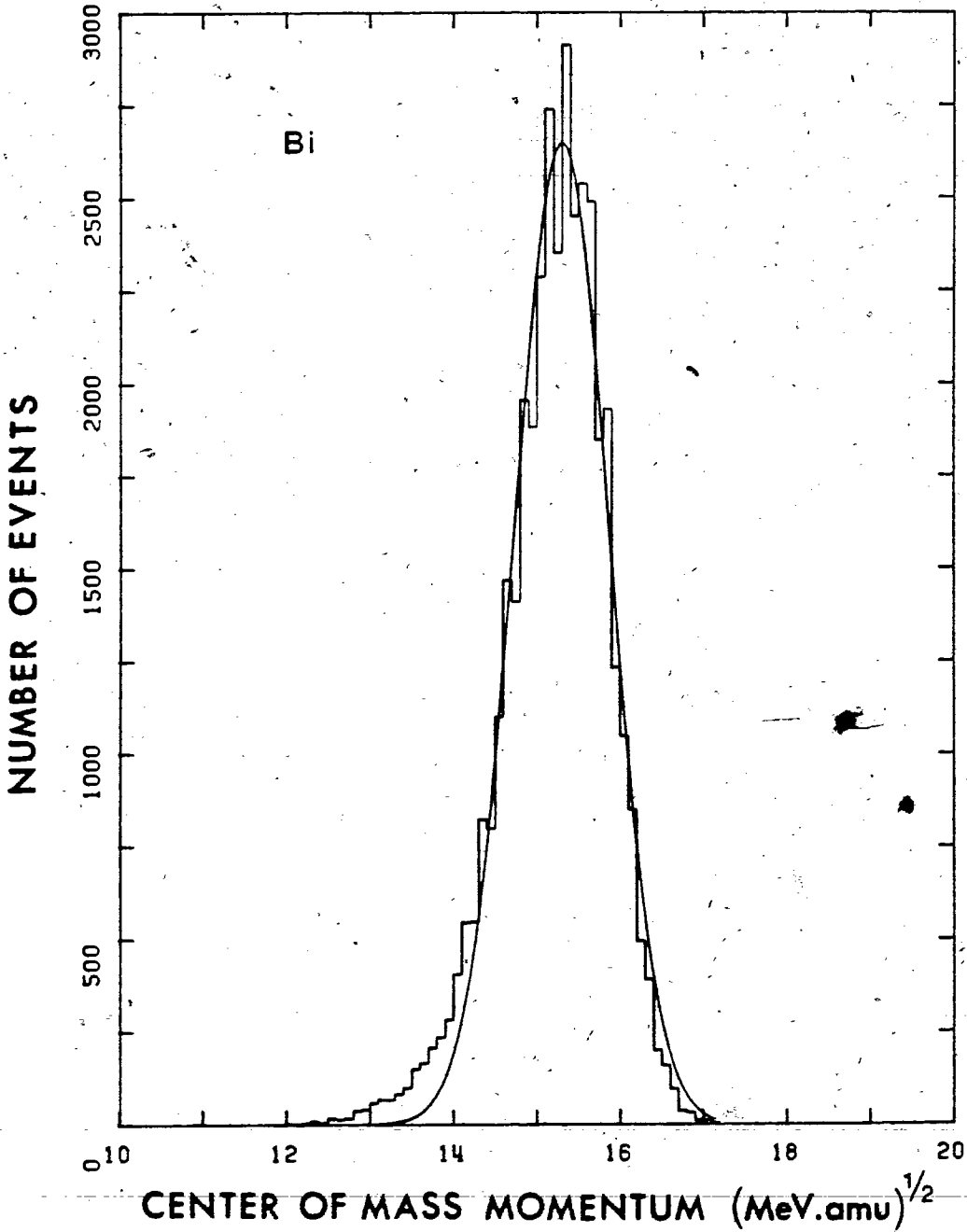
- The option 2 of the MANIAC program was applied first in order to obtain distributions in fragment masses (A_1, A_2), energies in the center of mass (E'_1, E'_2), in the total kinetic energy (E_{tot}) and in the center of mass momentum (P_{cm}). Examples of such data from a Bi target are shown in Fig.59-60-61-62-63-64. The information on the energies E'_1, E'_2, E_{tot} and on the center of mass momentum was retained as such. The mass distributions were only used as a test of the symmetry of the fission process since their most probable value was artificially set when the mass of the fissioning system was given. The values entered were 190 a.m.u for Au, and 234 a.m.u for U obtained from the analysis of angular distributions by the program RADICS. The values of 202 a.m.u for Bi and 228 a.m.u for Th were estimated assuming similar trends.

- In a second step, the data were analyzed through option 1 where the difference in time of flight Δt had an important role. It was then checked that the results of this option were similar to those of option 2 since, here again, the mass of the fissioning system was given to the program as an input. If a discrepancy was present, then, the zero time was readjusted in order to obtain an agreement between the results of options 1 and 2.

Fig.65: Sum of the fission fragment masses for the system Bi+480 MeV protons.

Bi

NUMBER OF EVENTS

TOTAL MASS (a.m.u.)
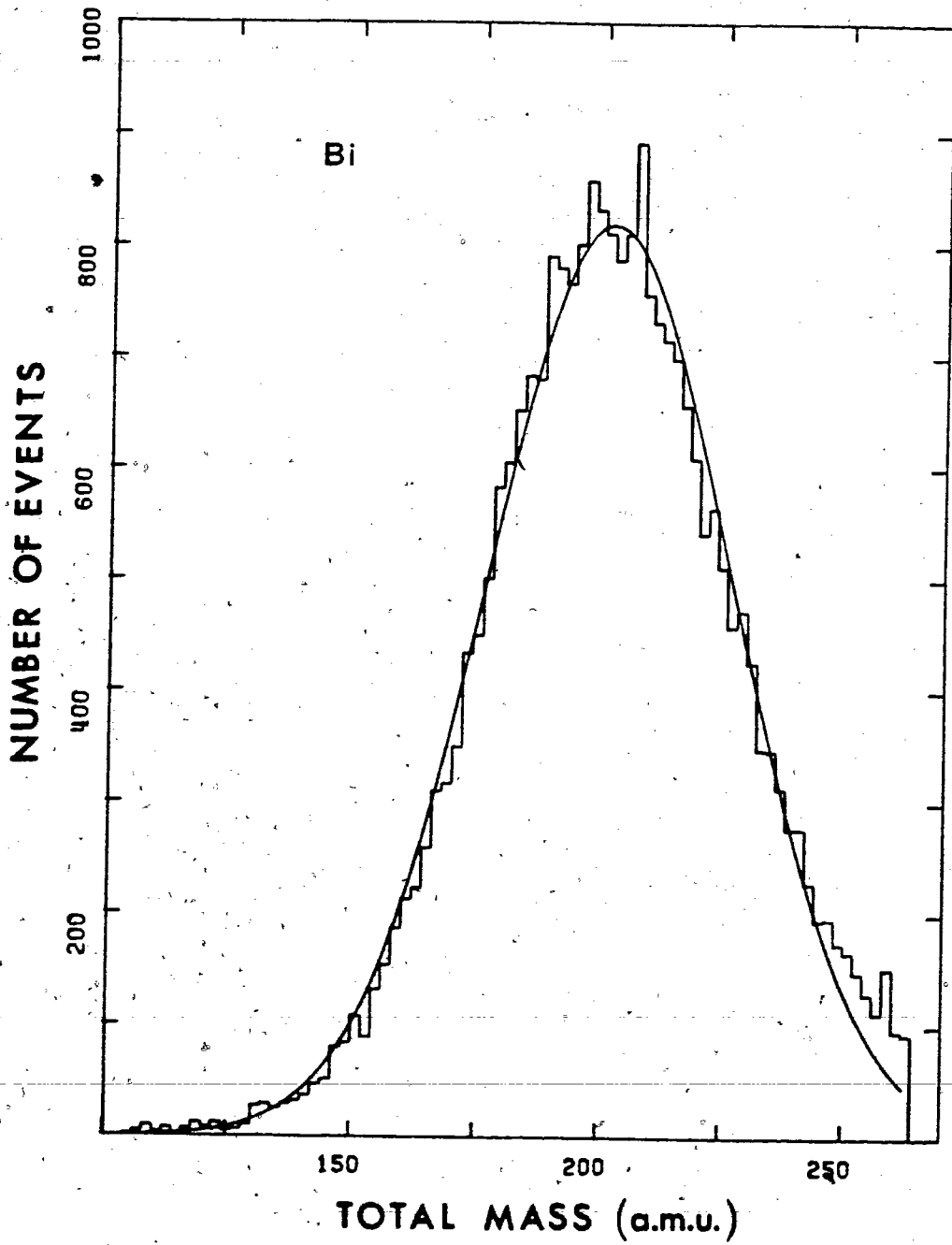
- Finally, the option 3 was used in order to extract the distribution of the fissioning system mass A_t. Such data are shown also for a Bi target in Fig.65.

    b) Influence of the different parameters on the
       results and estimate of the errors

The errors involved in the time of flight experiments arose from two different sources:

- errors related to the experimental setup such as errors in detector position (distance from the target and angle compared to the beam) and in experimental measurements such as the energy and the difference in time Δt.

- errors introduced into the calculations during the analysis of the data which proceeded from assumptions made or from a lack of knowledge on the fission process itself such as the most probable mass of the fissioning system, or from corrections for the energy loss by the fission fragments in the target, backing and foils.

Some of these errors are straightforward to correct for but the second type is somewhat difficult to estimate and an evaluation was often made by testing the sensitivity of the results to a variation of some input parameters to the computer program. Following is an evaluation of the

uncertainties involved in the determined quantities from the whole analysis process.

- Energy -

The uncertainty in the energy values in the laboratory system was a result of errors in the detectors calibration and in corrections made for the energy loss in the target material, the backing and the detectors protective foils. The calibration step involved a fitting of a Gaussian function to the energy spectra obtained experimentally in order to extract the most probable energy values for the two peaks (in channel number) and relate them to the known energies of the spontaneous ^{252}Cf fission. This fitting procedure was estimated to lead to an uncertainty of 0.2 MeV on the energy value for each detector. When correcting for the energy loss in the target, it was assumed that the fission events were all taking place in the center of the target and, therefore, that the fragments always traversed half of the target thickness. Taking into account the thickness uncertainties for the target, the backing and the foils, this correction involved an error of 0.6 MeV for each detector.

The energy in the laboratory was thus measured with an uncertainty of around 1 MeV.

- Mass of the fission fragments -

As described previously, the calculation of the fragment mass is carried out in a different way depending upon the option (1 or 2). The case of option 1, involving the time of flight Δt will be discussed later. For option 2, as can be seen from equation (III.8), the uncertainty in the mass A_1 (or A_2) will depend upon the errors in the energy measurements, the angles at which the detectors were positioned and the mass of the fissioning system. The angles at which the detectors were set in the scattering chamber were quite well known and the error on their value was 0.1°. However, owing to the finite detector size, there is an angular range ($\pm 5.8^\circ$ in the case of tne detector close to the target) within which the fragments can enter the detectors. This angular uncertainty will not affect the position of the maximum of the mass distributions but will contribute significantly to their widths, as will be seen later.

The assumed mass of the fissioning system was chosen according to the results of the analysis through the RADICS program. The associated uncertainty has been determined previously and found to be +5 a.m.u. All of these uncertainties combined will give an error of ± 6 a.m.u on the value of the masses A1 and A2.

It should be pointed out that the most probable mass value of the mass distributions was (of course) very strongly dependent upon the A_t value assumed. In all the cases studied, the most probable values of A_1 and A_2 were found to be equal and therefore half of the given A_t value.

- Center of mass momentum -

The parameters involved in the center of mass momentum calculation are: the energy and mass of the fragments and the angles of the detectors compared to the beam. The errors on these different quantities have been already discussed and combine to produce an error of 0.3 $(Mev.amu)^{1/2}$ on the most probable value of p_{cm}.

- Energy in the center of mass system -

Since the uncertainties on all the parameters used in the conversion of the energy through equation (III.9) have now been evaluated, it is possible to estimate the error on the value of E' in the center of mass. The main contribution to this error on E' will be the uncertainty in the measured energy E. The second and third terms of the sum in relation (III.9) will contribute around 0.5 MeV and 0.05 MeV respectively. The value of E' will thus carry an uncertainty of 1.6 MeV.

- Fissioning system mass -

The results of option 3 proved to be extremely sensitive to the assumed zero time value, that is the time origin at which the fission event took place. A shift of one nanosecond in this zero time will displace the distribution of the total fissioning mass by about 20 a.m.u (a difference corresponding to that produced by a change from first chance to last chance fission).

The zero time, which was not experimentally accessible, had to be calculated (knowing the energy in both detectors) but again with an assumed mass for the fissioning system. This choice of the A_t value was reflected in the calculation and an iterative procedure between options 3 and 1 failed to converge towards a constant value of A_t. This difficulty was also encountered during the procedure described in a). The choice, in a first step, of a A_t value in order to apply option 2, was reflected in the second step when the zero time was adjusted as to obtain the same results through option 1. Then, this dependence upon A_t was carried implicitly through the option 3 even if A_t did not intervene directly in that option. As a consequence, the end result for the distribution of A_t was very close to the value given to start with, whatever this value was.

It is therefore well understood that the results given for the experimentally determined most probable mass of the fissioning system are artificial since they can vary greatly with the time of flight Δt. However, the A_t distributions obtained are of interest as to their shape and width.

The same remarks could be made with regard to the fragment masses A_1 and A_2 obtained with option 3. Therefore, uncertainties will not be assigned to these masses nor to the most probable A_t values.

- Unfolding of the distributions width

The fragment mass distributions resulting from option 2 show a standard deviation σ of the order of 15 to 21 a.m.u that is to say a full width at half maximum (FWHM) between 35 and 50 a.m.u. This FWHM contains a contribution from errors on the parameters involved in the measurement and analysis which are themselves distributed with a finite width. The contribution of these parameter errors to the width of the fragment mass distributions can be calculated through the relation:

$$\sigma^2_z = \sum_{i,j=1}^{n} \left(\frac{\partial f}{\partial x_i} \bigg|_P \right) \left(\frac{\partial f}{\partial x_j} \bigg|_P \right) \sigma_{x_i x_j} \qquad (\text{III.10})$$

where $z = f(x_1, \ldots, x_i, \ldots, x_n)$ and $(\partial f / \partial x_i\ P)$ is the partial derivative of f with respect to x_i evaluated at the point $P = (\langle x \rangle, \langle y \rangle, \ldots)$.

The parameters involved here will be the time, energy and angles of detectors location. Since they are independent, relation (III.10) becomes:

$$\sigma^2_z = \sum_{i=1}^{n} \left(\left| \frac{df}{dx_i} \right|_P \right)^2 \sigma^2_{x_i} \qquad \text{(III.11)}$$

An application of this last relation to equation (III.8) will give for example:

$$\sigma^2 A_1 = \left(\frac{dA_1}{dE_1} \right)^2 \sigma^2 E_1 + \left(\frac{dA_1}{dE_2} \right)^2 \sigma^2 E_2 + \left(\frac{dA_1}{d\theta_1} \right)^2 \sigma^2 \theta_1 + \left(\frac{dA_1}{d\theta_2} \right)^2 \sigma^2 \theta_2 \qquad \text{(III.12)}$$

In this particular case, A_t was given as a single value and thus was not distributed : $\sigma A_t = 0$.

The numerical evaluation of the partial derivatives had to be made at the point corresponding to the maximum of each distribution. The quantities $\sigma E_1, \sigma E_2, \sigma \theta_1$ and $\sigma \theta_2$ were estimated considering the experimental conditions that is the energy resolution of the detectors and the solid angles they subtended. The resolution of the detectors for the measurement of a 100 MeV energy was taken as 100 keV (FWHM), while the standard deviations on the angles θ_1 and θ_2 were respectively 5.8 and 1.3 degrees.

As an example , in the case of the Bi target, the experimental standard deviation of the A_1 distribution was $\sigma(\exp) = 15.75$ a.m.u. With relation (III.12), the contribution of angles and energy distributions was calculated to be

σ(parameters)=10.5 a.m.u. From this, it was possible to
deduce the true standard deviation of the mass distribution:

$$\sigma^2(true) = \sigma^2(exp) - \sigma^2(parameters)$$

which led to a true standard deviation around 12 a.m.u.
The corresponding FWHM of this distribution will then be
27 a.m.u compared with 37 a.m.u as measured.

This calculation revealed an interesting feature,
namely the relative importance of the different parameter
errors. It was found that the greatest contribution to the
width of the A_1 distribution came from the solid angle θ_1
which accounted for 10.2 a.m.u. The solid angle θ_2 had a
much smaller influence with a contribution of 2.3 a.m.u to
the total width while the errors on the energy measurements
could be considered as negligible since each accounted for
only 0.03 a.m.u.

Following is a comparison of the FWHM of the fragment
mass distributions obtained via the above analysis.

A$_1$ or A$_2$ distributions			
Target	FWHM (exp) in a.m.u	FWHM (calc) in a.m.u	FWHM (true) in a.m.u
Au	39	23	32
Bi	37	25	27
Th	50	28	42
UF$_4$	50	29	41

The same procedure was used in order to calculate the contribution of the different parameters to the width of the total mass distribution obtained from option 3. By solving the system of equations (III.2) and (III.6), one finds the following expression for the mass of the fissioning system:

$$A_t = \frac{2\Delta t 2E_1 E_2 (\sin^2\theta_1 + \sin^2\theta_2)}{(d_1 E_2 \sin\theta_2 + d_2 E_1 \sin\theta_1)^2}$$

As previously:

$$\sigma^2 A_t = (\frac{dA_t}{d\Delta t})^2 \sigma^2 \Delta t + (\frac{dA_t}{dE_1})^2 \sigma^2 E_1 + (\frac{dA_t}{dE_2})^2 \sigma^2 E_2 + (\frac{dA_t}{d\theta_1})^2 \sigma^2 \theta_1 + (\frac{dA_t}{d\theta_2})^2 \sigma^2 \theta_2$$

The time resolution of the system was measured from the distribution obtained with a pulse generator replacing the detector signals at the inputs to the preamplifiers in Fig.49: $\sigma\Delta t$ = 0.8 nanosecond. The following table shows separately the calculated standard deviation contributions from all parameters involved, which combine to lead to the total standard deviation σ(par). From this and the experimental results, the true standard deviation σ(true) was obtained.

A_t distributions							
Target	$\sigma(\Delta t)$ amu	$\sigma(E)$ amu	$\sigma(\theta_1)$ amu	$\sigma(\theta_2)$ amu	σ(par) amu	σ(exp) amu	σ(true) amu
Au	7.4	0.1	20.8	5.5	22.8	26.55	13.6
Bi	7.8	0.1	21.8	5.7	23.8	25.27	8.5
Th	8.5	0.1	24.4	6.4	26.6	30.88	15.6
UF$_4$	9.1	0.1	25.5	6.7	27.9	21.36	----

Here again, it can be seen that the main contributing factor to the total mass distribution width is the solid angle θ_1 while the time and the second solid angle have a much smaller influence.

c) Results

The results obtained from the three different options are given for all the targets studied in Table VII.

The distributions of the total kinetic energy in the center of mass system are shown in Fig.66-67-68 for Au,Th and UF$_4$ targets respectively while the corresponding center of mass momentum distributions are given in Fig.69-70-71. The center of mass momenta expressed in different units are related as follows:

p in MeV/c = p in (Mev.amu)$^{1/2}$ x 30.52

30.52 being the quantity (amu in MeV/c^2)$^{1/2}$.

TABLE VII

Tar get	option	A_1 a.m.u	A_2 a.m.u	E'_1 in MeV	E'_2 in MeV	E_{tot} in Mev	P_{cm} in $\sqrt{MeV.amu}$	A_t amu
Au	option 1	96±6	95±6	66.9±1.6	67.2±1.6	133.5±3.2	--------	----
	option 2	96±6	94±6	66.3±1.6	67.7±1.6	133.4±3.2	14.4±0.3	---
	option 3	92	96	66.7±1.6	66.9±1.6	133.6±3.2	--------	189
Bi	option 1	101±6	102±6	71.0±1.6	70.7±1.6	141.4±3.2	--------	---
	option 2	101±6	101±6	70.6±1.6	71.1±1.6	141.3±3.2	15.3±0.3	---
	option 3	97	103	71.0±1.6	70.6±1.6	141.4±3.2	--------	202
Th	option 1	114±6	115±6	75.1±1.6	76.1±1.6	151.3±3.2	--------	----
	option 2	115±6	113±6	76.2±1.6	74.8±1.6	151.4±3.2	16.8±0.3	---
	option 3	111	117	74.6±1.6	76.5±1.6	151.1±3.2	--------	230
UF_4	option 1	117±6	118±6	81.7±1.7	81.9±1.7	164.0±3.4	--------	---
	option 2	118±6	117±6	81.7±1.7	82.4±1.7	164.4±3.4	17.7±0.3	---
	option 3	110	119	81.8±1.7	81.7±1.7	163.9±3.4	--------	231

Fig.66: Measured total kinetic energy in the center of mass system for Au+480 MeV protons.

Au

NUMBER OF EVENTS

TOTAL ENERGY (MeV)
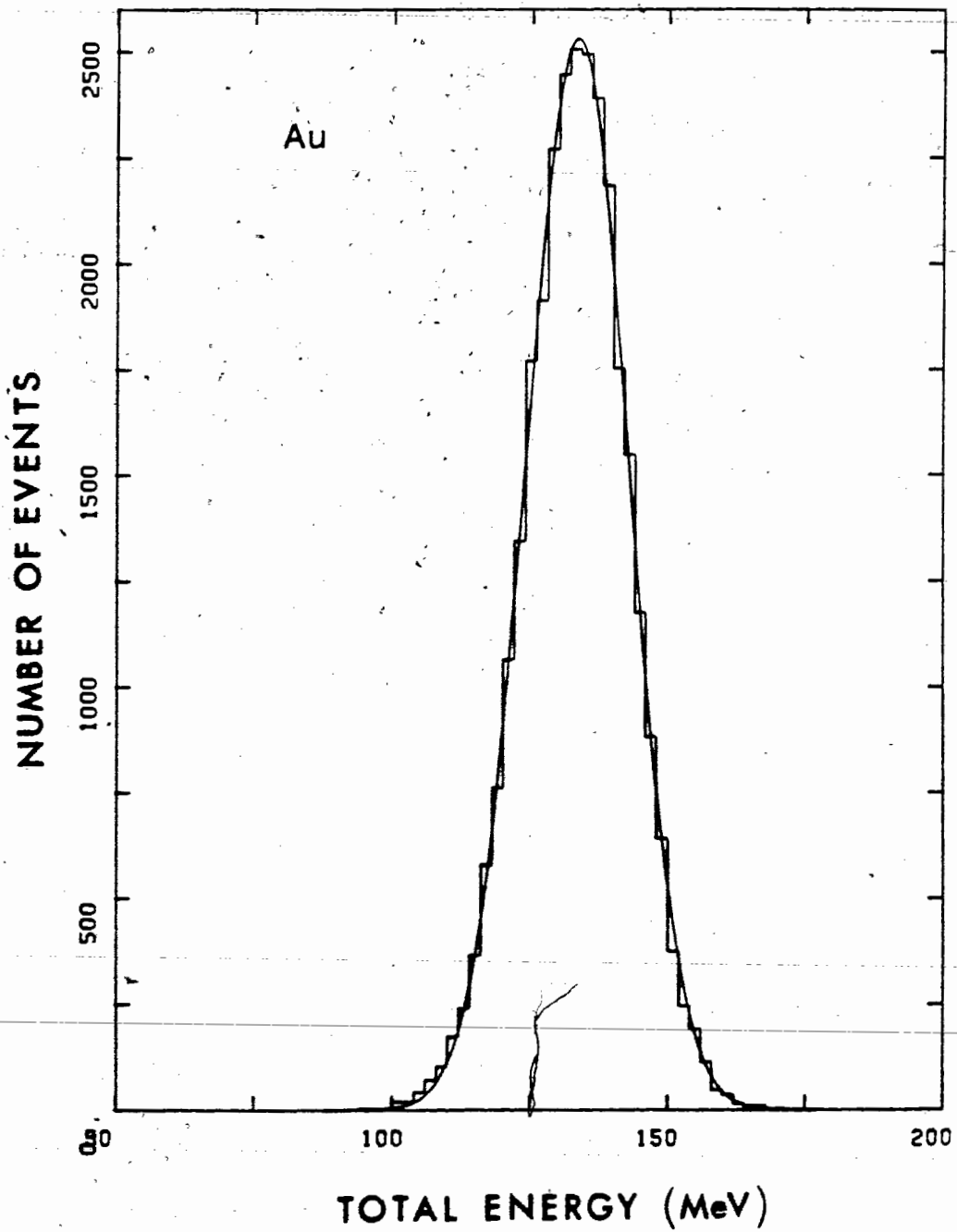
194 - a

Fig.67: Measured total kinetic energy in the center of
mass system for Th+480 MeV protons.
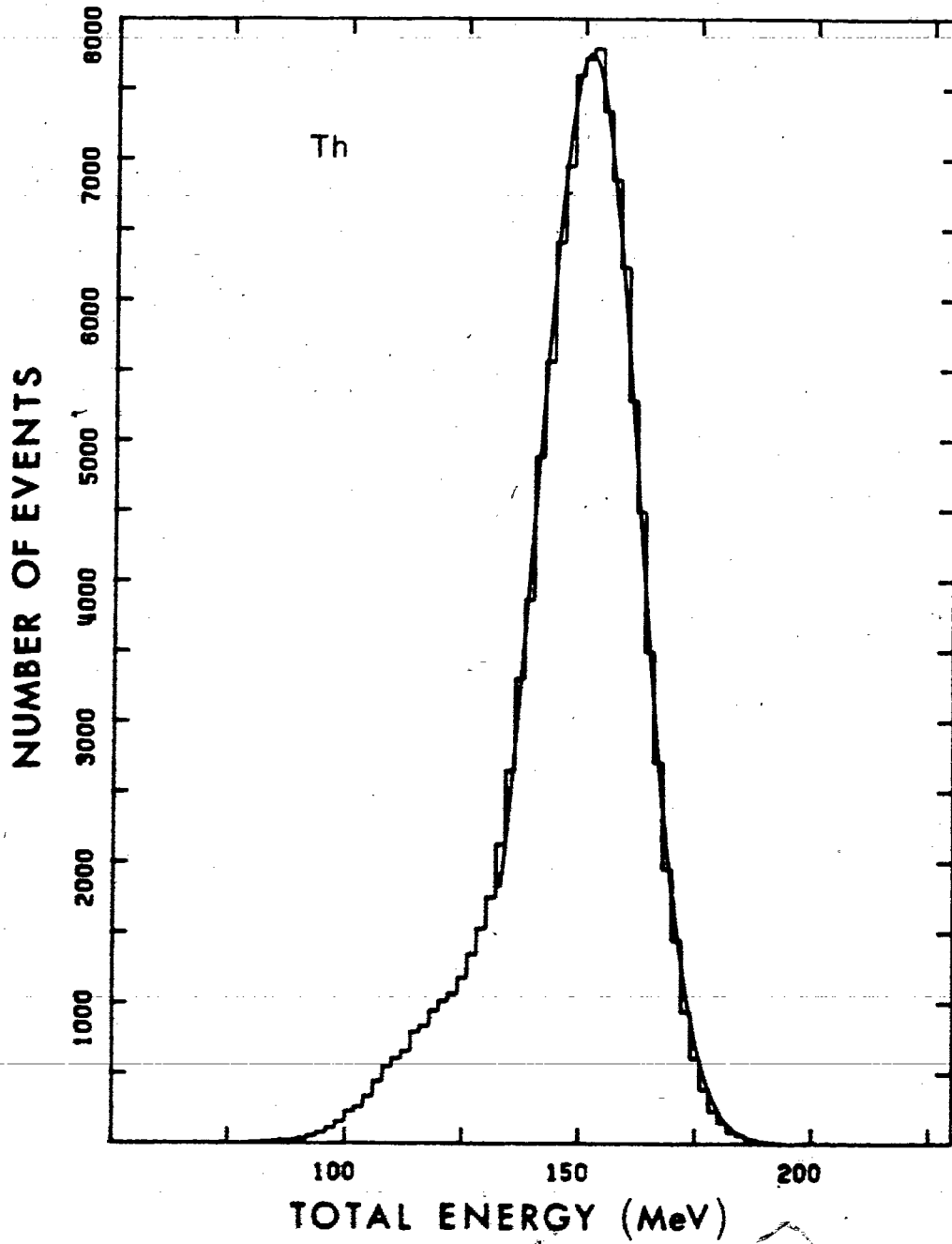
Fig.68: Measured total kinetic energy in the center of

mass system for UF_4+480 MeV protons.

UF$_4$

NUMBER OF EVENTS

TOTAL ENERGY (MeV)
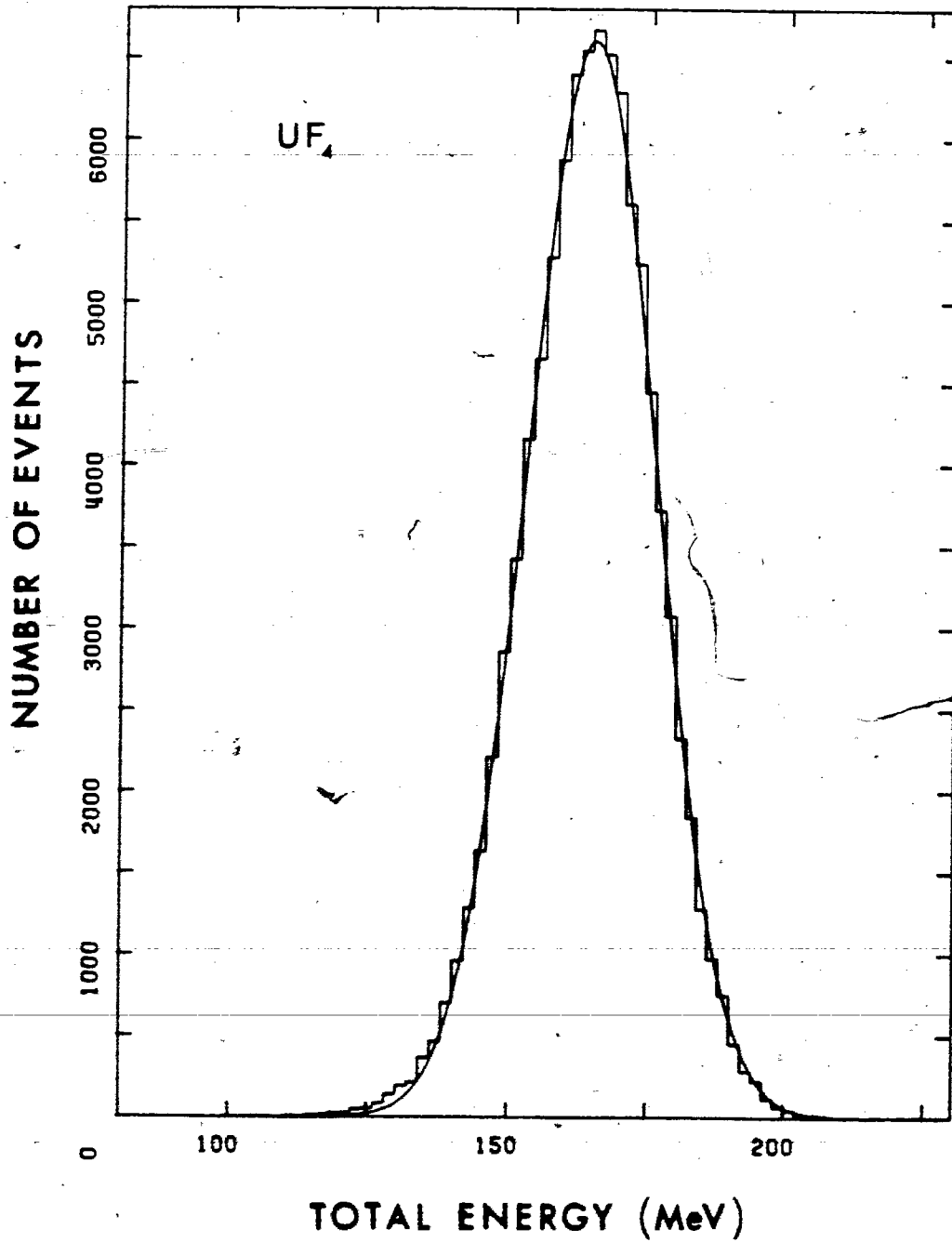
Fig.69: Deduced center of mass momentum distribution of the fissioning system from Au+480 MeV protons.
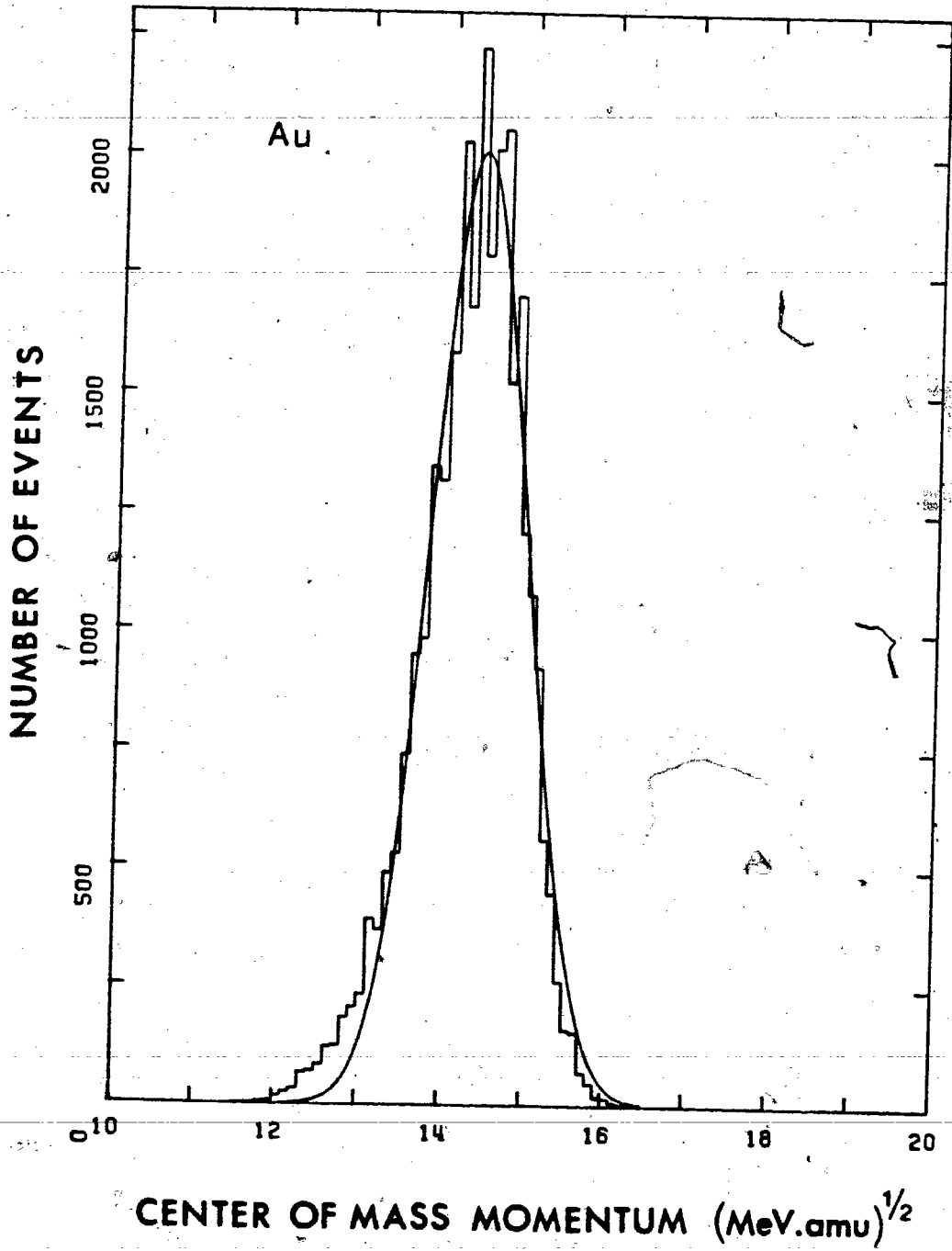
Fig.70: Deduced center of mass momentum distribution of
the fissioning system from Th+480 MeV protons.

CENTER OF MASS MOMENTUM $(MeV.amu)^{1/2}$
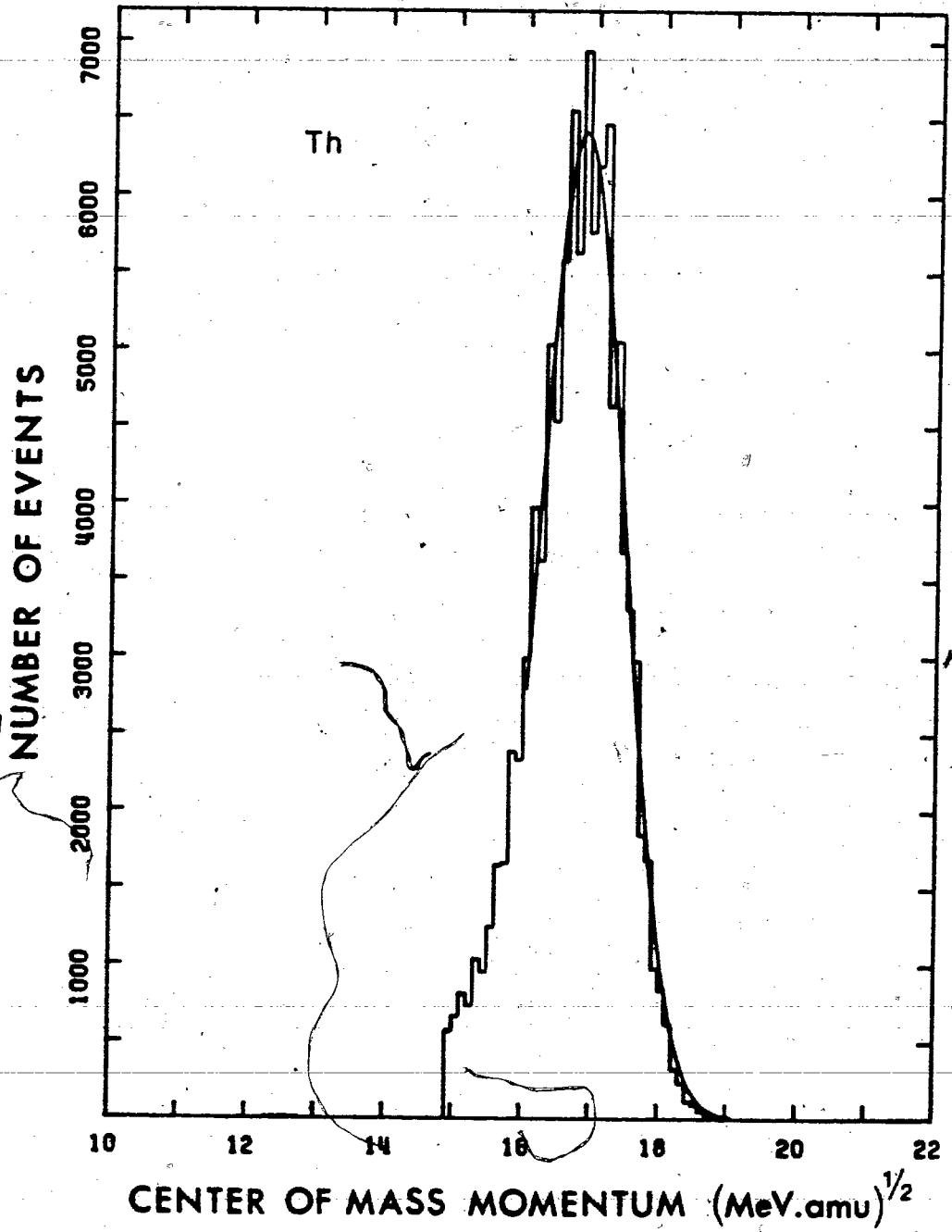
Fig.71: Deduced center of mass momentum distribution of the fissioning system from UF_4+480 MeV protons.

UF$_4$

NUMBER OF EVENTS

CENTER OF MASS MOMENTUM (MeV.amu)$^{1/2}$
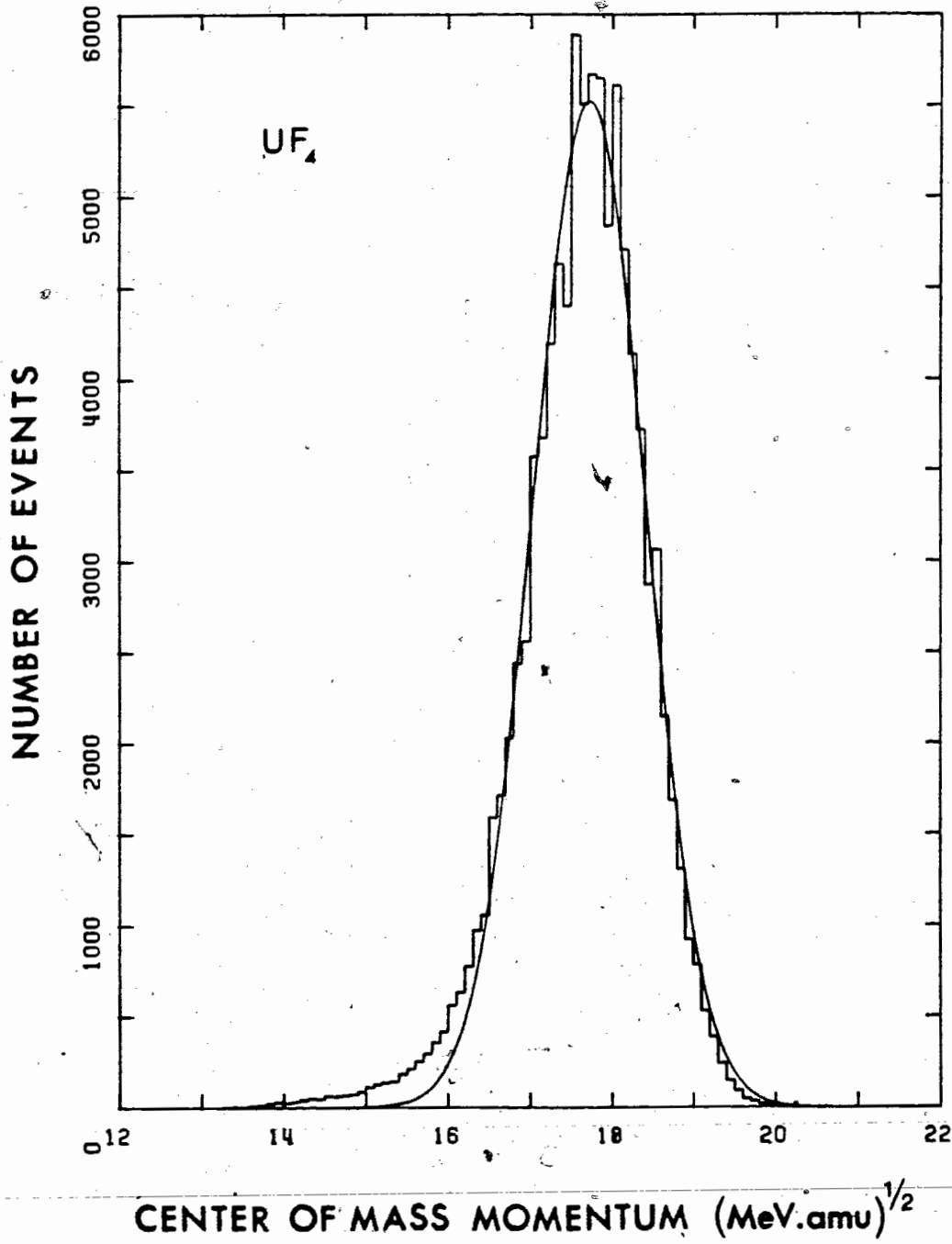
IV DISCUSSION

A) Techniques

1) Mica calibration

It is believed that the calibration data presented here constitute an advance on those available previously. Indeed, from the point of view of the use of mica for fission fragment spectroscopy, they may represent almost the best that can be achieved, short of the measurement of range curves for mass-separated ions of all relevant masses accelerated to a series of energies in the range of interest. Given the variation in the range-energy relationships from ion to ion already observed, plus the limitations in the application of the mica technique from other causes, further such calibration measurements are probably not worth the effort. Application of the present techniques to measurement of the most probable fission fragment energies in the case of low energy neutron induced fission of uranium (where some of the complications of the

higher energy systems are absent) in any case produced data evidently in satisfactory agreement with the literature.

2) Semiconductor detector experiments

The techniques employed in these experiments were evidently adequate to obtain data of good quality on fragment energies; the analysis of errors presented above shows that the energy uncertainties were small compared with the width of the energy distributions to be measured, and made only a small contribution to the uncertainty of the most probable values extracted from such distributions.

The angular data suffered from the effects of the size of the angular aperture of the detectors needed to achieve practical counting rates and random coincidence rates. Nonetheless, given the width of the angular correlations measured, the angular uncertainties are considered reasonable for the present purposes, and the data obtained to be of good quality.

In the case of the attempt to measure the fissioning system mass via fragment energies and time of flight, the techniques were clearly inadequate. They did, however represent about the best that could have been done with the

level of sophistication of the equipment at hand. To really
measure the required mass to useful precision would clearly
require experimental techniques (and a budget) well beyond
the scope of the work described above.

B) Results

1) Fissioning system mass

In the event that "first-chance fission" occurred in
the reaction systems studied here, then the fissioning
system mass distribution would be very narrow and centered
at or close to the mass of the target nucleus. Such a result
would (as noted above) be expected on the basis of
elementary considerations from the statistical model.

On the other hand, in the event that the opposite
extreme ("last-chance fission") is obtained, the fissioning
system mass would be distributed, with a width comparable to
that of the excited products from the prompt intra-nuclear
cascade widened still further by the variable effects of
evaporative de-excitation. Fig.72 shows the mass
distribution calculated by the ISOBAR code for the system
Bi+ 500 MeV protons and Fig.73 the result from the ISOBAR

Fig.72: Mass distribution results obtained from calculation by the ISOBAR code for the system Bi+500 MeV protons.
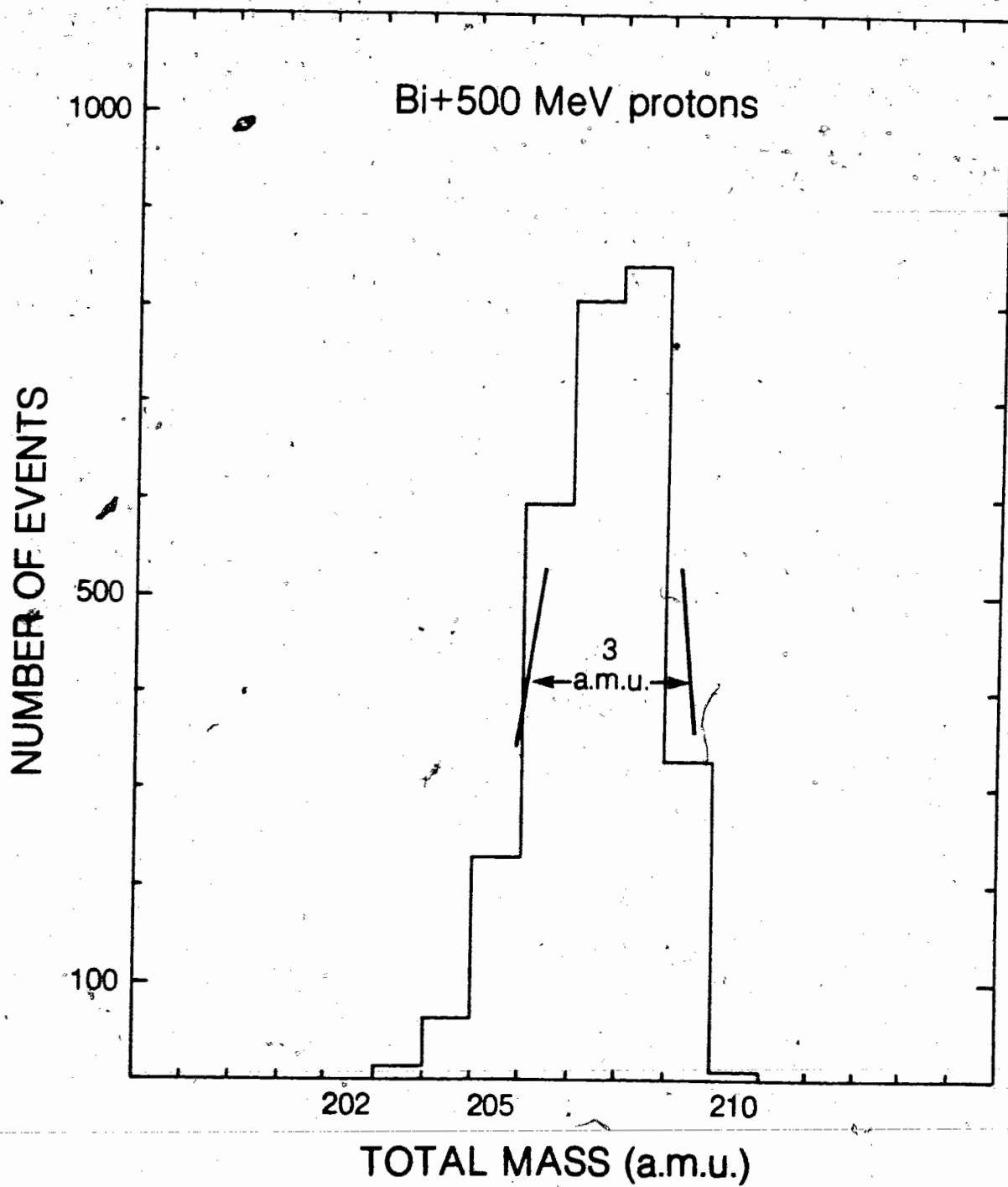
Bi+500 MeV protons

Fig.73: Mass distribution results obtained from calculation by the ISOBAR followed by EVA codes for the system Bi+500 MeV protons.
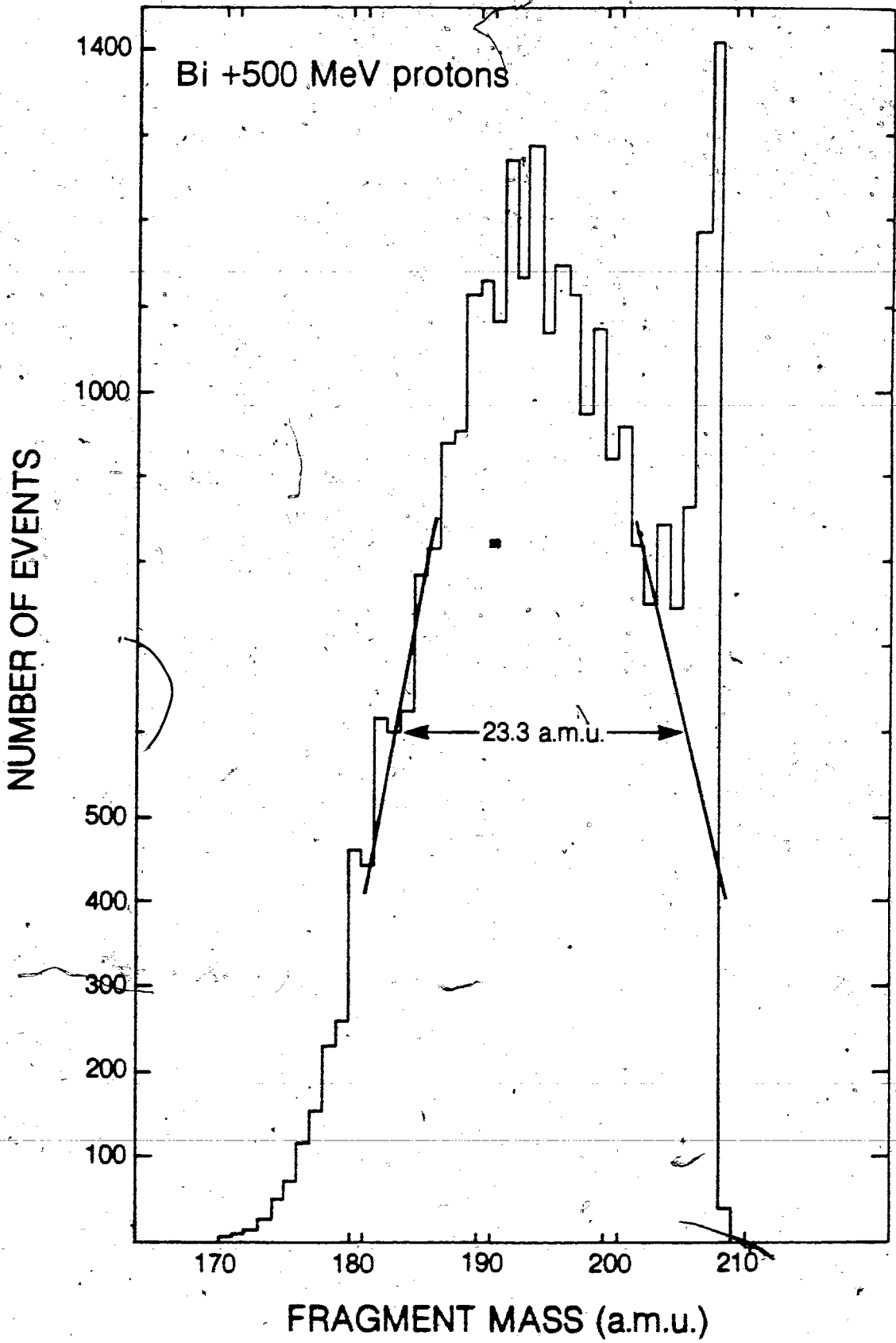
followed by EVA codes. As mentioned earlier, the EVA code does not consider fission in competition with evaporation for nuclei lighter than uranium, so that this latter distribution (modified for the effects of the substantial fission barrier for nuclei in this mass range) will approximate the mass distribution for nuclei undergoing last-chance fission. We also note that the EVA code is relatively rudimentary, but that it is probably adequate for the present discussion since the effects of angular momentum neglected by the code would be expected to be small.

The most probable mass value for distributions such as that in Fig.73, together with a distribution width expressed as a full width at half maximum height, are given in Table VIII for each of the targets studied here.

In the event that fission is neither first-chance nor last-chance in character, but occurs over many steps in the de-excitation chain (as predicted by the statistical model), then a different distribution of fissioning system masses will be obtained. However, the present experimental techniques for measurement of this quantity are sufficiently crude that a sophisticated calculation of it was not considered justified.

The results of analysis via the RADICS code of the

TABLE VIII

Target	⟨A⟩ amu ISOBAR+EVA	FWHM mass distribution ISOBAR+EVA	⟨A⟩ amu RADICS	⟨A⟩ amu TOF	FWHM mass distribution TOF
Au	179	23	190±5	188	32
Bi	192	23		202	20
Th	214	26		230	37
UF$_4$	218	26	234±2	231	--

angular distribution data obtained with mica detectors for the systems Au and U plus 800 MeV protons lead to values included in Table VIII in column 4.

Results obtained via semi-conductor detectors and the time of flight technique for protons energies of 480 MeV are shown in the same table in columns 5 (for the most probable mass) and 6 (for the distribution widths).

The two sets of data, where they overlap, are reasonably consistant, and indicate a most probable fissioning system mass distinctly displaced from that of the target. Thus, the data do at least indicate that first-chance fission was probably not the operative mechanism in general. However, while the width values extracted from the time of flight experiment are of the same order of magnitude as those calculated via ISOBAR+EVA, their quality is certainly not good enough to allow a distinction to be made between the distribution of masses resulting from last-chance fission and that from fission-evaporation competition occuring during much of the de-excitation process.

2) Momentum of the fissioning system and excitation
   energy

The component of the fissioning system momentum
parallel to the beam direction ($p_{//}$) is accessible, as seen
earlier, through the angular correlation measurements. It
can be evaluated from the angular distributions and with
time of flight experiments as well. If it is assumed that
any pre-fission neutrons are emitted isotropically in the
center of mass of the fissioning nucleus, and that their
evaporation has negligible effect on the value of $p_{//}$, then,
this momentum is the momentum given to the fissioning
nucleus by the intra-nuclear cascade.

The relationship expected between the excitation energy
E^* and the corresponding value of $p_{//}$ can be extracted from
the results of the ISOBAR code calculations. Fig.74 shows
these results in the case of a gold target bombarded with
500 MeV protons where the average excitation energy for a
given value of $p_{//}$ is plotted.

The most probable value of $p_{//}$ from the angular
correlation experiments together with the corresponding
excitation energy E^*(cal) calculated by means of the

Fig.74: Average value of the excitation energy (E^*) corresponding to a given momentum $p_{//}$ as calculated by the ISOBAR code for the system Au+500 MeV protons.

Au+500 MeV protons

AVERAGE EXCITATION ENERGY ⟨E*⟩ (MeV)

p// (MeV/c)
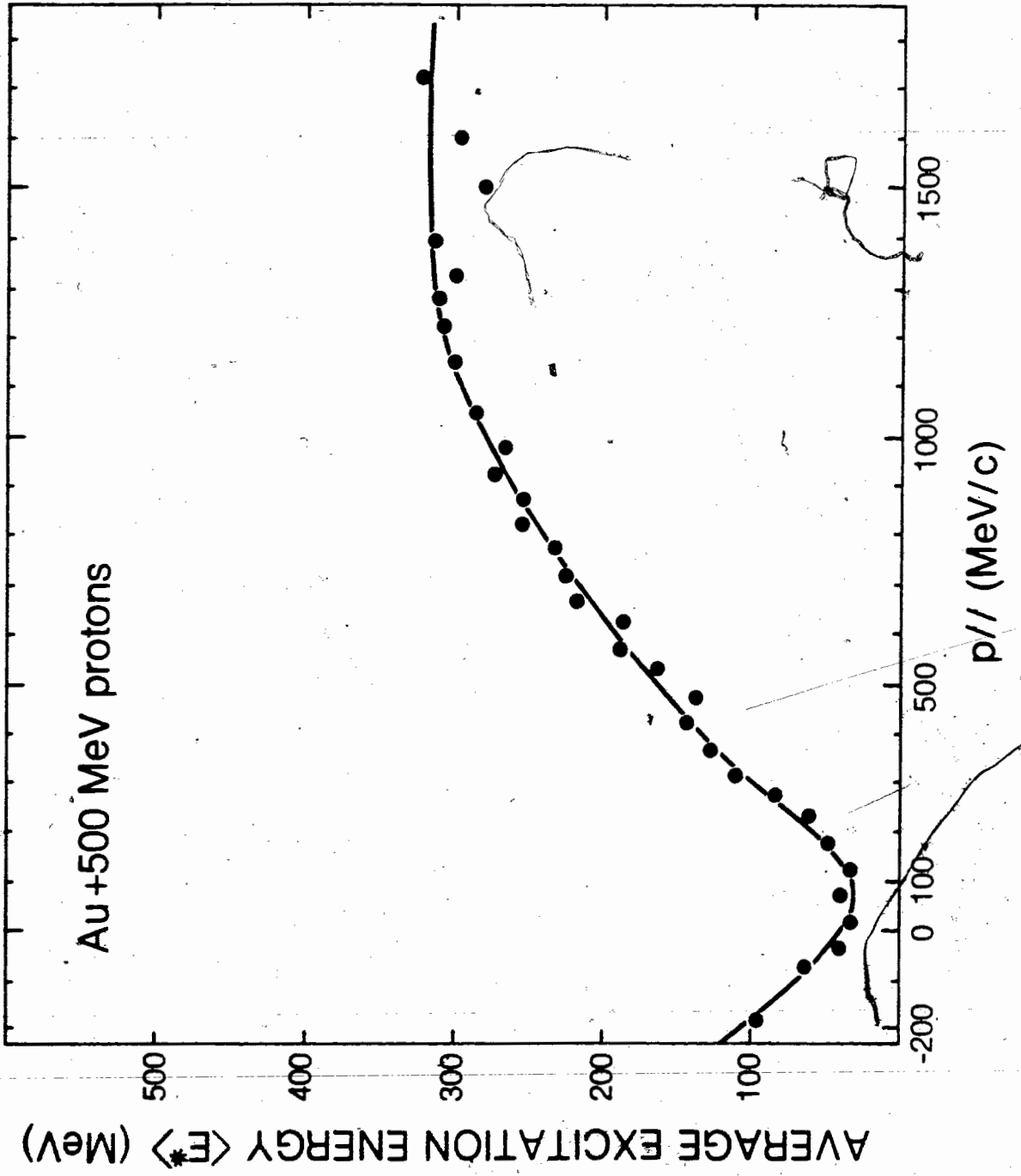
relationship of figure 74, is given in Table IX together
with the nuclear temperature t(exp) calculated through the
relationship (Nix.69):

$$at^2 - t = E^* - B_f$$

where the level density parameter a is taken as A/8 and B_f
is the fission barrier as calculated by Myers and Swiatecki
(Mye.66). In columns 5 and 6, the average value of the
excitation energy at the end of the cascade calculated by
means of the ISOBAR code, (E^*(isob)) is reported with the
corresponding nuclear temperature t(isob). In the last
column, the results from the analysis of the angular
distributions by the RADICS code are reported.

It can be seen from this table that, as the mass of the
target increases from Au to U, the average calculated
excitation energy (following the intra-nuclear cascade step)
of the nuclei leading to fission decreases. This effect is
observed in data from experiments both conducted with
semi-conductor detectors and with mica.

This could be explained in two ways:
  - one is the fact that, as the mass of the target
increases, the fission barrier decreases thus allowing
nuclei with a lower excitation energy to fission. However,
this cannot entirely account for the large decrease in the

TABLE IX

| Target | 480 MeV protons | | | 500 MeV protons | | 800 MeV p |
| | $p_{//}$(exp) | E^*(cal) | t(exp) | E^*(isob) | t(isob) | E^*(RADICS) |
	MeV/c	MeV	MeV	MeV	MeV	MeV
Au	483	160	2.43	160.4	2.43	150
Bi	471	150	2.27	163.3	2.38	
Th	267	80	1.62	169.4	2.41	
UF$_4$	231	77	1.59	171.7	2.41	95

average excitation energy from 160 MeV for gold to 77 MeV
for uranium.

      - the other more likely explanation can be given
by considering Fig.52-53-54-55 displaying the parallel
component of the fissioning system momentum obtained
experimentally and calculated through ISOBAR. It can be
observed that, while the two curves are in good agreement in
the case of the gold target, they disagree sharply in the
case of the uranium target (with intermediate situations for
the other targets). This discrepancy could be due to the
effects of evaporative de-excitation, and a simple
calculation can demonstrate if this is the case.

The average linear momentum $p_{//}$ given by ISOBAR at the
end of the cascade step has a value of 605 MeV/c in the case
of the uranium target. If, say, 20 neutrons are evaporated
before fission, the average velocity of the system will
remain the same (provided that the neutrons are emitted
isotropically in the center of mass of the fissioning
system) and the ratio of momenta before and after
evaporation will be as the ratio of the masses. Starting
from an average mass of 236 amu (as given by ISOBAR), one
obtains:

$$P_{after} = P_{before}(216/236) \text{ or } P_{after} = 554 \text{ MeV/c}.$$

If one assumes a first-chance fission mechanism with evaporation of an average 16 units of mass from each of the fission fragments (isotropically in their center of mass), one obtains a similar result for the value of $p_{//}$ after evaporation.

This average value of $p_{//}$ after evaporation is still quite far from the value of 231 MeV/c obtained experimentally, meaning presumably that the discrepancy between the experimental and calculated curves cannot be explained by evaporation alone.

Another explanation for the reduced average excitation energy of the nuclei which fission (in the case of Th and U targets) may be obtained by considering Fig.75 which is a three dimensional plot of data on the angular momentum versus the excitation energy of the nuclei resulting from the intra-nuclear cascade as calculated by ISOBAR. It can be seen that there is a tendency for the angular momentum to decrease with increasing excitation energy; this can be understood through the notion that highly excited nuclei are the result of collisions in which the incoming projectile hits the target nucleus at or near its center thus resulting in a low angular momentum, while the nuclei with low excitation energy result from collisions with large impact

Fig.75: Three dimensional plot of the angular momentum versus the excitation energy of the nuclei following the intra-nuclear cascade as calculated by the ISOBAR code for the system UF_4+500 MeV protons. The center of the figure gives the number of nuclei possessing an excitation energy E^* (shown horizontally in 25 MeV bins) and an angular momentum J (listed vertically). The total number of nuclei having a given angular momentum and their average excitation energy (<E>) are shown in the column on the right while the total number of nuclei possessing a given excitation energy and their average angular momentum (<J>) are listed at the bottom.

J \ E*	0	25	50	75	100	125	150	175	200	225	250	275	300	325	350	375	400	425	450	475	500	ΣN	\<E\>
0				1																	5	7	418
1							1			1	2	2	2		1		1		2			10	306
2								1	1	2	2	4	3	2	4	2	1	1		2		20	330
3			1		1	2	3	2	3	6	6	4	8	3	7	3	1					34	324
4					1	2	1	1	5	5	6	7	8	6	5	3	2					50	300
5			1		1	1	2	5	5	6	7	9	5	9	6	4	1					53	304
6				3	2	2	6	5	6	6	7	6	8	6	3	4	1	1				59	308
7					3	2	6	10	5	7	12	10	9	5	4	2						60	292
8				1		4	6	11	7	12	11	10	12	6	3	1	1					71	270
9			1		3	5	6	7	8	11	10	10	14	6	5	1		2				97	271
10			1	1	3	4	6	3	8	7	5	8	12	6	1	5	1					104	276
11		1		3	3	5	6	7	9	18	9	6	6	6	1	1	3					83	254
12			3	4	3	6	3	4	7	9	10	9	7	3	2							75	237
13		1	2	1	3	6	7	15	9	17	7	6	6	6		5						80	241
14	1		1	4	5	6	7	11	14	9	13	7	6	2	1	1						99	232
15				1	2	7	7	11	4	6	8	6	6									77	223
16			3	5	8	10	9	13	13	7	13	4	7	6								82	195
17		3	5	7	2	7	13	13	4	8	4	2	1									84	187
18		2	2	7	3	13	10	13	6	7	8	2	1									94	200
19	1	2	5	4	11	7	10	9	13	10	7	1	1			1						75	188
20		2	2	7	8	11	13	13	14	5	7	1			1							73	174
21		2	3	3	11	10	13	12	6	7	2	2										77	169
22	1	2	4	7	14	10	10	7	7	3	2	1										87	150
23	1	3	2	1	8	10	13	9	13	6	3											69	161
24		2	4	8	6	15	5	6	7	2	1	1										54	143
25		4	7	6	6	6	10	9	4	2	3	3										78	133
26	6	4	9	7	10	12	5	7	3	2												67	143
27	6	6	9	12	8	12	8	6	4	1			2									57	107
28	4	6	10	7	10	4	7	9	3	1			1									69	114
29	4	9	8	5	5	12	11	6	1	1												52	105
30	4	5	10	9	11	10	5	7	4													66	112
31		8	9	15	5	8	2	3	1		1											58	93
32	8	7	7	4	11	6	2	1														44	92
33	5	11	8	6	7	9	2			2												47	73
34	11	12	8	5	6	3	2	2														46	67
35	20	14	9	4	3	1	2	2	1													57	54
36	7	10	8	5	1	1	2	1		1												39	73
37	18	14	8	4	2	2	2		1													44	40
38	15	12	8		1	1	1															37	37
39	21	11	8	2																		46	39
40	24	4	6	3	2	1																41	34
41	19	9	6	2	1	2																39	41
42	18	5	3	2			1															28	25
43	22	3	3																			29	18
44	21	3	2																			27	21
45	14	2	2																			18	14
46	16	2	2	1																		21	17
47	17	2																				19	9
48	6																					6	6
49	4	1																				5	11
50	2																					2	2
51	1	1																				1	0
52	1																					1	13
ΣN	308	193	185	174	173	218	205	209	178	183	167	135	114	95	74	44	42	19	13	4	5		
\<J\>	39	32	29	26	24	21	19	18	16	14	14	11	11	9	8	8	6	7	6	3	0		

parameter and thus imparting to the struck nucleus a larger angular momentum.

It has been observed by many authors (Mil.78) that the probability for fission was greatly enhanced, at a given excitation energy, by an increase in angular momentum while, at constant angular momentum, an increase in excitation energy does not lead to a greater fission probability. This effect would clearly favour the fission of nuclei with high angular momenta and hence with low excitation energies.

The foregoing may seem to be in contradiction to the results of the present angular distribution measurements (see section III-B-1) which indicated very small anisotropies; however, an analysis of the orientation of the angular momentum vectors at the end of the prompt cascade as calculated by the ISOBAR code indicates that, except for those rare events with maximum angular momentum, the component parallel to the beam axis is of the order of 25% of the component perpendicular to the beam axis for all the present target nuclei. This might very well wash out to a great degree the correlation between the angular momentum vector and the symmetry axis of the fissioning system, thus attenuating the expected preferential emission of fission fragments in the forward and backward directions.

The angular correlation measurements with the mica
sandwich technique (which lead to values of the center of
mass momentum) do not offer the quality of data of those
performed with the semi-conductor detectors, owing to the
difficulty in scanning very deep and very shallow tracks
with respect to the mica surface. However, it is interesting
to look at the change in this momentum when π^+ particles
are used as projectiles instead of protons. Unfortunately,
the experimental facilities available did not permit this to
be done at the same projectile energy, and the effects of
increased proton mass are added to those of the increased
energy (800 MeV) of the proton beam compared to that
(400 MeV) of the pions. Fig.76 shows the momentum parallel
to the beam axis $(p_{//})$ as calculated by ISOBAR in the case
of a gold target bombarded with 400 MeV π^+ and of a 800 MeV
proton bombardment. The average momentum given to the nuclei
by the proton projectile is clearly greater than the average
momentum imparted by the pions. This trend is consistent
with that observed in the results of the mica sandwich
measurements where the average value of $p_{//}$ was found to be
bigger with 800 MeV protons than with 400 MeV π^+ particles
(see TableVI).

Fig.76: Momentum parallel to the beam axis ($p_{//}$)
transferred from the projectile to the struck nucleus as
calculated by the ISOBAR code for the systems Au+400 MeV
pions (———) and Au+800 MeV protons (————).
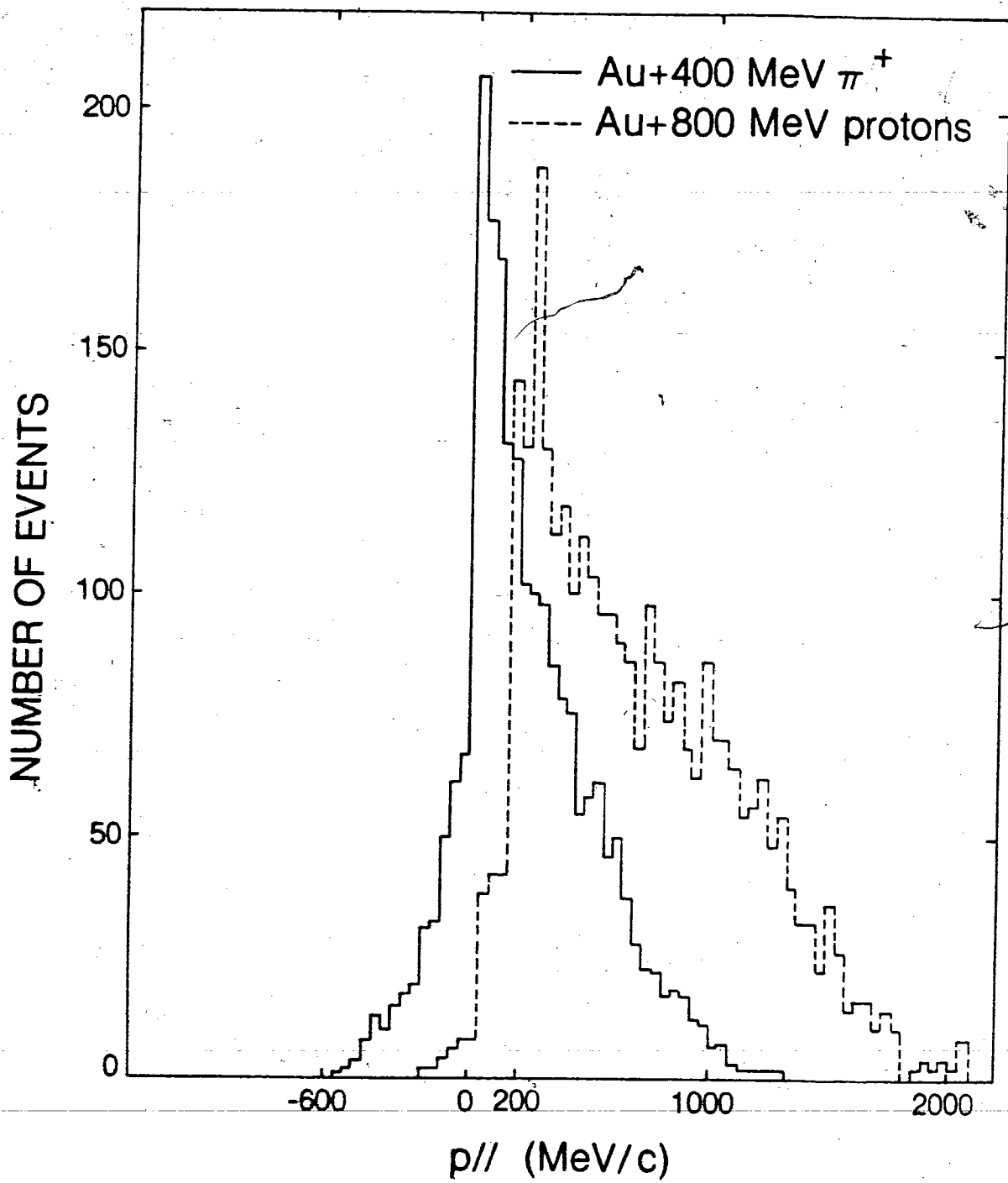
3) Fission fragment energies and masses

These two quantities will be considered together since, in the experiments, measurements of the first were used to extract the second, and the effects of excitation energy on their respective distribution widths are expected to be connected.

This effect of excitation energy was considered (inter alia) by Nix (Nix.69). Fig.77 reproduced from this reference shows the calculated widths of the distributions in total kinetic energy and in fission fragment mass as a function of the nuclear temperature. The average value of the nuclear temperature calculated from the experimentally determined excitation energy is reported in Table X. Column 3 of this table lists the most probable total kinetic energy calculated by Nix and columns 4 and 5 the energy and the fragment mass distribution widths corresponding to the temperature in column 2. The data from experiments with mica sandwiches are reported in columns 6 and 7 while the experimental data from semi-conductor detectors measurements are listed in columns 8 to 10.

While the average values of the total kinetic energy

Fig.77: Calculated widths (FWHM) of the mass and energy distributions for fragments from various fissioning systems as functions of the fissility parameter x. The curves are for various values of the nuclear temperature θ at the saddle point.
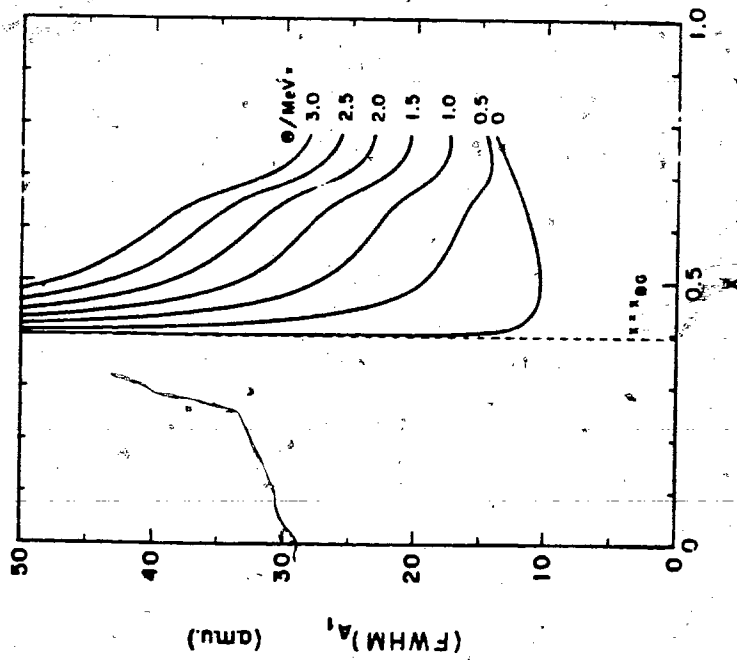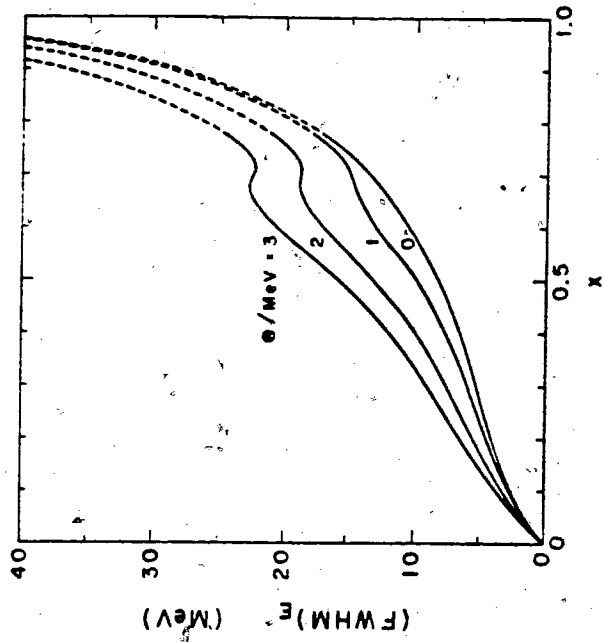
TABLE X

Target	t	NIX			MICA		Semi-cond. detec.		
		$\langle E_K \rangle$	FWHM E_K	FWHM A_1	$\langle E_K \rangle$ 400 MeV pions	$\langle E_K \rangle$ 800 MeV protons	$\langle E_K \rangle$	FWHM E_K	FWHM A_1
Au	2.43	146	21	33	123±9	123±9	133.4	22.1	32
Bi	2.27	160	20	29			141.3	21.9	27
Th	1.62	190	18	22			151.4	25.5	42
UF$_4$	1.59	197	19	21	162±15		164.4	27.5	41

experimentally obtained with the two techniques used are in reasonable agreement, they are consistently low compared with the calculated values. This discrepancy between several experimental determinations of the total kinetic energy and the theoretical predictions has been already noticed by Nix (Nix.69) and led him to improve the model used, in order to produce better agreement with experiment. As seen earlier, this model was based on the liquid drop model by assuming a non viscous irrotational flow inside the nucleus. More recent investigations (Dav.76), (Dav.77) taking viscosity into account led to more satisfactory results. Fig.78 taken from (Nam.75) shows a comparison of experimental and theoretical values of the total kinetic energy of the fission fragments for several values of the viscosity coefficient. The results from the present work have been added to this figure and are found to be in good agreement with the other experimental investigations.

The experimental values of width of the distributions (FWHM) reported in Table X agree well with the calculated ones (both for the kinetic energy and the fragment mass distributions) for the gold and bismuth targets. However the widths are much larger for the heavy targets. This disagreement between experimentally determined FWHM values

Fig.78: Comparison of experimental and theoretical values of the most probable total kinetic energy of the fission fragments from various fissioning systems. The solid curves represent the results of calculations for different values of the viscosity coefficient μ. The dashed curves give the calculated translational kinetic energies acquired prior to scission. Data (X) are from the present work.
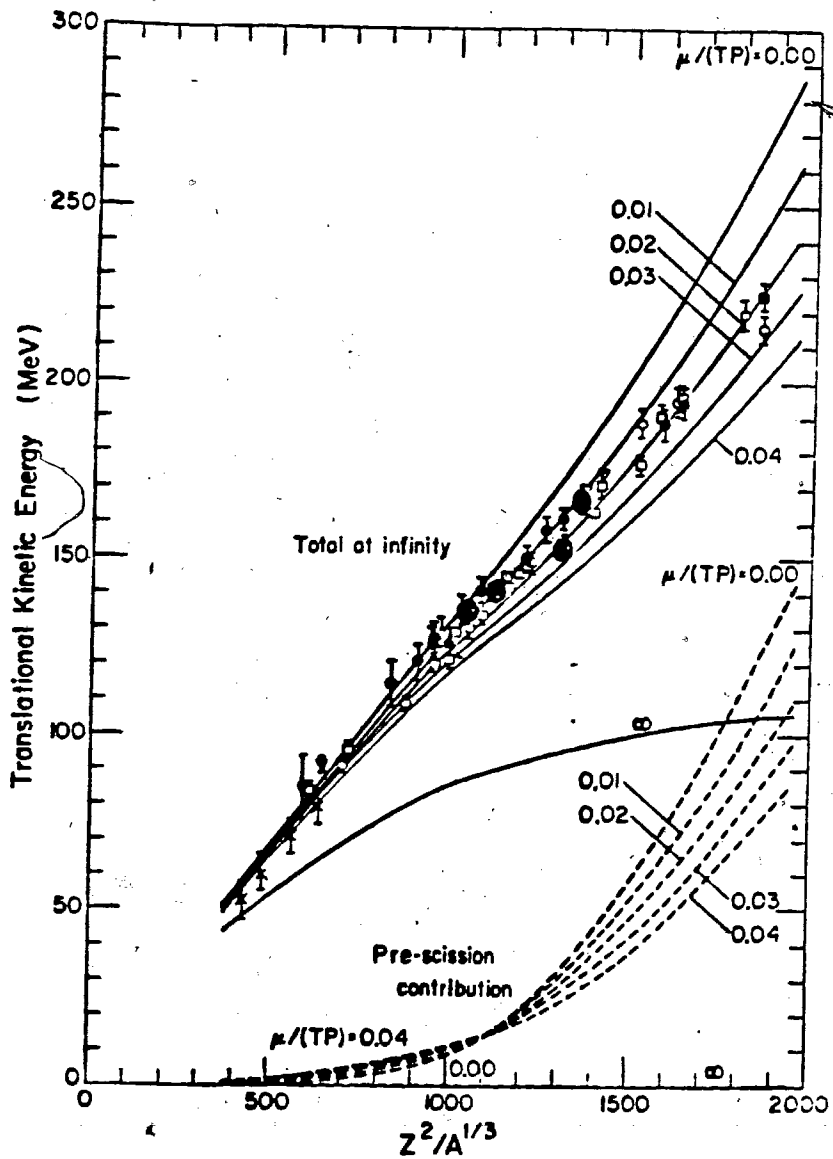
and theoretical ones was also found by other authors (see
Nix.69)).

The width (FWHM) value of the fragment mass
distribution was also obtained through calculations via the
ISOBAR and EVA codes where fission was included in the
process of de-excitation. The results of such a calculation
are given in Fig.79 for an uranium target bombarded with
500 MeV protons. The distribution in fragment mass shows a
most probable value of 109 amu and a FWHM of 23.5 amu (very
similar to the value calculated by Nix). The fact that the
experimental width of the fragment mass distribution is
almost twice the calculated width could be explained by some
significant proportion of the fission events taking place at
a low enough energy to lead to a significant proportion of
asymmetric events. It may be noticed that this is in
agreement with the results obtained from angular correlation
measurements, which seem to indicate that fission occurs
with a greater probability among the nuclei left with a low
excitation energy (and a high angular momentum) after the
intra-nuclear cascade. The computer code EVA did not take
into account the effects of angular momentum and predicted
fission of nuclei soon after the cascade step, and therefore
at a higher average value of the excitation energy

Fig.79: Fragment mass distribution as calculated by the
ISOBAR and EVA codes (where fission has been included as a
means of de-excitation) for the system UF_4+500 MeV protons.
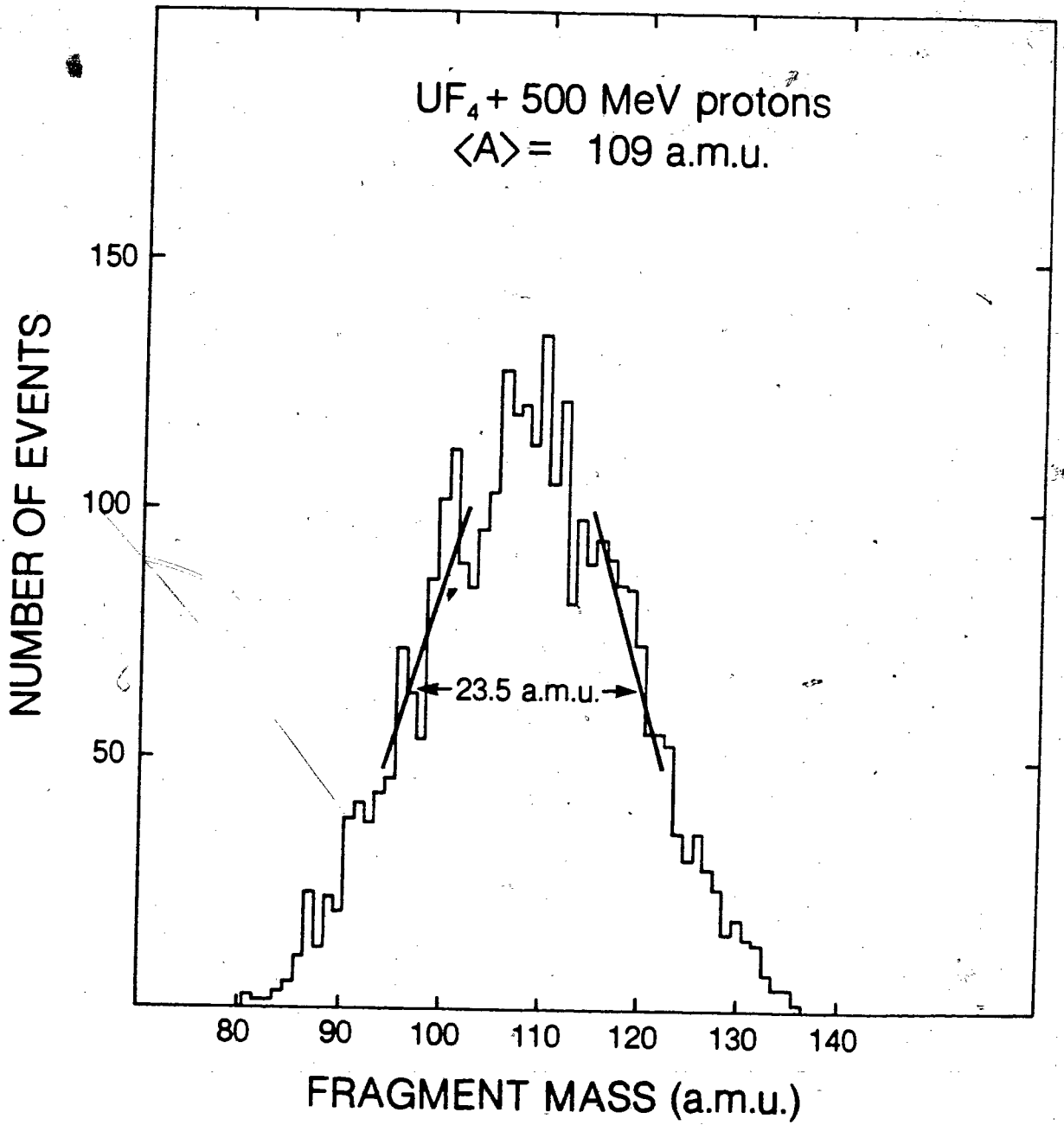
(~170 MeV). As a result, the fragment mass distribution
calculated by the code is perhaps narrower than the
experimental one arising from nuclei with an average value
of the excitation energy of the order of 80 MeV.

As mentioned earlier, the EVA code does not consider
fission, in the evaporation process, for elements lighter
than thorium, and it would be of great interest to extend
the calculations of this code to elements such as gold and
bismuth, in order to compare the width of the calculated
fragment mass distributions with those measured
experimentally.

Fission occuring at low excitation energy, thus with a
greater tendency towards asymmetry, would explain why the
experimental results are in disagreement with the
theoretical predictions of Nix in the case of thorium and
uranium targets. Indeed, the non-viscous irrotational liquid
drop model considered was found (Nix.69) incapable of
accounting for the properties of heavy nucleus fission at
low excitation energies (i.e for mass asymmetry).

V CONCLUSION

The present study provided information on fission induced by intermediate energy projectiles by means of two different techniques: mica track detector experiments and semi-conductor detector measurements.

The total kinetic energy of the fission fragments was measured and found to be in good agreement with published values obtained with different projectiles and bombarding energies.

For the same target, the measured average fragment kinetic energies were constant within experimental error whether protons (of 500 MeV or 800 MeV) or 400 MeV pions were used as projectiles. The widths of the total kinetic energy distributions were compared with the theoretical predictions of Nix for the expected nuclear temperatures and were found to be in reasonable agreement for gold and bismuth targets. However, for thorium and uranium, the experimental widths were larger than the calculated ones, a fact which has been observed in previous experimental investigations. A further test of the model proposed by Nix

was performed by comparing the widths of the fission
fragment mass distributions obtained experimentally (from
the fragment energy data) and theoretically. Here again,
good agreement was obtained for gold and bismuth but the
present experimental results for thorium and uranium were
greater than the calculated values by a factor of two. This
discrepancy could be due to the contribution of asymmetric
fission events (coming from low energy fission) to the
fragment mass distribution.

Angular correlation measurements led to average values
of the momentum of the fissioning system parallel to the
beam direction, and the corresponding average value of the
excitation energy was determined via a relationship between
the two derived from the results of the ISOBAR code. The
behaviour of the gold and bismuth targets was again
different from that of the heavier elements. In the case of
thorium and uranium, it was found that the probability of
fission was apparently higher among the nuclei possessing a
low excitation energy (and a high angular momentum) at the
end of the prompt cascade. These nuclei (with an average
excitation energy of the order of 80 MeV) would not possess
enough energy for the evaporation of a great number of
neutrons; therefore the fission process would take place (on

the average) after only a few evaporation steps.

When gold and bismuth targets were used, the measured average momentum was approximately equal to that calculated as given to the nuclei by the intra-nuclear cascade, indicating that the fission is not restricted to those nuclei with low excitation energy; the fission probability will be similar for all nuclei after the cascade step.

The measurements carried out for the determination of the fissioning system mass were not of a sufficient quality to obtain a definite value. However, indications on the competition between fission and particle evaporation were obtained when the experimental data (mainly the widths of the distributions) were compared with the calculated results of the computer codes ISOBAR and EVA (with or without fission as a de-excitation means).

The distributions of the fissioning system mass indicated a most probable value distinctly displaced from that of the target. This indication and the fact that the experimental width (FWHM) value was much greater than the calculated value for the nuclei after the intra-nuclear cascade seem to show that a simple "first-chance" fission is probably not the operative mechanism. It was not possible, however, to distinguish between "last-chance" fission and fission occurring over several stages of the de-excitation

chain.

The extension of the EVA code to include the
possibility of fission for the light targets (such as Au and
Bi) plus the inclusion of angular momentum effects could be
very useful as a means of comparison with experimental data.

The quality of the fissioning system mass measurements
could be improved by reducing the solid angle within which
the fission fragments entered the detectors. Since the
greatest uncertainty in the time-of-flight measurements was
the determination of the zero time (or time at which the
fission event took place), a method to provide a measurement
of its absolute value would be a distinct advantage. The
time of flight resolution could be improved by increasing
further the flight path of the fission fragments (i.e. the
detector giving the start signal could be located farther
away from the target). However, this increased time of
flight path added to the effects of a reduced solid angle
could result in an impractically low coincidence rate.

The current experimental approach of measuring the
evaporated particle spectra in coincidence with the fission
fragments (Wil.79), (Fra.75), (Blo.80), seems to offer more
possibilities.

LIST OF REFERENCES

(Ait.68) : M.Ait-Salem, H.Gerhardt, F.Gonnenwein, H.Hipp
            and H.Paap Nucl. Instr. and Meth. 60(1968) p.45

(Ale.63) : J.M.Alexander, C.Baltzinger and M.F.Gazdik Phys.
            Rev. 129(1963) p.1826

(And.76) : G.Andersson, M.Areskoug, H.A.Gustafsson, G.Hylten,
            B.Schroder and E.Hagebo Phys. Lett. 64B(1976) p.421

(And.79) : G.Andersson, M.Areskoug, H.A.Gustafsson, G.Hylten,
            B.Schroder and E.Hagebo Nucl. Instr. and Meth.
            163(1979) p.165

(Ara.65) : N.K.Aras, M.P.Menon and G.E.Gordon Nucl. Phys.
            69(1965) p.337

(Are.72) : N.Arena, S.Lo Nigro and C.Milone Lett. al Nuovo
            Cimento 3(1972) p.147

(Asg.70) : M.Asghar, C.Carles, R.Chastel, T.P.Doan, M.Ribrag
            and C.Signarbieux Nucl. Phys. A145(1970) p.657

(Asg.77) : M.Asghar, P.D'Hont, C.Guet, P.Perrin and C.Wagemans
            Nucl. Phys. A292(1977) p.225

(Asg.78) : M.Asghar, F.Caitucoli, P.Perrin and C.Wagemans
            Nucl. Phys. A311(1978) p.205

(Ber.63) : H.W.Bertini Phys. Rev. 131(1963) p.1801

(Ber.78) : H.W.Bertini, A.H.Culkowski, O.W.Hermann, N.B.Gove
            and M.P.Guthrie Phys. Rev. C17(1978) p.1382

(Blo.72) : H.Blok, F.M.Kiely and B.D.Pate Nucl. Instr. and
            Meth. 100(1972) p.403

(Blo.74) : H.Blok, F.Hanappe, F.M.Kiely, B.D.Pate and J.Peter
            Nucl. Instr. and Meth. 119(1974) p.307

(Blo.75) : H.P.W.L.Blok PhD. Thesis Simon Fraser University
            (1975)

(Blo.77) : H.Blok and B.D.Pate Z. Physik A281(1977) p.255

(Blo.80) : H.P.E.Blok, H.Dautet, Z.Fraenkel and B.D.Pate
to be published

(Boh.37) : N.Bohr Science 86(1937) p.161

(Boh.39) : N.Bohr and J.A.Wheeler Phys. Rev. 56(1939) p.426

(Bon.61) : G.Bonfiglioli, A.Ferro and A.Mojoni J. Appl. Phys.
32(1961) p.2499

(Bri.54) : J.A.Brinkman J. Appl. Phys. 25(1954) p.961

(Bri.56) : J.A.Brinkman Am. J. Phys. 24(1956) p.246

(Bri.63) : H.C.Britt, H.E.Wegner and J.C.Gursky Phys. Rev.
129(1963) p.2239

(Bro.62) : K.M.Broom Phys. Rev. 126(1962) p.627

(Cha.63) : L.T.Chadderton and H.M.Montagu-Pollock Pro. Roy.
Soc. A274(1963) p.239

(Che.52) : G.F.Chew and M.L.Goldberger Phys. Rev. 87(1952)
p.778

(Che.68) : K.Chen, Z.Fraenkel, G.Friedlander, J.R.Grover,
J.M.Miller and Y.Shimamoto Phys. Rev. 166(1968)
p.949

(Che.70) : E.Cheifetz, Z.Fraenkel, J.Galin, M.Lefort,
J.Peter and X.Tarrago Phys. Rev. C2(1970) p.256

(Che.71) : K.Chen, G.Friendlander, G.D.Harp and J.M.Miller
Phys. Rev. C4(1971) p.2234

(Cie.66) : E.Cieslak, J.Piekarz, J.Zakrzewski, M.Dakowski,
H.Piekarz and M.Sowinski Nucl. Instr. and Meth.
39(1966) p.224

(Cre.68) : V.P.Crespo, J.B.Cumming and A.M.Poskanzer Phys.
Rev. 174(1968) p.1455

(Cun.47) : B.B.Cunningham, H.H.Hopkins, M.Lindner, D.R.Miller,
P.R.O'Connor, I.Perlman, G.T.Seaborg and
R.C.Thompson Phys. Rev. 72(1947) p.739

(Cun.57) : J.G.Cuninghame J. Inorg. Nucl. Chem. 5(1957) p.1

(Dau.78) : D.Dautet and B.D.Pate Z. Physik A285(1978) p.253

(Dav.65) : J.A.Davies, L.Eriksson and P.Jespersgaard Nucl.
           Instr. and Meth. 38(1965) p.245

(Dav.76) : K.T.R.Davies, A.J.Sierk and J.R.Nix Phys. Rev.
           C13(1976) p.2385

(Dav.77) : K.T.R.Davies, R.A.Managan, J.R.Nix and A.J.Sierk
           Phys. Rev. C16(1977) p.1890

(Dem.72) : F.Demichelis, R.Liscia and A.Tartaglia Il Nuovo
           Cimento Vol.10B, N.2(1972) p.523

(Den.58) : G.F.Denisenko, N.S.Ivanova, N.R.Novikova,
           N.A.Perfilov, E.I.Prokoffieva and V.P.Shamov Phys.
           Rev. 109(1958) p.1779

(Dos.58) : I.Dostrovsky, P.Rabinowitz and R.Bivens Phys.
           Rev. 111(1958) p.1659

(Dos.59) : I.Dostrovsky, Z.Fraenkel and G.Friedlander
           Phys. Rev. 116(1959) p.683

(Dou.54) : E.M.Douthett and D.H.Templeton Phys. Rev. 94
           (1954) p.128

(Fas.65) : B.Fastrup, P.Hvelplund and C.Sautter Nucl. Instr.
           and Meth. 38(1965) p.26

(Fas.66) : B.Fastrup, P.Hvelplund and C.A.Sautter Mat. Fys.
           Medd. Dan. Vid. Selsk 35 N.10(1966)

(Fle.63a): R.L.Fleischer and P.B.Price J. Appl. Phys.
           34(1963) p.2903

(Fle.63b): R.L.Fleischer and P.B.Price Science 140(1963)
           p.1221

(Fle.64a): R.L.Fleischer, P.B.Price, R.M.Walker and
           E.L.Hubbard Phys. Rev. 133A(1964) p.1443

(Fle.64b): R.L.Fleischer and P.B.Price Geochim. Cosmochim. Acta 28(1964) p.1705

(Fle.65a): R.L.Fleischer, P.B.Price and R.M.Walker Science 149(1965) p.383

(Fle.65b): R.L.Fleischer, P.B.Price and R.M.Walker Ann. Rev. Nucl. Sci. 15(1965) p.1

(Fle.65c): R.L.Fleischer, P.B.Price and R.M.Walker J. Appl. Phys. 36(1965) p.3645

(Fle.67a): R.L.Fleischer, P.B.Price, R.M.Walker, R.C.Filz, F.Fukui, E.Holeman, M.W.Friedlander, R.S.Rajan and A.S.Tahmane Science 155(1967) p.187

(Fle.67b): R.L.Fleischer, P.B.Price, R.M.Walker and E.L.Hubbard Phys. Rev. 156(1967) p.353

(Fle.69) : R.L.Fleischer, P.B.Price and R.T.Woods, Phys. Rev. 188(1969) p.563

(Fle.75) : R.L.Fleischer, P.B.Price and R.M.Walker "Nuclear tracks in solids" University of California Press (1975)

(Fle.77) : R.L.Fleischer Nucl. Instr. and Meth. 147(1977) p.1

(Fra.75) : Z.Fraenkel, I.Mayk, J.P.Unik, A.J.Gorski and W.D.Loveland Phys. Rev. C2(1975) p.1809

(Fri.63) : G.Friedlander, L.Friedman, B.Gordon and L.Yaffe Phys. Rev. 129(1963) p.1809

(Fri.65) : G.Friedlander "Physics and chemistry of fission" Vol.2 IAEA Vienna (1965) p.265

(Fuj.49) : Y.Fujimoto and Y.Yamaguchi Proc. Theor. Phys. (Kyoto) 4(1949) p.468

(Fuj.50) : Y.Fujimoto and Y.Yamaguchi Proc. Theor. Phys. (Kyoto) 5(1950) p.76; 5(1950) p.787

(Gay.77) : A.Gayer and Z.Fraenkel Phys. Rev. C16(1977) p.1066

(Gil.64) : J.Gilat and J.M.Alexander Phys. Rev. 136(1964) p.B1298

(Goe.49) : R.H.Goeckermann and I.Perlman Phys. Rev. 76(1949)
p.628

(Gol.48) : M.L.Goldberger Phys. Rev. 74(1948) p.1269

(Gom.76) : M.A.Gomaa and M.A.El-Kolaly Nucl. Instr. and Meth.
134(1976) p.253

(Gom.77) : M.A.Gomaa and M.A.Hamdan Nucl. Instr. and Meth.
146(1977) p.527

(Gon.67) : F.Gonnenwein and E.Pfeiffer Z. Phys. 207(1967)
p.209

(Gri.59) : J.J.Griffin Phys. Rev. 116(1959) p.107

(Gun.57) : S.R.Gunn, H.G.Hicks, H.B.Levy and P.C.Stevenson
Phys. Rev. 107(1957) p.1642

(Hag.75) : E.Hagebo and T.Lund J. Inorg. Nucl. Chem. 37
(1975) p.1569

(Hal.58) : I.Halpern and V.M.Strutinski Proc. Intern. Conf.
Peaceful Uses of Atomic Energy, Geneva Vol 15
(1958) p.408

(Hal.59) : I.Halpern Nucl. Phys. 11(1959) p.522

(Han.70) : "Handbook of Chemistry and Physics" R.C.Weast
editor, The Chemical Rubber Co. Publisher (1970)

(Har.56a): G.N.Harding and F.J.M.Farley Proc. Phys. Soc.
(London) A69(1956) p.853

(Har.56b): G.N.Harding Proc. Phys. Soc. (London) A69(1956)
p.330

(Har.74) : G.D.Harp Phys. Rev. C10(1974) p.2387

(Hen.40) : M.C.Henderson Phys. Rev. 58(1940) p.774

(Hen.71) : R.P.Henke and E.V.Benton Nucl. Instr. and Meth.
97(1971) p.483

(Hog.69) : J.J.Hogan and N.Sugarman Phys. Rev. 182(1969)
p.1210

(Hon.71) : S.Hontzeas and H.Blok Phys. Scrip. 4(1971) p.229

(Hud.69) : J.Hudis and S.Katcoff Phys. Rev. 180(1969) p.1122

(Hui.69) : J.R.Huizenga, A.N.Beckami and L.G.Moretto Phys.
             Rev. 177(1969) p.1826

(Hve.68) : P.Hvelplund and B.Fastrup Phys. Rev. 165(1968)
             p.408

(Iva.57) : N.S.Ivanova and I.I.P'Ianov Sov. Phys. JETP
             4(1957) p.367

(Iva.58) : I.S.Ivanova Sov. Phys. JETP 34(7) (1958) p.955

(Jac.56) : J.P.Jackson Can. J. Phys. 34(1956) p.767

(Jen.57) : F.A.Jenkins, H.E.White, "Fundamentals of optics"
             Mc Graw-Hill book Company Inc. (1957)

(Jod.55) : L.G.Jodra and N.Sugarman Phys. Rev. 99(1955) p.1470

(Kap.66) : M.Kaplan and A.Ewart Phys. Rev. 148(1966) p.1123

(Kat.68) : R.Katz and E.J.Kobetich Phys. Rev. 170(1968) p.401

(Kha.72) : H.A.Khan and S.A.Durrani Nucl. Instr. and Meth.
             98(1972) p.229

(Kie.73) : F.M.Kiely and B.D.Pate Nucl. Instr. and Meth.
             109(1973) p.355

(Kow.62) : L.Kowalski, C.Stephan,H.Langevin-Joliot, et
             P.Radvanyi Phys. Lett. 2(1962) p.356

(Kow.63) : L.Kowalski and C.Stephan J. Phys. (Paris) 24
             (1963) p.901

(Kow.64) : L.Kowalski Ann. Phys. (Paris) 9(1964) p.211

(Kru.55) : P.Kruger and N.Sugarman Phys. Rev. 99(1955) p.1459

(Lag.76) : M.Lagarde-Simonoff, S.Regnier, H.Sauvageon and
             G.N.Simonoff Nucl. Phys. A260(1976) p.369

(Lea.52) : R.B.Leachman Phys. Rev. 87(1952) p.444

(Lea.55) : R.B.Leachman and W.D.Schafer Can. J. Phys.
33(1955) p.357

(Lec.50) : K.J.Le Couteur Proc. Phys. Soc. (London) A63
(1950) p.259

(Lec.52) : K.J.Le Couteur Proc. Phys. Soc. (London) A65
(1952) p.718

(Lef.68) : M.Lefort "Nuclear Chemistry" D.Van Nostrand
Company Ltd London Publisher (1968)

(Lin.61) : J.Lindhard and M.Scharff Phys. Rev. 124(1961)
p.128

(Loz.55) : O.V.Lozhkin, N.A.Perfilov and V.P.Shamov Sov.
Phys. JETP 1(1955) p.292

(Loz.56) : O.V.Lozhkin, N.A.Perfilov and V.P.Shamov Sov.
Phys. JETP 2(1956) p.116

(Mau.66) : M.Maurette J. de Physique 27(1966) p.505

(Mea.58) : J.W.Meadows Phys. Rev. 110(1958) p.1109

(Met.58) : N.Metropolis, R.Bivens, M.Storm, A.Turkevich,
J.M.Miller and G.Friedlander Phys. Rev.110(1958)
p.185; 110(1958) p.204

(Mil.59) : M.Miller and J.Hudis Ann. Rev. Nucl. Sci. 9(1959)
p.159

(Mil.62) : J.C.D.Milton and J.S.Fraser Can. J. Phys.
40(1962) p.1626

(Mil.78) : J.M.Miller, D.Logan, G.L.Catchen, M.Rajagopalan,
J.M.Alexander, M.Kaplan, J.W.Ball, M.S.Zisman
and L.Kowalski Phys. Rev. Lett. 40(1978) p.1074

(Mor.70) : D.V.Morgan and D.Van Vliet Contemp. Phys.
11(1970) p.173

(Mye.66) : W.D.Myers and W.J.Swiatecki Nucl. Phys. 81(1966)
p.1

(Nak.69) : H.Nakahara, J.W.Harvey and G.E.Gordon Can. J.
Phys. 47(1969) p.2371

(Nat.68) : J.B.Natowitz, A.Khodai-Joopari, J.M.Alexander and
T.D.Thomas Phys. Rev. 169(1968) p.993

(Nam.75) : M.N.Namboodiri, J.B.Natowitz, E.T.Chulick, K.Das
and L.Webb Nucl. Phys. A252(1975) p.163

(Ner.60) : W.E.Nervik Phys. Rev. 119(1960) p.1685

(Nix.69) : J.R.Nix Nucl. Phys. A130(1969) p.241

(Nor.70) : L.C.Northcliffe and R.F.Schilling Nucl. Data Tables
A7(1970) p.233

(Obu.59) : A.I.Obukhov Sov. Phys. JETP 8(1959) p.727

(Obu.61) : A.I.Obukhov and N.A.Perfilov Sov. Phys. JETP 13
(1961) p.881

(Obu.62) : A.I.Obukhov and N.A.Perfilov Phys. Rev. 126
(1962) p.2196

(Orm.63) : J.H.Ormrod and H.E.Duckworth Can. J. Phys.
41(1963) p.1424

(Orm.65) : J.H.Ormrod, J.R.Macdonald and H.E.Duckworth
Can. J. Phys. 43(1965) p.275

(Ost.55) : V.I.Ostroumov Proc. Acad. Sci. USSR 103(1955) p.409

(Pat.55) : B.D.Pate and L.Yaffe Can. J. Chem. 33(1955) p.15

(Pat.61) : B.D.Pate and A.M.Poskanzer Phys. Rev. 123(1961)
p.647

(Pla.66) : F.Plasil, D.S.Burnett, H.C.Britt and S.G.Thompson
Phys. Rev. 142(1966) p.696

(Por.57) : N.T.Porile and N.Sugarman Phys. Rev. 107(1957)
p.1410; 107(1957) p.1422

(Por.60) : N.T.Porile Phys. Rev. 120(1960) p.572

(Por.64) : N.T.Porile and S.Tanaka Phys. Rev. 135B(1964) p.122

(Pri.62a): P.B.Price and R.M.Walker Phys. Lett. 3(1962) p.113

(Pri.62b): P.B.Price and R.M.Walker Phys. Rev. Lett. 8(1962) p.217

(Pri.62c): P.B.Price and R.M.Walker J. Appl. Phys. 33(1962) p.3407

(Pri.67) : P.B.Price, R.L.Fleischer, D.D.Peterson, C.O'Ceallaigh, D.O'Sullivan and A.Thompson Phys. Rev. 164(1967) p.1618

(Pri.68a) : P.B.Price, R.L.Fleischer, D.D.Peterson, C.O'Ceallaigh, D.O'Sullivan and A.Thompson Phys. Rev. Lett. 21(1968) p.63

(Pri.68b) : P.B.Price, R.L.Fleischer, D.D.Peterson, C.O'Ceallaigh, D.O'Sullivan and A.Thompson Can. J. Phys. 46(1972) p.S1149

(Pri.68c) : P.B.Price, R.L.Fleischer and C.D.Moak Phys. Rev. 167(1968) p.277

(Pri.71) : P.B.Price and R.L.Fleischer Ann. Rev. Nuc. Sci. 21(1971) p.295

(Rem.70) : G.Remy, J.Ralarosy, R.Stein, M.Debeauvais et J.Tripier J. de Physique 31(1970) p.27

(Ros.65) : B.Rossi "Optics" Addison-wesley publishing Company Inc. (1965)

(Rud.56) : G.Rudstam "Spallation of medium weight elements" Doctoral Thesis University of Uppsala, Uppsala, Sweden (1956)

(Rut.11) : E.Rutherford Phil. Mag. 21(1911) p.669

(Sch.66) : H.W.Schmitt, J.H.Neiler and F.J.Walter Phys. Rev. 141(1966) p.1146

(Ser.47) : R.Serber Phys. Rev. 72(1947) p.1114

(Sha.56) : V.P.Shamov and O.V.Lozhkin Sov. Phys. JETP 2(1956) p.111

(Sil.59) : E.C.H.Silk and R.S.Barnes Phil. Mag. 4(1959) p.970

(Som.73) : G.Somogyi and S.A.Szalay Nucl. Instr. and Meth. 109(1973) p.211

(Som.77) : G.Somogyi, R.Scherzer, K.Grabisch and W.Enge Nucl. Instr. and Meth. 147(1977) p.11

(Ste.57) : W.E.Stein Phys. Rev. 108(1957) p.94

(Ste.58) : P.C.Stevenson, H.G.Hicks, W.E.Nervik and D.R.Nethaway Phys. Rev. 111(1958) p.886

(Ste.60) : P.C.Stevenson, H.G.Hicks, J.C.Armstrong Jr. and S.R.Gunn Phys. Rev. 117(1960) p.186

(Ste.67) : C.Stephan and M.L.Perlman Phys. Rev. 164(1967) p.1528

(Sug.56) : N.Sugarman, M.Campos and K.Wielgoz Phys. Rev.101 (1956) p.388

(Sug.66) : N.Sugarman, H.Munzel, J.A.Panontin, K.Wielgoz, M.V.Ramaniah, G.Lange and E.Lopez-Menchero Phys. Rev. 143(1966) p.952

(Tep.62) : Ya.A.Teplova, V.S.Nikolaev, I.S.Dmitriev and L.N.Fateeva Sov. Phys. JETP 15(1962) p.31

(Ula.47) : S.Ulam and J.Von Neumann Bull. Am. Math. Soc. 53(1947) p.1120

(Uni.74) : J.P.Unik, J.E.Gindler, L.E.Glendenin, K.F.Flynn, A.Gorski, R.K.Sjoblom Proc. 3rd Symp. on physics and chemistry of fission, Rochester, 1973 vol.2 (IAEA,Vienna,1974) p.19

(Val.60) : U.L.Vallinder and H.Tyren Nucl. Phys. 15(1960) p.152

(Vio.63) : V.E.Viola Jr. and T.Sikkeland Phys. Rev. 130 (1963) p.2044

(Wat.69) : R.L.Watson and J.B.Wilhelmy UCRL-18632 (1969)

(Wei.37) : V.Weisskopf Phys. Rev. 52(1937) p.295

(Wil.79) : B.D.Wilkins, E.P.Steinberg and S.B.Kaufman
           Phys. Rev. C19(1979) p.856

(Yam.50) : Y.Yamaguchi Prog. Theor. Phys. 5(1950) p.142

(You.58) : D.A.Young Nature 182(1958) p.375